THE UNIVERSITY OF CALGARY

Fluidized Bed Steam Methane Reforming with High-flux Membranes and Oxygen Input

by

Surajit Roy

A DISSERTATION

SUBMITTED TO THE FACULTY OF GRADUATE STUDIES

IN PARTIAL FULFILLMENT OF THE REQUIREMENTS FOR THE

DEGREE OF DOCTOR OF PHILOSOPHY

DEPARTMENT OF CHEMICAL AND PETROLEUM ENGINEERING

CALGARY, ALBERTA

DECEMBER, 1998

Abstract

The aim of the present investigation was to improve the performance of fluidized bed membrane reforming (FBMR) by improving the permeation of hydrogen using High-flux membranes and introducing oxygen to provide for the heat of reaction. Developments and modifications, which were made to the FBMR process, are summarized in six different sections. A study on the economics of FBMR showed that configuration with High-flux membranes had a lower capital and operating cost than conventional steam-methane reforming (SMR), and had a hydrogen supply cost 5% lower than commercial SMR, showing the promise of this new technology.

Second, palladium coated metal alloy tubular (High-flux) membranes for use at high temperatures and differential pressures were successfully developed. Mr. M. Islam tested them for permeation characteristics and abrasion. Then spring reinforced High-flux membrane (U-tube) modules were developed for use in the FBMR pilot plant reformer.

Thirdly, U-tube spring reinforced High-flux membrane modules were used in a pilot plant reformer, and performed successfully in the reactor environment. A greatly improved performance was observed compared to the equilibrium reactor, and the hydrogen permeate flow was ten to fifteen times greater than published studies by others. The dependent variables, methane conversion and hydrogen yields, behaved as anticipated and were about 15% higher than equilibrium.

Fourth, oxygen was introduced successfully into a steam methane fluidized bed reforming reactor to provide for the endothermic heat of reforming reactions. There was

100% conversion of oxygen under all conditions and most runs reached and maintained autothermal conditions. Methane conversion and hydrogen yield were compared to that expected from equilibrium.

Fifth, an autothermal FBMR unit producing hydrogen was successfully developed and tested. The hydrogen permeate flow (mol/h) in the autothermal FBMR study was on an average seven to ten times greater than in the previous study (Adris, 1994). The comparison with FBMR proved that the autothermal configuration gives increased methane conversion but decreased hydrogen yield and permeation.

Sixth, a comprehensive computer model to simulate the FBMR (High-flux membranes) with or without oxygen input was developed and verified using data from the work. The model showed very good agreement with experimental data.

Acknowledgments

I express my sincere appreciation to Dr. Barry Pruden for his critical evaluation, insightful suggestions, invaluable guidance, encouragement and support during the entire course on the Ph.D. project. It has been a marvelous three and half years working with him.

It was a pleasure to work with Mr. M. T. Islam, Dr. R. E. Buxbaum and Mr. B. G. Cox for various studies conducted during the project. Their suggestions and contributions are gratefully acknowledged.

I am grateful for the help rendered by Derek Verhegge, Rob Scory and others in the workshop for the experimental setup.

Especially, I would like to thank Dr. J. R. Grace and Dr. A. M. Adris for their interest, ideas and suggestions.

I would like to thank Dan Wong for lending a helping hand with the pilot plant experiments.

Above all I am grateful to my parents and rest of the family for their encouragement, support and infinite patience in my prolonged pursuit for education.

I would also like to thank my friends Ramki, Harpreet, Simant, Jayanta, Amitava, Subodh, Amit, Patrick, and others, who all have made my stay in Calgary pleasant.

Dedicated to my father

Late Shri. Ranjit Kumar Roy

Table of Contents

List of Tables

List of Figures

Nomenclature

a_b : ratio of bubble surface area to volume, m^{-1}

a_c : overall decay constant for catalyst particles in the dilute phase, m^{-1}

A_i : internal cross sectional area of the reactor, m^2

A_m : inside surface area of the membrane tube, m^2

Ar : dimensionless Archimedes number

C_{Hh} : concentration of hydrogen atoms at the high pressure side, mol H/m^3

C_{Hl} : concentration of hydrogen atoms at the low pressure side, mol H/m^3

C_i : concentration of component i

C_{ib} : concentration of component i in the bubble phase, kmol/m^3

C_{ie} : concentration of component i in the emulsion phase, kmol/m^3

C_o : hydrogen solubility in the metal, kmol/m^3.$Pa^{0.5}$

D : internal diameter of the reactor, m

d_b : bubble diameter at any height, m

d_{bm} : maximum bubble diameter, m

d_{bo} : initial bubble diameter, m

DEN : denominator of the kinetic rate expressions defined by Equation 2.4

d_i : inner diameter of the membrane tube, mm

D_{id} : effective diffusivity of component i in a mixture, cm^2/s

D_{ij} : binary diffusivity of components i and j, cm^2/sec

D_M : diffusivity of atomic hydrogen, m^2/sec

d_o : outer diameter of the membrane tube, mm

d_p : mean particle diameter of the catalyst particles, μm

E_p : activation energy for permeation, kJ/mol

g : gravitational acceleration, m/s^2

g_i^o : standard Gibbs energy of formation of component i, J/mol

G : total Gibbs free energy, J

h : height above the distributor level, m

h_{bed} : height of the fluidized catalyst bed surface, m

h_{dil} : distance from the catalyst bed surface in the dilute phase, m

h_{DIL} : distance from the catalyst bed surface in the dilute phase, m

h_{exit} : total height of the fluidized bed reformer, m

h_{EZN1} : height of Zone 1 in the FBMR model, m

h_{EZN2} : height of Zone 2 in the FBMR model, m

h_{EZN3} : height of Zone 3 in the FBMR model, m

h_{EZN4} : height of Zone 4 in the FBMR model, m

J_H : flux of hydrogen atoms, mols of atomic hydrogen/(m^2.s)

J_{H2} : molar flux of hydrogen, mol/(m^2.s)

k_1, k_2 : rate coefficients for Equations 7.21 and7.22, respectively, kmol/(kg cat.h)

K_3 : equilibrium constant for Equation 2.1, bar^2

k_3, k_5 : rate coefficients for Equations 2.1 and 2.3, respectively, kmol.$bar^{0.5}$/(kg cat.h)

K_4 : equilibrium constant for Equation 2.2, dimensionless

k_4 : rate coefficient for Equation 2.2, kmol/(kg cat.h.bar)

K_{CH4} : adsorption constants for CH_4, bar^{-1}

K_{CO} : adsorption constants for CO, bar^{-1}

k_H : permeation rate constant, kmol/h.$Pa^{0.5}$

K_{H2} : adsorption constants for H_2, bar^{-1}

K_{H2O} : dissociative adsorption constant for water, dimensionless

k_{iq} : interphase mass exchange coefficient for component i , m/s

K_R : sorption coefficient for hydrogen, mols of atomic hydrogen/(m^3.Pa)

K_S : Sieverts constant, mols of atomic hydrogen/(m^3.$Pa^{0.5}$)

l : length of the membrane tube, cm

L : thickness of the ceramic membranes, μm

M_i : molecular weight of component i , g/mol

n : exponent for hydrogen partial pressure & total number of mols for Equations 5.3 & 5.4, mol

N_{H2} : molar flow rate of permeate hydrogen, mol/s

n_i : molar flow rate of component i, mol/s & mols of component i, for Equations 5.3 &5.4, mol

n_{ib} : molar flow rate of component i in the bubble phase, mol/s

n_{ibf} : molar flow rate of component i in the bubble phase and at the end of catalyst bed, mol/s

n_{ibo} : molar feed rate of component i in the bubble phase, mol/s

n_{idil} : molar flow rate of component i in the dilute phase, mol/s

n_{ie} : molar flow rate of component i in the emulsion phase, mol/s

n_{ief} : molar flow rate of component i in the emulsion phase and at the end of catalyst bed, mol/s

n_{ieo} : molar feed rate of component i in the emulsion phase, mol/s

n_{if} : molar flow rate of component i at the end of the reactor, mol/s

n_{io} : molar feed rate of component i in the reactor, mol/s

N_{or} : number of orifices in the distributor plate

P : pressure, Pa and for Equations 5.3 & 5.4, bar

P_{CH4} : partial pressure of CH_4, bar

P_{CO} : partial pressure of CO, bar

P_{CO2} : partial pressure of CO_2, bar

P_{H2} : partial pressure of H_2, bar

P_{H2} : partial pressure of hydrogen, Pa

P_{H2h} : partial pressure of hydrogen in the feed or high pressure side, Pa

P_{H2l} : partial pressure of hydrogen in the permeate or low pressure side, Pa

P_{H2O} : partial pressure of H_2O, bar

P_i : partial pressure of component i for Equation 5.4, bar

p_i : partial pressure of component i, MPa

P_M : permeability in terms of molar flow, mol/(m.s.$Pa^{0.72}$)

P_{Meff} : effective permeability of the High-flux membrane tubes, mol/(m.s.$Pa^{0.72}$)

P_{MO} : permeation pre-exponential factor, mol/(m.s.$Pa^{0.72}$)

R_1 to R_5 : rate of reaction, kmol/(kg cat.h)

R_c : constant resistance, m^2.sec.$Pa^{0.72}$/mol

R_{CH4} : rate of formation of CH_4, kmol/(kg cat.h)

R_{CO} : rate of formation of CO, kmol/(kg cat.h)

R_{CO2} : rate of formation of CO_2, kmol/(kg cat.h)

R_g : universal gas constant, J/(mol.K)

R_{H2} : rate of formation of H_2, kmol/(kg cat.h)

R_{H2O} : rate of formation of H_2O, kmol/(kg cat.h)

R_{ib} : rate of formation of component i in the bubble phase, kmol/(kg cat.h)

R_{idil} : rate of formation of component i in the dilute phase, kmol/(kg cat.h)

R_{ie} : rate of formation of component i in the emulsion phase, kmol/(kg cat.h)

R_{tot} : total transport resistance through composite metal membrane, $m^2.s.Pa^{0.72}/mol$

SC : steam-methane ratio, dimensionless

T : temperature, K

t : thickness of the metal membrane, μm

T_{ci} : critical temperature of component i, K

t_{tot} : total thickness of the High-flux membrane tube, μm

U_{abs} : absolute rise velocity of bubbles, m/s

U_{br} : relative rise velocity of bubbles, m/s

U_{mf} : minimum fluidization velocity, m/s

U_o : superficial velocity, m/s

V_{ci} : critical molar volume of component i, cm^3/mol

X_{CH4} : conversion of methane, %

X_i : conversion of component i

y_{CH4} : mole fraction of methane

y_i : mole fraction of component i, in general

y_{ib} : mole fraction of component i in the bubble phase

y_{id} : mole fraction of component i in the dense catalyst bed

y_{ie} : mole fraction of component i in the emulsion phase

y_{O2} : mole fraction of oxygen

Symbols

$\frac{\partial G}{\partial n_i}$: partial derivative of Gibbs free energy with respect to moles of component i

$\frac{\partial X_{CH4}}{\partial F_{O2}}$: partial derivative of methane conversion with respect to oxygen flowrate

$\frac{\partial X_{CH4}}{\partial P}$: partial derivative of methane conversion with respect to pressure

$\frac{\partial X_{CH4}}{\partial SC}$: partial derivative of methane conversion with respect to steam-methane ratio

$\frac{\partial X_{CH4}}{\partial T}$: partial derivative of methane conversion with respect to temperature

μ : absolute viscosity of gas, kg/(m.s)

ϕ : equivalence ratio

Ψ_∞ : entrainment flux of solids above the transport disengagement height, kg/(m^2.s)

ε_b : volume fraction of bed occupied by bubbles

ϕ_b : volume fraction of bed occupied by solids dispersed in the bubble phase

ϕ_{dil} : catalyst mass concentration in the dilute phase, kg/m^3

ϕ_e : volume fraction of bed occupied by solids in the emulsion phase

ΔF_{O2} measurement accuracy of oxygen flow rate

ρ_g : density of gas stream, kg/m^3

ΔH : heat or reaction, kJ/mol

Ψ_{hdil} : entrainment flux of solids at any height h_{dil}, kg/(m^2.s)

ν_I : mole fraction of component i

ϕ_m : permeance, mol/(m^2.s.$Pa^{0.72}$)

ε_{mf} : voidage at minimum fluidization velocity

Ψ_o : entrainment flux of solids at the catalyst bed surface, kg/(m^2.s)

ρ_p : density of catalyst particles, kg/m^3

η_p : effectiveness factor for permeation

ΔP : measurement accuracy of pressure

ρ_s : density of catalyst, kg/m^3

ΔSC : measurement accuracy of steam-methane ratio

ΔT : measurement accuracy of temperature

Subscripts

b : bubble phase

CH4 : methane

d : dense catalyst bed

dil : dilute phase (freeboard region)

e : emulsion phase

f : final or exit

h : feed or high pressure side

H2 : hydrogen

i : component

l : permeate or low pressure side

o : feed

O2 : oxygen

Superscript

a, ao : exponents of temperature in milti-variate analysis

b, bo : exponents of temperature in milti-variate analysis

c,co : exponents of steam-methane ratio in milti-variate anlysis

do : exponent of oxygen flow rate in milti-variate anlysis

n : exponent of partial pressure of hydrogen in permeation rate equations

o : standard Gibbs energy of formation

Chapter 1

Introduction

1.1 Purpose of the study

The major objective of this study was to improve the process for production of hydrogen by utilizing High-flux palladium coated metal alloy membranes in a fluidized bed membrane reformer (FBMR).

A second objective was to study the addition of oxygen to the hydrogen production process, which would provide the heat of the reforming reaction directly to a fluidized bed reformer and a FBMR.

Finally, in the course of the study, a computer model was developed to simulate the experimental results. The economics of the fluidized bed membrane reforming process were evaluated and were compared to the conventional steam methane reforming (SMR) process.

1.2 SMR process

The application of nickel catalysts to produce hydrogen from hydrocarbons and steam was first claimed by Mond (Rostrup-Nielsen, 1984). The initial industrial patent for the reforming process was taken by BASF (Mittasch and Schneider) in 1912; numerous patents were issued in 1930s to other inventors. Presently, the conventional steam methane reforming (SMR) process is the primary method of hydrogen production

for industrial use. Steam methane reforming is defined as the process by which hydrogen or syngas is produced by the reaction of steam with methane. It is the process used to produce hydrogen and synthesis gas for ammonia production, methanol production, hydrocracking, hydrotreating, oxo-alcohol synthesis, Fischer-Tropsch synthesis and other essential processes in the petroleum and petrochemical industries. The endothermic SMR process generally uses nickel catalyst and is carried out in tubular reactors located in furnaces, where radiant heat from the combustion of fuel provides for sensible heat plus the endothermic heat of reaction.

Depending on the feedstock ratio and reaction conditions in the SMR process, numerous reactions may occur. The most likely reactions in steam methane reforming are listed in Table 1.1. In a commercial reformer, conditions are set to ensure that carbon formation reactions do not occur, and hence reactions 1.6 to 1.11 can be ignored. Only two of the reactions 1.1 to 1.5 are independent, Reactions 1.1 and 1.3 are generally used to describe the thermodynamics of the process. Other than the water gas shift reaction (1.2), reactions 1.1 to 1.5 are all highly endothermic, which means that high temperatures promote them. Only reaction 1.2, being exothermic, is favored at lower temperatures. This explains the higher carbon monoxide to carbon dioxide ratio in high temperature reformers compared to lower temperature reformers. Although most of the reactions are thermodynamically favored at low pressures, commercial reformers are generally operated at pressures ranging from 1.5 to 4.0 MPa to offset hydrogen compression costs.

To enhance the reaction rate, catalyst is used in SMR processes. Commercial catalysts have three important characteristics: high activity to increase the reaction rate and maximize conversion and hence yield of hydrogen; high thermal and mechanical

strength to maintain constant pressure drop across the reforming tube at high operating temperatures; and resistance to carbon formation. The most widely used commercial catalyst is nickel supported over alumina of various kinds, depending upon the conditions in which the catalyst is used (Rostrup-Nielsen, 1984; Wagner & Froment, 1992). Cobalt and noble metals are also active but are more expensive than nickel.

Table 1.1: Most likely reactions in steam methane reforming.

						ΔH_{298}, kJ/mol	
CH_4	+	H_2O	=	CO	+	$3H_2$	206.1	(1.1)
CO	+	H_2O	=	CO_2	+	H_2	-41.1	(1.2)
CH_4	+	$2H_2O$	=	CO_2	+	$4H_2$	165.0	(1.3)
CH_4	+	CO_2	=	2CO	+	$2H_2$	247.3	(1.4)
CH_4	+	$3CO_2$	=	4CO	+	$2H_2O$	330.0	(1.5)
CH_4			=	C	+	$2H_2$	74.8	(1.6)
2CO			=	C	+	CO_2	-173.3	(1.7)
CO	+	H_2	=	C	+	H_2O	-131.3	(1.8)
CO_2	+	$2H_2$	=	C	+	$2H_2O$	-90.1	(1.9)
CH_4	+	2CO	=	3C	+	$2H_2O$	-187.6	(1.10)
CH_4	+	CO_2	=	2C	+	$2H_2O$	-15.3	(1.11)

The activity of Ni/Al_2O_3 catalyst depends on the surface area of the active nickel component. The chemisorption of methane on nickel involves the breakage of a C-H bond, this breakage requires that molecules have sufficient energy to overcome a barrier of about 52 kJ/mol (Rostrup-Nielsen, 1975). The activated chemisorption of methane is the rate determining step in steam reforming (Rostrup-Nielsen, 1984). The water-gas shift reaction occurs at a much faster rate than chemisorption of methane and therefore can be safely assumed to be at equilibrium at all positions within the reformer. The catalyst properties are dictated by the severe operating conditions that are used in the commercial process, with temperatures of 450-950 °C and with steam partial pressures up to 3.0 MPa.

1.3 Applications of SMR

The petrochemical industry and other energy related industries use reforming technology for a variety of purposes. The reforming process is essential for many commercially important chemical processes such as ammonia synthesis, hydrogen production, methanol synthesis, oxo-synthesis, carbon monoxide production and Fisher-Tropsch synthesis. Approximately 76% of all the hydrogen produced comes from steam reforming of natural gas (Balthasar, 1984). Most of the world ammonia production is based on steam reforming of hydrocarbons, with natural gas being the preferred feedstock. Oil refineries use hydrogen from steam reforming for desulphurization and hydrocracking. In the petrochemical industry, steam reforming is used for the production of synthesis gas that is then used to manufacture methanol, oxo-alcohols, acetic acid and other chemicals. Applications also include gases for direct reduction for iron ore, conversion of hydrocarbons for fuel cells, and advanced energy transfer systems in which nuclear heat or

solar energy are absorbed by the endothermic steam reforming process. The total consumption of hydrogen/ syngas in industrial processes is apportioned as follows: 36% ammonia synthesis; 47% petroleum refining; 10% methanol synthesis; 7% miscellaneous uses (Balthasar, 1984).

Based on the intended use of the product gases, SMR applications can be broadly classified into three categories as described in sections 1.3.1 to 1.3.3.

1.3.1 Production of hydrogen for ammonia synthesis

Steam reforming is the first step in ammonia production. Steam reacts with methane and other hydrocarbons in the primary reformer to produce H_2, the desired product of the process, as well as CO_2 and CO. For a typical steam to carbon ratio of 3.5 and a temperature of 800 °C, the effluent gas composition (dry basis, mole %) is H_2-68.3%, CO-10.4%, CO_2-10.1%, CH_4-10.3% and N_2-0.9% (Xu, 1988). Air is added to the reformer products in a secondary reformer. The oxygen in air reacts with the excess methane and hydrogen to raise the temperature and provide the heat of reaction. The amount of air is such that the molar ratio of hydrogen to nitrogen is about 3:1 prior to entering the ammonia converter. Oxidation occurs in a combustion chamber, and steam reforming reactions occur in the secondary reformer catalyst bed. A typical composition (dry basis, mole %) of the effluent gas from the secondary reformer is as follows: H_2-55.7%, CO-13.8%, CO_2-7.2%, CH_4-0.4% and N_2-22.7% (Xu, 1988).

After leaving the secondary reformer, carbon monoxide is converted into carbon dioxide in high and low temperature shift converters. Carbon dioxide is absorbed by a suitable solvent and subsequently removed. The remaining traces of carbon monoxide

are converted to methane in a methanator. The hydrogen/ nitrogen mixture, which also contains some methane, enters the ammonia synthesis reactor at a ratio of close to 3:1. Sulfur compounds such as H_2S, CS_2, RSH, COS, RSR', RS_2R" poison the reforming catalyst and therefore are removed from the natural gas before being fed to the primary reformer.

1.3.2 Hydrogen production

When hydrogen is the desired product, the temperature and steam-to-carbon ratios are kept at high values to maximize the production of hydrogen. At a typical operating condition (steam-to-carbon molar feed ratio 3.0; outlet temperature 815 °C; and pressure 1.9 MPa), the composition (dry basis, mole %) of the effluent gas from the primary reformer is as follows: H_2 69%, CO 12%, CO_2 8.8%, CH_4 6.1% and N_2 4.1% (Xu, 1988). After the primary reforming stage the gases are processed using different schemes depending on the hydrogen purity required. In conventional SMR plants, the reforming stage is followed by high and low temperature shift converters (to convert CO to CO_2), a carbon dioxide absorption process, and a methanator (to convert remaining CO and CO_2 to CH_4). Modern plants utilize pressure swing adsorption (PSA) to produce high-purity hydrogen from the primary reformer effluent gas. Hydrogen purity of about 98% is achieved with conventional purification schemes whereas PSA can produce hydrogen at 99.99% purity (Balthasar, 1984). When, in addition to hydrogen, CO production is also desired, the reformer is followed by a cryogenic partial condenser. Carbon monoxide, along with methane as a resulting impurity is condensed in the process and subsequently distilled to produce a CO stream with 99.5% purity.

1.3.3 Syngas production

The steam reforming reaction can be controlled to maximize production of syngas (H_2+CO). When maximizing syngas production, CO_2 is undesirable since it is in a completely oxidized state and lowers the reactivity of the syngas. An important parameter to consider in syngas production is the ratio (H_2+CO) to (H_2O+CO_2). Typical values of this ratio are between 9 and 10 for reducing gas applications. High temperature, low pressure and a low steam to carbon ratio favor production of an effective reducing gas. The H_2/CO ratio suitable for methanol synthesis is about 2.5 which requires a feed hydrogen to carbon ratio of about 2.0. This ratio is difficult to achieve when natural gas or a light hydrocarbon is used as feedstock. Recycling carbon dioxide to the reformer can solve this problem. However, this carbon rich environment can cause considerable carbon deposition and hence catalyst deactivation. In response to this, Haldor Topsoe Inc. developed a sulfur passivated catalyst which prevents carbon deposition at low H_2/CO ratios (Dibbern et al., 1986).

1.4 Limitations and design features of conventional SMR process

In conventional SMR units, the steam reforming reactions are carried out in high alloy tubes placed inside a furnace equipped with burners. Depending on the furnace type and application, there are typically 40 to 400 tubes of 6 to 12 m in length. The tubes are made from expensive high alloy nickel chromium steel (e.g. HK 40) and account for a large part of the reformer cost. The internal tube diameter is in the range of 70 to 160 mm with a tube wall thickness of 10 to 20 mm. Typical inlet temperatures are 450-650

°C; product gases leave the reformer at temperatures between 700-950 °C depending on the application (Adris et al., 1996).

1.4.1 Intraparticle diffusion

The size of particles and shape of reforming catalysts are optimized to achieve maximum activity and maximum heat transfer while minimizing the pressure drop. The intrinsic rates of the reforming reactions are very high compared to the rate of mass transfer. The mass transfer restrictions are located mainly in pore diffusion, whereas the heat transfer restrictions are located in the gas film. De Deken et al. (1982) computed the effectiveness factors for both carbon dioxide production and methane disappearance (η_{CO2} and η_{CH4} respectively) using Langmuir-Hinshelwood type kinetics. Their reported values for maximum effectiveness factors were less than 0.05 and 0.04 for CO_2 and CH_4 respectively. Another study by Soliman et al. (1988) has shown effectiveness factors for steam and methane disappearance in the range of 0.05 to 0.008. Both studies confirm that at least 95% of the catalyst surface area is not utilized in SMR and the activity is roughly proportional to the external surface area. Use of catalyst pellets with high voidage (to give low pressure drop) and high external surface area has been suggested to overcome this problem. The Haldor Topsoe cylindrical pellets that consist of a number of cylindrical holes in each pellet and catalytically active material concentrated on the external surface of the pellets have been used. However, no dramatic improvements in the effectiveness factors have been reported even after these modifications.

1.4.2 Heat transfer limitations

Heat is needed to achieve the endothermic steam reforming reactions and to provide for sensible heat to raise the reaction mixture to the high temperatures necessary for high rates of reaction and resulting high conversions. Heat is supplied by burning natural gas or other fossil fuels in the furnace that accommodates the catalyst tubes. The fuel consumption rate is typically between 30% and 50% of the feed rate. Approximately 50% of the heat produced by combustion in the burners is transferred through the reformer tube walls and absorbed by the process. The other half of the heat duty is available in the hot flue gas and is recovered in the convection section of the reformer for preheat duties and steam production. The balance between heat input through the reformer tube walls and the heat consumption in the endothermic reforming reaction is the central problem in steam reforming (Rostrup-Nielsen, 1983). The walls of the reformer tubes must be capable of withstanding extreme operating conditions, such as skin temperatures in the range of 750 °C to 880 °C, very large temperature gradients, and a pressure difference of between 1.5 and 4.0 MPa. The maximum allowable stress value in the tubes is strongly influenced by the maximum tube wall temperature and by the maximum heat flux.

Typical values of the average heat flux in modern reformers are about 45 to 90 kW/m^2. The average heat flux is, however, not a very good measure of the operating severity of reformer tubes. More important than the average heat flux is the maximum local heat flux and the outside wall temperature corresponding to the peak heat flux. Even a slight increase in the maximum tube wall temperature may result in a serious decline in the expected tube lifetime. Tube materials are limited by design temperature and creep rupture

strength. Consequently, reformer tubes are generally made of expensive high alloy nickel-chromium steels having a limited operating life under such extreme conditions.

1.4.3 Constraints of thermodynamic equilibrium

The steam reforming reactions reach thermodynamic equilibrium quite rapidly at higher temperatures. The equilibrium compositions are dependent on only three variables, temperature, pressure and inlet composition (steam-methane ratio). Equilibrium compositions can be calculated by Gibbs free energy minimization that will be explained in Chapter 5. Figures 1.1 and 1.2 plot the methane conversion and hydrogen yield at equilibrium with temperature and steam-methane ratio, respectively. Hydrogen production is directly proportional to the methane conversion and hydrogen yield; high temperature is beneficial for higher hydrogen production. Higher steam-methane ratios also help increase hydrogen production. However, higher pressure is not favorable for hydrogen production.

1.4.4 Carbon formation

In conventional steam methane reformers, carbon formation is a major problem. This problem of coke formation has been studied rigorously by Rosturp-Nielsen (1978) and Paloumbis and Petersen (1982). Poor distribution and hot spots in the reformer tubes compound this problem. Carbon formation is inevitable if the concentration of steam or hydrogen falls below a certain limit. Paloumbis and Petersen (1982) reported that the experimental steam to carbon ratio was higher than the minimum thermodynamic value.

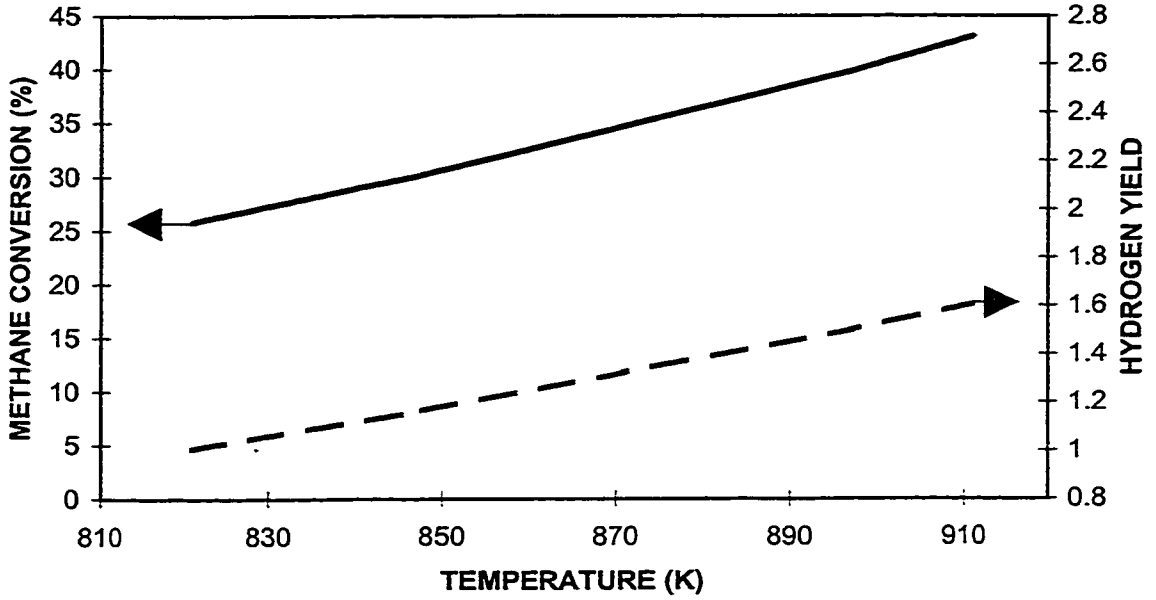

Figure 1.1: Methane conversion and hydrogen yield at equilibrium with temperature vatiation. P = 0.99 MPa and Steam-methane ratio = 3.1

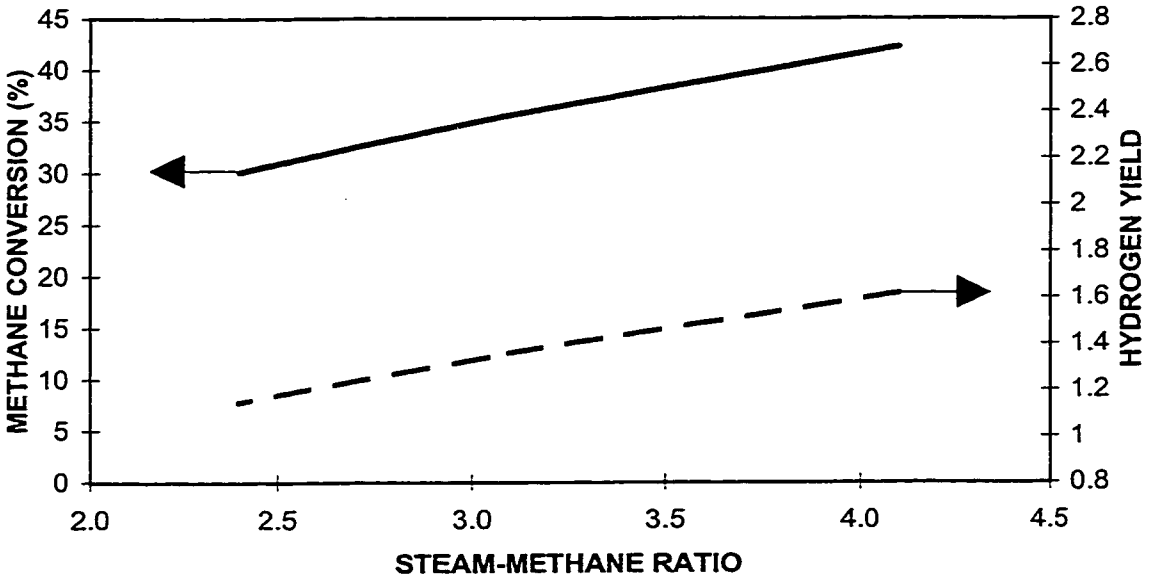

Figure 1.2: Methane conversion and hydrogen tield at equilibrium with steam-methane ratio variation. T = 873 K and P = 0.99 MPa.

At an operating temperature of 900°C, the minimum steam-methane ratio calculated thermodynamically is 1.0; the experimental value is maintained at more than 1.3 to prevent coke formation.

1.5 Improvements to the SMR process

There have been numerous attempts to improve the performance of the steam methane reforming process (Adris et al., 1996). Development efforts can be traced along two distinct lines: (1) improving the catalyst performance to provide higher activity, better catalyst effectiveness, higher mechanical strength, better resistance to carbon deposition and sulfur poisoning; (2) improving the performance of the reactor by using improved materials of construction or a different configuration.

The following discussion summarizes the attempts made to improve the steam methane reforming process through reconfiguration of the process.

1.5.1 Fluidized bed for better heat transfer

Guerrieri (1970) was the first to consider the use of fluidized bed reactors for SMR in his patent. The hydrodynamic property of the reforming catalyst was used for transport between the heating chamber and the reformer. The solids were heated directly and transported back to the reformer, providing most of the endothermic heat requirements.

1.5.2 Packed bed with membrane separation

Nazarkina and Kirichenko (1979) employed membranes to separate hydrogen selectively from fixed bed reformers. A palladium alloy membrane was used at 700°C producing a shift in thermodynamic equilibrium which resulted in higher conversions. Also, pure permeate hydrogen was produced. Oertel et al. (1987) studied a similar configuration and reported an increase of 36% in feed utilization, of 44% in hydrogen yield and of 17% reduced heat requirement. Uemiya et al. (1991) reported that a thin layer of palladium over a porous glass membrane increased hydrogen production. The palladium membrane reactor showed an increase in methane conversion with reactor pressure due to higher permeation rate, despite the fact that higher pressure is thermodynamically unfavorable.

1.5.3 Fluidized bed with heat pipes

Reichel and Lippert (1984) proposed a configuration, which carries out the reforming in a fluidized bed which is connected to a furnace by heat pipes. The heat pipes were hermetically sealed and contained sodium. The sodium in the heat pipes vaporized in the furnace and recondensed in the fluid bed giving off latent heat to provide for the heat of reaction.

1.5.4 Packed bed with metal supported membranes

The patent of Weirch et al (1987) is based on the conceptual design of Nazarkina and Kirichenko (1979). The proposed tubular reactor had a hydrogen collection chamber made of a porous material covered by a layer of hydrogen permselective membrane.

1.5.5 Carbon dioxide acceptor

Brun-Tsekhovoi et al. (1988) proposed a modified process for catalytic steam reforming of hydrocarbons in the presence of carbon dioxide acceptors. Reforming was carried out in a fluidized bed of catalyst containing calcium oxide, which reacts with carbon dioxide to form calcium carbonate, thus liberating the heat of reaction which provides 80 to 100% of the energy required for the endothermic reforming reactions. The calcium oxide plus calcium carbonate was shown to be almost completely separated from the catalyst particles. An equilibrium shift of the reaction conversion and reduction in fuel consumption were claimed to be further advantages of this process.

1.5.6 Rapid quenching of product stream from fluidized bed

Goetsch et al. (1989) suggested a process for synthesis gas production through a catalytic partial oxidation of methane in a fluidized bed autothermal reactor. In the fluidized bed, a light hydrocarbon feed primarily of methane was reacted with oxygen and steam in the presence of a supported nickel catalyst. The gases were maintained at elevated temperatures and pressures to favor the formation of synthesis gas and then quenched by indirect heat exchange. This quench or rapid cooling helped to prevent back reaction and carbon formation. Carbon formation could take place as outlined by the Boudouard reaction ($2CO \Rightarrow C + CO_2$) because low steam/carbon ratios were employed.

1.5.7 Combination of fluidized bed with membranes

The combination of a fluidized bed with permselective membrane was first used by Adris et al. (1991). Utilization of heat pipes to supply the reaction heat were also suggested (Adris, 1994). Adris et al.'s configuration combined the advantages of the fluidized bed, shift of thermodynamic equilibrium by hydrogen separation, and energy input by heat pipes. An experimental study was carried out to demonstrate the validity of the proposed configuration (Adris, 1994: Adris et al. 1994b). Since then it has also been patented (Adris et al. 1994a). The process used by Adris is of particular interest for the present investigation, as the objective of this study is to improve on it. A functional comparison of the major process units in FBMR to the process units in a conventional SMR plant is outlined in Table 1.2.

1.5.8 The Kellog reforming exchanger system (KRES)

LeBlanc (1991) patented a heat exchanger-type reforming reactor where the endothermic heat was supplied by the effluent gas from a separate autothermal reactor in which exothermic partial oxidation of hydrocarbons as well as hydrocarbon reforming took place. LeBlanc's design included a limited duty preheater. The KRES design replaces fuel burning on the outside of the reforming tubes by a limited duty preheater together with the heat generated from the exothermic partial oxidation reaction. The major accomplishments of this configuration are lower capital cost, improved energy efficiency and reduced NO_x and CO_2 emissions.

Among all the configurations that were mentioned earlier, fluidized bed membrane reforming (FBMR) is of special interest for this study. In a fluidized bed

membrane reactor, heterogeneous reactions take place in the fluidized bed of the reactor. The palladium membrane, owing to its permselective property, separates hydrogen as it is produced. The combination of fluidized bed and palladium membrane can be used for catalytic reactions that are limited by equilibrium. When one or more of the products are removed by a permselective membrane, the reaction equilibrium shifts towards the forward direction, i.e. towards more product formation.

Table 1.2: SMR vs. FBMR functional comparison

Function	SMR	FBMR
Feed Purification	ZnO Reactors	ZnO Reactors
Reformer Reactor	Packed Bed, Tubes	Fluidized Bed-Vessel
Effluent gas separation	Pressure Swing Adsorption	Membrane
Process Heating	Gas Fired Furnace	1. Sodium Heat Pipes 2. Sodium Vaporizer 3. Reheated Catalyst 4. Furnace 5. Direct O_2 input
Water Gas Shift	Co-Mo Fixed Bed Reactor	Not Required
Heat Recovery	Waste Heat Boiler Convection Steam Gen.	Waste Heat Boiler Steam Generators (Exchangers)
Product Permeation	Not present	Pd. Membranes

Therefore, using the permselectivity of the membrane, a given conversion can be achieved at a lower operating temperature or an enhancement in conversion can be achieved at a fixed temperature for a thermodynamically unfavorable reaction. FBMR has many advantages compared to the conventional SMR process and will be discussed in detail in Chapter 2. Table 1.2 gives a functional comparison between the two processes.

1.6 Membrane literature review

Palladium membranes have been studied extensively due to their unique ability to permeate hydrogen selectively. Titanium, tantalum and vanadium are capable of sorbing and easily permeating hydrogen, whereas silver is permeable only to oxygen. Bhave (1991) discusses the theory and concepts of membrane reactors in detail. Tsotsis et al. (1993) have classified a number of different configurations of membranes and reactors. Of importance to the current study is the fluidized bed membrane reactor designated as FBMR.

Two membrane properties are of utmost importance, the permeability or the ease of transport through the membrane, and the selectivity, a measure of membrane capability to separate gaseous components. For a given reaction in presence of a membrane, two important parameters are the ratio of the permeation rate to the reaction rate, and the separation factor for all reactants and products with respect to the fastest permeating component, which is generally one of the products of the reaction. When a component's permeability is small, either a large membrane surface area or a high sweep gas flow rate can be used to increase the permeation rate.

Much of the early pioneering work on membranes of pure palladium and rhuthenium and their alloys was performed by V. M. Gryaznov and co-workers who studied hydrogenation and dehydrogenation reactions while testing a number of reactor designs containing flat foil, thin walled tube, and double spiral membranes. Continuous addition or removal of hydrogen has been shown to increase the reaction yield and selectivity. For the hydrogenation of benzene to cyclohexane, Gryaznov et al. (1977) reported an increase in equilibrium conversion from 0.1% to 4% at 390 °C. Other reaction studies (Gryaznov et al., 1973a, 1977, 1979b) examine the hydrogenation of: cyclopentadiene to cyclopentene, napthalene to tetralin, furan to tetrahydrofuran, furfural to furfuryl alcohol and nitrobenzene to aniline. In all of these reactions high selectivities were obtained. The reactor used for all these reactions consisted of two chambers, which were separated by a flat metallic membrane.

Mischenko et al. (1981) described a process for the production of aniline by the catalytic hydrogenation of nitrobenzene using a 92-97% Pd and 3-8% Ru hydrogen permselective membrane. At 170 °C, the nitrobenzene vapor apparently reacted with active atomic hydrogen on the membrane surface. Mischenko et al. claimed that participation of atomic hydrogen provided a 100-fold increase in the productivity.

Ermilova et al. (1985) demonstrated the hydrogenation of 1,3- and 1,5-cyclooctadiene and cyclooctatetraene with a 0.1 mm thick Pd-Ru (90.2:9.8) foil. The controlled diffusion of hydrogen helped to achieve high yields and selectivities.

Nagamoto and Inoue (1985) studied hydrogenation reactions of several olefins and found that reaction rates for palladium membrane reactors can be more than 10 times greater than in conventional reactors.

The dehydrogenation of hydrocarbons is normally carried out at very high temperatures, yet obtains only low yields. If hydrogen is removed continuously from the product using a selective membrane, equilibrium can be shifted in favor of greater yields of hydrogen. Palladium membranes have been used for dehydrogenation reactions since the 1960's. Pfefferie (1966) patented a process for the dehydrogenation of ethane to ethylene using palladium-silver alloy membranes. Smirnov et al. (1977) studied dehydrogenation and dehydrocyclization reactions of alkanes to olefins using Pd-W-Ru (94:5:1) membranes. They reported higher yields at lower temperatures. Mikahlenko et al. (1986) studied the dehydrogenation of isopropanol over a Pd-Ni (94.1:5.9) alloy membrane at 702 °C. They found that the conversion of isopropanol increased with the ratio of hydrogen partial pressure to isopropanol; a maximum conversion of 83% was achieved. Itoh (1987) studied the dehydrogenation of cyclohexane to benzene using 200 micron thick palladium membranes containing 0.5% (w/w) Pt/Al_2O_3. The palladium tubes were packed with catalyst, the reaction took place in the catalyst bed, and hydrogen permeated through the membrane walls into the shell side. Argon was used as sweep gas in the shell side to remove the hydrogen permeating the membrane tubes. At 746 °C, 1 atm pressure and using an argon purge, an essentially complete conversion (99.5%) of cyclohexane was achieved with an equilibrium value of 18.7%.

Clayson and Howard (1987) used a 0.1 mm Pd-Ag (76:24) alloy membrane at 550 °C for the dehydrocyclodimerization of propane to aromatics. The reactant side of the reactor was filled with activated zeolite catalyst and argon was used as sweep gas in the permeate side. Clayson and Howard obtained 87% conversion of propane with 64%

selectivity to aromatics. Using the same conditions but without the membrane, they obtained 89% conversion with 53% selectivity. Nazarkina and Kirichenko (1979) studied the steam reforming of methane using palladium alloy membranes. Uemiya et al. (1991c) carried out steam reforming of methane in a packed bed reactor incorporating a hydrogen-permeable membrane, which consisted of a thin palladium film supported on a porous glass cylinder. Both studies have been described earlier in this chapter. Kikuchi et al. (1989) performed experiments for the water-gas shift reaction with the use of dense palladium membranes and complete conversion was achieved.

In membrane reactor studies, palladium alloys have been preferred over pure palladium membranes for two reasons. First, pure palladium is susceptible to hydrogen embrittlement after it undergoes repeated cycles of hydrogen adsorption and desorption. Second, catalytic activity and hydrogen permeability of some of the palladium alloys are higher than those of pure palladium. Gryaznov et al. (1983) examined different alloys and found that the metals of the Group VI to VII (e.g. Ru, Rh, Ni, Cu, Ag) form preferred binary alloys with palladium. The optimum composition of the metal other than palladium usually ranges from 2% to 15% of the alloy.

Konno et al. (1988) prepared a composite membrane tube by impregnating a porous alumina film with palladium formed from an aqueous solution of $[Pd(NH_3)_4]Cl_2$. At 300 °C, they obtained a hydrogen selectivity of 100 relative to nitrogen.

Uemiya et al. (1991a) manufactured a composite membrane consisting of a 13 μm palladium film on a porous glass tube. The permeation rate was higher than previously obtained with commercially available palladium-silver alloy membranes. Selectivity studies using a mixture of nitrogen and hydrogen showed that the membrane was only

permeable to hydrogen in the temperature range of 400-500 °C, while nitrogen permeated at temperatures below 300 °C. Uemiya et al. (1991b) coated a palladium-silver alloy of 4.5-6.4 μm thickness on the outer surface of a porous alumina tube by an electroless plating method. They obtained infinite hydrogen selectivity at temperatures above 200 °C. The rate of permeation was measured up to a temperature of 527 °C. They reported that the hydrogen permeation rate through the supported membrane (5.8 μm coating thickness) was 77.2 $cm^3(STP).cm^{-2}.min^{-1}$ at 500 °C, whereas the permeation rate of a commercial palladium-silver alloy membrane under identical conditions was 2.3 $cm^3(STP).cm^{-2}.min^{-1}$.

Li et al. (1993) prepared a Pd-Ag alloy coated (coating 1.5-2 μm thick) composite membrane by spray pyrolysis of a palladium and silver nitrate solution on a porous alumina hollow fiber support. They obtained higher permeation rates, but the separation factor for hydrogen with respect to nitrogen was only 24 at 500 °C. Although this separation factor is much higher than that of pure alumina membranes, it falls far below the accepted separation factor of infinity for Pd-Ag alloy membranes. Another negative feature is that, the membrane was easily abradable.

Collins and Way (1993) deposited palladium films of thickness ranging from 11.4-20 μm on the inside surface of asymmetric tubular ceramic membranes by an electroless deposition method. The permeability experiments were conducted with hydrogen, nitrogen and helium at temperatures from 450 °C to 640 °C and feed pressures from 160 to 2445 kPa. They reported a hydrogen permeability of 3.23 X 10^{-9} $mol.m/(m^2.s.Pa^{0.602})$ at 550 °C for the 11.4 μm coated membrane tube. The separation

factor for hydrogen with respect to nitrogen was 380 at 550 °C and at a differential pressure of 1500 kPa.

Yan et al. (1994) formed a very thin palladium film in the macropores of an α-alumina support tube by metal-organic chemical vapor deposition. The permeabilities were high (equivalent to those of the membranes demonstrated by Uemiya et al. (1991a,b), and the separation factor between hydrogen and nitrogen was higher than 1000 at permeation temperatures of 100-300 °C. They performed experiments at up to 500 °C and claimed that, even at high temperatures the membranes were resistant to abrasion. A microporous membrane was prepared by coating a metal (Pd, Ru, Rh, Pt, Co, Fe or Cu) on a porous alumina substrate using the sol-gel method (Chai et al., 1994). Permeabilities and separation factors were measured up to 400 °C, and values exceeded those expected from Knudsen diffusion. However, the separation factor was too low (2.5 - 6) compared with the separation factor expected for a metal membrane. Lee et al. (1994) prepared a palladium impregnated γ-alumina membrane using a sol-gel technique. Direct impregnation of palladium was achieved by mixing the alumina sol with a palladium precursor. Dispersion of the palladium particles was performed by sonication. Their highest temperature for permeation experiments was 477 °C. They enhanced the selectivities of hydrogen relative to both carbon dioxide and nitrogen up to 8.1 and 9.9, respectively, which are low.

Athayde et al. (1994) of Membrane Technology and Research, Inc. prepared ultrathin metal composite membranes using sputter deposition of a palladium-silver (76:24 atomic ratio) alloy layer onto a conventional polymeric gas separation membrane.

The thickness of the metal layer was 250-1000 A°. The permeation rate of hydrogen at 25 °C was 10^{-5} cm^3(STP)/ (cm^2.s.cmHg) and a hydrogen/carbon dioxide selectivity greater than 100 was reported. Even the best commercial polymeric membranes have a hydrogen/carbon dioxide selectivity of up to only 6.

1.7 Mechanism of hydrogen permeation

Hydrogen permeates through dense metallic membranes by a "solution-diffusion" mechanism. When a permselective metal separates two regions containing hydrogen at high and low partial pressures, P_{H2h} and P_{H2l}, respectively, hydrogen will be adsorbed on the metal surface on the high pressure side and then diffuse to the low pressure side where it will be desorbed into the gas phase.

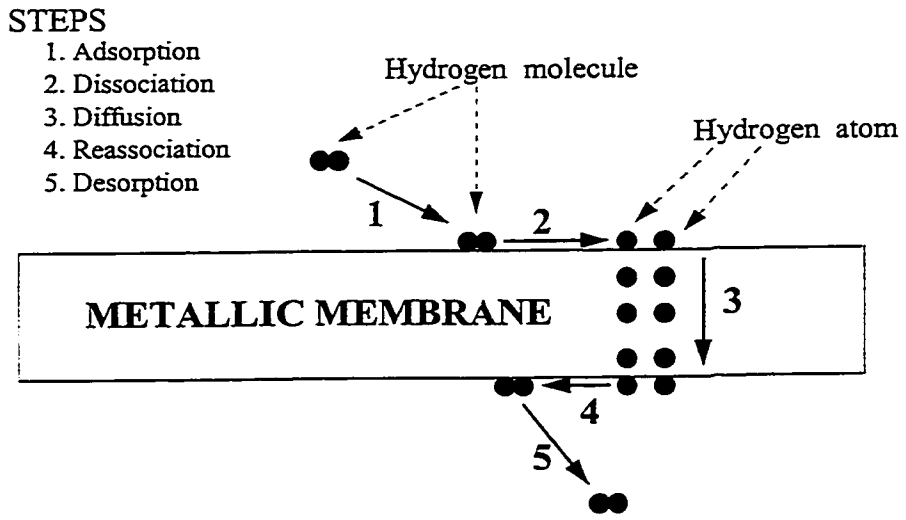

Figure 1.3: Hydrogen permeation mechanism through a metal membrane

Figure 1.3 illustrates the mechanism of permeation of hydrogen through a metal membrane. The basic processes essential for permeation of hydrogen to occur are (Barrer, 1951):

1) adsorption of hydrogen molecules onto the surface of the metal from the gas phase at the high pressure side;

2) dissociation of hydrogen molecules into atoms on the surface and dissolution of surface atomic hydrogen in the bulk layers of the metal;

3) diffusion or transport of atoms through the metal due to concentration gradient;

4) passage out of atoms from the solution of the surface layers and their recombination to molecules on the surface of the low pressure side.

5) desorption of hydrogen molecules from the surface to the gas phase.

In some cases, dissociation occurs simultaneously with adsorption with no identifiable molecular phase on the surface; this process, "direct dissociative chemisorption", is believed to provide hydrogen transport through many transition metal surfaces, including Pd, Nb and Ni (LeClaire, 1983). Only hydrogen is transported through the membrane by this mechanism (Athayde et al., 1994) providing infinite selectivity. The term permeation is used to describe the overall transport of molecular hydrogen across the membrane, whereas the term diffusion refers only to the movement of hydrogen atoms inside the metal. Hydrogen is readily adsorbed onto palladium, and the resultant diffusion of atomic hydrogen through the palladium lattice is a rapid process. Pure palladium can absorb 600 times its volume of hydrogen at room temperature (Partington, 1954).

Figure 1.4 shows the phase behavior of the hydrogen/ palladium system. The system exhibits two-phase behavior below a critical temperature of 300 °C and a critical pressure of 20 atm. For example, at 30 °C temperature and ~18 mmHg pressure, the atomic hydrogen to palladium (H/Pd) ratio is 0.03 for the hydrogen-deficient α phase and 0.57 for the hydrogen-rich β phase (Hunter, 1963). Due to the expansion and contraction of the metal lattice as hydrogen is adsorbed and released, palladium membranes are subject to mechanical failure (hydrogen embrittlement) below the critical temperature.

Discontinuous lattice expansion occurs due to the phase transformation from α to β hydride, since β-phase hydride has a considerably expanded lattice compared to α-phase palladium hydride. Hunter (1963) reported that the dimensions of the unit cell in the palladium lattice expand from 3.89 to 3.96 A° upon saturation with hydrogen.

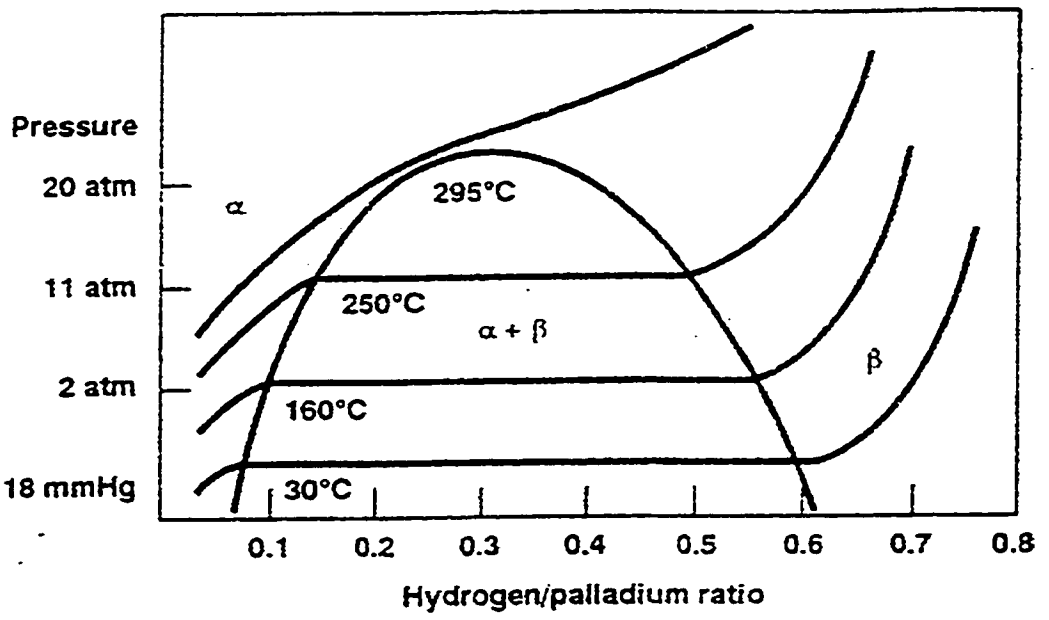

Figure 1.4: Absorption relationship of the palladium-hydrogen system (Athayde et al., 1994)

1.8 Palladium coated metal or metal alloy membranes

From a theoretical point of view, there are several common metals such as niobium, tantalum, zirconium and vanadium which are more permeable to hydrogen than palladium, the usual metal employed for hydrogen purification and extraction (Figure 1.5). As these metals are much stronger than palladium, even thin walled membranes of these materials could provide the necessary thermal and mechanical strength. As flux is inversely proportional to membrane thickness, it is possible that thin walled membranes of these metals could have fluxes that are in orders of magnitude greater than that of palladium alone. At high temperatures, these metals are impermeable to all gases except hydrogen, therefore the hydrogen purity will still be 100%. However, these metals are not used for hydrogen separation because the experimentally obtained fluxes have been far below the predicted values. In the case of pure uncoated refractory metals, surface resistances slow hydrogen entry and exit from the metal.

Several techniques have been used to reduce the surface resistance of these metals. The most widely used techniques are annealing in high vacuum, and using ion bombardment. The transport fluxes obtained experimentally for metals treated through these processes are less than those predicted, indicating that a surface resistance is either inherent in these metals, or may be caused by a very tightly held oxide film which impedes absorption (Brown and Buxbaum, 1988). If there was no surface resistance, these refractory metals could be used for hydrogen separation with high permeability and at a considerably lower price than with palladium or its alloys (Markides et al., 1967). The surface resistance of these metals can be reduced if a very thin layer of palladium is coated on to their surface. In the resultant type of composite membrane, the palladium

coat serves two purposes: it catalyzes the molecular hydrogen dissociation and recombination reactions on the surface, and it decreases the transport barrier for hydrogen atom absorption into the refractory metal (Sawatzki and Ledoux, 1977). In addition, the palladium layer protects the refractory metal from oxidation. The palladium coated metal alloy membrane literature has been referred to in detail in Chapter 3.

The High-flux membranes (palladium coated niobium-tantalum alloy tubular membranes) used for this study were manufactured by REB Research and Consulting (Ferndale, Michigan, USA).

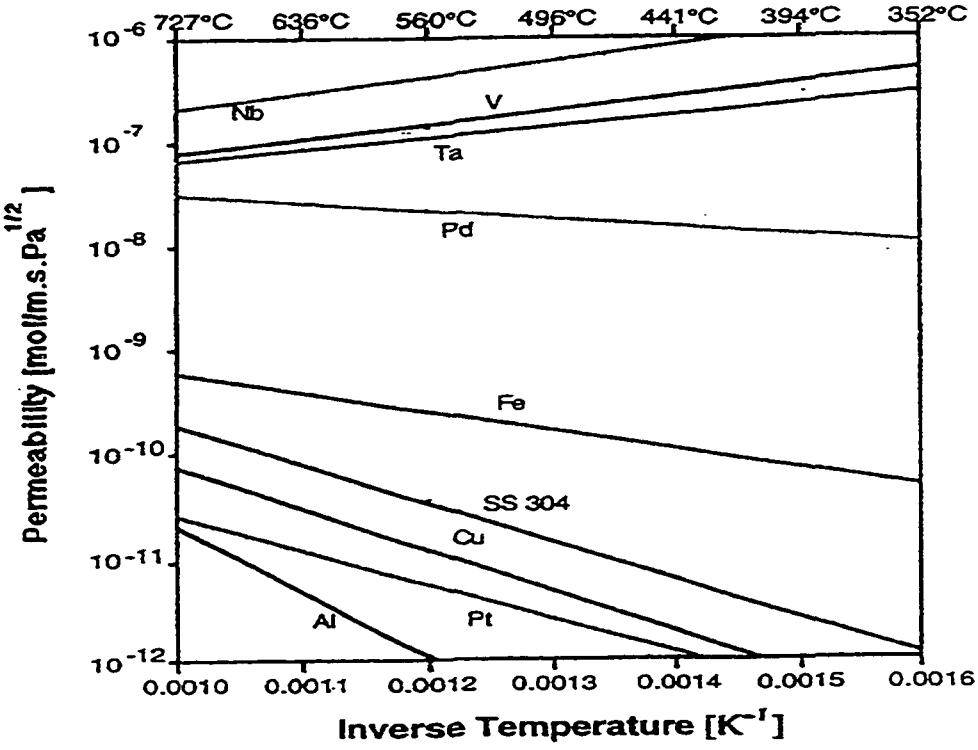

Figure 1.5: Hydrogen permeabilities for some metals (Buxbaum and Kinney, 1996)

The permeability of palladium increases with higher temperatures; the relationship is an Arrhenius type with an activation energy of 20.5 kJ/mol (Katsuta et al., 1979). In a contrary relationship, the permeability of niobium and tantalum decrease with increasing temperature in an Arrhenius manner (Figure 1.5). This is due to hydrogen absorption in these metals which is more exothermic than the endothermic activation energy for diffusion.

Tubular membranes have been selected for this study because the tubular geometry is the most suitable for a fluidized bed membrane reactor. Tubular membranes are also useful for other applications. For example, they can easily be fabricated into large scale hydrogen extractors using a shell and tube heat-exchanger design. Another advantage of using tubular membranes is that they can be constructed with a thin wall for a given pressure differential, thus allowing higher hydrogen fluxes. A schematic diagram of a High-flux membrane tube is shown in Figure 1.6.

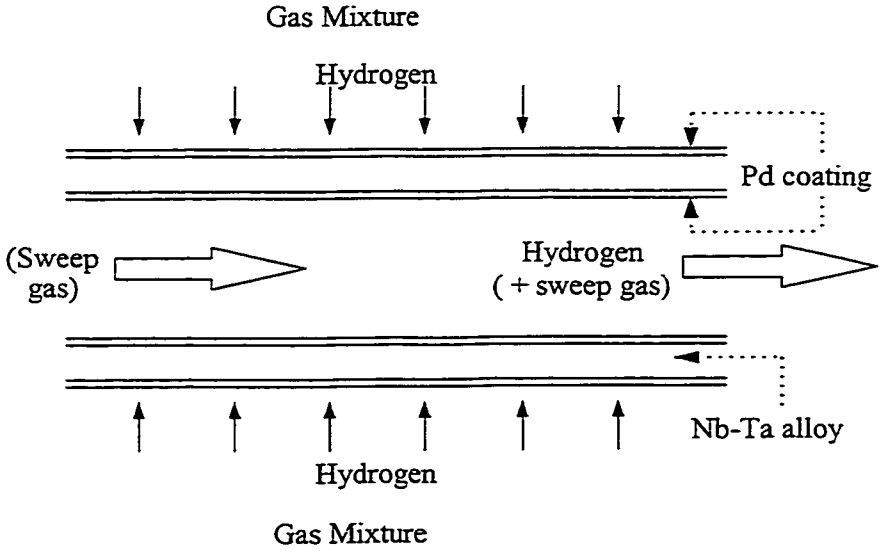

Figure 1.6: Section of a High-flux membrane tube

1.8.1 Method used for coating palladium

Palladium can be deposited on any refractory metal by various methods (Shu et al., 1991). Each method has its advantages and disadvantages and any choice is necessarily a compromise. The most important techniques currently used for this kind of deposition are conventional cold rolling, thermal evaporation, chemical vapor deposition, electroplating and electroless plating (Chopra, 1969; Lee, 1978; Hsieh, 1989). Electroless plating was used for coating the composite membrane tubes in this study. A brief description of the coating method is given below.

In electroless plating, deposition takes place as a result of controlled autocatalyzed decomposition or reduction of a metastable salt complex(es) onto target substrates (Lowenhiem, 1974). The substrate is dipped into a solution containing a salt of the metal to be deposited. The metal salt reacts with a reducing agent in the solution and a thin, uniform metal film is deposited on the surface of the substrate.

To deposit palladium, salts like $PdCl_2$ or amine complexes such as $Pd(NH_3)_4(NO_2)_2$, $Pd(NH_3)_3Br_2$ or $Pd(NH_3)_4Cl_2$ are generally used in the presence of a reducing agent such as hydrazine (Uemiya et al., 1990), ammonium hydroxide, or sodium hypophosphite (Athavale and Totlani, 1989). In some cases, the substrate is preseeded with palladium nuclei to reduce the induction period of the autocatalytic plating reaction (Uemiya et al., 1990). Usually other inorganic and organic agents which act as stabilizers are added to the solution.

Prior to electroless plating, the substrate goes through several pretreatment and surface activation steps. Use of ultrasound, alkaline solution, deionized water, isopropyl

alcohol, or any other suitable reagent performs surface cleaning. Sometimes the surface of the substrate metal is roughened by emery cloth, steel wool or a steel brush to facilitate the deposition of the coated metal (Buxbaum and Hsu, 1992).

Electroless plating has the obvious advantage of being able to deposit a uniform film on complex shapes. For this reason large tubular membranes are easier to coat by electroless deposition than by any other technique. Palladium and some of its alloys are among the few metals that can be deposited on various substrates using this method. Possible decomposition in the bath, difficulties in controlling thickness, and entrainment of other reagents in the deposited film are the major pitfalls of this method. The thickness of the palladium film is calculated either gravimetrically - dividing the weight difference in the unplated and plated membranes by the plated surface area and the palladium density - or by taking a scanning electron microscope (SEM) micrograph of the film.

This technique has been widely used for the preparation of palladium-based membranes (Itoh et al., 1989; Kondrasheva et al., 1985; Uemiya et al., 1988; Kikuchi et al., 1989; Govind and Atnoor, 1991; Athavale and Totlani, 1989; Buxbaum and Marker, 1993; Buxbaum and Kinney, 1996).

1.9 Present investigation

The present investigation can be summarized in six different sections, each of which comprises a chapter in this thesis. The following paragraphs explain the objectives and achievements of each of these studies.

1.9.1 Economic study of FBMR

The objective of this study was to estimate capital, operating, and supply cost economics for fluidized bed membrane reforming and compare these economies to those of a conventional steam methane reforming plant. This study considers five configurations for providing the heat of reforming reaction. Supply cost economics were determined for the five separate cases in order to identify the most economic configuration compared to the conventional steam methane reforming process. The study also revealed the constraints faced by this process, particularly those that require further research. Hence the economic study also outlined the general direction of the balance of the present investigation.

1.9.2 Development of High-flux membrane module

The primary objective of the study was to develop a module containing tubular palladium coated metal alloy (High-flux) membranes. The writeup details the development of the High-flux membrane, its modifications, and the final design that was deemed suitable for our specific application. The module was primarily intended for use in a fluidized bed membrane reformer to separate hydrogen at high temperatures (up to 650^{o}C) and differential pressures (up to 1250 kPa). A U-tube spring reinforced High-flux membrane module was also developed for this specified application.

1.9.3 FBMR with High-flux membranes

The objective of this investigation was to utilize the U-tube spring reinforced High-flux membrane module in a fluidized bed membrane reforming reactor and prove its

viability. The chapter analyzes the results obtained from the FBMR (High-flux membranes) experimentation. Pressure, temperature, steam-methane ratio, superficial gas velocity, sweep gas flowrate, and membrane pressure were varied, and the methane conversion, hydrogen yield, and hydrogen recovery were evaluated. The study compared the results obtained from this investigation to those of previous investigations and also to the equilibrium values. It proved conclusively the viability of the application of the High-flux membranes in the FBMR.

1.9.4 Fluidized bed steam methane reforming with oxygen input

The objective of this experimental study was to investigate the addition of oxygen directly to a fluidized bed reformer to provide the heat of the reforming reaction. The aim was to add sufficient oxygen to attain autothermal conditions at the desired process conditions. Pressure, temperature, steam-methane ratio and oxygen flowrate were varied, and the methane conversion and hydrogen yields evaluated. The experimental results of these runs were compared with the respective equilibrium compositions evaluated from a Gibbs free energy minimization method. Autothermal conditions were obtained for most experimental runs.

1.9.5 FBMR with High-flux membranes and oxygen input

The objective of this investigation was to develop an autothermal fluidized bed membrane reformer. This system could sustain steam methane reforming by itself and simultaneously produce pure hydrogen from a single modular unit. Pressure, temperature, steam-methane ratio, superficial gas velocity, sweep gas flowrate, oxygen

flowrate, and membrane pressure were varied, and the methane conversion, hydrogen yield, and hydrogen recovery were evaluated. The experimental results from these runs were compared to the values obtained in a FBMR without oxygen input and were also compared to the equilibrium results. Experimentation performed in the pilot scale unit validated this new concept.

1.9.6 Computer simulation of FBMR

The primary objective of this study was to develop a comprehensive computer model to simulate the FBMR (High-flux membranes) with or without oxygen input. The simulation work is based on a two-phase bubbling bed reactor model with the membrane considered as a separate side selectively separating hydrogen from the reacting gas mixture. Reaction on the entrained catalyst in the freeboard region has been included in this model. The experimental results obtained from the present investigations were used to validate the computer model.

Chapter 2

Economics of Fluidized Bed Membrane Reforming

2.1 Objective

The objective of this study was to estimate capital, operating, and supply-cost economics for fluidized bed membrane reforming (FBMR) and to compare these to conventional steam methane reforming (SMR) plant. This study considers four configurations for providing the heat of reaction. A fifth alternative similar to the furnace reactors configuration using High-flux membranes is also considered. The supply cost economics were determined for the five separate cases in order to identify the most economic configuration compared to the conventional steam methane reforming process.

2.2 Introduction

Steam reforming of natural gas is an important chemical process for manufacturing hydrogen or syngas required for ammonia and methanol production, hydrocracking and hydrotreating, oxo-alcohol and Fisher-Tropsch synthesis as well as many other essential processes in the petroleum and petrochemical industries (Rosturp-Nielsen; 1983, Wagner and Froment 1992). More stringent environmental regulations are increasing the demand to use hydrogen in refineries to produce fuels with lower sulphur and aromatics content. Hydrogen is considered by many to be the fuel of the future, as it

burns cleanly to form only water. Conventional steam methane reforming (SMR) is a well-established process that has been highly optimized over the years.

In an attempt to determine a process with improved performance over conventional SMR, the economics of the fluidized bed membrane reforming (FBMR) process have been evaluated. The FBMR process modifies the conventional SMR in four major areas by:

1. Changing the reactor's operation from a fixed bed to a fluidized bed
2. Changing the heat supply from external firing to direct heating
3. Separating of hydrogen using membrane technology to drive the reaction beyond the normal thermodynamic equilibrium for the stated temperature pressure and steam/methane feed rates.
4. Using High-flux palladium coated niobium/tantalum membranes.

Adris (1992, 1994) summarized the attempts and investigations by others to improve the SMR process as reported in Chapter 1. Adris, Elnashaie and Hughes (1991) developed a two-phase model to explore a fluidized bed reactor equipped with a bundle of membrane tubes which would remove the hydrogen from the reacting gas mixture and drive the reaction beyond its thermodynamic equilibrium. Steam methane reforming (SMR) is the most common process for the manufacture of hydrogen. The process is highly endothermic, utilizing a reformer furnace with hundreds of parallel catalyst-filled tubes. Heat of reaction is supplied by radiant natural gas burners positioned in a top-firing, bottom-firing or side-firing configuration. The process feed, containing natural gas and superheated steam, is passed through the bank of furnace tubes over a fixed bed of nickel reforming catalyst to form a mixture of hydrogen and carbon monoxide. The

reformer stage is followed by a water gas shift and final purification, typically via a pressure swing adsorption (PSA) unit to produce up to 99.8% pure hydrogen (Balthasar, 1984).

The process is limited by the equilibrium of reforming reactions, as discussed in Chapter 1. The Equations 1.1, 1.2 & 1.3 (Chapter 1) are sufficient to describe the catalytic reforming process. The state of thermodynamic equilibrium is dependent on temperature, pressure and the steam-to-carbon molar ratio. The reforming reaction is strongly endothermic and high temperature and low pressure favor the forward reaction. The rate of the reforming reactions is controlled by the kinetics of the reaction, the rate of mass transfer from the bulk gas to the surface of the catalyst, the diffusion rate through the pores of the catalyst. and the heat transfer through the walls of the high alloy reformer tubes.

The CO produced is further reacted to yield hydrogen via the water gas shift, and four moles of hydrogen can theoretically be produced from each mole of methane feed. Recent improvements in metallurgy have allowed significantly increased heat flux in new reformers, and new catalysts have been developed to optimize conversion in the PSA systems. PSA yields 99.9% pure hydrogen and returns unreacted methane to reformer fuel so that 98% conversion per pass is no longer required to obtain high purity hydrogen.

A conventional Steam Methane Reforming (SMR) process is made up of five sections as shown in Figure 2.1:

- feed desulphurization
- steam reforming
- water gas shift

- purification
- steam generation

Overall hydrogen yield which includes methane fuel is between 2.2 to 2.7 moles/mol of CH_4 fed, and typically about 2.5. Methane conversion is typically about 73% when PSA is used. The balance of the methane is burned as fuel in the reformer along with auxiliary methane.

The Fluidized Bed Membrane Reforming (FBMR) process is made up of five sections as shown in Figure 2.2:

- feed desulphurization
- steam reforming
- membrane separation
- compression
- steam generation

Traces of sulfur in the form of H_2S are removed prior to processing, as sulfur will poison reforming catalysts. The reforming unit is gas fired with internal membrane separation. Hydrogen permeates through the palladium membranes placed in the reformer and hydrogen permeate gas is cooled by a waste heat boiler and heat exchangers before being compressed.

In the reforming section, provision for the heat of reaction was found to be the most difficult part of the process design. This study considers four configurations for providing this heat of reaction. A fifth alternative similar to the furnace reactors configuration but using High-flux membranes has also been considered.

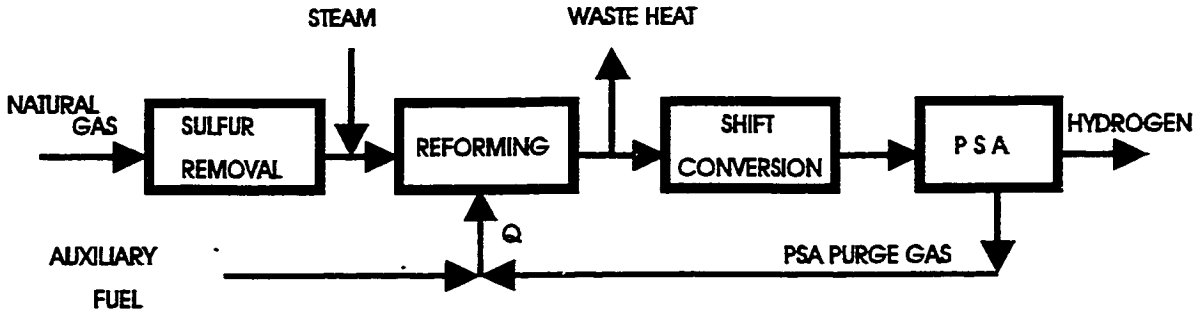

Figure 2.1: Schematic of steam methane reforming

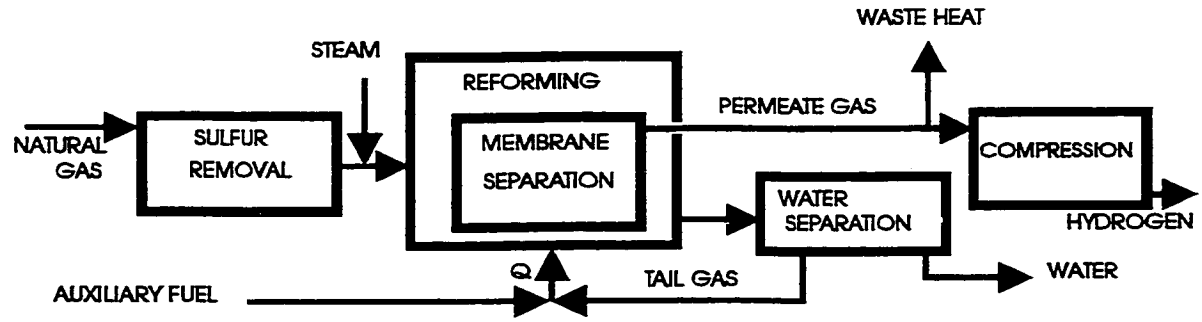

Figure 2.2: Shematic of fluidized bed membrane reforming

2.2.1 Reactor design configurations

Five alternative reformer design configurations were studied for the FBMR process. The primary difference between Configurations 1-4 was in the method of heat transfer. Configurations 1-4 used thin-walled palladium membranes while Configuration 5 used a membrane made of niobium/tantalum alloy tubes coated with a few micron thick palladium layer (High-flux membranes).

Configuration 1: Sodium Heat Pipes. This is shown schematically in Figure 2.3. The reformer is a fluidized bed reactor with a thermal liquid heating system using sodium heat pipes to supply the heat of reaction into the fluidized bed. Individual vertical sodium heat pipes are externally heated in a furnace under the reactor. The sodium is vaporized and rises in each of the hermetically sealed heat transfer pipes up into the reactor (Richardson, 1988). As the sodium condenses, the latent heat of vaporization is transferred through the walls of the heat pipes into the fluidized bed of catalyst. Liquid sodium falls down the inside walls of the pipes to the furnace where it is again vaporized and superheated to 1173 K. The furnace is fueled by purge gas and auxiliary natural gas.

Configuration 2: Sodium Heat Tubes/Vaporizer. This is shown schematically in Figure 2.4. The reformer is a fluidized bed reactor with an internal sodium heat pipe tube bundle integrated with a composite metal membrane. The sodium is vaporized externally in a separate 'Dowtherm' type furnace/boiler. The sodium vapour rises to the horizontal tube bundle inside the reactor where it condenses releasing heat. The liquid sodium leaving the tube bundle returns through gravitational force to the condensate drum where it is again vaporized by radiant and convective heat from the furnace. The furnace is fueled by purge gas and auxiliary natural gas.

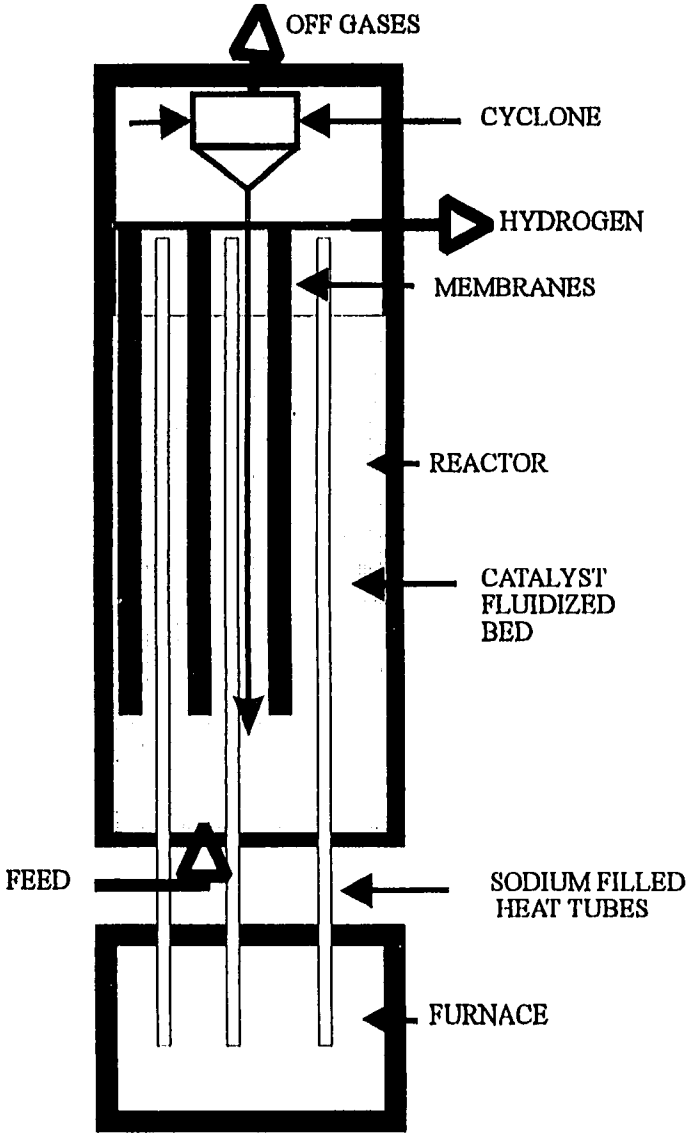

Figure 2.3: Sodium heat pipes / furnace heater

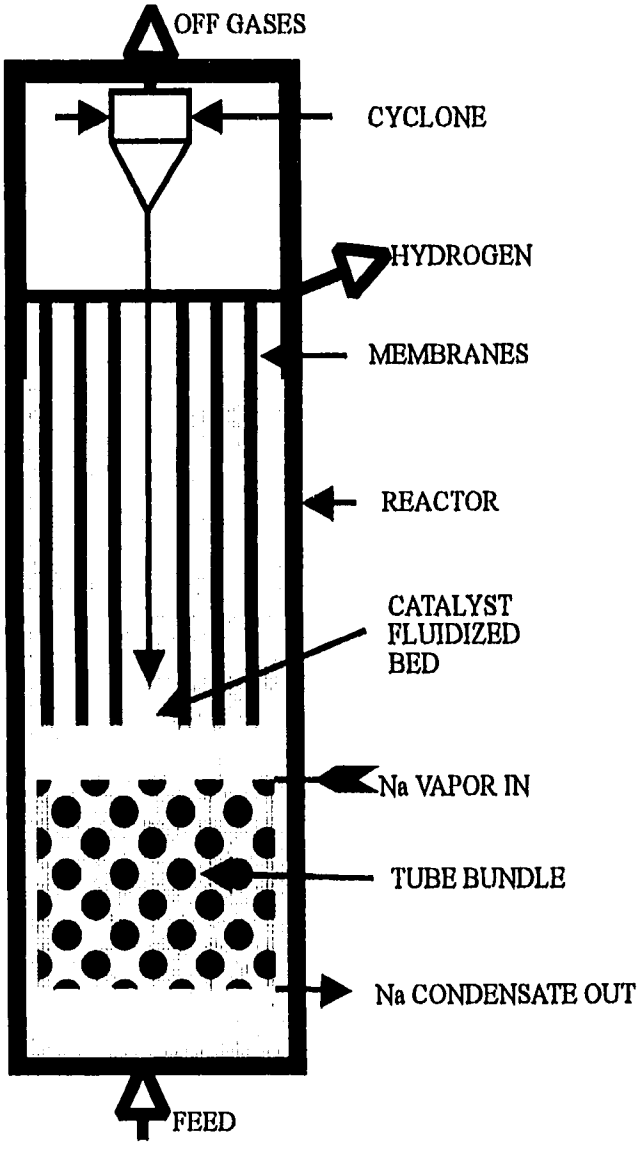

Figure 2.4: Sodium heat tubes/dowtherm vaporizer

Configuration 3: Two Bed Circulating Catalyst. This is shown schematically in Figure 2.5. The reformer is a two bed system similar to a fluidized catalytic cracker reactor/regenerator. The catalyst is reheated in the 'Regenerator' and recirculated to the reactor through a hydraulic solids transport system to provide the heat of reaction. The metal membrane unit is placed inside the reactor to remove hydrogen. The catalyst is reheated to 1273 K in the regenerator by burning natural gas and purge gas. Energy from the flue gas leaving the regenerator is recovered in a waste heat boiler to generate steam and preheat the feed gas. The flue gas is released to the atmosphere through a separate stack. Cyclones in each vessel remove catalyst particulates from the reactor effluent and flue gas.

Configuration 4: Multiple Reactors. In Configuration 4, shown schematically in Figure 2.6, the reformer consists of multiple reactors inside a furnace. Each reactor has its own membrane unit and external cyclone. Heat of reaction is supplied by radiant and convective heat from the gas fired reformer furnace. Packed bed tubes (about 60 in this size of reformer) common in conventional steam methane reformer furnaces are replaced by twelve separate fluidized bed reactors. Each of the fluidized bed reactors is about 900 mm in diameter by 7 m long compared to 125 mm by 12 m tubes in the conventional reformer. The reactor vessels are made of HK40 high alloy chromium steel, cast to withstand the high radiant temperatures. The inside of each reactor is operated at 1073 K by controlling the feed rate. Each reactor has its own membrane module to separate product hydrogen. External cyclones located on top of each reactor remove entrained catalyst particulate from the retentate gases.

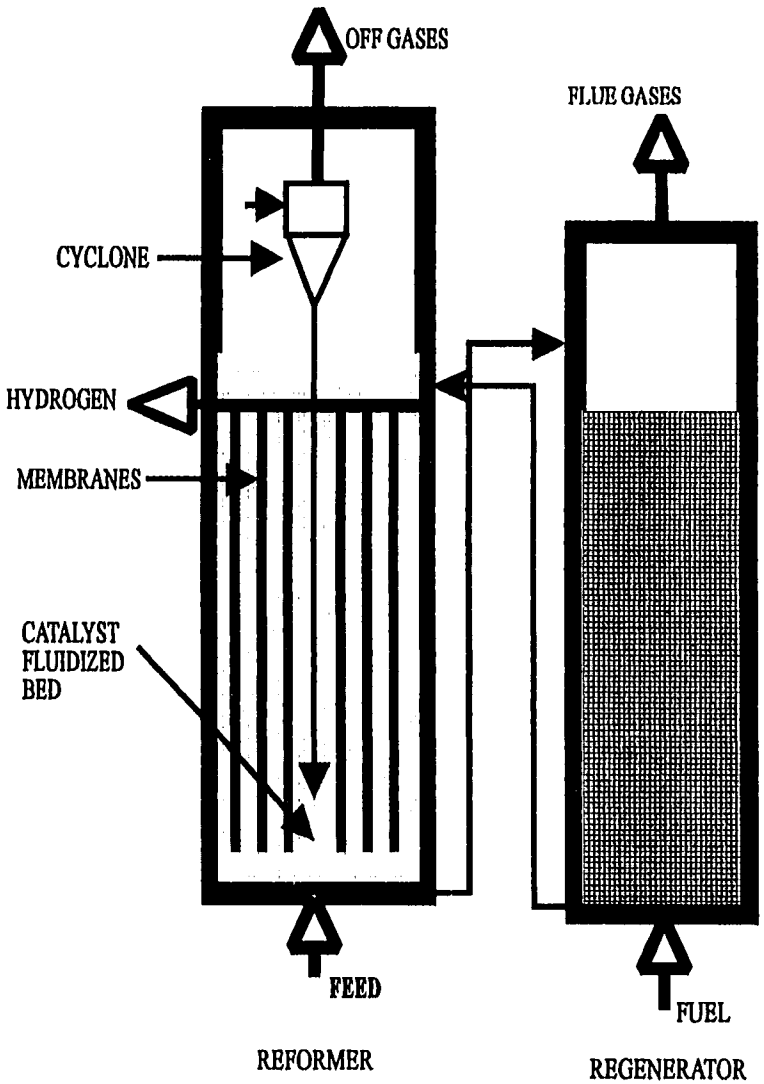

Figure 2.5: Two bed circulating catalyst

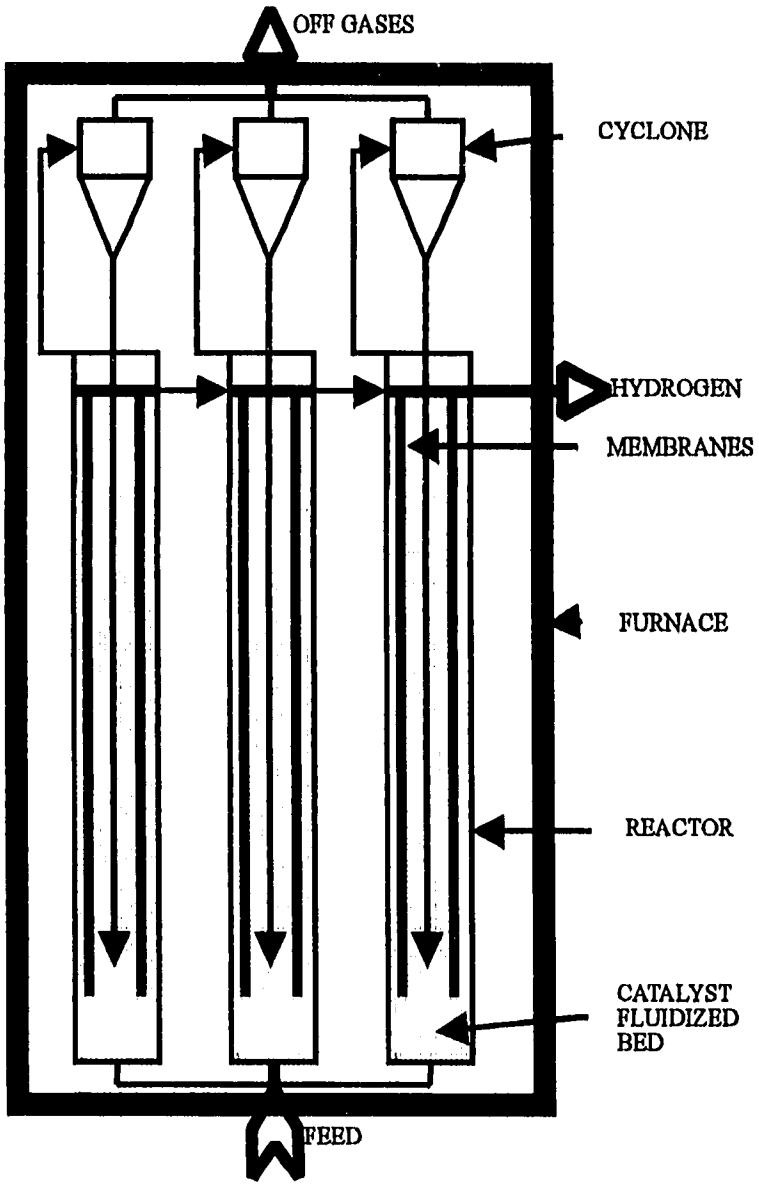

Figure 2.6: Multiple furnace reactors

Configuration 5: Multiple Reactors with High-flux Membranes. This configuration is similar to that in Configuration 4 except that it has High-flux membranes (Buxbaum, 1996). The reactor is operated at 948 K, a considerably lower temperature than is used in the other configurations.

2.3 Computer simulation

2.3.1 Model assumptions

A mathematical model was developed to simulate the reforming reactions in the fluidized bed. The simulation consists of a bubbling bed model with some gas flow in the dense phase. Reaction in the freeboard region (the region between the fluidized bed surface and the reactor exit) has also been considered. Model validation has been performed against experimental reaction data. The model is based on the following assumptions:

1) Steady state operation.

2) Dense catalyst bed consists of a bubble phase and dense phase.

3) No axial dispersion of gas in either phases.

4) Reaction mostly occurs in the dense phase with some reaction in the bubble phase on the surface of entrained solids.

5) The internal diffusional resistance of the catalyst particles is negligible.

6) The membrane permeates hydrogen from both the dense phase and the bubble phase.

7) Permeating gases are in plug flow.

8) The membrane permeates hydrogen only.

9) Gases are in plug flow in the freeboard region and react on the entrained catalyst particles.

10) The solids concentration in the freeboard region decreases exponentially with height.

2.3.2 Reaction kinetics

A large number of kinetic rate expressions for the steam reforming of methane are reported in the literature (Akers and Camp, 1955; De Deken et al., 1982). Most of the rate equations are either empirically based power law kinetics or are obtained by applying a large number of assumptions on a proposed mechanism. Although the rate equations are quite different from one another, most of them suggest that the rate of disappearance of methane is first order with respect to its concentration. Singh and Saraf (1979) and Rostrup-Nielsen (1984) have ascribed the observed differences among the various rate equations to the neglect of pore diffusional resistance. While the reaction is very fast, most studies have been carried out with large size catalyst pellets for which intraparticle resistance is very large. However, the interparticle mass transfer resistance is negligible in the high mass flow rate conditions existing in reformers (Singh and Saraf, 1979; De Deken et al., 1982). These facts make the rate equations obtained valid only for a certain range of reaction conditions. In addition, the rate equations led to certain discrepancies such as the disappearance of certain reactants and/or products from the rate equations. One of the most interesting contradictions noticed in these rate equations is the prediction of positive, as well as negative effective reaction orders with respect to steam.

Xu and Froment (1989) developed rate expressions based on the Langmuir-Hinshelwood-Hougen-Watson (LHHW) approach after correlating data over a wide range of operating conditions. This adsorption-surface reaction-desorption model considered a 13-step reaction scheme of which 3 were rate determining. The 13 steps represent 3 global reactions given by Equations 1.1, 1.2 and 1.3 of Chapter 1. Elnashaie et al. (1990) analyzed reforming rate expressions developed by different workers and concluded that the expressions developed by Xu and Froment (1989) are the most reliable and general in nature. Xu and Froment's (1989) expressions also resolved some of the contradictions among previous rate expressions. For example, they successfully explained the prediction of a positive, as well as, a negative order dependence of methane disappearance upon steam partial pressure. The functional forms of these expressions are:

$$R_3 = k_3\left(\frac{P_{CH_4}.P_{H_2O}}{(P_{H_2})^{2.5}} - \frac{(P_{H_2})^{0.5}.P_{CO}}{K_3}\right) / DEN^2 \qquad (2.1)$$

$$R_4 = k_4\left(\frac{P_{CO}.P_{H_2O}}{P_{H_2}} - \frac{P_{CO_2}}{K_4}\right) / DEN^2 \qquad (2.2)$$

$$R_5 = k_5\left(\frac{P_{CH_4}.(P_{H_2O})^2}{(P_{H_2})^{3.5}} - \frac{(P_{H_2})^{0.5}.P_{CO_2}}{K_3.K_4}\right) / DEN^2 \qquad (2.3)$$

$$DEN = 1 + K_{CO}P_{CO} + K_{H_2}P_{H_2} + K_{CH_4}P_{CH_4} + K_{H_2O}P_{H_2O} / P_{H_2} \qquad (2.4)$$

where R_3, R_4, ... are rate of reactions; k_3, k_4, ... are rate constants; K_{CO}, K_{H2}, ...are adsorption constants; K_3, K_4 are equilibrium constants; and P_{CH4}, P_{H2O}, ... are partial pressures.

All the rate constants (k_3, k_4 & k_5), adsorption constants (K_{CO}, K_{H2} etc.) and equilibrium constants (K_3, K_4) follow Arrhenius type temperature dependence. The pre-exponential factors and activation energies are given in Table 2.1.

Table 2.1: Rate expression parameters and equilibrium constants

Rate/ Adsorption constants	Pre-exponential factor	Activation energy/ Heat of adsorption kJ/mol
k_3	9.49×10^{15}	240.1
k_4	4.39×10^{6}	67.13
k_5	2.29×10^{15}	243.9
K_{CO}	8.23×10^{-5}	-70.65
K_{CH4}	6.65×10^{-4}	-38.28
K_{H2O}	1.77×10^{5}	88.68
K_{H2}	6.12×10^{-9}	-82.9
K_3	1.20×10^{13}	223.1
K_4	1.77×10^{-2}	-36.58

The disadvantage to the rate expressions described by the Equations 2.1 to 2.4 is that the partial pressure of hydrogen (P_{H2}) is in the denominator. Therefore, it is not possible to calculate the rates of the above reactions initially when there is no hydrogen in the feed (P_{H2}=0). To overcome this problem, a small amount of hydrogen was always considered to be present in the feed for the purpose of simulation. The addition of a small amount of hydrogen would have little impact on the overall performance of the reactor simulation.

If constant differential pressure is maintained across the membrane and isothermal conditions are assumed, the permeation rate can be approximated by a half power law (Bohmholdt, 1967):

$$N_{H2} = k_H [(P_{H2h})^{1/2} - (P_{H2l})^{1/2}] \quad (2.5)$$

where the permeation rate constant k_H is defined as :

$$k_H = (A_m / t) D_m C_o \quad (2.6)$$

The mass balance equations for each component are solved simultaneously. The flowchart of the solution algorithm program in Fortran 77 is shown in Figure 2.7.

2.4 Simulation results

Table 2.2 - Simulation results for Configurations 1-5

	Configurations 1-4	Configuration 5
Given plant capacity and reactor conditions		
Capacity of plant (kg of hydrogen/h)	2000	2000
Steam-methane ratio	2.5	2.5
Reactor bed temperature (K)	1073	948
Reactor pressure (kPa)	3000	3000
Permeate hydrogen pressure (kPa)	200	400
Simulation Results		
Reaction conversion of CH_4 (%)	85.4	80.0
Reaction conversion of steam (%)	61.0	61.0
Total percentage of hydrogen permeated	87.9	95.5
Total moles hydrogen/moles of methane	3.3	3.2

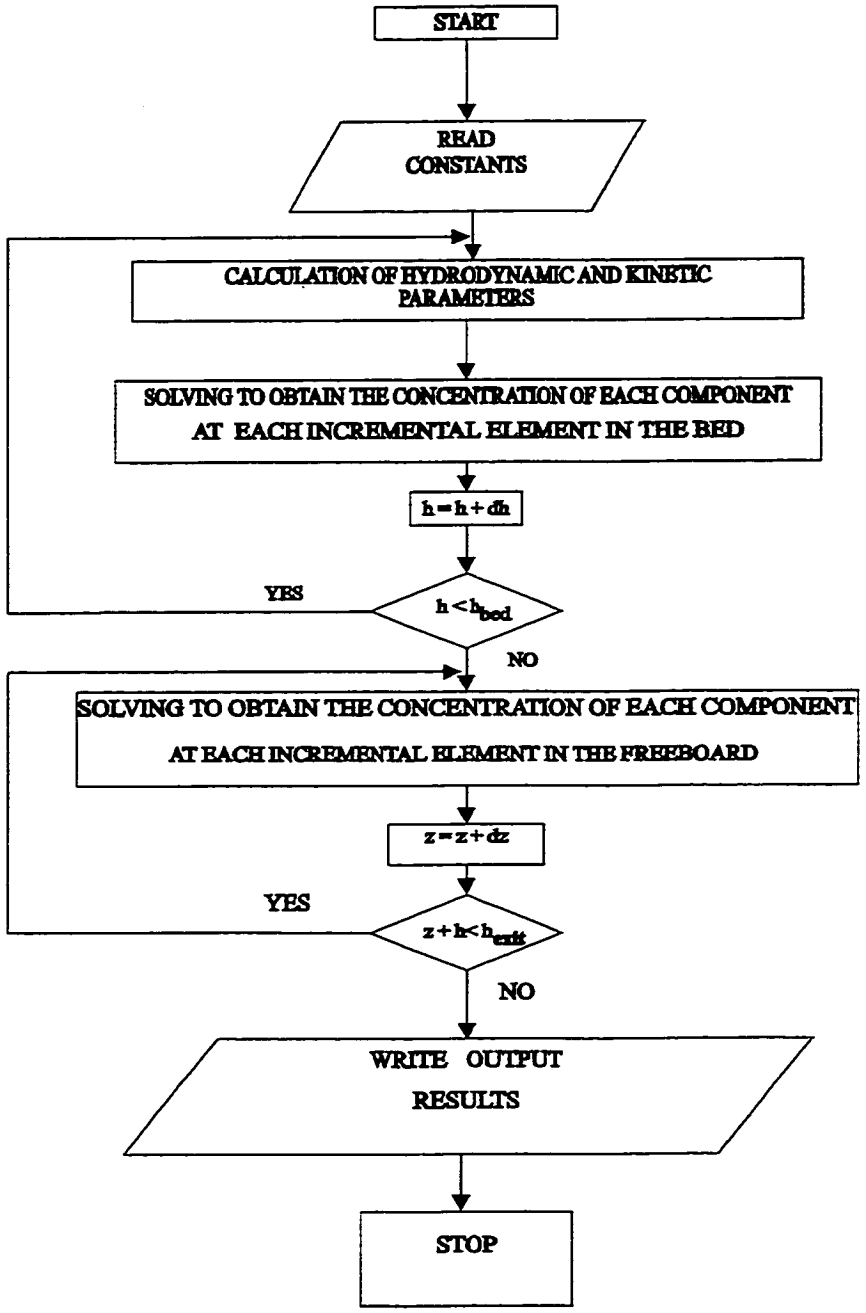

Figure 2.7: Flowchart for model solution algorithm

The plant capacity, reactor conditions and the simulation results for configurations 1-5 are given in the following Table 2.2. Configurations 1-4 utilize similar thin walled palladium membranes. Hence the same parameters have been used for input and reactor conditions. Also for these configurations, reactor size and membrane area were computed for identical conversion and hydrogen permeation respectively. Configuration 5 utilized High-flux membranes (Buxbaum, 1996) and parameters used for this simulation were adjusted to accommodate the higher permeation rate.

2.5 Capital and operating costs

Table 2.3 - Economics of FBMR vs SMR

	.....Configurations.....					
	1	2	3	4	5	SMR
CAPITAL (million [1997] $ Cdn) Installed @ Edmonton						
INITIAL	48.2	49.7	55.4	47.3	39.2	41.1
OPERATING COST (million [1997] $ Cdn/y) @ 95% SF						
NATURAL GAS	5.4	5.5	5.6	5.5	5.4	6.2
ALL OTHER NON-GAS	3.5	3.5	3.8	3.1	2.6	2.1
TOTAL OPERATING COSTS	8.9	9.0	9.4	8.6	8.0	8.3
SUPPLY COST ($ Cdn/ton) @ 10% DCFR (DEVELOPER)						
HYDROGEN	**863**	**881**	**943**	**837**	**748**	**779**

Direct material and labor costs were developed using historical industrial cost correlations. Costs were expressed in the second quarter 1997 constant Canadian dollars (Pruden et al., 1995; Roy et al. 1998) at an Edmonton location.

The indirect costs, engineering costs, contingency costs and a process development contingency were applied. Each configuration assumes a service factor (SF) of 95%. All process configurations were compared to the equivalent size SMR hydrogen plants using supply cost economics. The supply cost is the product price required for a developer to achieve a 10% Discounted Cash Flow Return (DCFR). An economic model was used to determine the supply cost given the capital, operating costs, taxation assumptions and annual production.

For example, hydrogen would require a price of $863/t to realize a 10% DCFR for Configuration 1. All costs are in 1997 Canadian dollars.

2.6 Results and discussion

The following key results were obtained during this study:

1. FBMR increases conversion.

Use of a fluidized bed membrane reactor increases conversion up to 35% more than the conventional SMR at comparable operating temperature and pressure if hydrogen can be removed efficiently. The operating temperature for the FBMR process is considerably lower than for the conventional SMR process. The furnace reactor High-flux membrane type configuration requires an operating temperature of 948 K compared to the conventional SMR process which requires about 1173 K at 3000 kPa.

2. Membranes eliminate PSA but require compression.

Use of highly selective membranes eliminates the need for a PSA unit to purify the product hydrogen, but produces low pressure hydrogen that must be compressed for distribution, storage and use in other processes.

3. Direct fired heating is more efficient than indirect heating.

The study focused on alternate methods of heat input. Use of indirect heat input methods such as a thermal heating system using liquid sodium or catalyst reheating to supply the heat of reaction is less efficient than direct fired heating in a furnace. Locating the reactor inside the furnace takes advantage of radiant heat transfer that is prevalent at these high temperatures and minimizes heat loss.

4. High-flux membranes reduce the capital cost:

The High-flux membrane which is made of a metal alloy coated with a few micron thick layer of palladium reduces the capital cost due to its high permeation rate; hence, lesser membrane material is required and the reformer is smaller in size.

5. FBMR is more economical than conventional SMR:

Four of the configurations studied were more expensive for the production of H_2 than SMR and one was less expensive. The supply cost of producing hydrogen for Configurations 1-4 was 7-20% higher than for a conventional SMR plant, capital costs were 15-35% higher than SMR; and operating costs were 4-14% higher than for SMR. However, Configuration 5 had a lower capital and operating cost than SMR and the supply cost of hydrogen is about 5% lower than SMR. FBMR produces ultra pure hydrogen as compared to the SMR process, there was no credit taken for the superior quality of product hydrogen.

6. Improved membranes are essential for improving FBMR process:

The FBMR process holds great promise for the future of hydrogen technology. However, future viability of the process is dependent on the feasibility of making a High-flux membrane that will operate at 923 K or above for long periods.

2.7 Conclusions

The study confirmed that fluidized bed membrane reforming has up to a 35% gain in conversion of methane over conventional technology at comparable operating temperature and pressure when hydrogen can be efficiently removed in the reactor. A scheme using direct fired fluidized bed reactors located in the radiant section of a reformer type furnace was the most efficient for heat transfer when compared to alternate configurations. The product hydrogen is ultra pure due to very high membrane selectivity. The configuration with High-flux membranes had a lower capital and operating cost than conventional SMR, thus demonstrating the promise of this new technology.

Chapter 3

Membrane Permeation and Abrasion

3.1 Objective

The primary objective of the study described in this chapter was to develop a module containing palladium coated metal alloy tubular membranes (High-flux). The module was primarily intended for use in a fluidized bed membrane reformer to separate hydrogen at high temperatures (up to 923 K) and differential pressures (up to 1.25 MPa).

3.2 Background

A membrane is a barrier, which is capable of redistributing components in a fluid stream utilizing a driving force such as a pressure, concentration, or electrical potential difference. Membranes are used extensively in separation processes to provide mass transfer in the desired direction.

One of the most promising applications of membranes occurs in membrane reactors as mentioned in Chapters 1 & 2 where product separation or purification takes place in conjunction with chemical reactions. Use of membranes is particularly important for reactions that are equilibrium limited, as significant enhancement of the equilibrium conversion can be achieved by selectively removing one or more reaction products through the membrane wall. At high temperatures, metal membranes are preferred; among all metals, palladium and its alloys are the most widely used due to their high

permeability, chemical compatibility with many hydrocarbon-containing gas streams, and infinite hydrogen selectivity. Some of the potential reactor applications of palladium based membranes include: steam reforming of methane, water gas shift and dehydrogenation of various compounds including hydrocarbons such as cyclohexane, ethylbenzene, ethane, propane and butane (Collins and Way, 1993) as explained in Chapter 1. Palladium based membranes can also be used for hydrogenation reactions in which a controlled addition of hydrogen increases the reaction yield and/or selectivity. However, the productivity of these membrane reactors is limited by the low permeability of the palladium membrane; a major challenge lies in developing a thin membrane which will be highly permeable and at the same time will be able to withstand high temperatures and differential pressures.

From a theoretical point of view, there are several common metals such as niobium, tantalum, zirconium and vanadium which are more permeable to hydrogen than palladium, the usual metal employed for hydrogen purification and extraction. As these metals are much stronger than palladium, even thin-walled membranes of these materials could provide the necessary thermal and mechanical strength. As flux is inversely proportional to membrane thickness, it is possible that thin-walled membranes of these metals could have fluxes that are orders of magnitude greater than that of palladium alone. However, these alternative metals are not used for hydrogen separation because the transport fluxes obtained for these metals are less than those predicted theoretically. Indicating that a surface resistance may be inherent in these metals, or a very tightly held oxide film may impede absorption (Brown and Buxbaum, 1988) as described in Chapter 1. The surface resistance of these metals can be reduced if a very thin layer of palladium

is coated onto the metal surface. In the resulting type of composite membrane, the palladium coat serves two purposes: it catalyzes the molecular hydrogen dissociation and recombination reactions on the surface, and it decreases the transport barrier for hydrogen atom absorption into the refractory metal (Sawatzki and Ledoux, 1977). In addition, the palladium layer protects the refractory metal from oxidation. For the above reasons, composite membranes were chosen for this study.

3.2.1 Composite palladium membrane literature

Markides et al. (1967) prepared the first palladium coated composite membrane by cleaning a niobium metal and then vapor depositing palladium onto it. Permeation experiments showed much greater hydrogen permeability with the niobium-palladium membrane than with pure palladium or palladium alloy membranes. The problem with the process of vapor deposition used to coat the niobium is that it cannot be used to coat the inside of a tube, so the surface resistance remained high on the inside. Palladium coated alloy membranes have been used continuously for over 10,000 hours in a nuclear reactor where they removed hydrogen from metal-cooled nuclear reactor fluids (Hill, 1982). Sawatzki and Ledoux (1977) reported a palladium-coated zirconium membrane that had been tested successfully for removing embrittling deuterium from CANDU reactor bundles. Amano et al. (1991) demonstrated a membrane prepared by plating palladium on a vanadium-nickel alloy. The resulting alloy prevents hydrogen embrittlement as it suppresses the appearance of the two-phase hydride region below room temperature.

Buxbaum and Marker (1993) used a solution method called electroless plating for palladium deposition as explained in Chapter 1. Using electroless plating they coated discs of niobium, tantalum and vanadium and made the first tubular membranes. They reported a permeability as high as 0.32 μmol/(m.s.$Pa^{0.5}$) at 425 °C and 2 atm pressure for palladium-coated niobium discs of 2 mm thickness. For palladium coated niobium tubes of 0.25 mm wall thickness, the permeability was lower, about 0.16 μmol/(m.s.$Pa^{0.5}$), but the flux was higher because of the thin wall. Buxbaum and Kinney (1996) reported experiments with hydrogen extraction membranes made of palladium-coated niobium and tantalum heat exchanger tubes. Before applying palladium coats of 1-3 μm thickness using a solution method, the tubes were cleaned, electropolished and hydrided. Permeation studies were performed at temperatures as high as 420 °C and with differential pressures up to 0.3 MPa. Using 9.53 mm OD tubular membranes, the maximum flux obtained was 0.00147 mol/(m^2.s) which corresponds to an effective permeability of 0.145 μmol/(m.s.$Pa^{0.5}$).

The High-flux membranes (palladium coated alloy tubular membranes) used for this study were supplied by REB Research and Consulting (Ferndale, Michigan, USA). Palladium was coated on both the inside and outside of the alloy tube. The method and conditions used for coating palladium were described in detail by Buxbaum and Hsu (1992) and Buxbaum and Kinney (1996).

These tubular membranes were selected for this study because they have the most suitable geometry for use in a fluidized bed membrane reactor. They can be fabricated easily into large scale hydrogen extractors using a shell and tube heat-exchanger design.

Also, tubular membranes can be constructed with a thinner wall for a given pressure differential.

In this section, no sweep gas was used on the permeation side of the membrane although most of the reported membrane studies were performed using sweep gas. The use of sweep gas is impractical in commercial applications as it would require a separation step for recovering hydrogen from the sweep gas stream. In addition, the sweep gas must be heated to reaction temperatures, which requires a significant heat input and is thus economically unattractive.

3.3 Membrane model

It is generally accepted that hydrogen permeates dense metallic membranes by a "solution-diffusion" mechanism. The essential steps were described by Barrer (1951) and Athayde et al. (1994). The flux of hydrogen through a metal membrane can be estimated by the following equation (Collins and Way, 1993; Uemiya et al., 1991b; Hurlbert and Konecny, 1961):

$$J_{H2} = P_M\left(\frac{P_{H2h}^n - P_{H2l}^n}{t}\right) \tag{3.1}$$

The above equation can be derived from Fick's first law. According to Fick's law, the flux of hydrogen atoms through a homogeneous metal phase can be calculated from the equation:

$$J_H = D_M\left(\frac{C_{Hh} - C_{Hl}}{t}\right) \tag{3.2}$$

When diffusion through the metal is the rate limiting step (i.e. dissolved hydrogen atoms are in rapid equilibrium with the hydrogen molecules in the gas phase) and hydrogen atoms form an ideal solution in the metal, C_H is related to the partial pressure of hydrogen in equilibrium with the metal expressed via Sieverts thermodynamic equation:

$$C_H = K_S(P_{H2}^{0.5}) \tag{3.3}$$

Combining Equations 3.1 and 3.2, the value obtained for n is equal to 0.5 (Buxbaum and Kinney, 1996; Buxbaum and Marker, 1993; Collins and Way, 1993; Hurlbert and Konecny, 1961).

If the surface adsorption of hydrogen on palladium is the rate-determining step, the concentration of hydrogen at the interface of the membrane can be written as follows (Wijmans and Baker, 1995):

$$C_{Hh} = K_R.P_{H2} \tag{3.4}$$

Combining Equations 3.2 and 3.4, the value obtained for n is equal to 1.0 (Wijmans and Baker, 1995).

Several factors influence the value of 'n'. When the rate of permeation is governed by both surface adsorption of hydrogen molecules and diffusion of hydrogen atoms through the bulk of the metal, the value of 'n' is between 0.5 to 1.0 (Hurlbert and Konecny, 1961; Collins and Way, 1993; Yan et al., 1994).

Deviation from "ideal solution behavior" (Sieverts law, Equation 3.3) is one of the influences on the value of the pressure exponent 'n'. At low concentrations, hydrogen atoms form an ideal solution in the metal and there is no interaction between the hydrogen atoms as they diffuse through the metal. When the partial pressure of hydrogen

in the gas phase is high, the atomic hydrogen concentration in the metal also increases and the adsorbed hydrogen atoms attract each other. Therefore, at high hydrogen partial pressures, the atomic hydrogen concentration in the metal (C_H) is more than the value predicted by Sieverts law (Equation 3) (Buxbaum and Kinney, 1996). If K_S is taken as constant, this effect increases the value of the pressure exponent from the 0.5 value in Equation 3.3. The deviation from ideal behavior (i.e. deviation from n=0.5 behavior) is more pronounced in metals such as palladium which form hydrides with hydrogen atoms (Le Claire, 1983). In these metals, the deviation from ideal behavior is encountered even at comparatively low pressures.

Another factor which influences the value of 'n' is the leakage of gas through metal film or membrane seals (Collins and Way, 1993). Since flow through any leak is hydrodynamic, the flow rate depends on the absolute pressure difference and not on the difference in hydrogen partial pressures.

The value of 'n' may depend on temperature since it is affected by the Sieverts constant (K_S), diffusivity (D_M) and the ratio of the rates of surface processes and bulk diffusion which all depend on temperature.

Hydrogen permeation experiments conducted with palladium have yielded n values of 0.5 (Buxbaum and Kinney, 1996; Buxbaum and Marker, 1993; Uemiya et al., 1991b; Holleck , 1970), 0.68 (Hurlbert and Konecny, 1961), 0.76 (Uemiya et al., 1991a), 0.80 (De Rosset, 1960), 0.53-0.62 (Collins and Way, 1993) and 1.0 (Yan et al., 1994). All these experiments were conducted at temperatures ranging from 340 °C to 460 °C and with hydrogen feed pressures ranging from 101 to 4926 kPa.

Since both the diffusivity and Sieverts constants vary in an Arrhenius manner with temperature, the permeation constant can be expressed in terms of a pre-exponential factor, P_{MO}, and an activation energy, E_p, by the equation:

$$P_M = \frac{D_M K_S}{2} = P_{MO} \exp\left(-\frac{E_p}{R_g T}\right) \tag{3.5}$$

Two other quantities, "permeance" and "total resistance to transport" can be derived from Equation 3.1. "Permeance" (ϕ_m) is defined as the flux divided by the pressure driving force as:

$$\phi_m = \frac{J_{H2}}{(P^n_{H2h} - P^n_{H2l})} = \frac{P_M}{t} \tag{3.6}$$

The inverse of permeance is the "total resistance to transport",

$$R_{tot} = \frac{1}{\phi_m} = \frac{(P^n_{H2h} - P^n_{H2l})}{J_{H2}} = \frac{t}{P_M} \tag{3.7}$$

For the High-flux membranes used for this study, the total resistance to transport will be the sum of the resistance offered by the palladium coating and the constant resistance R_C.

$$R_{tot} = \left.\frac{t}{P_M}\right|_{Pd} + R_C \tag{3.8}$$

R_C accounts for the resistance of the niobium/tantalum alloy plus the interfacial resistances between the palladium coatings and the alloy. The diffusion rates for palladium membranes reported by various authors differ by orders of magnitude. For example, the rates reported for a 50 μm palladium membrane at 300 °C by Jost and Widman (1940), Silberg and Bachman (1958), Barrer (1940) and Hurlbert and Konecny

(1961) are in the ratio of 0.005:0.01:0.3:1 respectively. Also the reported activation energy (E_P) for permeation of hydrogen through palladium differs considerably between studies. For example, Holleck (1970) reported an activation energy (E_P) of 43.97±0.42 kJ/mol whereas Katsuta et al. (1979) determined E_P to be 20.5±1.4 kJ/mol.

The data reported by various authors demonstrates variability which is probably a result of the purity of the palladium and the state of the palladium surface, the permeability pre-exponential factor (P_{MO}), the activation energy (E_P) and the pressure exponent (n) were determined for our membranes from experimentally obtained permeation rates. At a particular temperature, the effective permeability of the high flux membrane tube (P_M) and pressure exponent (n) were determined from nonlinear regression analysis of Equation 3.1. Using experimental results obtained at different temperatures, the permeation pre-exponential factor and the activation energy were estimated using linear regression analysis of the following equation:

$$\ln P_M = \ln P_{MO} - \frac{E_p}{R_g T} \tag{3.9}$$

Similarly, the total resistance of the High-flux membrane was determined from Equation 3.7. The resistance and permeability of the palladium coating and the constant resistance were determined by linear regression analysis of Equation 3.8.

3.4 Apparatus and procedure

Permeabilities and selectivities of membrane tubes were studied using the permeation and abrasion test assembly shown in Figure 3.1. The permeation and abrasion unit consisted of a cylindrical vessel flanged at both ends with a distributor plate

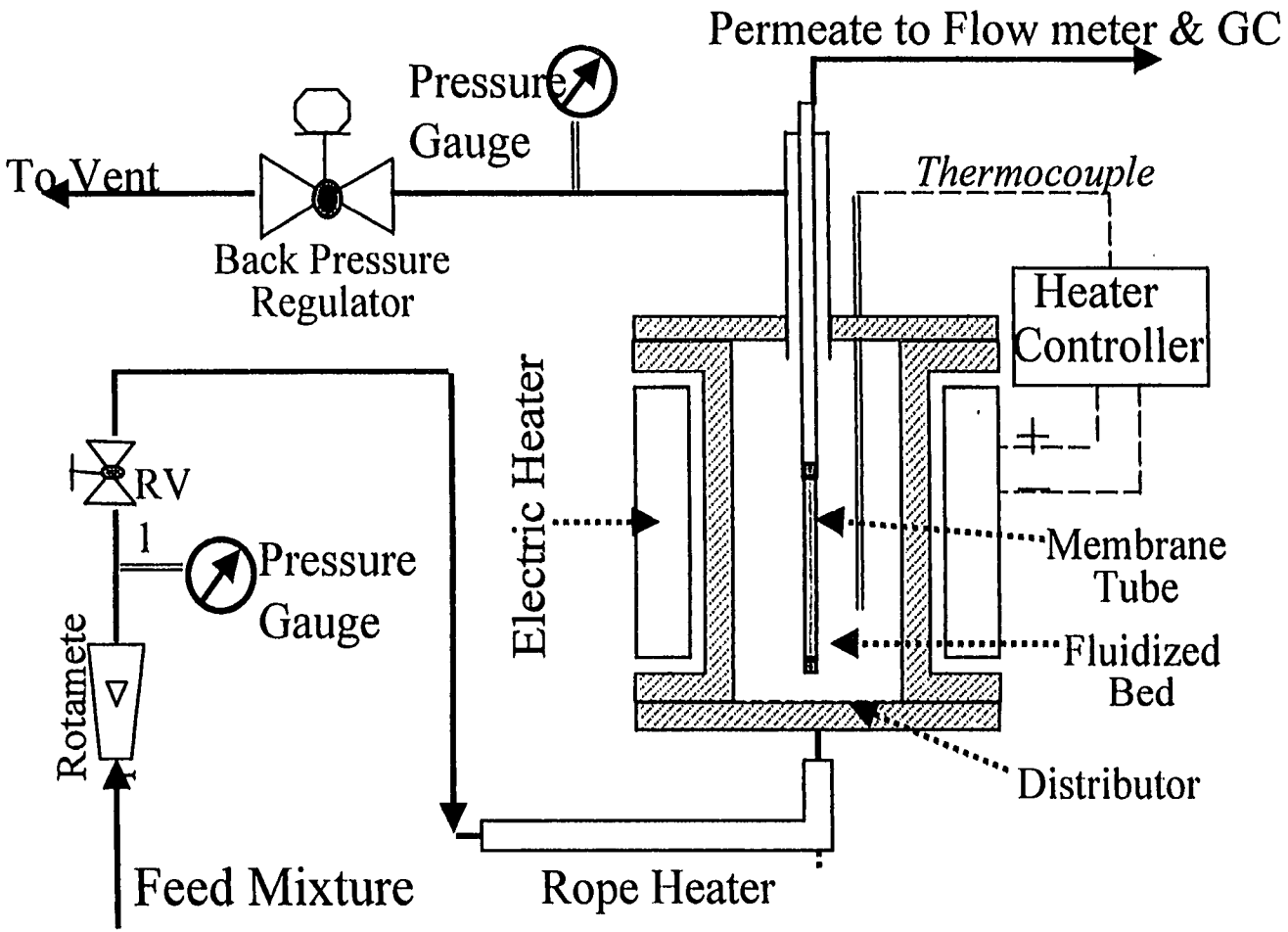

Figure 3.1: Permeation and abrasion test unit

at the bottom. As the feed gas (a mixture of N_2 and H_2) flowed up the catalyst bed, a small amount of hydrogen permeated through the membrane and the retentate exited from the top of the vessel. The flow rate of the permeate was measured using a water displacement method and its composition was analyzed at regular intervals by a Shimadzu GC-8A IT Chromatograph. At each temperature and pressure, steady state was assumed when two successive flow rate measurements were within 4%. The pressure in the permeation unit was maintained at various set points by a back pressure regulator, whereas the permeate side was always at atmospheric pressure. The membrane tubes used for permeation studies were 6.0 to 9.0 cm long. Sufficient reforming catalyst, which is essentially Ni supported on alumina (Al_2O_3), was added to the vessel to ensure that all of the membrane tube remained submerged in the fluidized bed. The substrate metal (alloy) thickness of all the high flux tubes was 76.2 μm and the palladium coating varied from approximately 3 to 9 μm on the inside and the outside of the tubes. The top ends of the membrane tubes were brazed to 316 SS tubes of slightly larger diameter using a commercially available high temperature braze UTP 6 (Bohler UTP Welding Canada, Ltd.) and the bottom ends were sealed using 316 SS plugs brazed with UTP 6. The 316 SS tube was sealed to the permeation unit by Swagelok fittings. The retentate gas passed through a catalyst trap, filter and a back pressure regulator before being vented. Before introducing the feed gas, the catalyst bed and the permeation unit were preheated to 673 K with nitrogen flow to prevent damage to the palladium layer, as pinholes or cracks could be formed by phase transformation of palladium hydride from the α- to the β-phase on exposure to hydrogen at temperatures below 573 K.

For the first set of experiments, each of the two membrane tubes had an outside diameter of 1.98 mm and a substrate metal alloy thickness of 38 μm. One end of each membrane tube was first brazed to a 3.34 mm ID 316 SS tube which was then brazed to a 4.93 mm ID 316 SS tube while the other end was plugged by brazing. The brazed tubes, supplied by REB Research, had a palladium coating of 4 and 6 μm on both the inside and the outside. Both of the tubes collapsed and resembled thin sheets at an operating temperature of 873 K. This collapse caused stress in the braze and a leak developed at the point where the membrane tube was brazed to the stainless steel tube. Normally these tubes have pressure in the inside, and the thickness was computed to be able to adequately contain pressure at 973 K. However, computations for tubes with pressure on the outside are approximate, as much depends on tubes being perfectly round.

New membranes with greater wall thickness (64 μm) were used for a second set of experiments. The outside diameter of the membrane tubes were 1.98 mm and they were brazed to 3.18 mm OD 316 SS tubes. These tubes had a palladium coating thickness of 4.2 and 6.2 μm, respectively. These membrane tubes were also crushed into the shape of thin sheets, although there was no leak (i.e. no nitrogen peak was detected in the permeate gas) as the brazing remained intact. Surprisingly, the permeate continued to flow through the continuous channels of the crushed tube.

3.5 Results and discussion

From the initial experiments, it was clear that the alloy tubes were unable to maintain their mechanical structure at high temperature. It was decided to reinforce the

membranes by inserting springs inside the tubes. Two spring-reinforced membranes were tested for permeation and high temperature and high pressure resistance. The membrane tubes had an outside diameter of 3.18 mm and a substrate metal thickness of 76 μm. Each tube was first brazed to a 3.34 mm ID tube which was subsequently brazed to another 1.75 mm ID SS tube. Both of the membrane tubes started leaking at approximately 873 K and 1378 kPa. The leak occurred due to the inability of the braze (performed by REB Research using Braze 505) to withstand this high temperature. However, the spring reinforcement prevented the tubes from collapsing. The brazing of all the tubes tested afterwards was carried out using a high temperature braze called UTP 6 (49.0% Cu, 10.6% Ni, 1.0% Ag and the balance Zn & other traces).

The High-flux membrane tubes used for the next set of experiments had outside diameters of 3.18 mm and substrate metal thickness of 76 μm. The palladium coating thickness of these tubes was 1.94, 4.05 and 6.33 μm. Because of the very thin palladium layer, it was not possible to braze the 1.94 μm membrane to a stainless steel tube, so that tube was not used. Permeation studies were performed with the 6.33 and 4.05 μm membranes at different temperatures and differential pressures. The 4.05 μm tube collapsed at 1330.3 kPa and 873 K. Since the spring inside the tube was not compact, the high outside pressure at this high temperature caused both the spring and the tube to collapse. For the same reason, the 6.33 μm membrane leaked nitrogen in to the permeating gas at 898 K and 1330.3 kPa. The following conclusions were drawn from all the experimentation up to this point:

i) Spring reinforcement is essential to provide strength at such high temperatures and differential pressures. Moreover, the spring needs to be packed compactly, even though it may decrease the surface area available for desorption.

ii) Brazing becomes difficult if the palladium coating thickness is very low. The coating should be a minimum of 3.0 μm and preferably above 4.0 μm.

iii) UTP 6 can withstand the high temperatures and differential pressures used in the present investigation.

3.5.1 Permeation characteristics

New membrane tubes were fabricated utilizing the conclusions of the previous experiments. Springs of the right dimensions were inserted snugly into the membranes, and a collapse at higher differential pressures and temperatures was prevented. These membrane tubes were utilized to evaluate the permeation characteristics. Mr. M. Islam conducted the experiments for membrane characteristics and abrasion (Islam, 1997).

All the tubes tested for permeation characteristics had an outside diameter of 1.98 mm and substrate metal thickness of 76 μm. One end of each tube was plugged with brazing and the other end was brazed to a 3.34 mm ID 316 SS tube.

Figure 3.2 shows the effect of change in superficial velocity on the permeabilities of pure palladium and High-flux membrane tubes. Each data point in this figure and all the figures used afterwards represent the average of three readings. The maximum percentage deviation from the mean value was ±5%. From the results of Figure 3.2, it

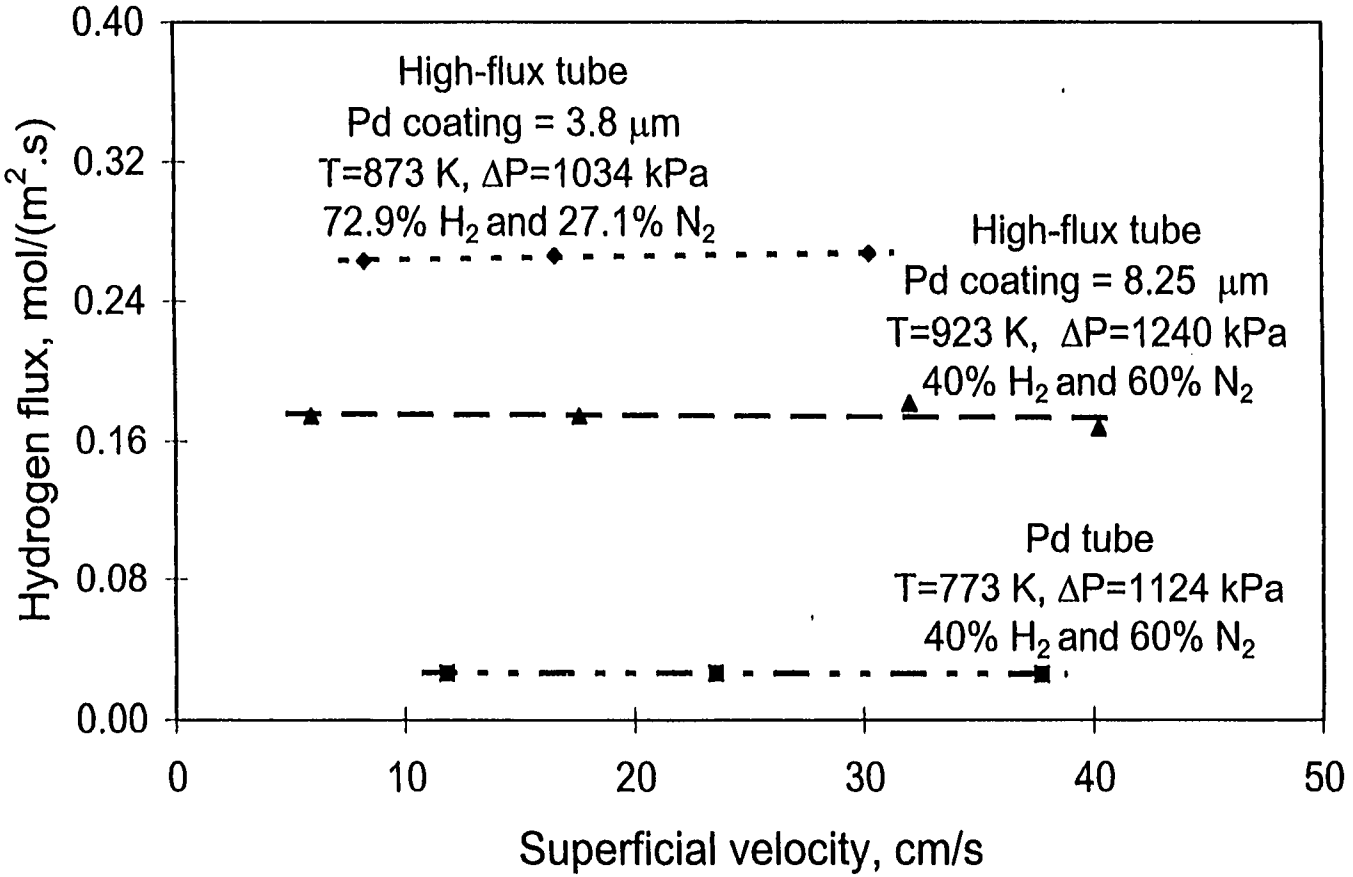

Figure 3.2: Effect of superficial velocity on permeation

can be concluded that the permeation rate was independent of superficial velocity i.e. there is no diffusional resistance in the catalyst bed.

Figures 3.3 and 3.4 show temperature effects on the flux and permeabilities of different High-flux membrane tubes respectively. Although there is considerable scatter in the data of Figure 3.4, the trend follows Arrhenius behavior. Experimentally, the scatter may be due to difficulties in controlling the temperature and pressure inside the permeation unit. The temperature varied by as much as 10 K from the mean whereas the pressure varied from the mean value by as much as ± 35 kPa.

The pre-exponential factors (P_{MO}) in Equation 3.9 for the 3.8, 5.4 and 8.25 μm membranes were determined to be 9.95 x 10^{-9}, 7.85 x 10^{-9}, and 5.48 x 10^{-9} mol/(m.s.$Pa^{0.72}$) respectively with corresponding activation energies (E_P) of 12.7, 11.5 and 9.6 kJ/mol. The above mentioned P_{MO} and E_P values account for the combined effect of the palladium coating and the alloy substrate. Activation energy is positive (i.e. permeation increases with increasing temperature) for palladium while it is negative for niobium and tantalum. As diffusion through the palladium coating is the rate limiting step, it dominates the overall activation energy of the High-flux membranes. The E_P for pure palladium is 20.5±1.4 kJ/mol (Katsuta et al., 1979). For High-flux membranes this value is clearly reduced because of the opposing effect of exothermic absorption in the substrate alloy.

The effect of hydrogen partial pressure on the permeation flux for different membrane tubes is shown in Figure 3.5. The pressure exponent 'n = 0.72' was determined from nonlinear regression analysis using the combined permeation data from three different membrane tubes in Equation 3.1. One of the reasons for the high value of n is

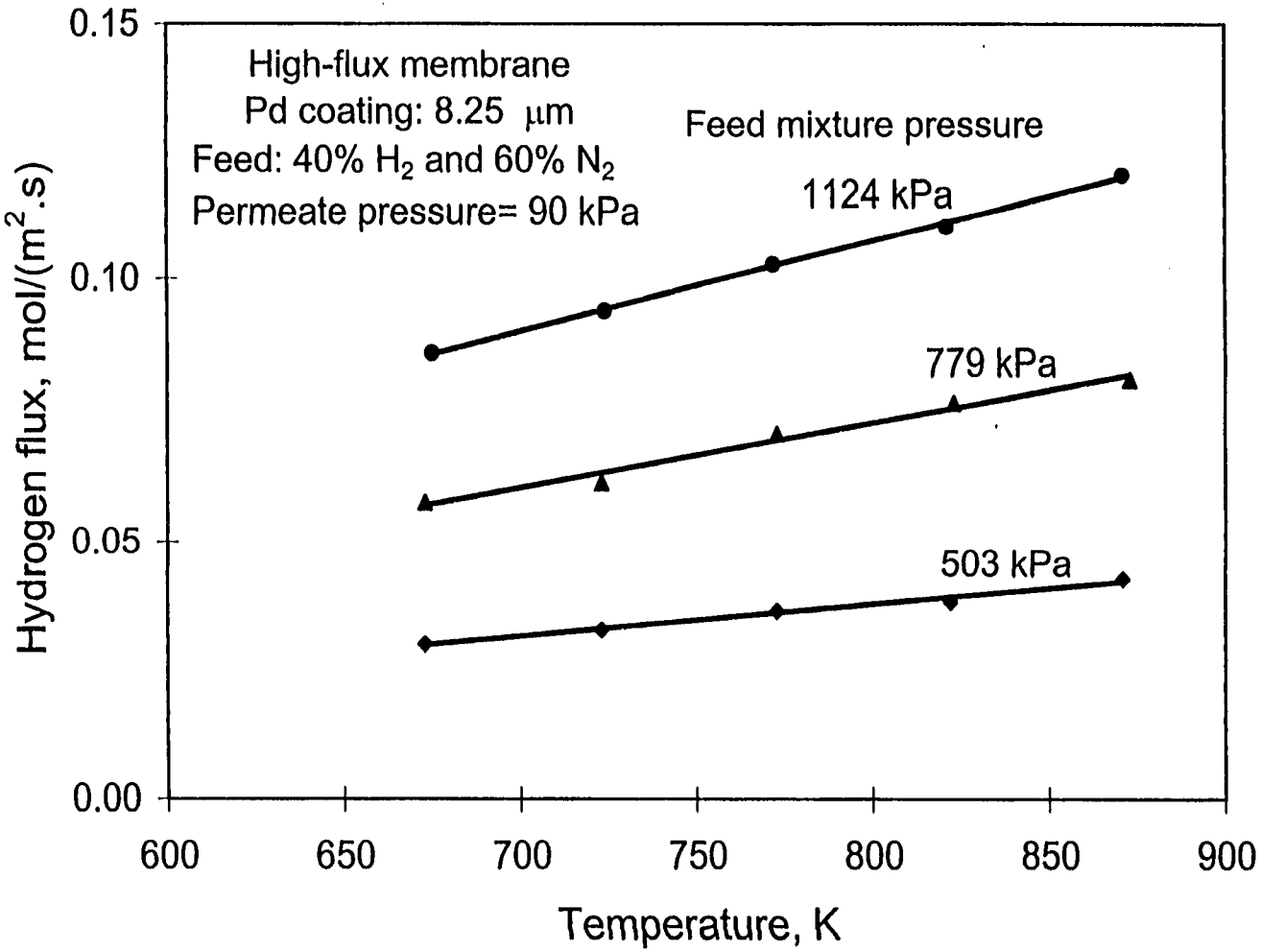

Figure 3.3: Effect of temperature on permeation rate with pressure as a parameter

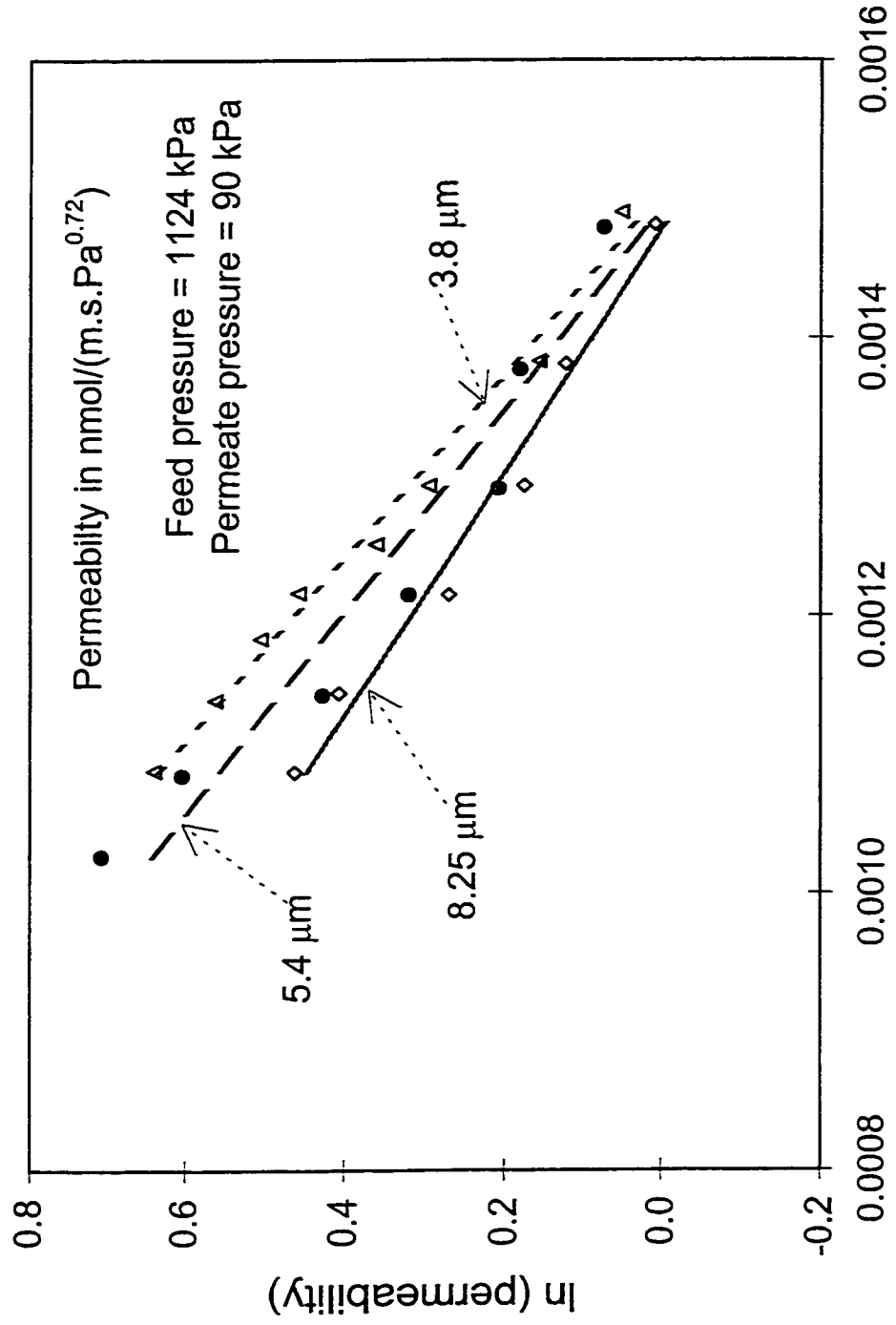

Figure 3.4: Permeability variation with temperature for different membrane tubes

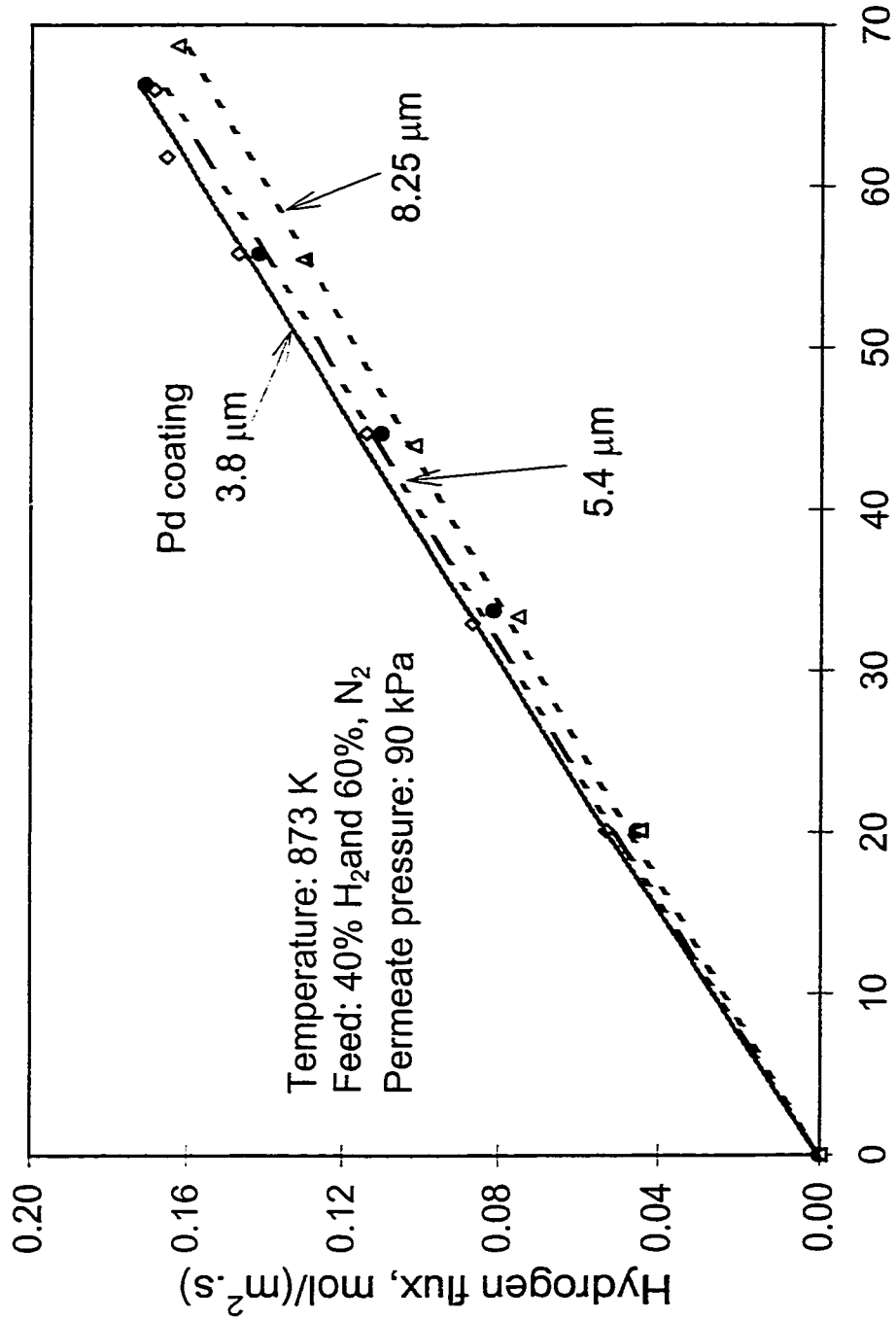

Figure 3.5: Effect of hydrogen partial pressure on permeate flux

that all the experiments were performed with a high hydrogen concentration (40% H_2 in the feed), which causes deviations from ideal solution behavior and thus from Sievert's law.

The reciprocal of the slopes of the best fit lines in Figure 3.5 are the transport resistances of different membrane tubes at 873 K. These resistances are plotted against the palladium coating thickness in Figure 3.6. The intercept of the line with the resistance axis, which was about 49700 $m^2.s.Pa^{0.72}/mol$, represents the constant resistance offered by the substrate alloy plus the metal-metal interfaces. The slope of the best fit line represents the resistance offered per 1 μm palladium coating and was about 1450 $m^2.s.Pa^{0.72}/mol$. For a single membrane tube, the variation of permeation rate with hydrogen partial pressure at three different temperatures is plotted in Figure 3.7. From this plot it is concluded that for the temperature range of 673 to 873 K, the pressure exponent 0.72 satisfactorily describes the permeation characteristic of the membrane.

In most of the experimental runs, the composition of the feed mixture was 40% H_2 and 60% N_2. The high concentration of nitrogen was used so that even a small leak could be detected by analyzing the permeate. Experiments were also conducted using a 27.1% CH_4 and 72.9% H_2 feed mixture. Figure 3.8 shows the variation of hydrogen flux with pressure for the two feed gas mixtures. The slopes of the best fit straight lines for the two sets of data are almost equal. From this result we concluded that the permeability is independent of the concentration of hydrogen and the choice of the non-permeating component.

For comparison purposes, a permeation study was performed using pure palladium tubes supplied by Johnson Matthey Ltd. (same type as used by Adris, 1994).

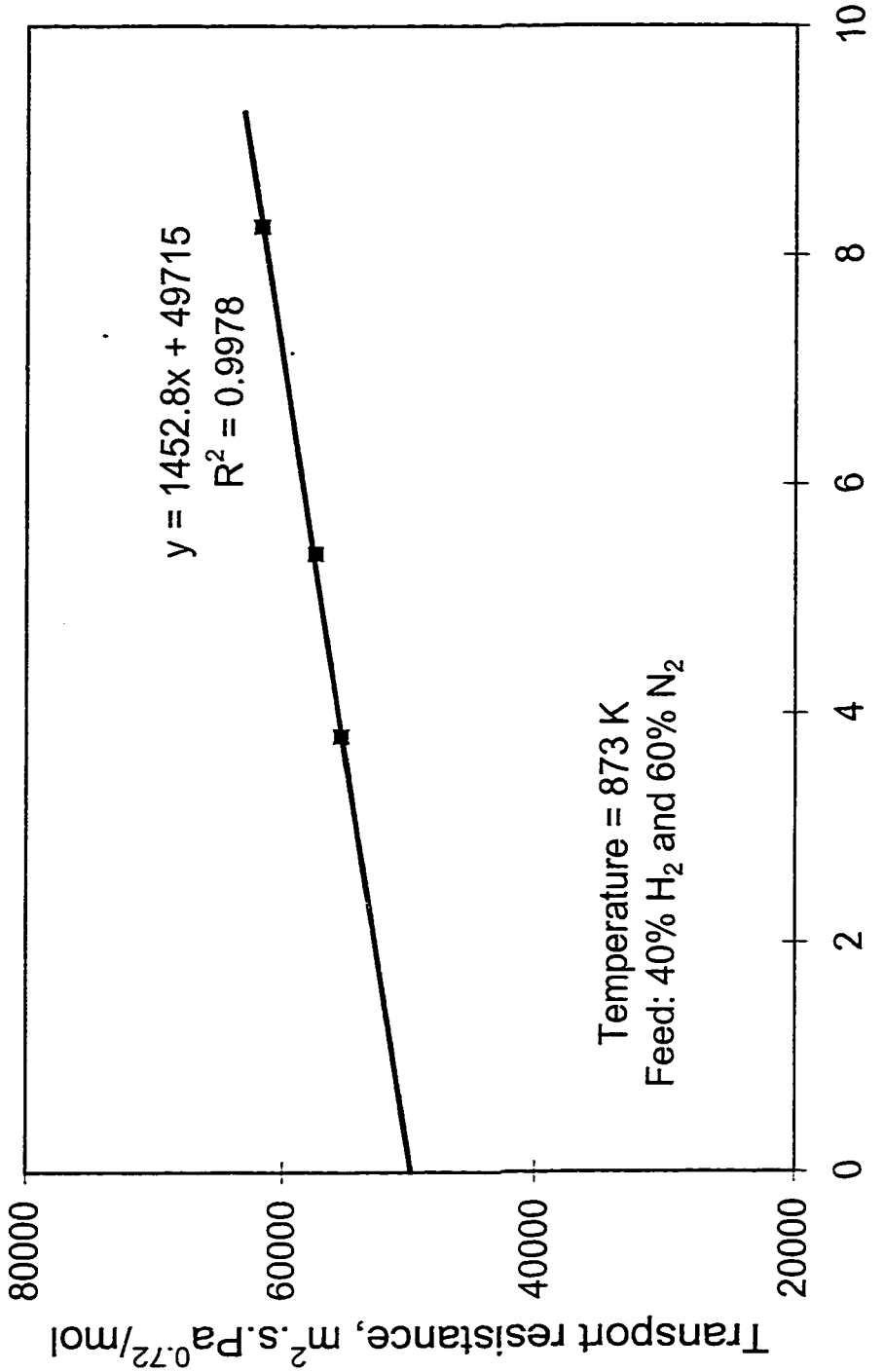

Figure 3.6: Effect of palladium coating thickness on overall transport resistance

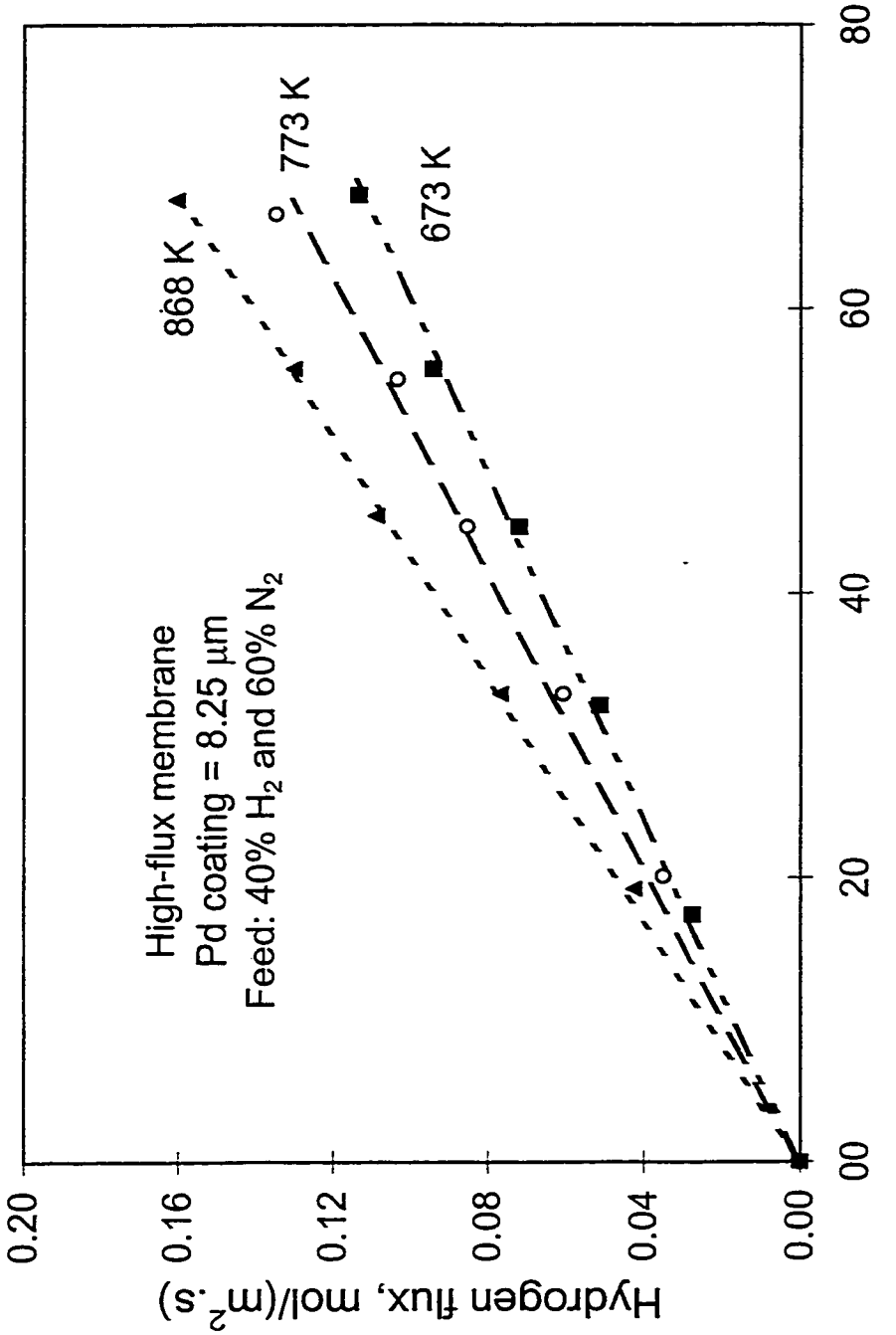

Figure 3.7: Effect of hydrogen partial pressure on permeate flux at different temperatures

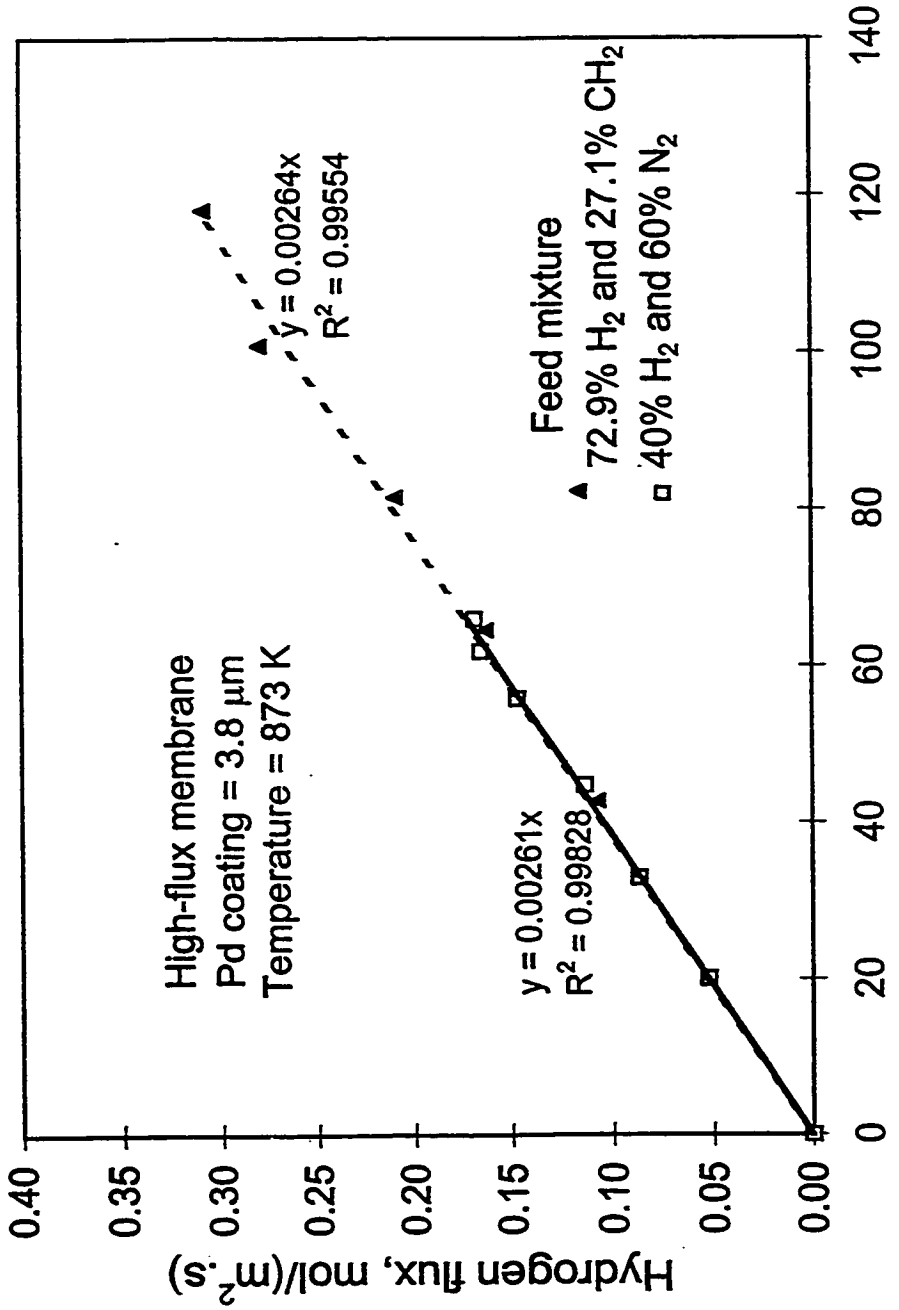

Figure 3.8: Variation of permeate flux with partial pressure for different feed mixtures

Figure 3.9 shows that the permeation rate was more than three times higher for the High-flux tubes than for the pure palladium tubes. The effect on permeability with temperature variation for the two kinds of membrane tubes is plotted in Figure 3.10. The permeation activation energies (E_p), calculated from the slopes of the lines, were 9.580 kJ/mol for the High-flux tube and 20.559 kJ/mol for the palladium tube. The E_p value for the palladium tube was close to the value (20.5±1.4 kJ/mol) reported by Katsuta et al. (1979).

The brazing with UTP 6 was not perfect as it failed on some occasions below a temperature of 923 K. As a result of this uncertainty, a different method was used to join the membrane tube and the stainless steel tube for a number of runs. A Conax™ PG gland with Grafoil sealant was used to connect the membrane tube to the 316 SS tube. A 3.18 mm OD SS tube was first machined to decrease its outer diameter so that it fit snugly inside the spring reinforced membrane tube. A Grafoil sealant was crushed on to the contacting/overlapping surface of the two tubes. Membrane tubes with Conax™ fitting at the top and braze at the bottom were tested successfully (without any leak) up to a temperature of 943 K and a differential pressure of 1410 kPa.

3.6 Conclusions

The spring reinforced High-flux membrane tubes were tested for permeation over the temperature range of 673-973 K and at differential pressures up to 1480 kPa. This is a significant improvement, as this type of membrane was tested in earlier studies only up to a temperature of 698 K and a differential pressure of 110.3 kPa. In addition, the abrasion resistance of the palladium coating was tested in the fluidized bed of catalyst particles and found to be satisfactory after 60 hour tests. Due to their stability at high

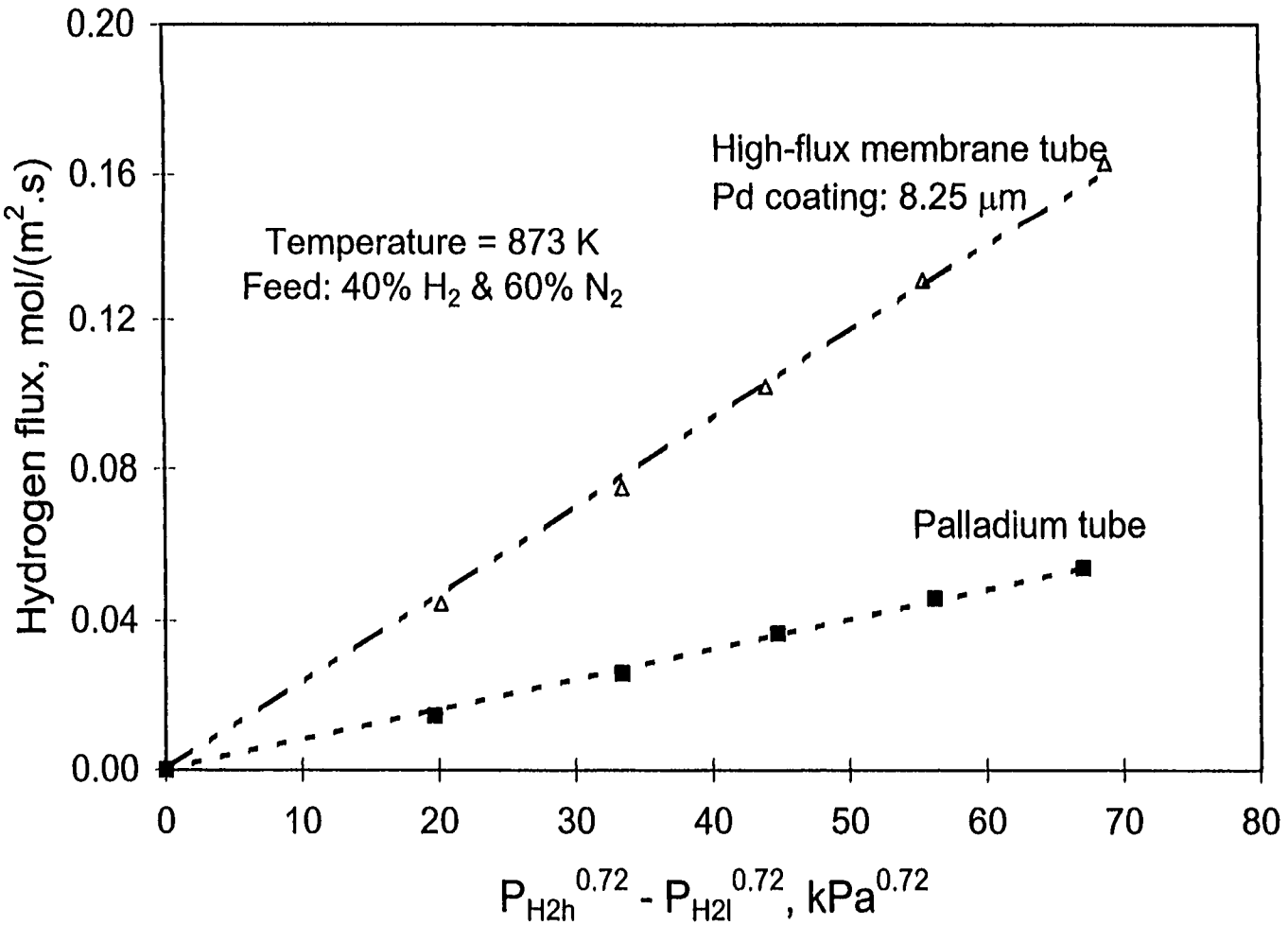

Figure 3.9: Variation of permeation rate with partial pressure for different membranes

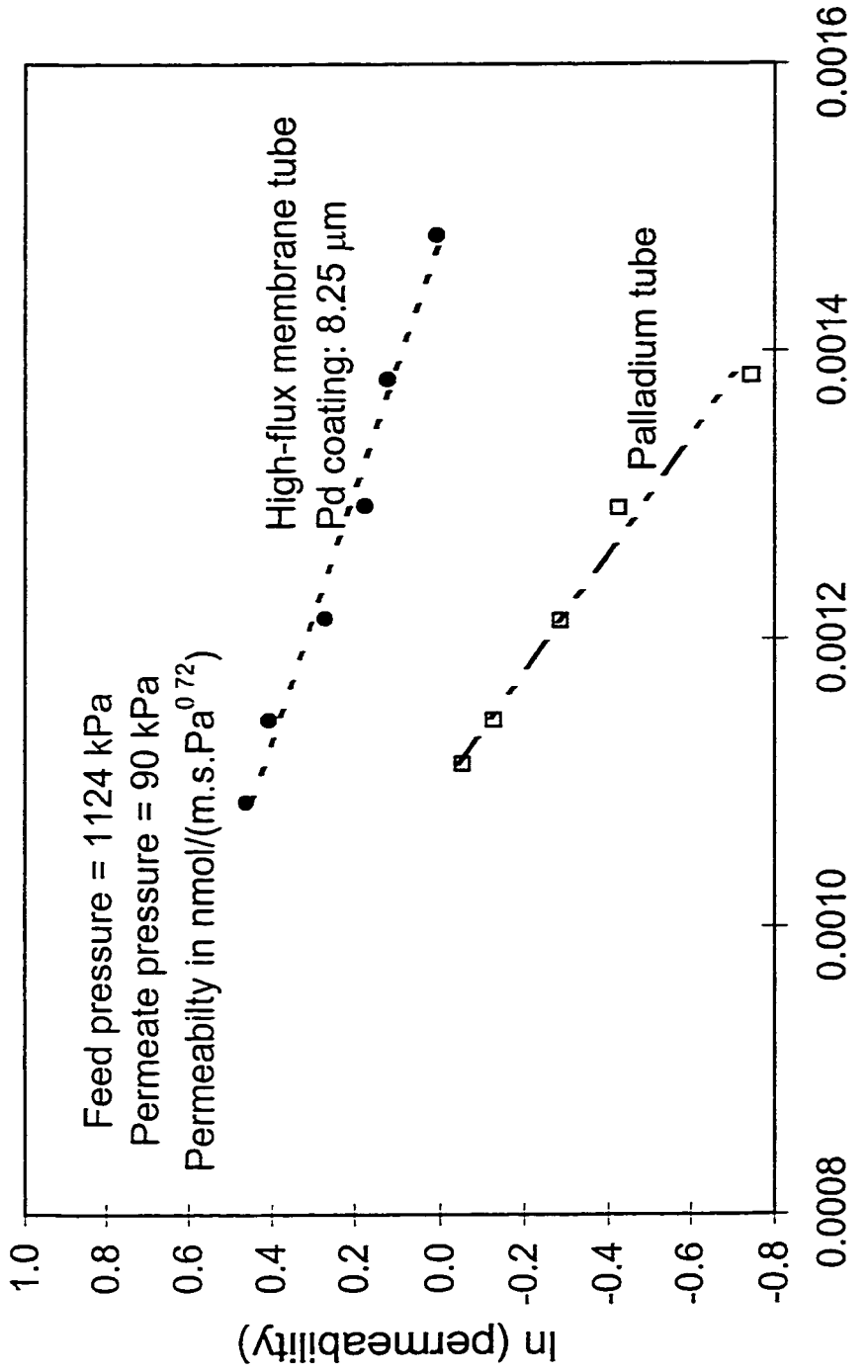

Figure 3.10: Permeability variation with temperature for different membranes

temperatures with high differential pressures and in a fluidized bed environment, the High-flux membrane tubes can be used in membrane reactors including fluidized bed membrane reformers which require operation at relatively high temperatures and with transmembrane pressure differences.

Chapter 4

Fluidized Bed Membrane Reforming Experimentation

4.1 Objective

The objective of this study was to prove the viability of U-tube spring-reinforced High-flux membrane modules in a pilot plant reformer. This chapter analyzes the results obtained from the FBMR with High-flux membrane experimentation and compares them to previous investigations and equilibrium values.

This chapter also describes the equipment used for all pilot plant experiments and details the experimental procedures.

4.2 Pilot plant description

The primary unit used for experimentation was the steam methane reforming pilot plant; the same unit was used for all other experimentation in the doctoral project. For the oxygen input experiments some changes were made to the reforming reactor which are detailed in Chapters 5 and 6. The instrumentation and chromatographic analysis have also been explained in this chapter. The system consisted of an industrial scale fluidized bed reforming pilot plant, which is represented, schematically in Figure 4.1. Table 4.1 summarizes the abbreviations assigned to the pilot plant process equipment; the dimensions, design conditions and materials of construction.

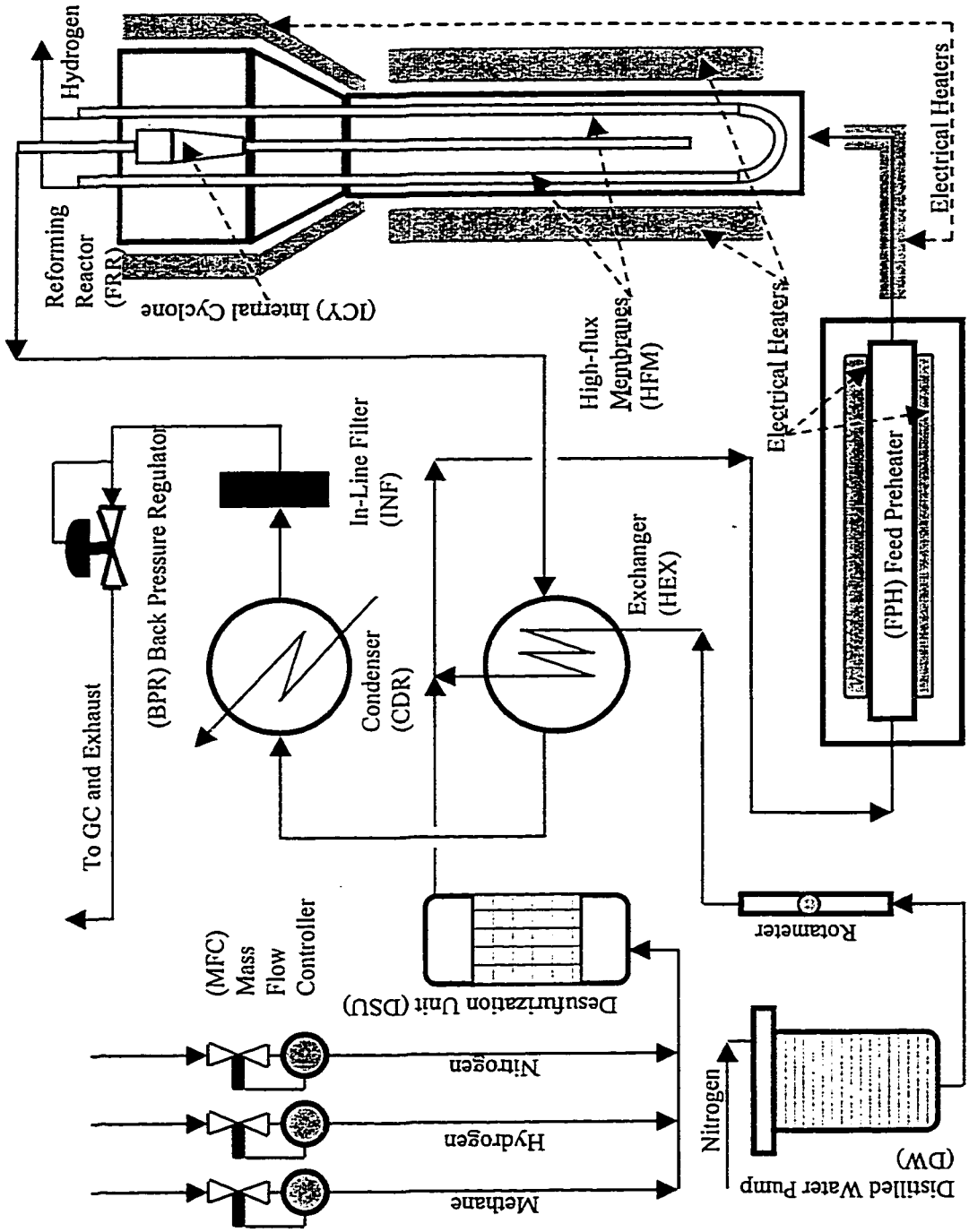

Figure 4.1: Schematic of the FBMR pilot plant

Table. 4.1: Main process equipment

Name	Description	Dimensions & Material
Reactor (FRR)	The reforming reactor consists of a main body, tapered section, windbox, expansion section and distributor plate. Reactor is flanged at both ends. Holes are provided in top flange to support vertical membrane tubes. Main body is surrounded by two semi-cylindrical electric heating elements each rated for 240 V at 2.8 kW each.	Reactor body: OD=114.3 mm, ID=97.2 mm, L=0.66m Tapered section:Angle=60^0, L=0.178 mm. Expansion section:OD=219 mm, ID=194 mm, L=0.305m. Windbox: Depth=25.4 mm, ID=88.9 mm, Vol.=0.158 lit. 316L stainless steel
Heat Exchanger (HEX)	This exchanger consists of two identical tubular coils inside one shell. The shell is top flanged pressure vessel rated at 1.35 MPa and 813 K.	Coil tubing: OD=6.25 mm, L=2.4m, coil circle dia.=152 mm, heat transfer area=0.047 m^2. Vessel OD=219 mm, ID=203 mm, L=1.22 m 316 stainless steel (both coil & shell)
Condenser (CDR)	Four identical coils inside one shell. The shell is similar to HEX	Coil tubing: OD=6.25 mm, L=1.2 m, coil circle dia.=152 mm, heat transfer area=0.0235 m^2 316 stainless steel
Feed Preheater (FPH)	This heater is made of two vessels, flanged at each end with one placed inside the other. Inside vessel is rated at 1.28 MPa and 1061 K and is surrounded by two semicylindrical	Inside vessel: ID=97.2 mm, L=1.32 m. Outside vessel: ID=289 mm, L=1.524 m.

	electric heaters rated at 240 V and 6 kW each. Outside vessel is rated at 1.64 MPa and 723 K.	Inside vessel: 316L stainless steel. Outside vessel: carbon steel.
Distilled Water Tanks (DW-1 & DW-2)	Two identical top-flanged vessels rated for pressure of 1.35 MPa at room temperature.	OD=114.3 mm, ID=102.3 mm, L=0.71 m. Vessel: 316 stainless steel Flange: carbon steel lined with stainless steel.
Desulfurization vessel (DSU)	Bottom flanged with a screen 0.3 m above the bottom flange supported from the bottom (flange). Pressure rating 1.35 MPa at room temperature.	Identical to DW-1 and DW-2
Back Pressure Regulator (BPR)	Pressure rating is 1.7 MPa at 453 K.	Inlet and outlet connections are 6.3 mm Swagelok fittings. 316 stainless steel casing.
Filter (INF)	In-line filter assembly consists of two identical filters with a filter element of 15 microns pore size sintered metal.	Inlet and outlet connections are 12.7 mm Swagelok fittings. 316 stainless steel
Internal Cyclone (ICY)	Consists of main body, tapered section, gas inlet, gas outlet and solids return pipe. Rated for 1033 K.	Main body: ID=26.6 mm, L=76.2 mm. Tapered section: L=102 mm. Gas inlet ID=9.6 mm, Gas outlet ID=6.8 mm, Solids return pipe: ID=6.8 mm, L=0.61 m. 316 stainless steel.

The desulfurization unit (DSU) was used to remove trace sulfur compounds from the methane/natural gas input steams. The unit was packed with 4.0 kg of zinc oxide. Sulfur compounds tends to deactivate the reforming catalyst and must be removed from the feed streams.

Distilled water was accurately measured and pumped from tanks DW-1 and DW-2, then preheated in the heat exchanger (HEX) by the reactor flue gases. Methane and hot water were then combined and fed into the feed preheater (FPH), and heated by electrical radiant heaters to the desired process temperature. The heated feed mixture was then introduced into the fluidized reforming reactor (FRR) through a heated pipe. The reactor was comprised of two sections: the main fluidized section and an expanded disengagement section. Semi-cylindrical electrical radiant heaters that were clamped on to the reactor's main section provided for the endothermic heat of reforming. The expanded section was heated with electrical band heaters to prevent a temperature decrease from heat loss to the surroundings. The reactor contained nine High-flux U-tube modules for removal of hydrogen.

The design of the distributor plate, the layout of the holes, and the orifice design are shown in Figure. 4.2. The elutriated catalyst particles were separated from the reactor exit gases by an internal cyclone (ICY) and returned to the reactor bed. The reactor flue gas stream exchanged heat with the feed water stream in the heat exchanger (HEX). The unreacted steam was then condensed in the condenser (CDR) using cold tap water. An inline filter (ILF) separated any residual catalyst particles before the exit stream was passed through a back pressure regulator (BPR), which controlled the upstream pressure to the desired value.

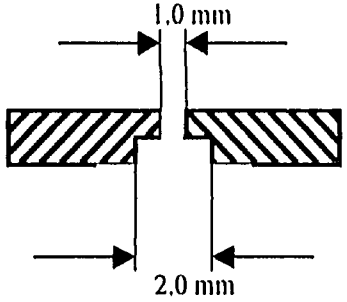

Orifice Design

Distribution of holes
44 holes on 91 mm circle
24 holes on 74 mm circle
24 holes on 58 mm circle
18 holes on 43 mm circle
16 holes on 31 mm circle
8 holes on 14 mm circle

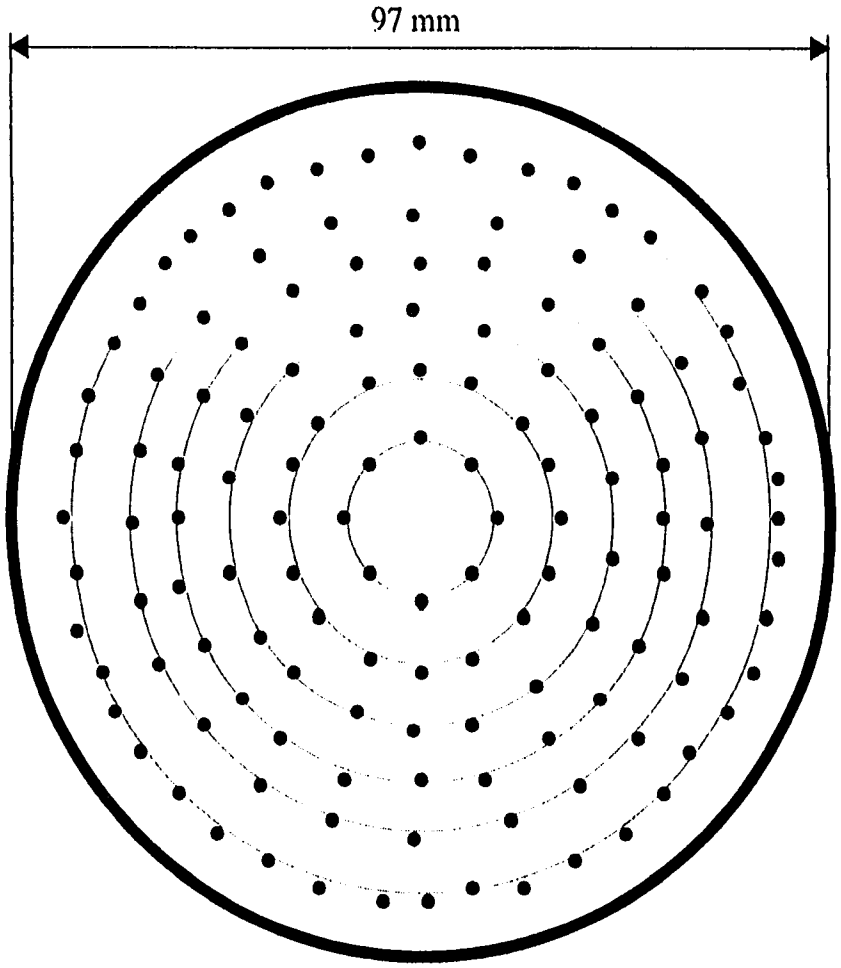

Figure 4.2: Distributor plate design for the pilot plant reactor

4.3 Instrumentation and data acquisition

Figure 4.3 schematically shows the instrumentation that is associated with the reactor. The reactor was provided with seven pressure probes, PR1 to PR7, along the height. PR1 to PR6 were equally spaced at 85 mm intervals along the height of the reactor's main section, with the lowest probe (PR1) 85 mm above the distributor plate. The seventh pressure probe (PR7) was near the top of the expanded section. Each pressure probe was connected to nitrogen purge lines attached to rotameters. The purge gas flow was regulated and controlled to an optimized value by rotameters (Cole-Palmer, tube number N022-13 with SS316 spherical float of density 8040 kg/m^3).

The purge gas velocities were maintained so that the fluidized catalyst of the reactor could not get entrained into the pressure probes. OMEGA PX750 differential pressure transducers calibrated to a range of 0 to 8 kPa and able to withstand a maximum of 13.8 MPa measured the differential pressures.

Figure 4.3 shows the location of the K type thermocouples (TR0 to TR7 and TRF) used to monitor the temperatures at different locations in and around the reactor. There also was a thermocouple TRW to monitor the temperature of the reactor outer wall. TR3 was used as the control thermocouple for the reactor heaters, while TRF was used as the control thermocouple for the freeboard heater.

The absolute pressure was measured using OMEGA PX603 pressure transmitters at five different points, including the reactor on the pilot plant.

Thermal mass flow controllers (MFC) (Brooks model 5850E) measured and controlled the flow rate of process gases. The three MFCs were calibrated for a

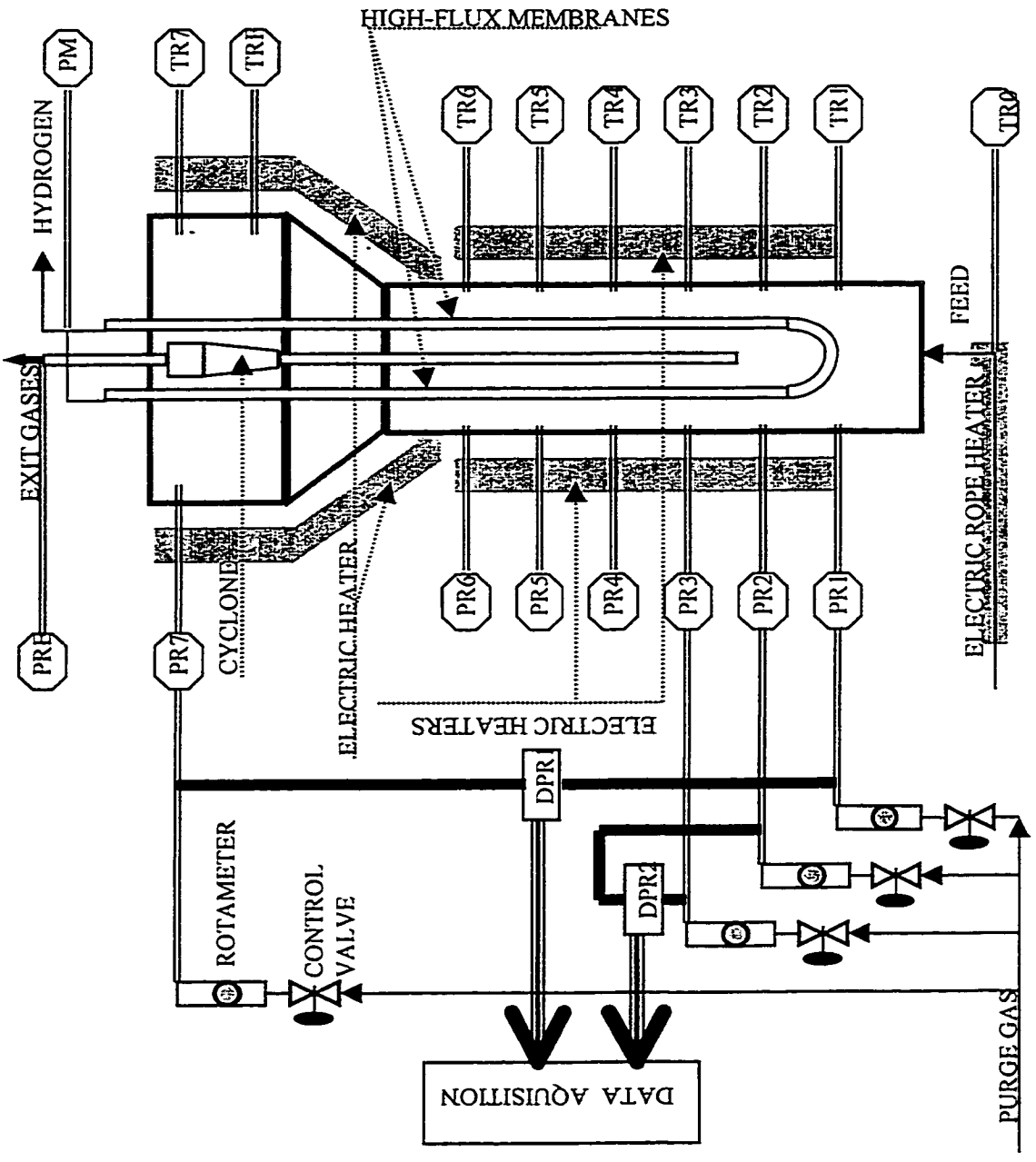

Figure 4.3: Schematic of the fluidized bed steam methane reformer

maximum flow of 1.2 m^3[STP]/h for nitrogen and hydrogen and 3.0 m^3[STP]/h for methane. A digital control unit (Brooks model 5857 – Mass Flow Secondary Electronic) was used to set and monitor the MFCs.

Two composite rupture discs (BS & B safety systems, 316 SS, rupture pressure 370 psig at 20 ^{o}C) provided for safe relief of pressure in case of a system over-pressure, one was located on the reactor top flange and the other at the inlet of the feed preheater.

Pressure was displayed on the pilot plant panel by OMEGA DP203 units. The absolute and differential pressure signals were sent to a STA-08PGA screw terminal accessory (Keithley Metrabyte) which was connected to a data acquisition board DAS-801 (Keithley Metrabyte) installed in an IBM PC386-33MHz. The DAS800 series boards used a 12 bit, successive approximation analog to digital converter with integral sample and hold and eight expandable analog-input channels. All of the temperature thermocouple signals were displayed on the pilot plant display panel using OMEGA 115K units. The control thermocouples were connected to process controllers (OMEGA CN76000) that in turn controlled the electrical heating elements. The temperature signals were simultaneously connected to a multiplexer EXP-16A (Keithley Metrabyte) which expanded one of the DAS801 channels to sixteen. The data from the DAS801 was analyzed, displayed and stored using Lab-Tech NoteBook software.

4.4 Membrane module configuration

Palladium-coated metal alloy membranes (High-flux) as mentioned and described in Chapter 3 were used to construct the membrane modules for the FBMR experimentation. Figure 4.4 shows a cross section of the spring reinforced High-flux

membrane being used for the FBMR experimentation. A total of nine U-tube modules were installed in the reforming reactor with the layout as shown in Figure 4.5. The U tube membranes were joined to 3.175 mm SS316 tubing using Conax™ fittings with Grafoil™ ferrules. The SS tubing was machined so that it slid into the membrane; the mating surface was sealed with Grafoil™ ferrules compressed by Conax™ fittings. This type of joints capable of withstanding a temperature of 800 °C was tested for leaks at 2.8 MPa. Each arm of the membrane U-tube was 0.5 m long and the SS tubing joined to each of them was a meter long. The SS tubing membrane units were attached to the top flange of the reforming reactor with Connax™ fittings.

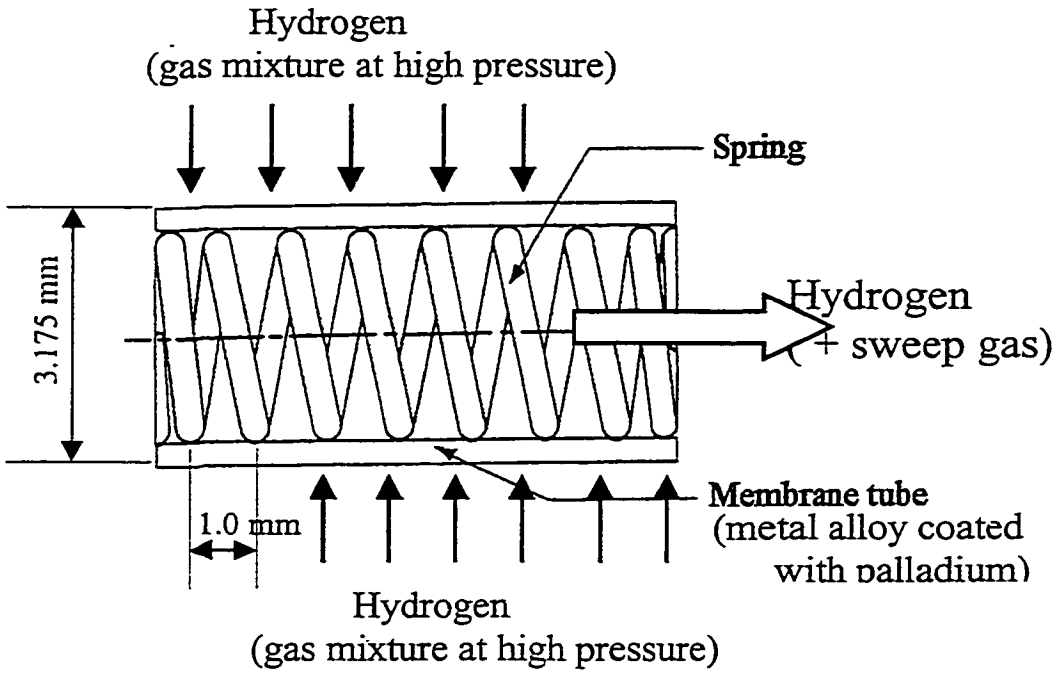

Figure. 4.4: Spring reinforced membrane tube

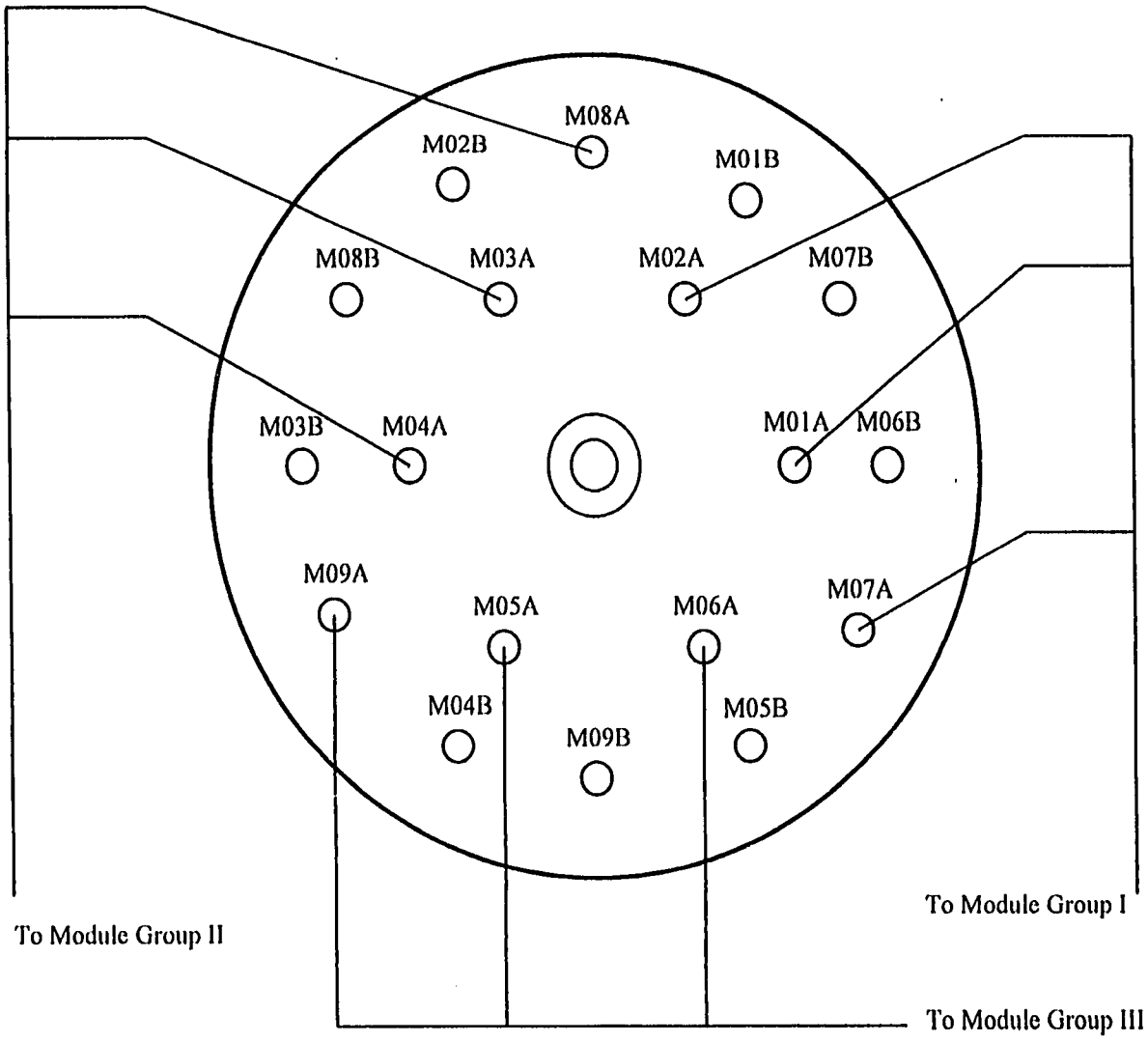

Figure 4.5: High-flux membrane module layout

The membrane module connections to the exhaust and sweep gas system are represented in Figure 4.6. Three U-tube modules were connected to a separate sweep gas system, each of which included a flow control valve and a rotameter at the flow inlet and a back pressure valve at the outlet. The outlet was connected to a dry test meter to measure the cumulative flow of the membrane exit gas. A stream was sent to the sample port for gas chromatograph analysis while the rest of the membrane exit gas was sent to the exhaust. The system could be operated with or without sweep gas and at any desired membrane pressure.

4.5 Chromatographic analysis

The gases exiting the pilot plant contained hydrogen, nitrogen, methane, carbon dioxide, carbon monoxide and oxygen. Hence, a suitable column was procured that could detect all of the above gases without resorting to SEQUENCE-REVERSAL or SERIES/BYPASS systems, as these systems have mechanical problems as well as added problems of poor resolution and ghost peaks (Adris, 1994).

A Shimadzu GC-8A IT Chromatograph was used to analyze the composition of the reformer and permeate exit gases. The GC had a thermal conductivity detector (TCD) and an isothermal mode of operation. Gas sample of sizes 80 μl were injected into the column. To detect component gases, a 9.14 m long, 3.18 mm OD and 2.16 mm ID stainless steel GC column packed with 100/120 mesh Haysep DB was used. The column was connected to the GC injection port by 3.18 mm stainless steel fittings.

The Thermal Conductivity Detector (TCD) had a 60 mA current supply connected with a tungsten filament. It detected the gas components in the sample based on the

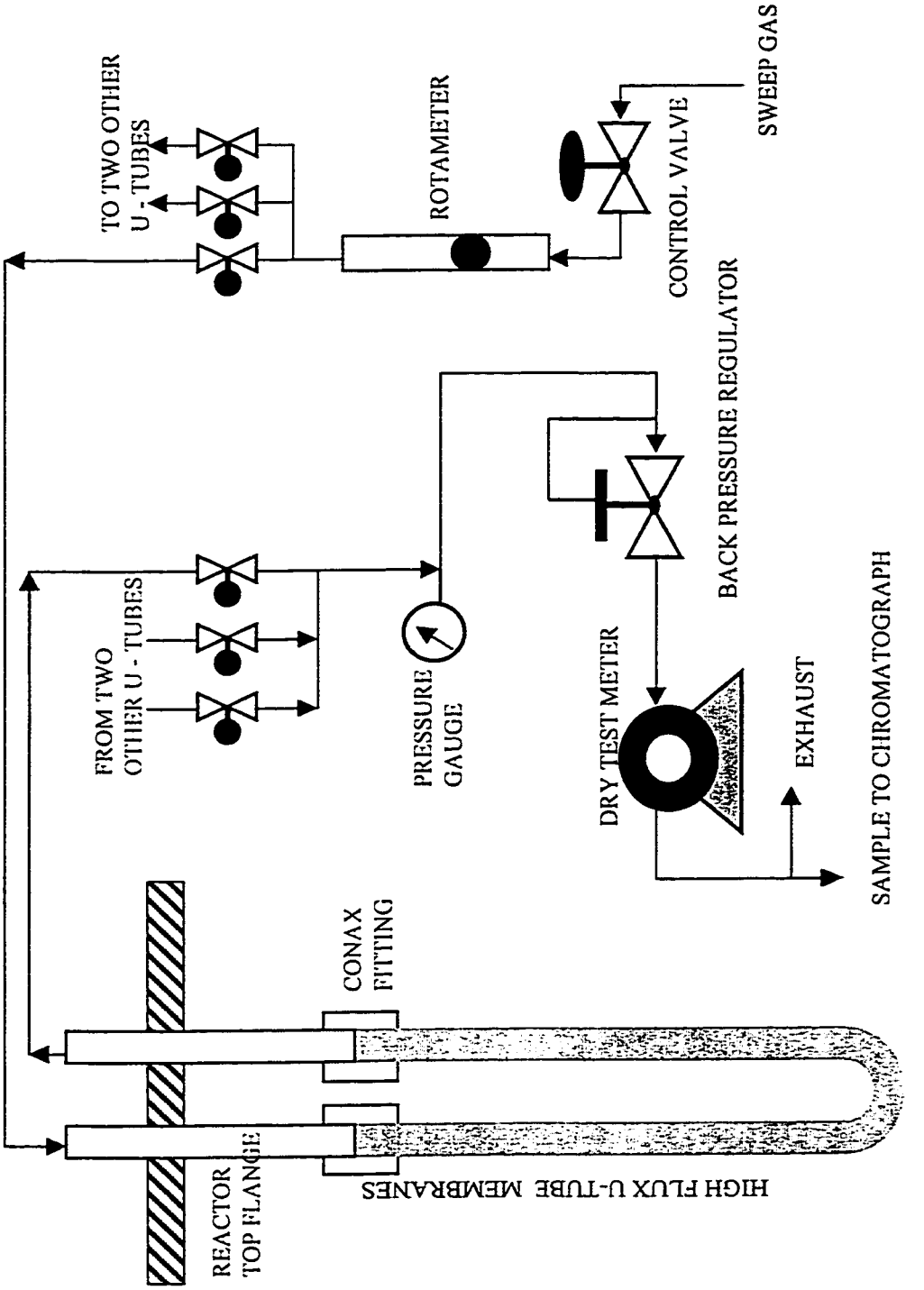

Figure 4.6: High-flux membrane module sweep and exhaust system

difference in thermal conductivity between the reference gas and the gas being analyzed. Argon was used as both carrier gas and reference gas. Column preconditioning was performed by passing argon at 25 ml/min through the column, which was connected to the injection port only. While performing this procedure the column temperature was maintained at 423 K while the injection/detection port temperature was kept at 443 K. The preconditioning was performed at room temperature for 30 minutes and 48 hours at the above-mentioned temperature. Calibration of the GC was carried out using two pre-analyzed gas mixtures. The injection/detection temperature, column temperature and carrier gas flow rate were optimized based on the separation and resolution of the various component gas peaks. The optimum conditions arrived at were as follows:

Column temperature: 393 K Injection/Detection temperature: 423 K

Carrier gas and reference gas: Argon Carrier gas flow rate: 25 ml/min

Reference gas flow rate: 34 ml/min

The Shimadzu CR601 Chromatopac integrator was programmed to record the results. The major integrator parameters are given below:

Width : 4 Minimum area rejection: 10

Slope: 400 Attenuation: 2

Drift: 0 Chart speed: 10 mm/min

A sample of a typical chromatogram of the exit gas is shown in Figure 4.7. Peaks appearing in the tail of the hydrogen peak were well resolved by the Chromatopac software.

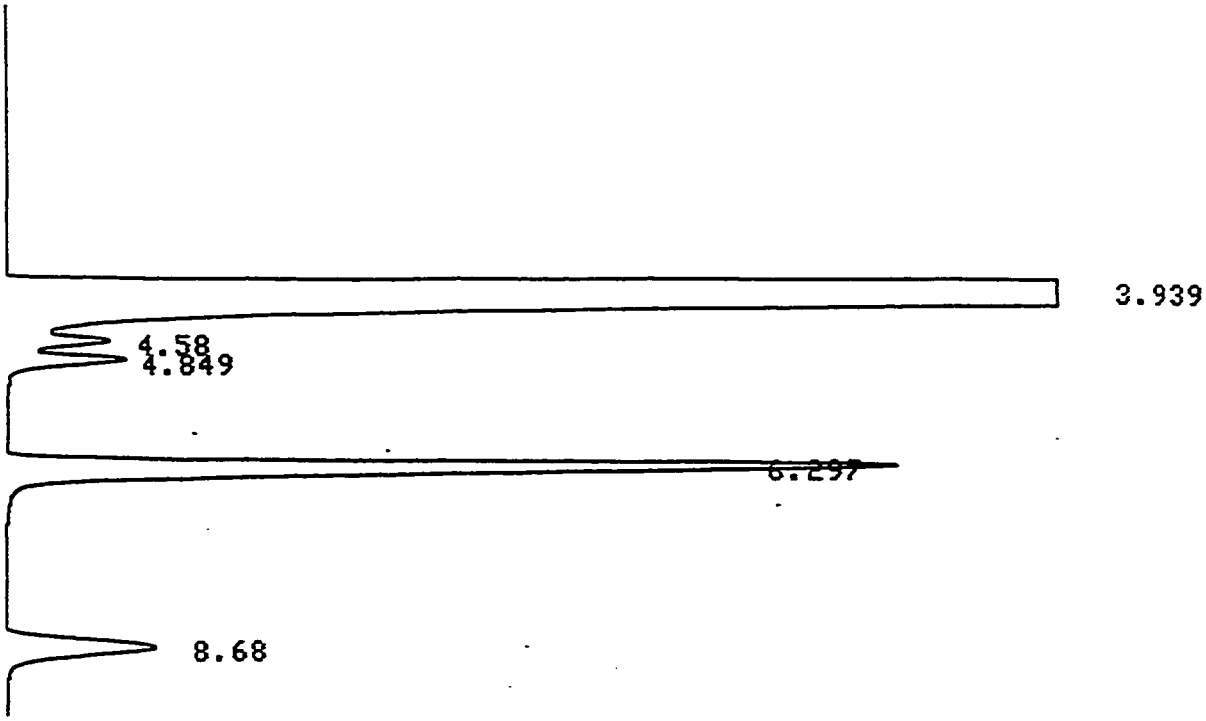

An exit gas sample of 80-microlitre size was injected giving the response:

Peak Number.	Time (min)	Response Area	Calibration Constant	Concentration Normalized (%)	Species Name
1	3.939	446533	$1X10^{-4}$	58	H_2
2	4.58	1883	$1.17X10^{-3}$	2.8	N_2
3	4.849	3214	$1.43X10^{-3}$	5.9	CO
4	6.297	36339	$4X10^{-4}$	18.8	CH_4
5	8.68	8239	$1.35X10^{-3}$	14.5	CO_2

Figure 4.7: A sample chromatogram of the reformer exit gas

4.6 Safety Systems

The pilot plant safety systems were set up for attended operations only. The system was prepared so that it could deal with runaway temperature, overpressure and leakage of combustible or poisonous gases. A hood was constructed over the entire pilot plant so that any leaking gas would be exhausted and not accumulate around the experimental area. Combustible gas sensors and carbon monoxide sensors were installed in the hood as well as outside to alarm personnel of any gas buildup. The sensors were connected to a controller which had an alarm to warn the operators. The system was explosion proof and had an independent electrical supply.

The fail-safe system for runaway conditions was essentially a magnetic switch and a manual start/stop switch. The power supplies to the radiant electric heaters and the shut off solenoid valves on the hydrogen, methane, and oxygen feeds were routed through this magnetic switch. The magnetic switch could be shut off either manually using the start/stop switch or by the fail-safe controller connected to the shell side thermocouple of the feed preheater (FPH). The pilot plant also had rupture discs connected to the process lines leading into and out the reactor. These discs would burst and release the system pressure through the vent system if system pressure went beyond 2.5 MPa.

4.7 Hydrodynamic investigation

Hydrodynamic properties of the steam methane reforming catalyst used for experimentation were essential for design and scale up of the reactor. The pilot plant was used for this investigation. The reforming catalyst, fluid bed height, minimum fluidization velocity and isothermality of the bed are discussed in this section. Adris

(1994) conducted a more detailed hydrodynamic investigation using similar catalyst in his Ph.D. thesis project.

4.7.1 Reforming catalyst

Steam methane reforming commercial catalyst supplied by United Catalysts Inc. was used for the experimentation. The catalyst contained the active component nickel oxide supported over α-alumina and was procured in the shape of Rashig rings which were then pulverized and reduced to a powder. The ground catalyst was sieved to a size range of 100 to 355 microns. This corresponded to a Geldart B type powder (Geldart, 1973). The reforming reactor was initially charged with 3.5 kg of powdered catalyst with the following sized distribution.

Size range (μm)	90-125	125-180	180-250	250-300	300-355
Mass %	11.8	24.7	35.3	13.6	14.6

The mean diameter of the catalyst particles was calculated to be 187 μm. The fresh catalyst was fluidized for twelve hours to round off the sharp edges of the fresh particles, which in turn led to some reduction in catalyst size.

The catalyst also required a reduction procedure before experimentation to reduce nickel oxide to active nickel. Passing a hydrogen nitrogen mixture through the catalyst bed at 623 to 823 K for six to eight hours was sufficient for this purpose.

4.7.2 Minimum fluidization velocity

The minimum fluidization velocity is a key parameter used to characterize the hydrodynamic properties of the catalyst. Experiments were devised to determine the minimum fluidization velocity as a function of bed temperature. One of the widely used correlations to determine the minimum fluidization velocity is given by Wen and Yu (1966) for small particles:

$$U_{mf} = \frac{d_p^2\left(\rho_p - \rho_g\right)g}{1650\mu} \qquad \left[Ar = \frac{\rho_g \cdot g \cdot \left(\rho_p - \rho_g\right)d_p^3}{\mu^2} < 10^3\right] \qquad (4.1)$$

The dependence of minimum fluidization velocity on temperature is pronounced because of the temperature effect on the viscosity of the fluid. Knowlton (1990) reviewed the effects of temperature and pressure on hydrodynamic parameters. A variation of pressure has a negligible effect on minimum fluidization velocity for low Archimedes numbers ($Ar < 10^3$). In the temperature and pressure range of our interest, the Archimedes numbers are well below 1000. Figure 4.8 shows the predictions of the Wen and Yu correlation as well as the experimentally determined values. There is a slight overprediction in the minimum fluidization velocity with temperature associated with this correlation.

4.7.3 Bed height

The bed height determines the active heating surface area as well as the volume for reaction conversion. Bed height was determined experimentally by differential pressure drop between the pressure taps. The pressure drop due to the entrained catalyst in the freeboard was found to be negligible compared to the pressure drop associated with

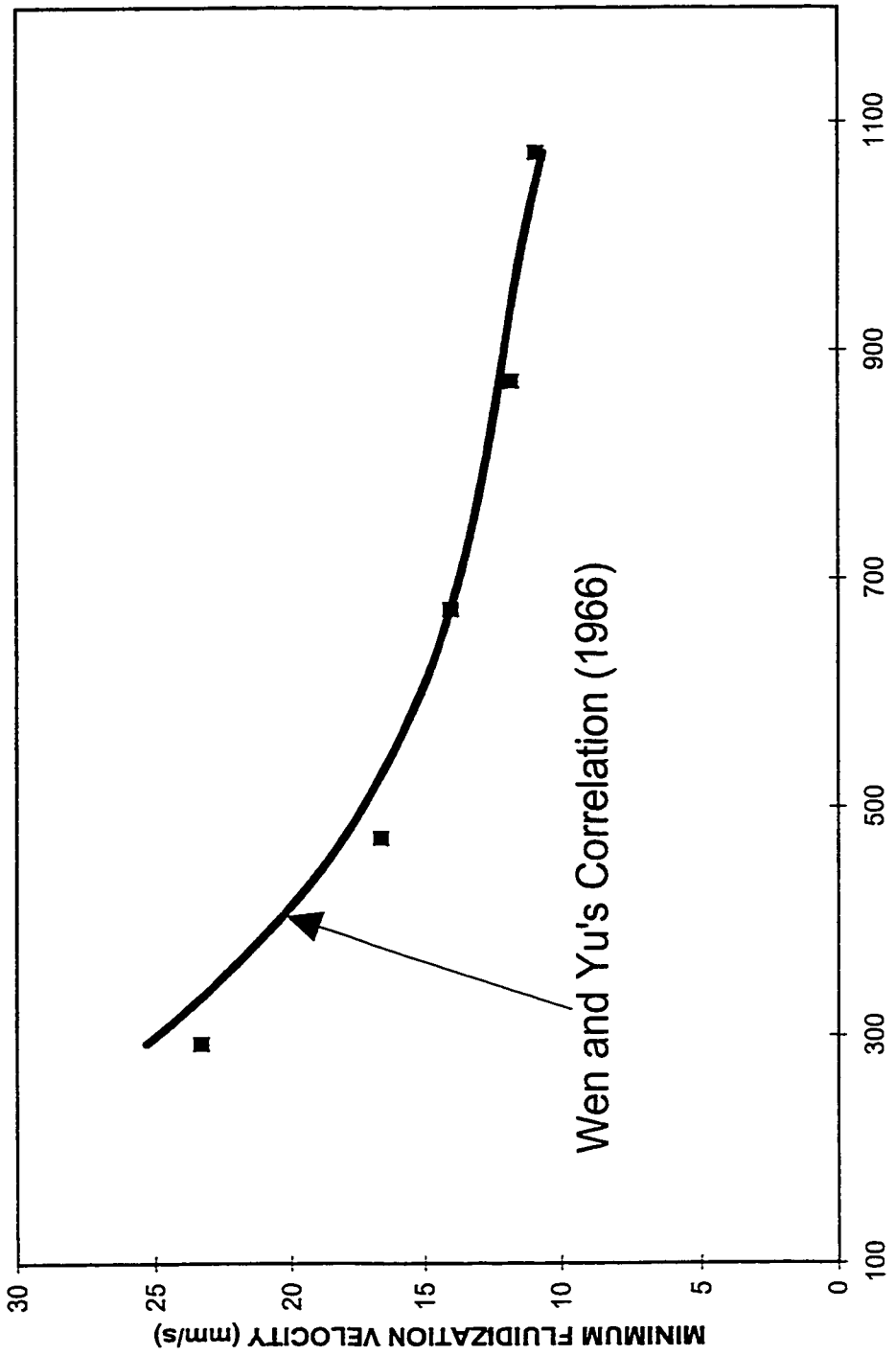

Figure 4.8: Minimum fluidization velocity versus bed temperature. [catalyst weight = 3.4 kg, bed height (static) = 0.24 m]

the bed. The packed bed (static) height was about 0.23 m, while the fluidized bed (expanded) height was between 0.35 to 0.39 m for the range of superficial gas velocities examined.

The pressure drop across PR7 and PR1 (Figure 3) plus the pressure drop from PR1 to the distributor gives the total pressure drop. The drop between PR2 and PR3 approximated the pressure drop from PR1 to the distributor. The total pressure drop was divided by the drop between PR2 and PR3, which were 85 mm apart, and multiplied by 85 mm to give the bed height. A plot of bed height with temperature is given in Figure 4.9. A plot of bed height as a function of superficial velocity is given in Figure 4.10.

The plots show that the bed height does not change appreciably in the range of temperatures and superficial velocities in which the reaction-permeation experiments were conducted. The procedure can be used to estimate bed height and maintain it to a desired level during experimentation.

4.7.4 Isothermality of the fluid bed

Before proceeding with reaction permeation experiments the thermal uniformity of the fluidized bed at any axial position with time were determined. In experiments with nitrogen, it was found that a superficial velocity of five times the minimum fluidization velocity was sufficient to attain isothermality of the fluidized bed. Hence, the gas velocity was maintained above five times the minimum fluidization velocity during the reaction permeation experiments. The temperatures recorded by the thermocouples immersed in the fluidized bed have been plotted for experimental runs at different bed temperatures in Figure 4.11 and demonstrate that the bed was isothermal.

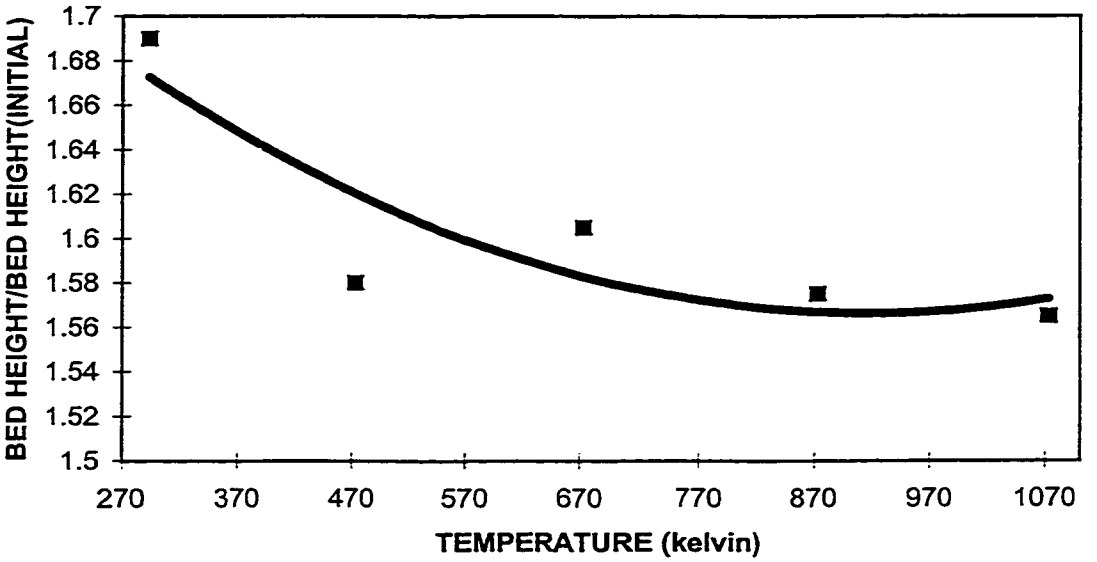

Figure 4.9: Bed expansion with increasing bed temperature at 110 mm/s superficial gas velocity {Bed height(initial)=0.23m}

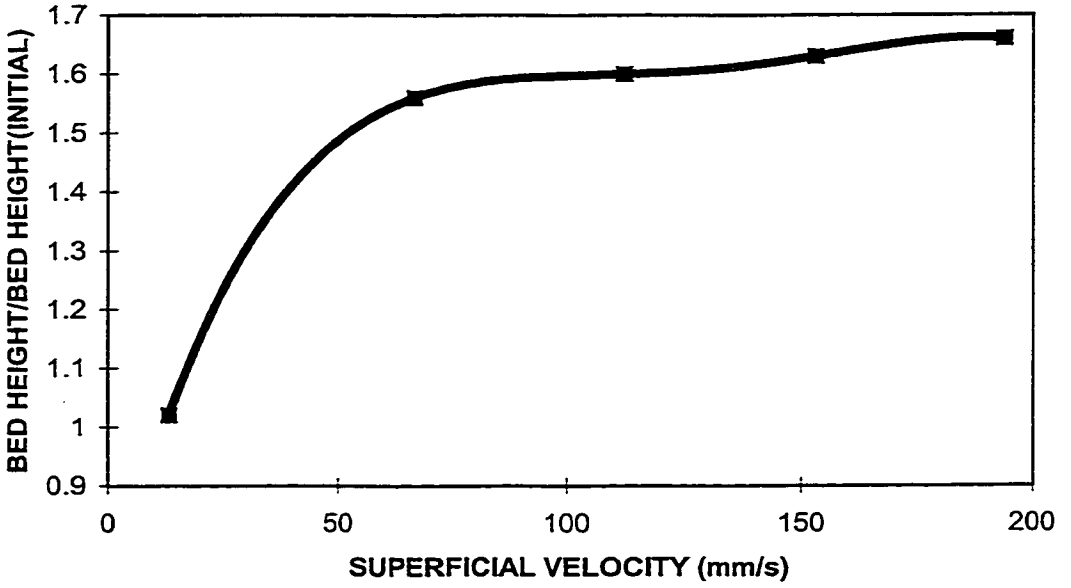

Figure 4.10: Bed expansion with increasing superficial gas velocity at 673 Kelvin {Bed height (initial)=0.23 m}

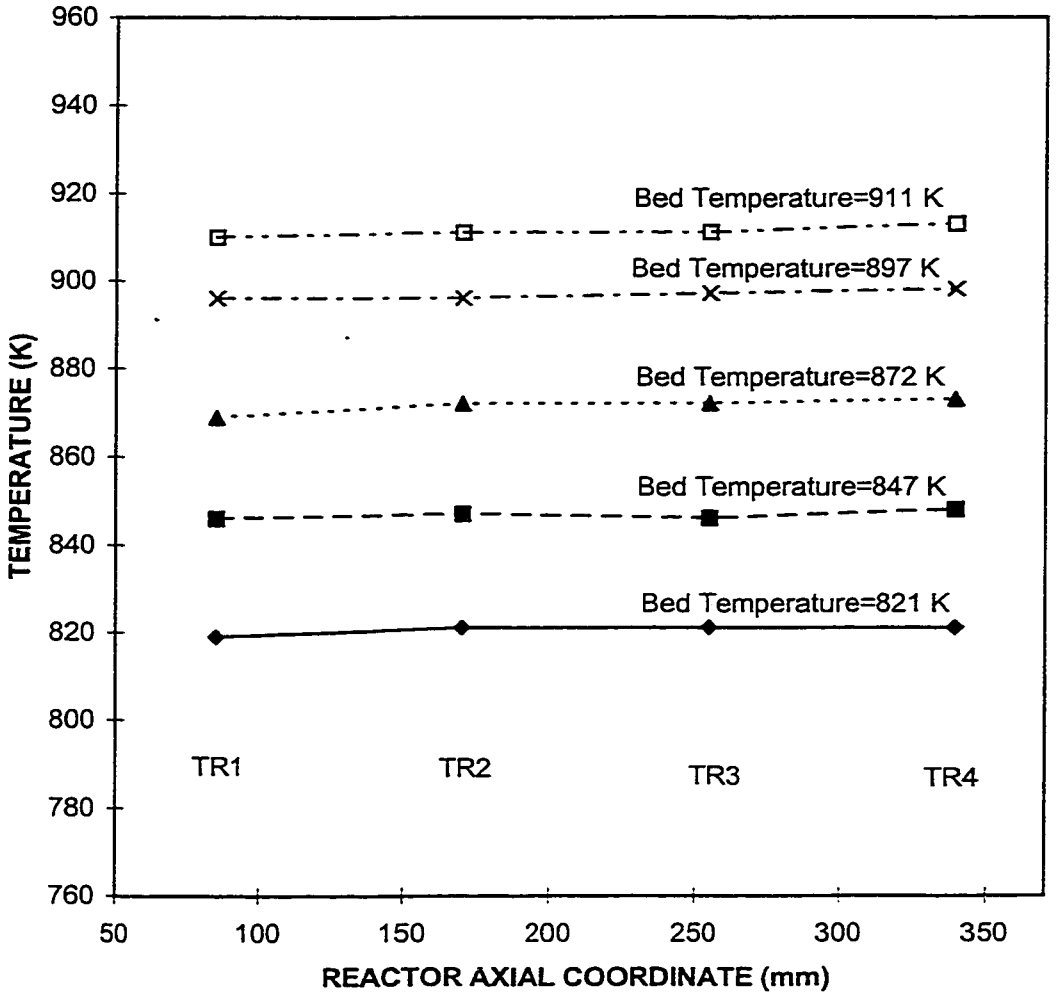

Figure 4.11: Bed temeperatures recorded by the thermocouples TR1 to TR4 immersed in the catalyst bed for runs at various bed temperatures showing isothermal behaviour

4.8 Experimental Procedures

The procedures followed during experimentation ensured that the pilot plant was started up, operated and shut down safely. The catalyst retained its activity, the results were at steady state and the High-flux membranes and other equipment were not damaged. These procedures also prevented any runaway conditions.

STARTUP

1.) Adjust N_2 purge gas at 1.2MPa, switch on the purge rotameters at the 30 mark on the scale, pressurize the external shell of the feed preheater to 0.5 MPa and open the nitrogen valve to pressurize the distilled water tanks.

2.) Initiate N_2 process gas through the mass flow controller, setting it at the 50% mark and pressure the system to 0.5 MPa. Switch on the feed preheater and the reactor (main and freeboard) heaters.

3.) When reactor reaches 623 K, introduce H_2 through the mass flow controller, setting it at the 40% mark; increase the pressure to 0.7 Mpa and equalize the feed preheater shell pressure.

4.) Maintain the same conditions for 6-8 hours until the effluent H_2 concentration remains unchanged.

5.) Introduce water into the system through the rotameter at the required ratio, heat up the reactor to the desired process temperature, and adjust to the required process pressure.

6.) After thermal stability is reached, initiate CH_4 flow through the mass flow meter and shut off process N_2 flow.

7.) After the chromatograph shows reproducible concentrations of CO and CO_2, shut off H_2 flow.

8) Start the sweep N_2 rotameters and adjust the membrane module pressure.

9) Wait until the reactor attains thermal equilibrium, which is indicated when TR1 to TR4 show similar temperatures.

10.) Continue at a steady state until the chromatograph shows reproducible concentrations of H_2, CO and CO_2 for the exit gas and H_2 for the membrane gas.

EXPERIMENTAL

11) Fix the parameters for the experiment and check the system for steady state in pressure, temperature and flow.

12) Chromatographic analysis is done repeatedly until three consecutive analyses give similar results.

12) Note results and record parameters.

SHUTDOWN

13.) Switch off the CH_4 supply and replace it with H_2. Switch the heaters off.

14) Shut off the sweep gas and isolate the membrane modules.

15.) Cool the reactor to 573 K and shut off the supply of H_2/N_2 mixture. Keep the purge meters on until the reactor cools down and completely depressurizes.

4.9 Variation of operating parameters

The major variables which were controlled were temperature, pressure, feed flowrate, feed steam methane ratio, membrane pressure and membrane sweep gas flowrate. Effort was made to vary only one of these variables during an experimental run

and to study the result. Methane conversion, hydrogen yield and hydrogen permeate flow were major dependent variables calculated from the experimental results.

4.10 Experimental results and discussion

In three separate sets of experimental runs, reactor pressure, reactor temperature and steam/methane ratio were varied while keeping other variables constant. These runs are described in the following paragraphs in detail. Methane conversion was a major calculated parameter indicating the extent of reaction and the consumption of methane by the reforming reactions. The hydrogen yield indicated the number of moles of hydrogen produced for every mole of methane fed at the given operating conditions. The reactor pressure was the time average values of the absolute pressures. Reactor temperature was an average of temperatures TR1, TR2, TR3 and TR4. The reactor had by experiment, sufficient catalyst such that if more was added, there was no change in exit composition, this was proven in a separate set of experiments reported in Chapter 6. The reactor freeboard contained entrained catalyst and was heated so that reverse reactions were probable. All the experiments were carried out at gas superficial velocities above the requirement of five times the minimum fluidization velocity. Additionally, runs were conducted with a range of superficial gas velocities to further verify this limitation. Several more sets of temperature and pressure variation runs were conducted and are documented in the Appendix. Also many runs were repeated several times to evaluate the repeatability of the experimentation.

Experimental runs were also conducted by varying the gas flowrate and pressure on the membrane sweep side. Runs were conducted with two different membrane side

pressures and the results were compared. Similarly results were plotted with and without sweep gas flow. A measured flowrate of nitrogen was used as the sweep gas; by evaluating its exit composition, the flowrate of permeate hydrogen could be determined.

The experimental results have been compared to the composition obtained by a batch reactor without permeation at equilibrium. A Gibbs minimization program, explained in detail in Chapter 5 was used to evaluate the equilibrium composition.

In one set of runs, the reactor temperature was varied. In these runs, the pressure in the reactor was kept constant at around 1.0 MPa. The methane and steam flowrates were maintained constant at 45 and 138 mols per hour respectively. The sweep gas pressure was maintained at 0.14 MPa and the sweep gas flowrate was constant at 45 mol/h. The methane conversion increased with an increase in reactor temperature. The conversions were found to be considerably higher than equilibrium reactor values as shown in Figure 4.12, a result of the hydrogen permeation through the High-flux membranes. At a reactor temperature of 821 K the methane conversion was 36.5% and increased to 57.5% at a temperature of 911 K as shown in Figure 4.12. The corresponding equilibrium conversions were 25.8% and 43.1% respectively. The experimental runs showed that the hydrogen yields are higher than the equilibrium values as shown in Figure 4.13 and increased considerably from 1.52 at 821 K to 2.16 at 911 K. The hydrogen permeate flow also increased from 23.6 mol/h to 32.6 mol/h due to increased permeation. The temperature run proves that a higher temperature is beneficial for increased methane conversion and hydrogen production.

In another set of runs, the reactor pressure was varied. During these runs the temperature in the reactor was kept constant at 873 K. The methane and steam flowrates

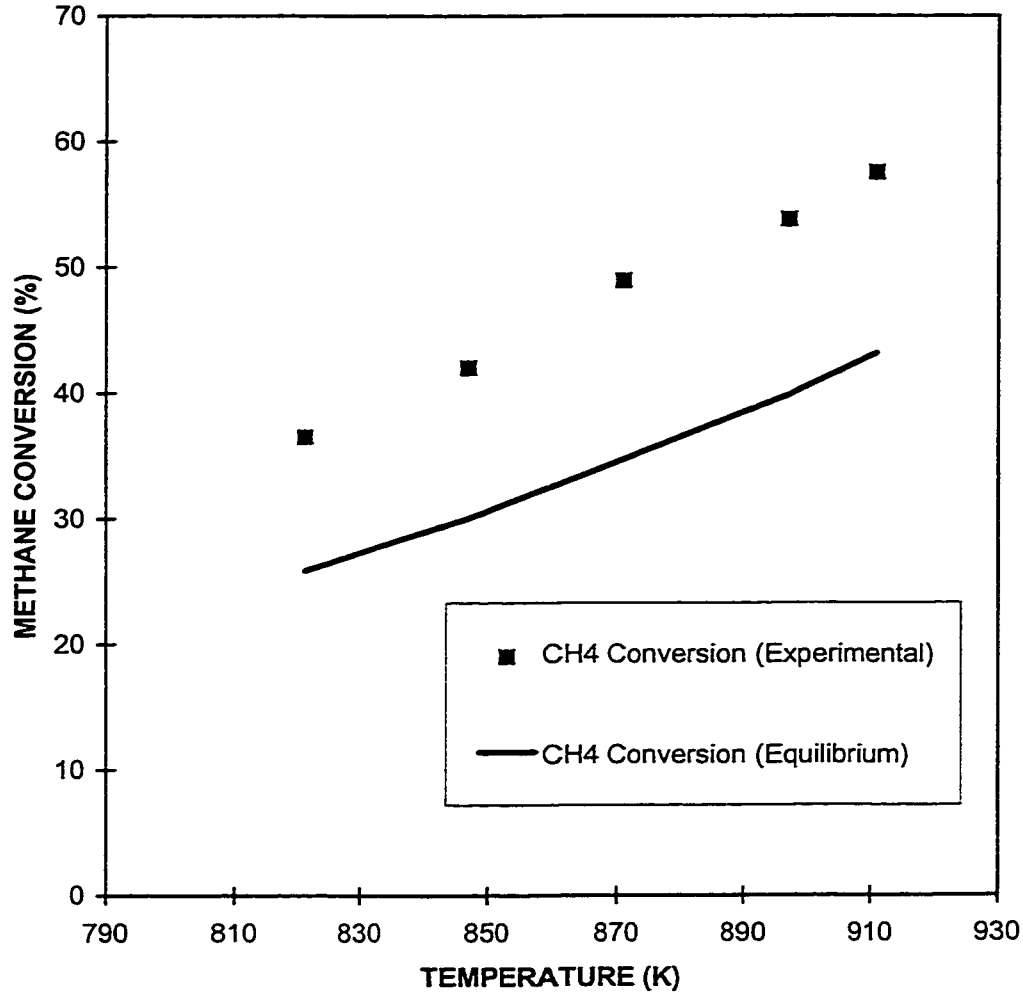

Figure 4.12: EFFECT OF TEMPERATURE VARIATION ON METHANE CONVERSION

P=0.99MPa., Methane flowrate=45mol/h. Steam flowrate=138mol/h. Steam methane ratio= 3.1. Sweepgas pressure=0.14MPa. Sweep gas flowrate=45mol/h.

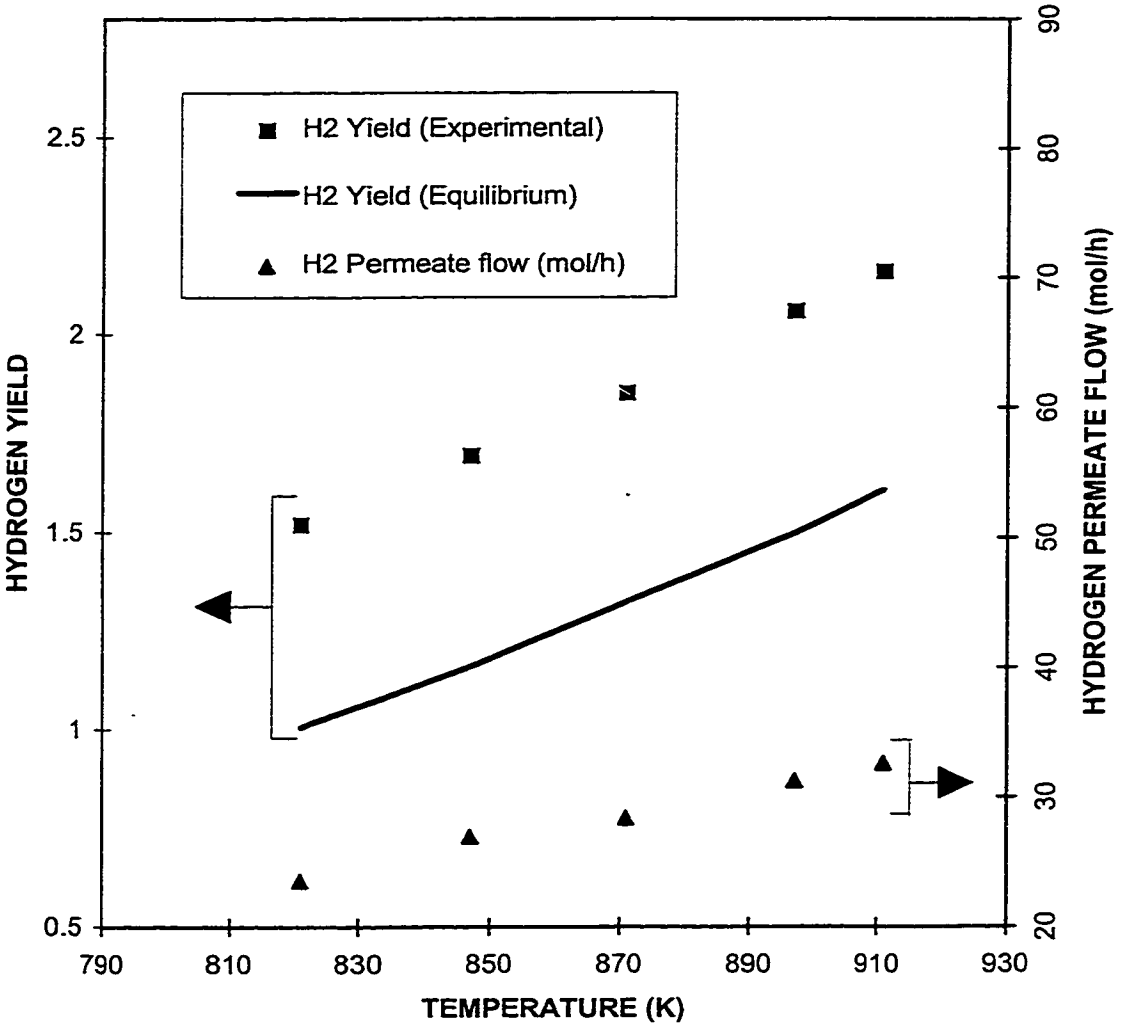

Figure 4.13: EFFECT OF VARIATION IN TEMPERATURE ON HYDROGEN YIELD AND PERMEATE FLOW

P=0.99MPa., Methane flowrate=45mol/h. Steam flowrate=138mol/h. Steam methane ratio= 3.1. Sweepgas pressure=0.14MPa. Sweep gas flowrate=45mol/h.

were maintained constant at 33.7 and 138 mols per hour respectively. The sweep gas pressure was maintained at 0.14 MPa and the sweep gas flowrate was constant at 45 mol/h. The methane conversion decreased marginally with an increase in reactor pressure. As shown in Figure 4.14, the conversions were found to be considerably higher than equilibrium reactor values due to hydrogen permeation through the High-flux membranes. At a reactor pressure of 0.7 MPa, the methane conversion was 60%, decreasing to 53% at a pressure of 1.0 MPa as shown in Figure 4.14. The corresponding decrease in the equilibrium reactor values were 50% and 42% respectively. These experimental runs showed that hydrogen yield decreased moderately from 2.35 at 0.7 MPa to 2.12 at 1.0 MPa. These yields are higher than the equilibrium values, as shown in Figure 4.15. Interesting to note are the increases in hydrogen permeate flow from 23 mol/h to 27 mol/h with increasing pressure even though hydrogen yield and methane conversion both show a decreasing trend. Increase in hydrogen permeation occurred because with an increase in reactor pressure there was a resulting increase in hydrogen partial pressure difference across the High-flux membrane. This hydrogen partial pressure difference is the driving force for permeation, hence the increased permeate flow. The pressure run proves that higher reactor pressures are beneficial for increasing hydrogen permeate flow.

In another set of runs, the steam methane ratio of the feed was varied from 2.4 to 4.1. In these runs, the temperature of the reactor was kept at 873 K and the pressure was maintained at 1.0 MPa. The steam flowrates were maintained at 138 mol/h while the methane flowrate was varied from 58 to 33.7 mols per hour to vary the ratio. The methane conversion increased from 37.2% for a steam-methane ratio of 2.4 to 54.6% for

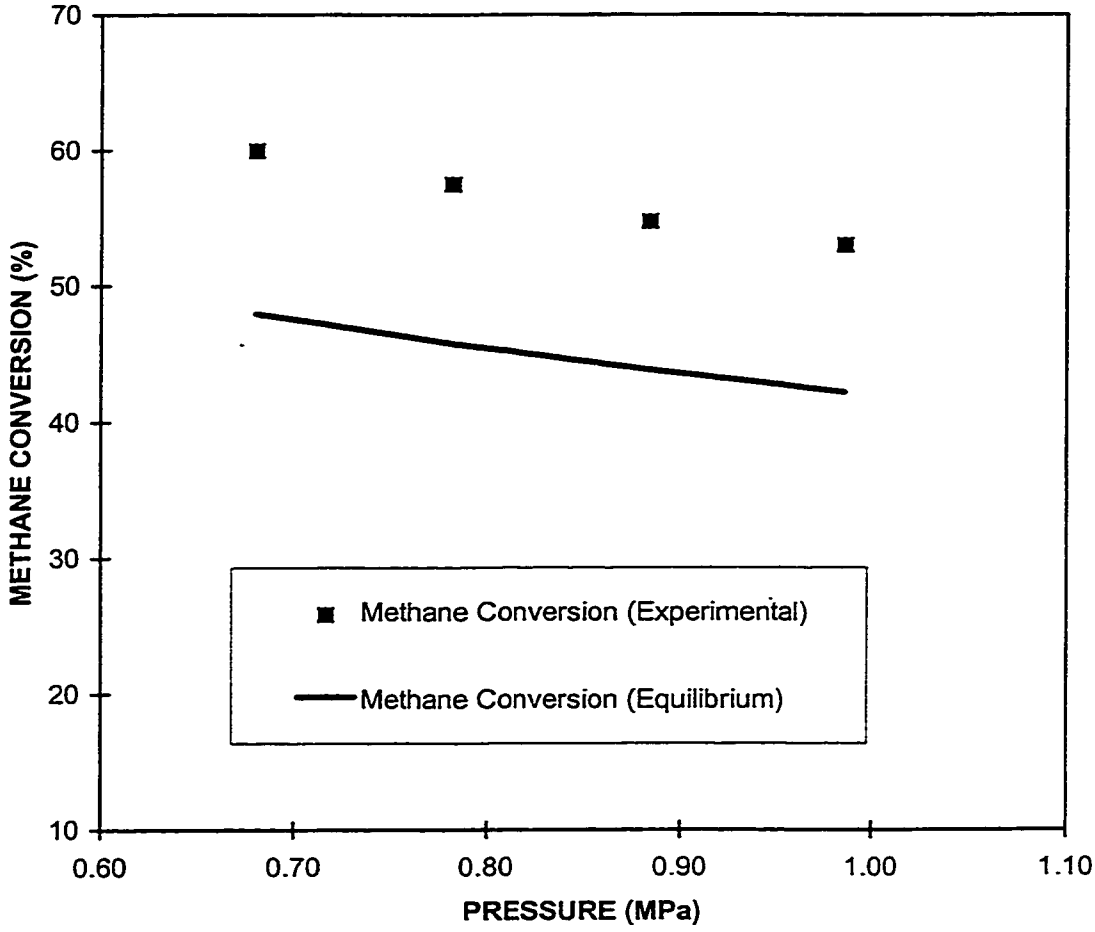

Figure 4.14: EFFECT OF VARIATION OF PRESSURE ON METHANE CONVERSION

T=873 Kelvin, Methane flowrate=33.74mol/h. Steam flowrate=138mol/h. Steam methane ratio= 4.1. Sweepgas pressure=0.14MPa. Sweep gas flowrate=45mol/h.

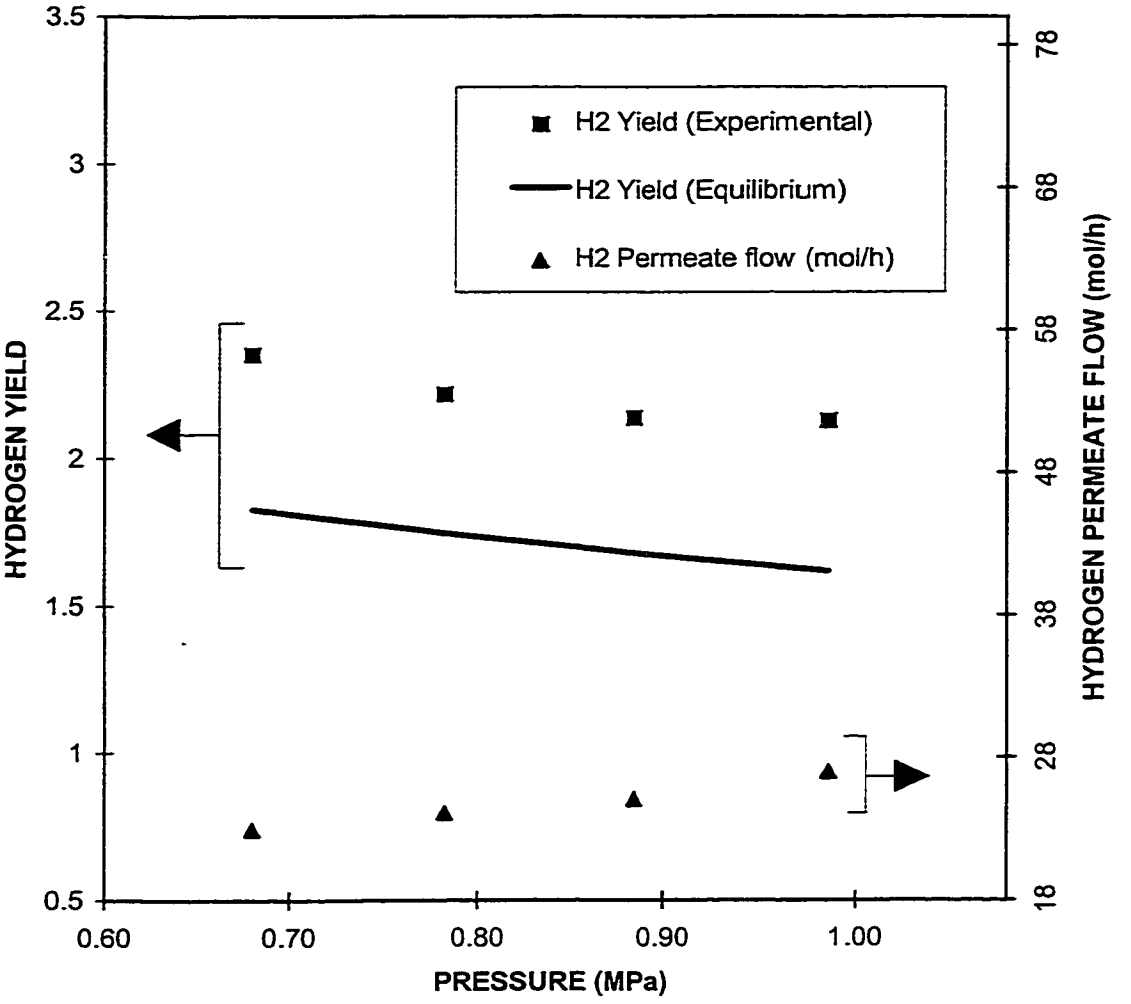

Figure 4.15: EFFECT ON HYDROGEN YIELD AND PERMEATE FLOW WITH PRESSURE VARIATION

T=873 Kelvin, Methane flowrate=33.74mol/h. Steam flowrate=138mol/h. Steam methane ratio= 4.1. Sweepgas pressure=0.14MPa. Sweep gas flowrate=45mol/h.

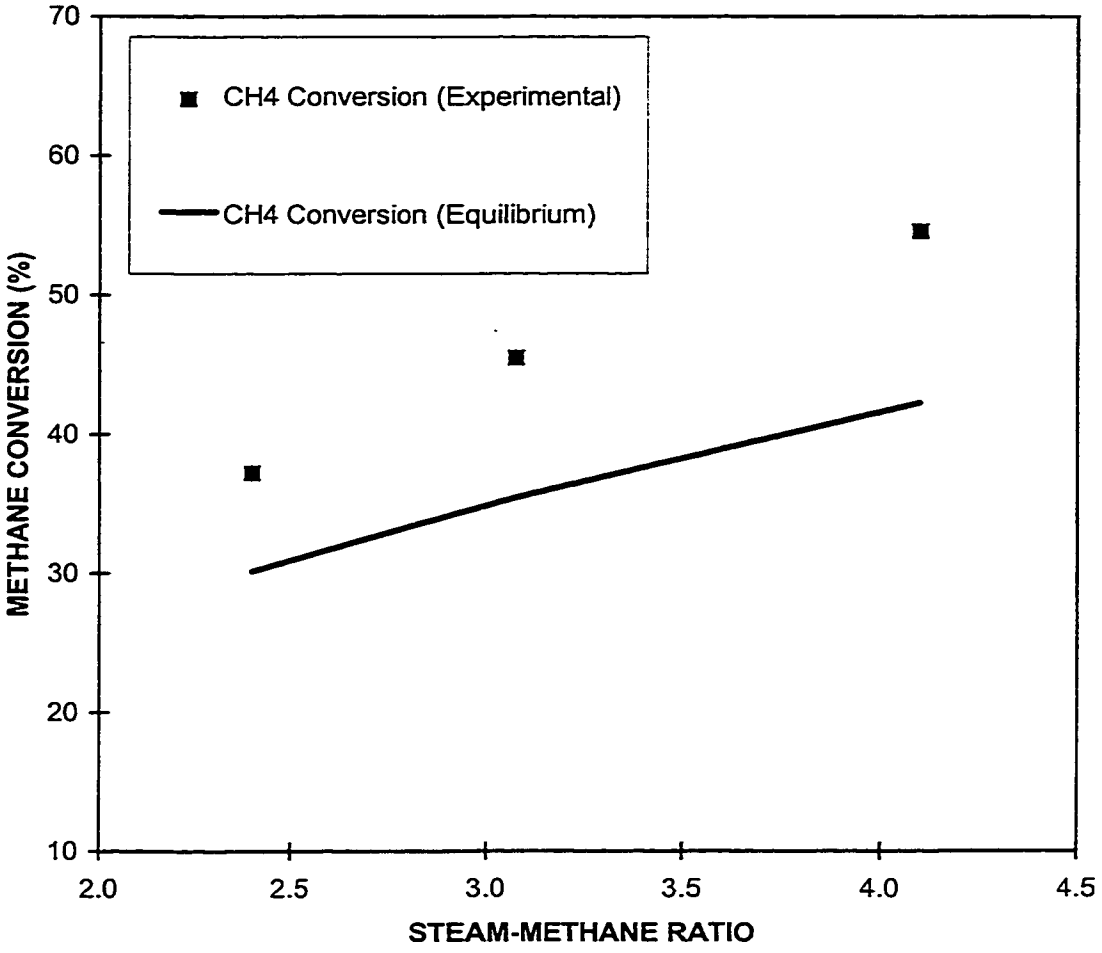

Figure 4.16: METHANE CONVERSION WITH STEAM-METHANE RATIO VARIATION

P=0.99 MPa, T=873 K. Steam flowrate=138mol/h. Sweepgas pressure=0.14MPa. Sweep gas flowrate=45mol/h.

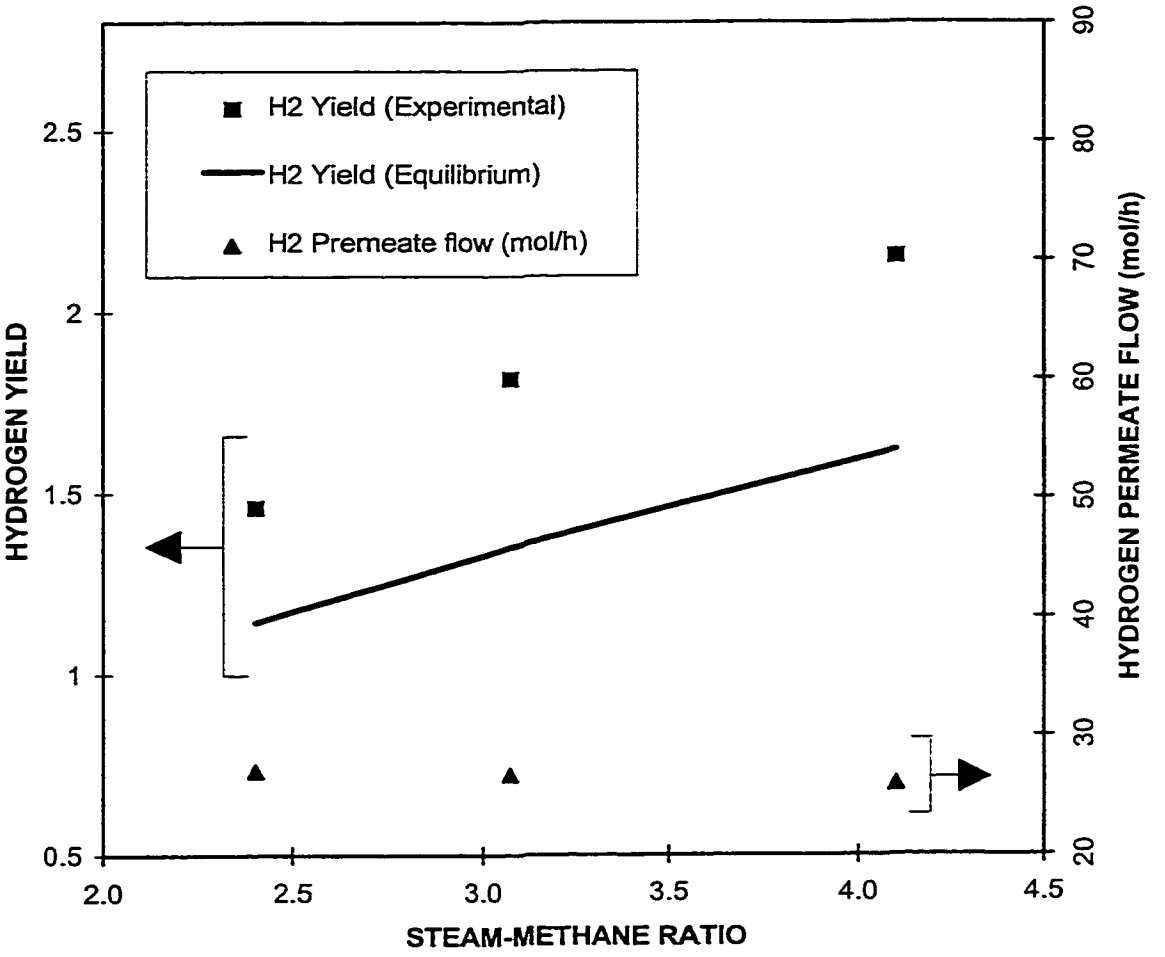

Figure 4.17: HYDROGEN YIELD AND PERMEATE FLOW WITH VARIATION OF STEAM-METHANE RATIO

P=0.99 MPa, T=873 K. Steam flowrate=138mol/h. Sweepgas pressure=0.14 MPa. Sweep gas flowrate=45mol/h.

a steam-methane ratio of 4.1 as shown in Figure 4.16. The corresponding equilibrium conversions showed the same trend but were considerably lower than the experimental values. The hydrogen yield increased with an increase in steam-methane ratio, though the hydrogen permeate flow decreased marginally as shown in Figure 4.17. This was due to the decrease of hydrogen partial pressure in the reactor with an increasing steam-methane ratio. This set of runs proved that increasing the steam-methane ratio results in higher methane conversion and hydrogen yield but will not provide an increased hydrogen permeate flow.

In Figure 4.18 a comparison has been made between the present study (FBMR with High-flux Pd membranes) and the previous study (FBMR with thin walled Pd membranes) conducted by Adris (1994). The hydrogen permeate flow (mol/h) in the present study is on an average ten to fifteen times higher than that in Adris's study, as the High-flux membranes have a better permeation than the thin-walled membranes and can also withstand a higher pressure differential. It should also be noted that the methane feed flow rate in most of the runs of the previous study was higher than in the present study. Therefore, the improvement in percentage hydrogen recovery for the present investigation is even better than the percentage hydrogen recovery in Adris work. This comparison (Figure 4.18) indicates the overall improvement achieved by the present study.

The pressure on the membrane sweep side was varied and its effect on the conversion and yield was evaluated. Two sets of reactor temperature variation runs with different membrane sweep pressures have been compared in Figures 4.19 and 4.20. The methane conversion with a membrane sweep pressure of 0.14 MPa is higher than the

Figure 4.18: Comparison of hydrogen permeate flow in FBMR(High flux Pd membranes) and FBMR(Thin walled Pd membranes)

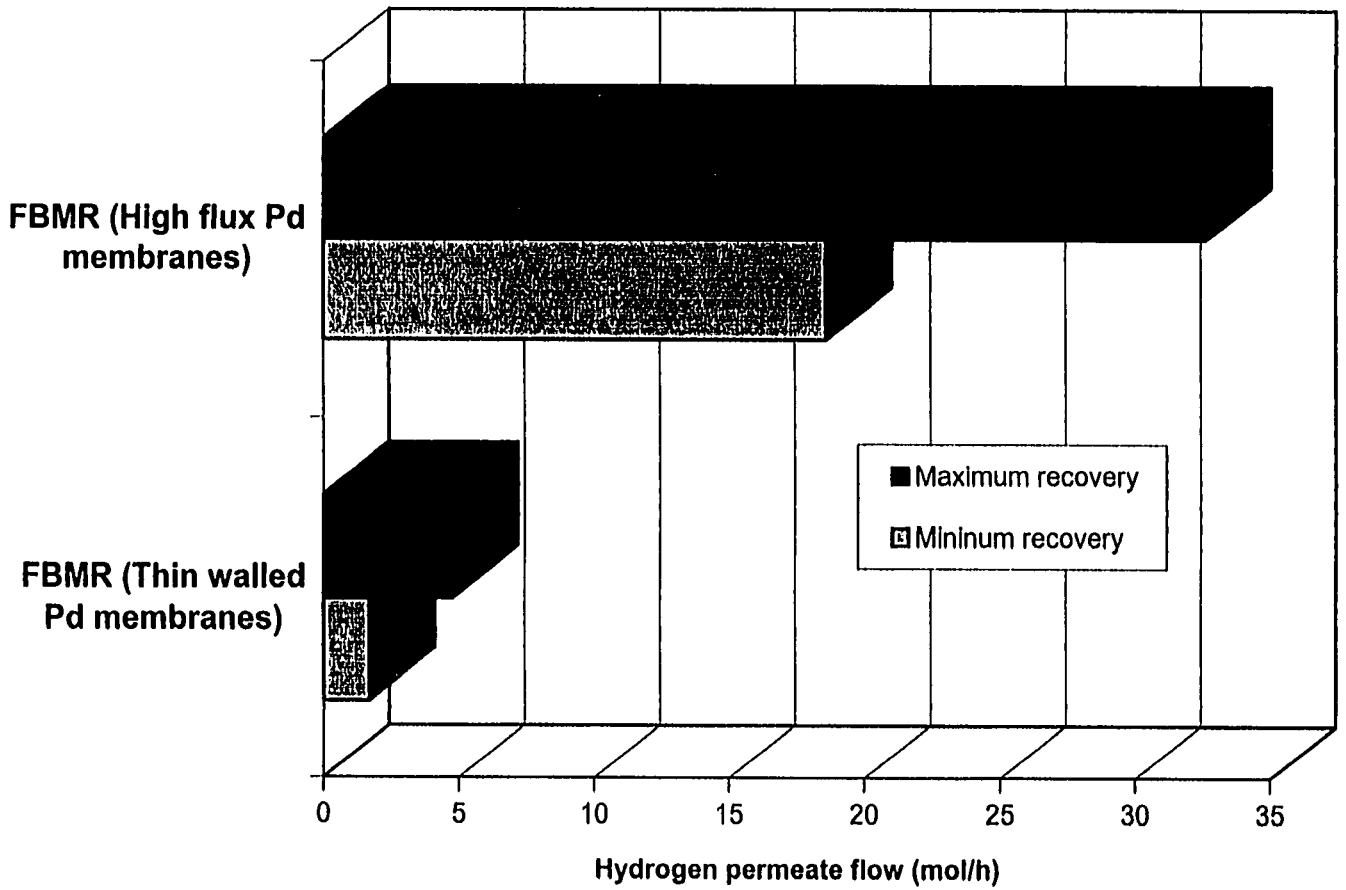

corresponding value for a pressure of 0.24 MPa (as shown in Figure 4.19). Lower membrane sweep pressure resulted in decreased partial pressure of hydrogen on the membrane side. This resulted in a higher hydrogen partial pressure difference across the membrane. The higher driving force for hydrogen separation resulted in higher hydrogen permeation leading to increased conversion of methane. Similar effects are also seen on hydrogen yield and permeate flow as shown in Figure 4.20. These comparative figures prove the benefits of decreased hydrogen partial pressure on the membrane sweep side.

Runs were conducted with and without sweep gas and the effect on the conversion and yield was evaluated. Two sets of reactor temperature variation runs; one with sweep gas and one without sweep gas on the membrane sweep side have been compared in Figures 4.21 and 4.22. The methane conversion is higher with than without sweep gas, as shown in Figure 4.21. Use of membrane sweep gas flow results in a decreased partial pressure of hydrogen on the membrane side, producing a higher hydrogen partial pressure driving force. The higher driving force for hydrogen separation results in higher hydrogen permeation, in turn leading to increased conversion of methane. The difference in hydrogen yields is not measurable, while the hydrogen permeate flow is moderately higher with sweep gas flow, as shown in Figure 4.22. These comparative figures conclusively prove the benefits of using sweep gas flow to reduce hydrogen partial pressure on the membrane side.

Another important design parameter is the superficial gas velocity through the bed. As we had an excess catalyst and the effectiveness factor was near 1.0, the effect of change in superficial gas velocity was expected to be negligible. Moreover, the superficial gas velocity changes with a variation in any parameter, pressure, temperature

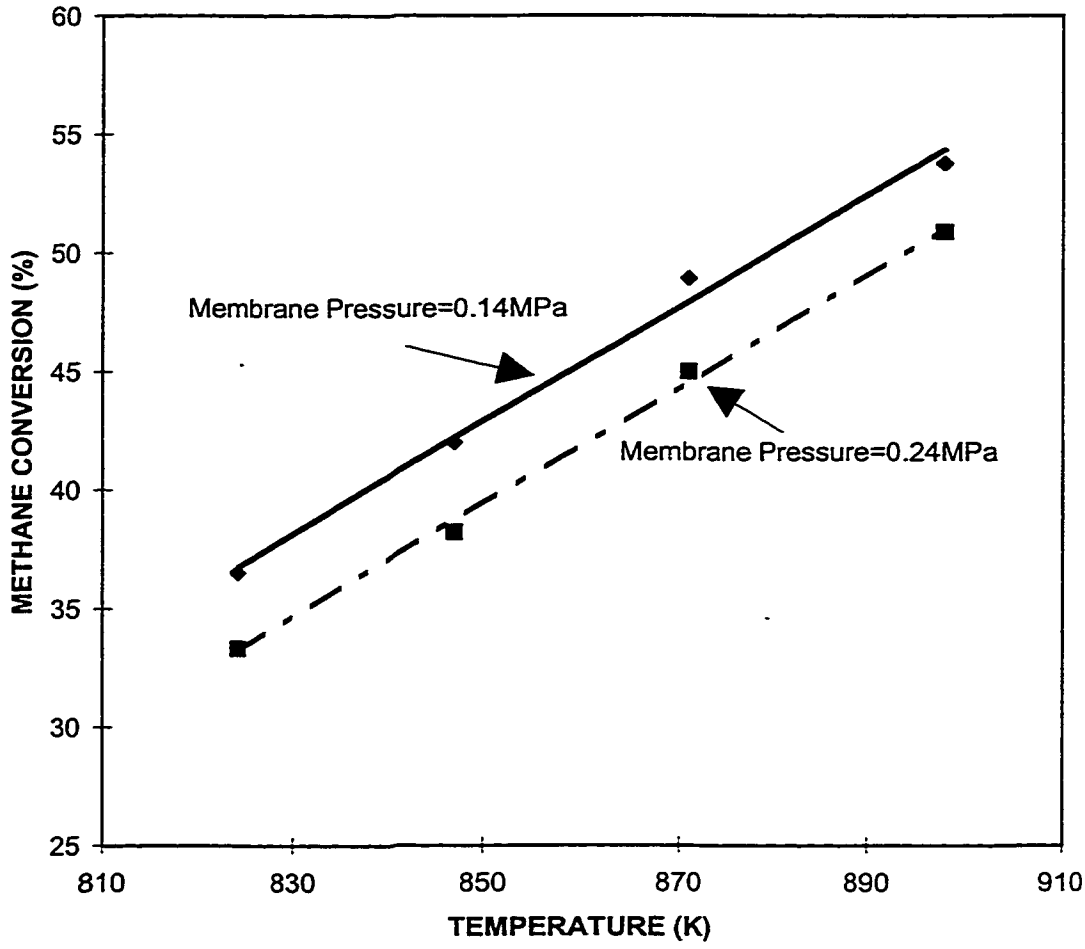

Figure 4.19: Comparison of methane conversions at two separate membrane pressures

P=0.99MPa., Methane flowrate=45mol/h. Steam flowrate=138mol/h. Steam methane ratio= 3.1. Sweep gas flowrate=45mol/h.

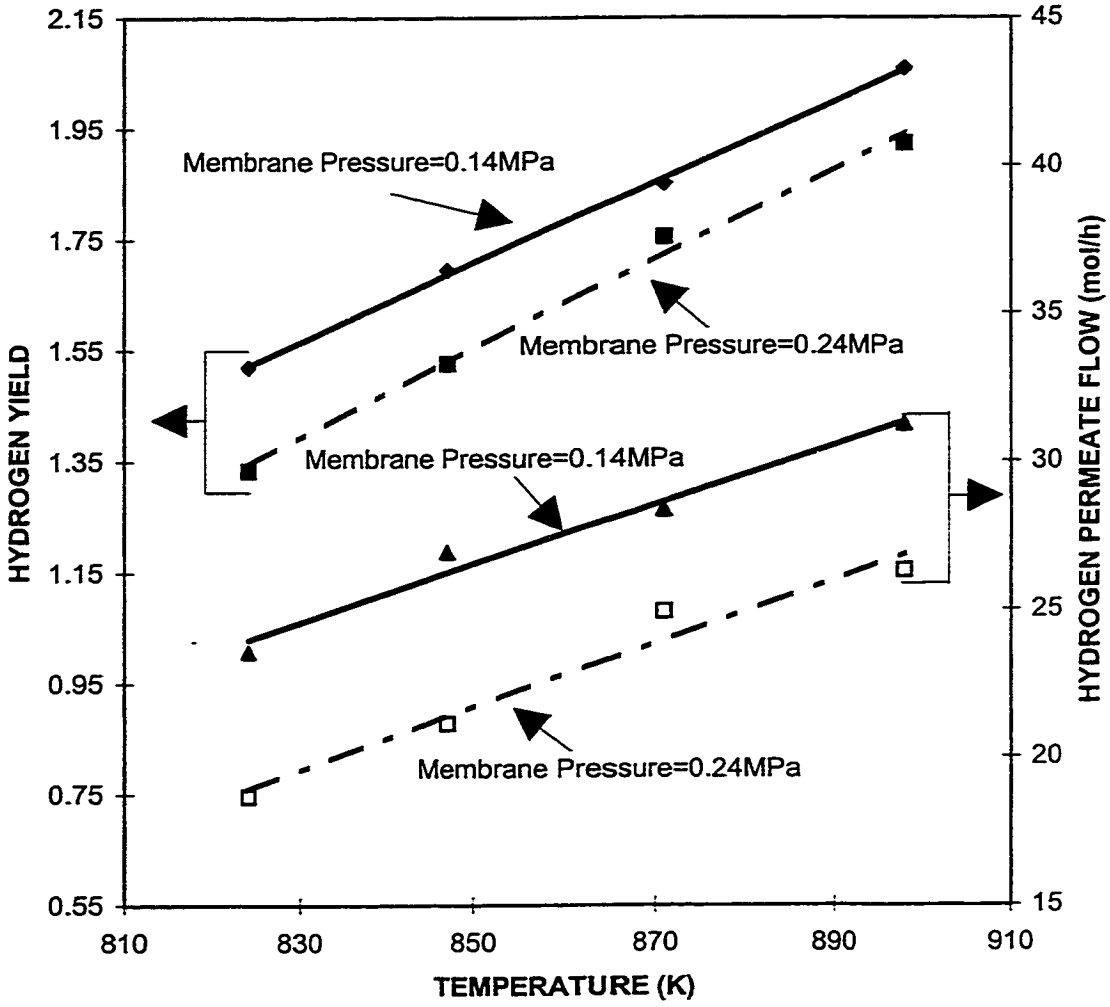

Figure 4.20: Comparison of hydrogen yield and permeate flow at two different membrane pressures

P=0.99MPa., Methane flowrate=45mol/h. Steam flowrate=138mol/h. Steam methane ratio= 3.1. Sweep gas flowrate=45mol/h.

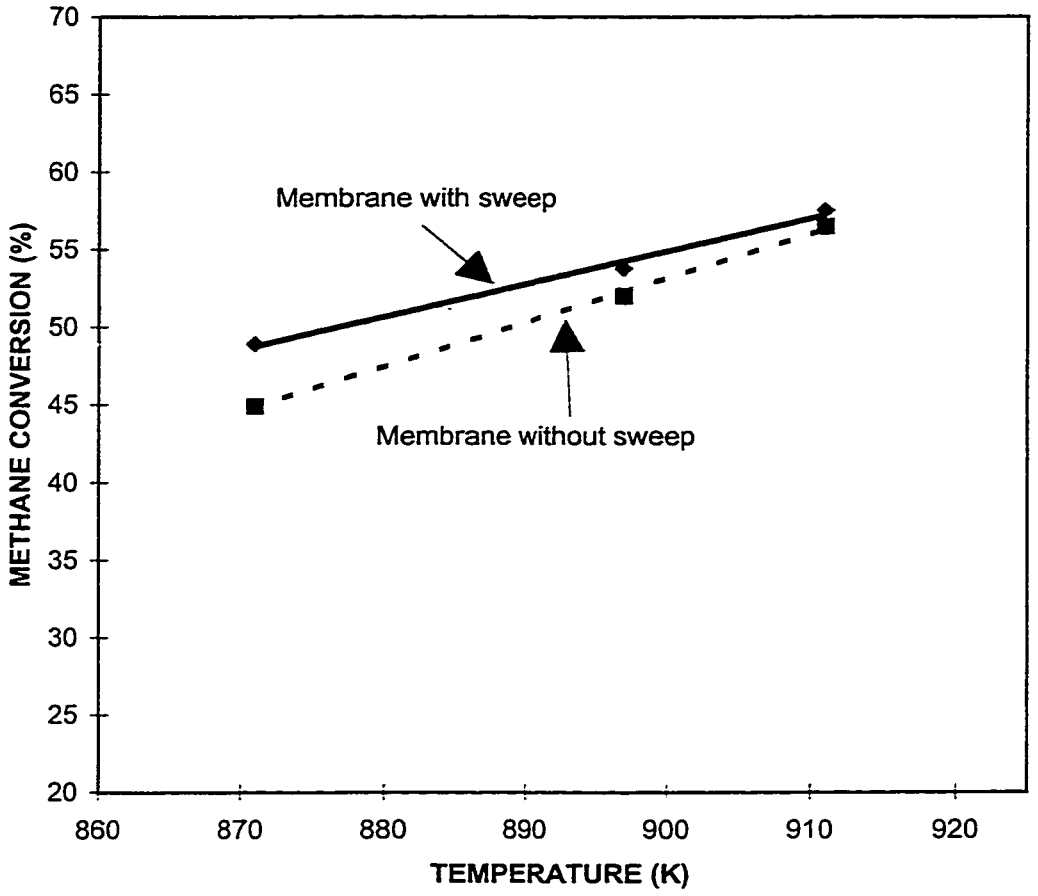

Figure 4.21: Comparison of methane conversions with and without sweep gas in the membrane

P=0.99MPa., Methane flowrate=45mol/h. Steam flowrate=138mol/h. Steam methane ratio= 3.1. Membarne pressure=0.14MPa. Sweep gas flowrate=45mol/h.

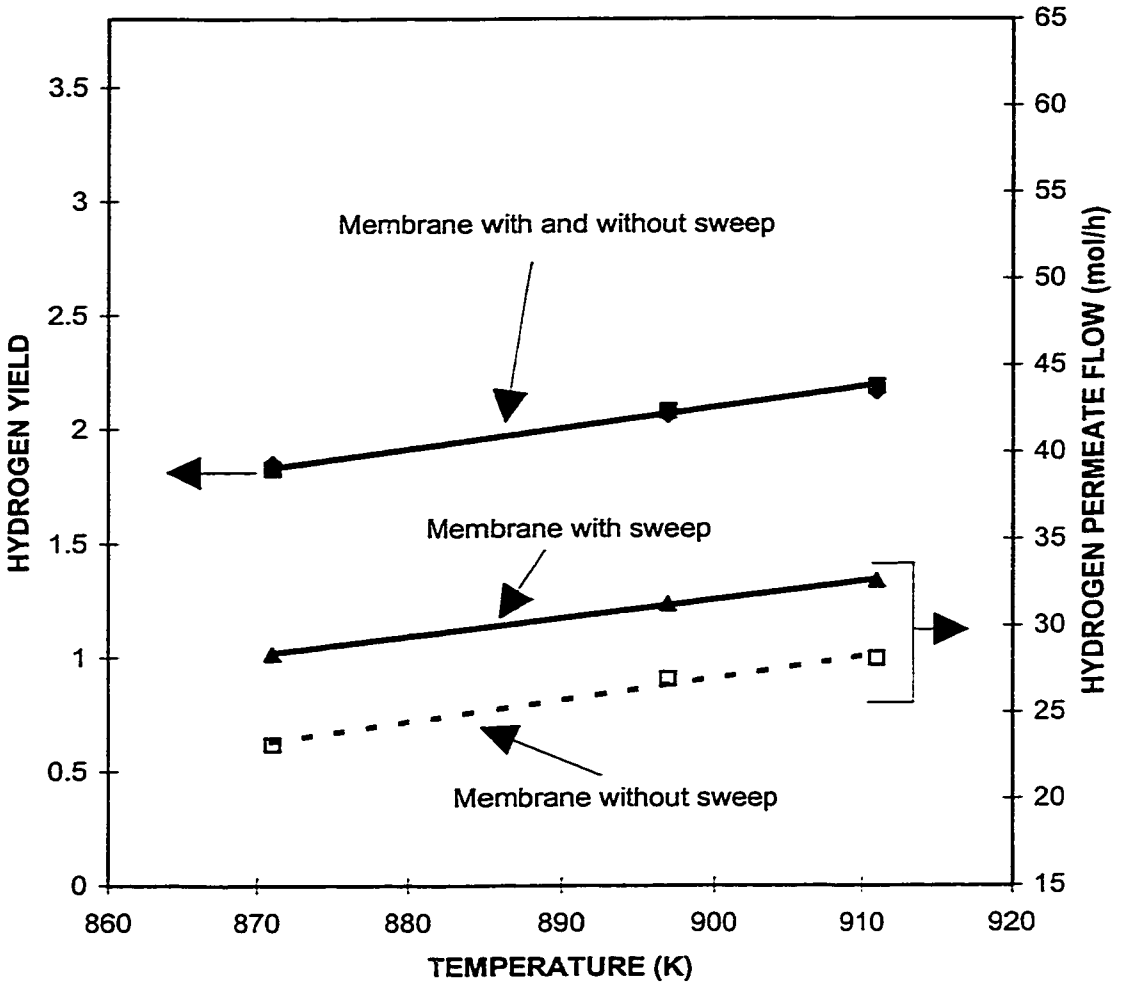

Figure 4.22: Comparison of hydrogen yield and permeate flow with and without sweep gas in the membrane

P=0.99MPa., Methane flowrate=45mol/h. Steam flowrate=138mol/h. Steam methane ratio= 3.1. Membarne pressure=0.14MPa. Sweep gas flowrate=45mol/h.

or feed flowrate. Thus it was crucial to prove that a change in superficial gas velocity would not affect the exit concentrations. The superficial gas velocity was varied and the other parameters were maintained constant. The resulting methane conversion and hydrogen yield were plotted as shown in Figure 4.23. The plot indicated that change in superficial gas velocity has a negligible or no effect on exit concentrations for our experimental runs.

As mentioned earlier the difference between the partial pressure of hydrogen in the reactor and on the membrane side is the driving force for permeation. The driving force at the exit of the reactor must be evaluated to indicate if additional membrane capacity would further help to increase permeation. The driving force at the reactor exit for a pressure variation run has been plotted in Figure 4.24. If the driving force is zero, there will be no permeation even if there is hydrogen in the reactor. Figures 4.24 shows that there is residual driving force at the exit of the reactor and hence room for an increase in permeation capacity. Another parameter of interest is the percentage (%) hydrogen recovery, which are the moles per hour of hydrogen recovered through the membrane divided by the total moles per hour of hydrogen produced in the reactor, expressed as a percentage. The percentage hydrogen recovery plotted in Figure 4.24 shows that a larger quantity of hydrogen could be recovered by increasing the permeation capacity.

4.11 Conclusions

The study proved the viability of U-tube spring reinforced High-flux membrane modules in a pilot plant reformer. The membranes were able to successfully perform in the reforming reactor environment.

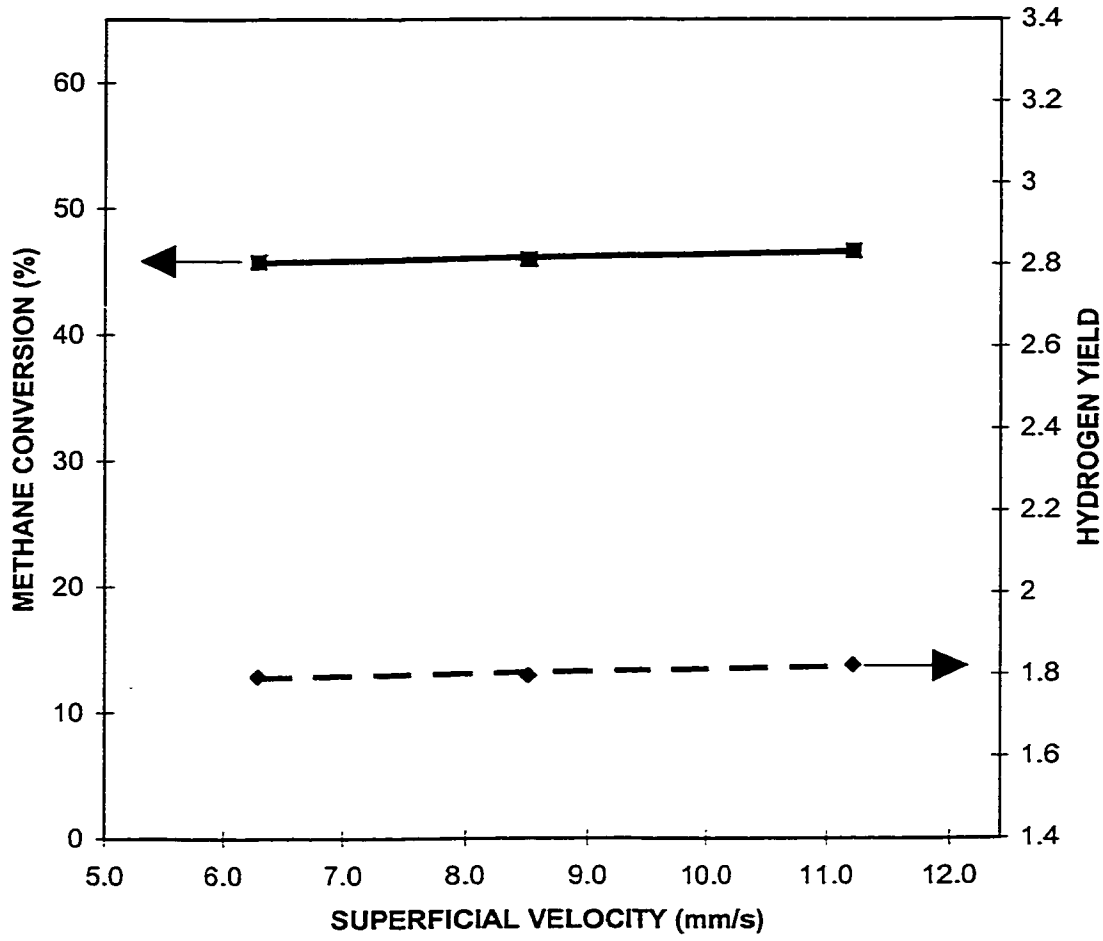

Figure 4.23: EFFECT OF SUPERFICIAL GAS VELOCITY VARIATION ON METHANE CONVERSION AND HYDROGEN YIELD

P=0.99 MPa, T= 873 K, Steam methane ratio= 3.1. Sweepgas pressure=0.14 MPa. Sweep gas flowrate=45mol/h.

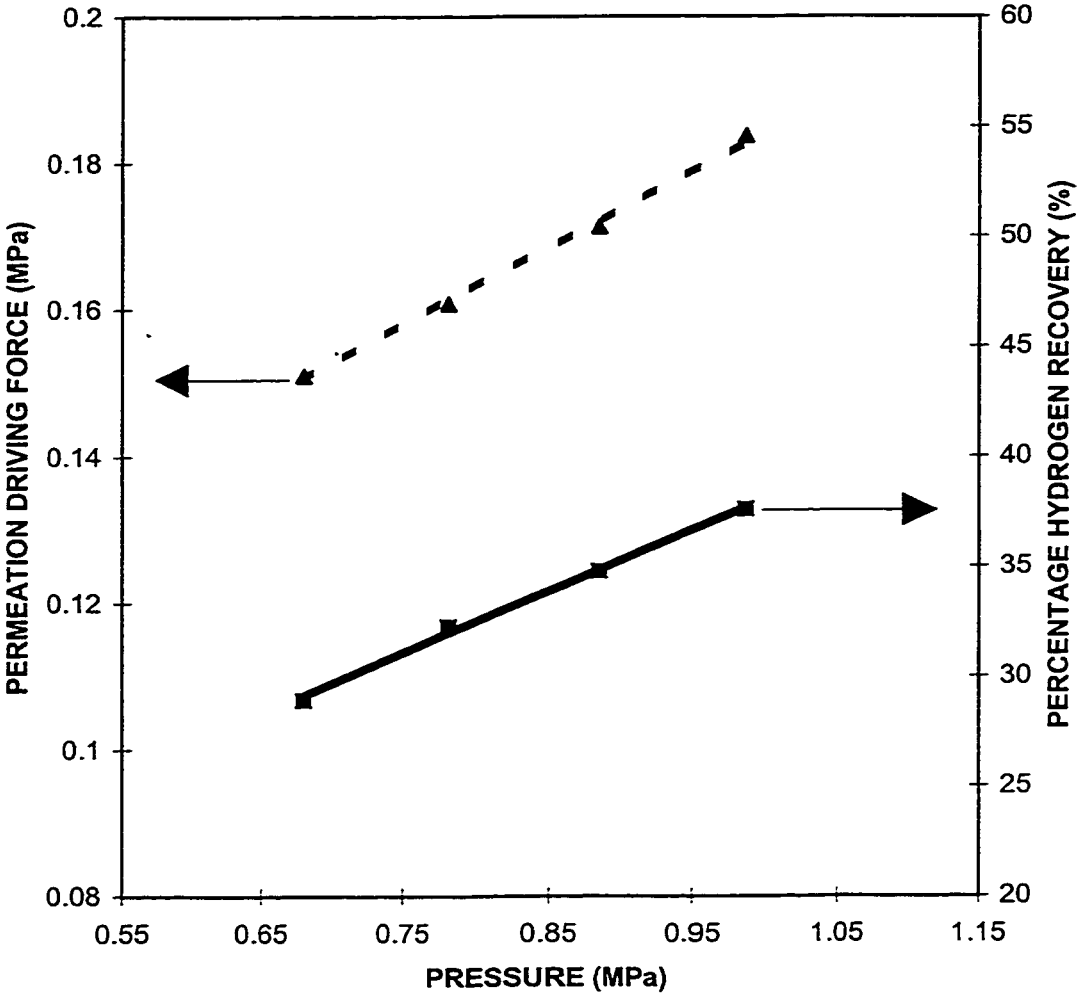

Figure 4.24: EFFECT OF PRESSURE VARIATION ON PERMEATION DRIVING FORCE AND PERCENTAGE HYDROGEN RECOVERY

T=873 K, Methane flowrate=33.74mol/h. Steam flowrate=138mol/h. Steam methane ratio= 4.1. Sweepgas pressure=0.14MPa. Sweep gas flowrate=45mol/h.

The experimental results showed a greatly improved performance compared to the equilibrium reactor and previous investigation. The hydrogen permeate flow was ten to fifteen times more than the previous study. The study also showed that there was room in the reformer to handle increased permeation capacity.

The dependent variables methane conversion and hydrogen yields behaved as anticipated and were higher than equilibrium values.

Chapter 5

Fluidized Bed Steam Methane Reforming with Oxygen Input

5.1 Objective

Study the addition of oxygen directly to a fluidized bed reformer to provide the heat of the reforming reaction with sufficient oxygen to attain autothermal conditions at the desired process conditions. To compare the experimental results of these runs with the respective equilibrium compositions.

5.2 Background of fluidized bed SMR

Conventional fixed bed steam methane reformers have some disadvantages such as low heat transfer rates, diffusional resistance in the catalyst pores, and large temperature gradients. In addition, steam methane reforming, a highly endothermic process, is affected by the efficiency of heat input into the reformer.

Improved heat transfer, catalyst bed uniformity, and virtual elimination of diffusional limitations are the major advantages of using a fluidized bed (Adris et al., 1996). The reforming catalyst is fluidizable when the particle size range is in the proper domain, and is able to withstand the mechanical environment of the fluidized bed reformer as shown in previous studies. Particles ranging in size from 90 to 355 μm and with mean diameters of 160 to 200 μm as mentioned were used successfully in earlier studies. The minimum superficial gas velocity needed for thermal uniformity of the fluidized bed was about five

times the minimum fluidization velocity (Adris, 1994). Another benefit of fluidized bed SMR is the low pressure drop through the bed.

5.3 Heat input to a steam methane reformer

Efforts have been made to overcome heat transfer limitations in a conventional packed bed, radiantly heated reformer, and to improve the thermal efficiency of the overall process by changing the mode of heat supply. Attempts previously made to improve the heat transfer in SMR are discussed in the following paragraphs.

Quartulli et al. (1966) analyzed the problems peculiar to primary and secondary reformer operations including the requirements for larger sized equipment and for the use of increasing amounts of steam and fuel. They suggested the use of a heat exchanger between the primary and secondary reformers for indirect heat exchange of the primary and secondary reformer effluents. Thus, the temperature of the primary reformer effluent can be raised and, at the same time, the temperature of the effluent from the secondary reformer is decreased. It is claimed that this configuration reduces the size of the external fuel-fired primary reformer.

Reichel and Lippert (1984) suggested a configuration in which the reaction takes place in a fluidized bed reactor which is thermally connected to a fired heater by means of a heat pipe provided with fins to facilitate transfer of heat to the reactor bed. However, some important issues such as reaction reversal in the freeboard, capital costs, and catalyst attrition were not addressed.

Fuderer (1987) suggested an integrated primary and secondary reforming process and apparatus for providing autothermal conversion of hydrocarbons and steam to hydrogen

and carbon oxides. Use of an external fuel-fired reformer was eliminated from the reforming process. In Fuderer's apparatus, hydrocarbon and steam feed is passed through the catalyst bed of the primary reformer. The partially reformed effluent enters as feed to the secondary reformer where preheated gas containing oxygen is introduced. The hot secondary reformer effluent gas does not leave the plant, but passes on to the shell side of the primary reformer, thereby supplying the endothermic heat required for the primary reforming reaction.

Brun-Tsekhovoi et al. (1988) proposed a modified process for catalytic steam reforming of hydrocarbons in the presence of carbon dioxide acceptors. Reforming was carried out in a fluidized bed of catalyst containing calcium oxide, which reacts with carbon dioxide to form calcium carbonate, thus liberating the heat of reaction which then provides 80 to 100% of the energy required for the endothermic reforming reactions. The calcium oxide plus calcium carbonate was shown to be almost completely separated from the catalyst particles. An equilibrium shift of the reaction conversion and reduction in fuel consumption were further claimed to be an advantage of this process.

Goetsch et al. (1989) suggested a process for synthesis gas production by catalytic partial oxidation of methane in a fluidized bed autothermal reactor. In the fluidized bed a light hydrocarbon feed of primarily methane was reacted with oxygen and steam in the presence of a supported nickel catalyst. The gases were maintained at elevated temperatures and pressures to favor the formation of synthesis gas then quenched by indirect heat exchange. This quench or rapid cooling helped to prevent back reaction and carbon formation. Carbon formation could take place by the Boudouard reaction ($2CO \Rightarrow C + CO_2$) as low steam/carbon ratios were employed.

LeBlanc (1991) patented a heat exchanger type reforming reactor where the endothermic heat was supplied by the effluent gas from a separate autothermal reactor in which exothermic partial oxidation of hydrocarbons as well as hydrocarbon reforming took place. This design included a limited duty preheater. The major accomplishments of this configuration are lower capital cost, improved energy efficiency, and reduced NO_x and CO_2 emissions.

5.3.1 Heat supply by in situ oxidation of methane in the reforming reactor

The partial oxidation of methane involves the combustion of methane to produce both carbon monoxide and carbon dioxide simultaneously. The combustion reaction is highly exothermic and very fast. This exothermicity adds to the large temperature gradients and hot spots generated in fixed bed reactors. The issue of temperature gradients gives rise to considerable experimental difficulties and complications in reporting accurate kinetic data (Choudhary et al., 1993; Dissanayake et al., 1991). The existence of hot spots poses serious problems for the operation of industrial reformers and makes fixed bed reactors unsuitable for oxygen input operation.

In contrast, fluid beds are best used in processing applications where temperature control, thermal uniformity, and heat transfer are important. The fluidized solid catalyst particles act as an internal heat carrier in the bed and provide a more uniform reactor temperature. Much of the recent work has been done primarily for natural gas or methane combustion in catalytic fluidized beds and the production of synthesis gas by catalytic partial oxidation of methane.

Most of the fluidized bed combustion studies considered a complete combustion of methane or natural gas with stoichiometric or excess amounts of air. Catalytic fluidized bed combustion has several advantages over homogeneous combustion.

The heterogeneous ignition (light-off) temperature at the surface of the catalyst is generally lower than the homogeneous ignition temperature, consequently combustion can be carried out at a much lower temperature in catalytic fluidized beds. Since limits of surface flammability are much wider, fluidized bed combustion can be carried out beyond the conventional homogeneous flammability limits. Also, the attainment of thermal uniformity (isothermality) is considerably easier with fluidized beds.

Foka et al. (1994) studied the combustion of natural gas in a fluidized bed of Pd/Al_2O_3 catalyst and produced an isothermal temperature profile in the bed. Van der Vaart (1992) studied methane combustion in a fluidized bed of inert solids. The combustion was homogeneous but the internal circulation of solid particles helped maintain a near isothermal profile in the emulsion phase.

Production of synthesis gas by catalytic partial oxidation of methane primarily involves the overall reaction given below:

$$CH_4 + 0.5\ O_2 = CO + 2\ H_2 \qquad \Delta H = -35.5\ kJ/mol \qquad (5.1)$$

This reaction is favored thermodynamically at temperatures greater than 900 °C. Selectivities are affected by the formation of water in highly exothermic combustion reactions which also produce carbon monoxide and carbon dioxide. Since the overall direct oxidation reaction is exothermic, a reactor incorporating this reaction would be much more energy efficient than the endothermic steam reforming process. As oxidation reactions are much faster than reforming reactions, a single stage process for syngas generation would be

a viable alternative to steam reforming, requiring much smaller reactors, and giving higher throughput (Bharadwaj and Schimdt, 1994).

Several reaction studies have examined the direct oxidation of methane to syngas (Tomiainen et al., 1994; Dissanayake et al., 1991; Choudhary et al., 1993). For the most part, work on the use of fluidized beds is not common although the results obtained by most studies in this area are encouraging. For the production of synthesis gas by catalytic partial oxidation of methane, Olsbye et al. (1993) reported an almost flat temperature profile within the bubbling phase of the fluidized bed with conversions and selectivities close to equilibrium values. The temperature drop in the freeboard decreased the conversion and selectivity due to reverse reactions taking place on the catalyst elutriating into this region.

Bharadwaj and Schimdt (1994) analyzed the production of synthesis gas in fluidized beds over Pt, Rh, and Ni catalysts coated on 100 μm α-Al_2O_3 beads. With methane and air feeds they achieved CO and H_2 selectivities as high as 95%, and methane conversions of higher than 90% for Rh and Ni catalysts with contact times of 0.1-0.5 s. The optimal selectivities were improved by heating the reaction mixtures above the autothermal reactor temperature and using oxygen instead of air. The bed operated with temperature variations less than 50 °C between two given positions in the bed. Santos et al. (1994) investigated similar reactions in a fluidized bed reactor of $NiO/NiAl_2O_4$ catalyst. They examined the axial temperature and concentration profiles and the amount of carbon deposited. Analyzing the profiles, they concluded that the conversion and selectivity can be maximized by minimizing the amount of catalyst entering the colder zones of the reactor such as the freeboard region. This can be accomplished by choosing the appropriate fluidization

conditions and by generating an adequate temperature and solids concentration profile in the disengagement section of the reactor.

The purpose of all the above mentioned work was to produce H_2 and CO (syngas) at a ratio of 2:1 which is more easily accomplished if no steam is used in the feed. For ammonia synthesis and for hydrogen production the desired product from the reformer is H_2. The aim of the present investigation is to produce hydrogen while still maintaining the autothermal conditions of the reformer. In this study, addition of steam to the feed is essential, since steam reacts with methane and carbon monoxide to produce more hydrogen. Steam also helps to prevent coke formation. Coke (carbon) formation will take place at temperatures below 1000 °C if only methane and oxygen (2:1 ratio) are used as feed. Coke formation starts at even lower temperatures (Bharadwaj and Schimdt, 1994) with leaner methane/oxygen mixtures. The minimum concentrations of steam and hydrogen below which coke forms can be calculated thermodynamically (Xu, 1988). Paloumbis and Petersen (1982) studied carbon formation in reformers and reported that the minimum thermodynamic steam to carbon ratio for carbon or coke formation is lower than the experimental value. For example, at an operating temperature of 900 °C, thermodynamically there is no carbon formation at steam to carbon ratios above 1.0, but experimentally they found that the steam to carbon ratio should be kept above 1.3 to avoid carbon formation.

With similar operating conditions, the likelihood of carbon formation in fluidized beds is always less than that in the fixed beds. The movement of solid particles within a fluidized bed reactor helps to limit the net amount of carbon formation by recirculation of the carbon-fouled catalyst to the oxygen-rich zones of the bed. In the present experimental

work, steam has always been included in the feed stream at ratios above 1.5 to avoid formation of coke and favor the production of hydrogen.

5.3.2 Flammability limits and ignition temperature

Homogeneous gas phase combustion occurs when the gas temperature is equal to or higher than the ignition temperature of the fuel and the fuel-air ratio is within the flammability limits. The ignition temperature of a gas defined by the occurrence of a visual flame is the lowest temperature at which the air-gas mixture will ignite by contact with a hot surface. Below this temperature, neither a spark nor a flame will ignite the mixture. For methane and air in stoichiometric amounts the homogeneous ignition temperature is 711 °C. The lower and higher flammability limits for homogeneous methane combustion are 5% and 15% methane in air respectively.

The ignition temperature is affected by various factors in varying degrees. It increases if a lesser than stoichiometric amount of air is used. For example, if 80% of stoichiometric air is used the increase is about 12 °C. The presence of inert gases raises the ignition temperature, whereas it decreases with increasing pressure (Vandaveer and Segeler, 1965). For the catalytic oxidation of methane, the heterogeneous ignition temperature is generally much lower and the flammability limits are broader relative to the homogeneous limits. For combustion to occur at the catalyst surface, the temperature inside the fluidized bed must be higher than the light-off temperature; also, it should always be below the homogeneous ignition temperature for safe operation of the reactor. The equivalence ratio is generally used as a parameter to define the flammability limits over catalyst surface:

$$\text{equivalence ratio } (\phi) = \frac{\left(\frac{\%\ \text{fuel}}{\%\ \text{air or oxygen}}\right)_{\text{actual}}}{\left(\frac{\%\ \text{fuel}}{\%\ \text{air or oxygen}}\right)_{\text{stoichiometric}}} \qquad (5.2)$$

A stoichiometric mixture corresponds to $\phi = 1$, fuel lean mixtures correspond to $\phi < 1$, and fuel rich mixtures correspond to $\phi > 1$.

The limits of flammability and light-off temperature on a metal surface are predicted from the bifurcation diagrams of metals. Veser and Schmidt (1996) studied the ignition-extinction behavior of different fuels on the surface of a platinum-foil catalyst over the entire range of fuel/air ratios at atmospheric pressure and generated a complete bifurcation diagram. For methane in air, the region of surface flammability ranges from an equivalence ratio of about 0.25 to about 7.3.

The complete bifurcation diagram for nickel, the active component of the catalyst used for this experimental study, is not available but the ignition temperatures can be estimated using other published data. Torniainen et al. (1994) studied the partial oxidation of methane in oxygen on monolith supported metal catalysts. At methane to oxygen ratios between 1.6 and 2.0, the ignition temperature on Pt catalyst was about 1100 °C, whereas the ignition temperature on Ni catalyst was between 950 °C to 800 °C.

Bharadwaj and Schmidt (1994) compared the catalytic oxidation of methane in fluidized bed reactors over Pt, Rh and Ni catalysts. At the same methane to air ratio the ignition temperature was between 775 °C and 850 °C for Pt catalyst and between 725 °C and 875 °C for Ni catalyst. In both studies the ignition temperature over Ni catalyst was found to be less than that over Pt.

The light-off temperature in a fluidized bed is generally higher than the ignition temperature estimated from bifurcation diagrams. For example, temperatures above 600 °C are required for heterogeneous ignition of methane air mixtures on Pt-foil. In a fluidized bed it was difficult to ignite a stoichiometric mixture of methane in air even at 700 °C (Bharadwaj and Schmidt, 1994). To overcome this problem, Bharadwaj and Schmidt used stoichiometric mixtures of propane in air (4%) or ammonia in air (15%) which light-off at much lower temperatures (370 and 300 °C respectively). The bed was first preheated in air or nitrogen to about 350 °C. The flow was then switched to a stoichiometric mixture of propane or ammonia in air. After catalyst light-off, the bed temperature steadily increased to about 800 °C within 3 to 4 minutes. Methane was then introduced and the propane or ammonia stream was simultaneously switched off. The catalyst bed stayed ignited and attained a steady-state temperature after a few minutes.

The present experimental work was performed at a temperature range of 550 to 675°C and with a CH_4/O_2 ratio between 0.25 and 0.65. This CH_4/O_2 ratio corresponds to an equivalence ratio (ϕ) between 3.0 and 8.0 which falls within the surface flammability limits of nickel catalyst, but is well outside the flammability limits ($0.53 < \phi < 1.5$) for homogeneous ignition. Therefore, the reactor can be operated in a safe and stable manner outside the explosion (flammability) limits for homogeneous combustion.

5.4 Apparatus and procedure

5.4.1 Pilot plant description

The experimental unit for this study was the Steam Methane reforming pilot plant, which has been described in detail in chapter four of this thesis. In the reforming reactor, modifications were made to feed oxygen directly into the fluidized bed reformer. The oxygen feed was measured using a mass flow meter. There were no hydrogen permeable membranes present in the reforming reactor during the course of this experimentation. The tapered and expanded sections of the reformer were not heated and hence were at a considerably lower temperature than the reformer bed. A wattmeter was attached to the electrical heaters which were in turn connected to the reforming reactor. At the autothermal condition, the electrical heaters supplying heat to the reactor remained off and the endothermic reforming heat was provided internally by the exothermic methane combustion.

5.4.2 Oxygen input

Figure 5.1 shows the modified pilot plant used for oxygen input experiments. The dimensions and the material specifications of the reforming reactor and other equipments are given in Chapter 4. The distributor plate in the reactor had 134 holes, similar to the reactor described in Chapter 4. The oxygen input sparger entered the reactor at 85 mm above the distributor plate. This horizontal sparger consisted of a 4.76 mm SS tube, 80 mm long with holes of 0.5 mm diameter. The oxygen was heated to a temperature of 723 K using a rope heater prior to being fed into the reformer.

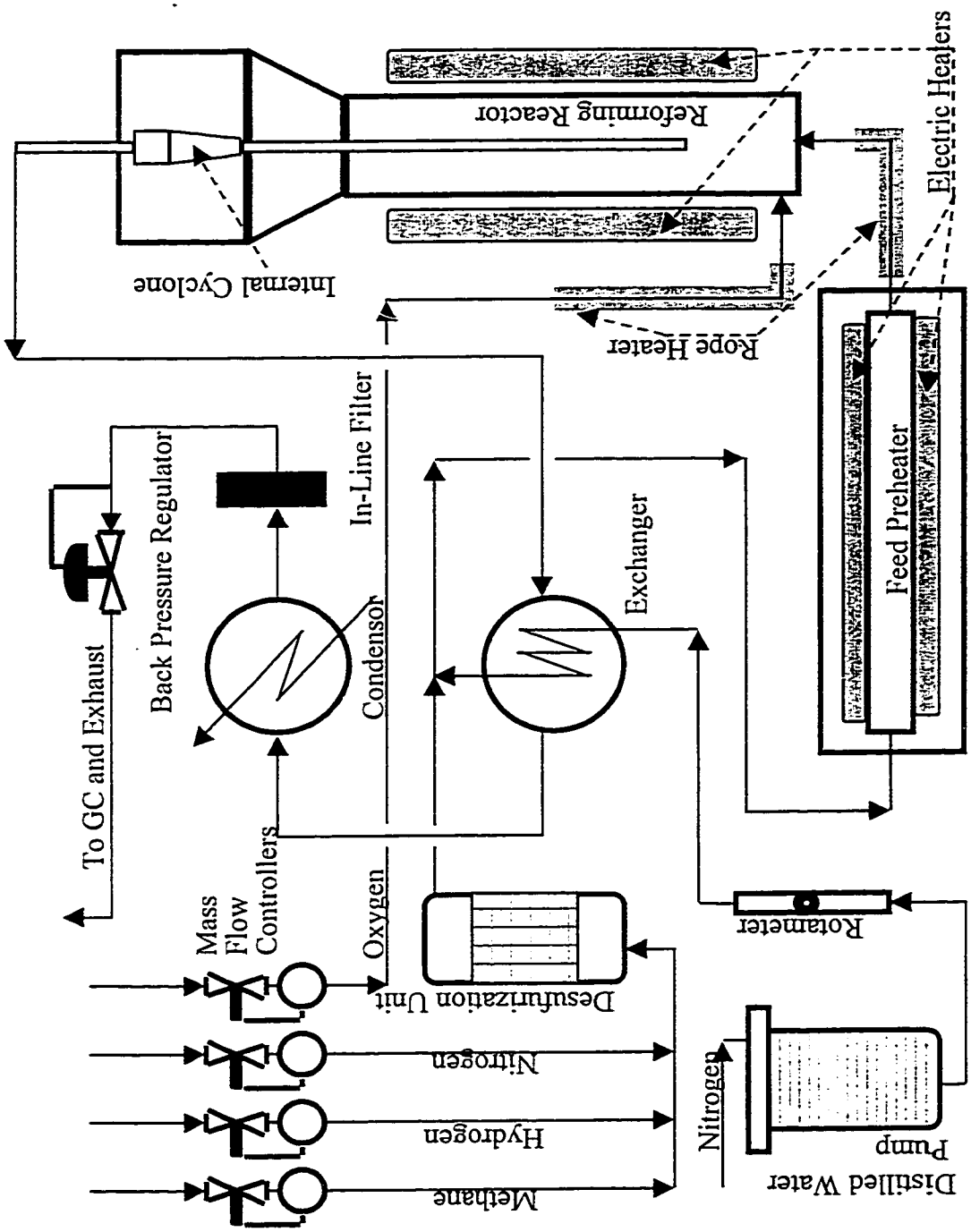

Figure 5.1: Schematic of fluidized bed reforming with oxygen input

5.4.3 Process description

Distilled water was heated by the exit gases from the reforming reactor in an exchanger and then mixed with the methane feed. The mixture was then heated in the feed preheater to boil the water and heat the vapors to the desired temperature and fed into the reforming reactor. Preheated oxygen was fed through a sparger into the fluid bed. The gases reacted in the catalyst fluid bed as well as in the freeboard region. The exit gases from the reactor were piped to the shell side of an exchanger which transfers sensible heat to the distilled water feed. Unreacted steam was condensed using a water-cooled condenser. The gases from the exit of the condenser passed through a 15 micron filter and were let down through a back pressure regulator. The electrical heaters used in the preheater and the reactor were controlled to maintain the desired process temperatures. A commercial steam methane reforming catalyst with particle size range from 100 to 350 μm and mean diameter of 180 microns was used.

Experimental procedures were similar to those described in Chapter 4 (section 4.8). Oxygen was introduced into the reactor bed after step 7 (section 4.8) of the startup procedure, and oxygen shut-off was the first step (section 4.8) of the shut down procedure. Other procedures were identical.

5.5 Computer model to evaluate equilibrium compositions

The principle that the Gibbs free energy of a system at a given temperature and pressure has to be minimum at equilibrium has been used to find the equilibrium composition of a reacting gaseous mixture. The sole information needed for such a calculation is the Gibbs free energy of formation for all chemical species expected at the

equilibrium. The gaseous mixture has been assumed to be ideal so that the fugacity coefficients are all 1.0. The method is robust and flexible with the possible species, as redundant ones will have negligible concentrations at equilibrium..

A conditional or constrained minimum of the Gibbs energy has to be evaluated because it is minimum at equilibrium, subject to conservation of the total amounts of individual chemical elements making up the chemical species found. There are several ways to solve for the minima; successive linear programming has been used in this study. The total Gibbs energy of a mixture is the sum of the contributions of the components and of mixing effects. In the case of an ideal gaseous reacting mixture, the Gibbs energy function is (Wallas, 1985):

$$G = \sum n_i [g_i^o + R_g T \ln(n_i P / n)] \tag{5.3}$$

and the derivative is:

$$\frac{\partial G}{\partial n_i} = \sum_i \nu_i [g_i^o + R_g T \ln P_i] = 0 \tag{5.4}$$

The minima is evaluated using successive linear programming and the Lagrange-Newtonian method is used for converging the estimates. The program is fast and accurate. The equilibrium compositions found by this method are compared with the experimental results.

5.6 Experimental results and discussion

5.6.1 Interdependence between operating parameters

The experiments were devised so that the effect of a single operating variable could be studied without altering the other variables. This was not a simple task, due to

the interrelation between the various variables and the controllability of the process parameters. The operating temperature, pressure and other major variables affect the outlet compositions and the reaction rate. This can be predicted from equilibrium computations, which give limiting compositions, and from rate equations which give reaction rates. Methane conversion and hydrogen production are favored by increased temperature and decreased pressure. Normally, the steam/methane ratio is set well above 1.3 to eliminate coke formation, and the actual ratio is determined commercially by a balance between steam costs and desired conversion. Oxygen will react with methane as well as hydrogen or carbon monoxide produced from the reforming and the partial combustion reaction. Hence, the net effect of oxygen in the reactor will be to increase methane conversion with a decreased hydrogen yield. The equipment used for this experimentation was an industrial scale pilot plant. This 97 mm internal diameter size had the advantage of being able to generate realistic conditions and results.

5.6.2 Results and discussion

In the four sets of experimental runs, oxygen input, reactor pressure, reactor temperature, and steam/methane ratio were varied while the other variables were kept constant. These runs are described below. Methane conversion was a major calculated parameter indicating the extent of reaction and the consumption of methane. The hydrogen yield gave the number of moles of hydrogen per mole of methane feed at the evaluated operating conditions. The reactor pressures are the time average values of the absolute pressures. The temperatures are an average of temperatures of the thermocouples immersed in the fluidized bed. The reactor had sufficient catalyst, such

that an incremental addition did not change outlet compositions, as discussed in the next chapter. The reactor freeboard contained entrained catalyst and was not heated, so that reverse reactions were possible. Consequently, all the experimental results show considerably lower methane conversion and hydrogen yield than the corresponding equilibrium values. All the experiments were carried out at gas superficial velocities well above that required for thermal uniformity (isothermality) of the fluidized bed.

In one set of runs, the oxygen input flowrate was varied and the exit gas compositions were measured. The temperature of the reactor was kept at 923 K and the pressure was at 0.55 MPa. The methane and steam flowrate were constant at 40 and 80 mols per hour respectively. Methane conversion increased from about 53% at an oxygen flowrate of 12 mols per hour to about 64% at an oxygen flowrate of 22 mols per hour (see in Figure 5.2). This result was expected as the increasing amount of oxygen reacted irreversibly with methane to produce CO or CO_2 and H_2O. The experiments also showed that at an oxygen input flowrate of 18 mol/h the reactor reached autothermal conditions. The experimental results show that the hydrogen yield is affected minimally by the oxygen input flowrate. There is a small decreasing trend as shown in Figure 5.3.

In another set of runs, the reactor pressure was varied. In these runs the temperature of the reactor was maintained at around 923 K and the oxygen input flowrate at 18 mols per hour. The methane and steam flowrates were maintained at 40 and 80 mols per hour respectively. The methane conversion decreased with an increase in reactor pressure. At a reactor pressure of 0.35 MPa, the methane conversion was 65.3%; the conversion decreased to 58.7% at 0.6 MPa, as shown in Figure 5.4. The equilibrium conversions indicate a similar trend but were higher than the experimental values as the

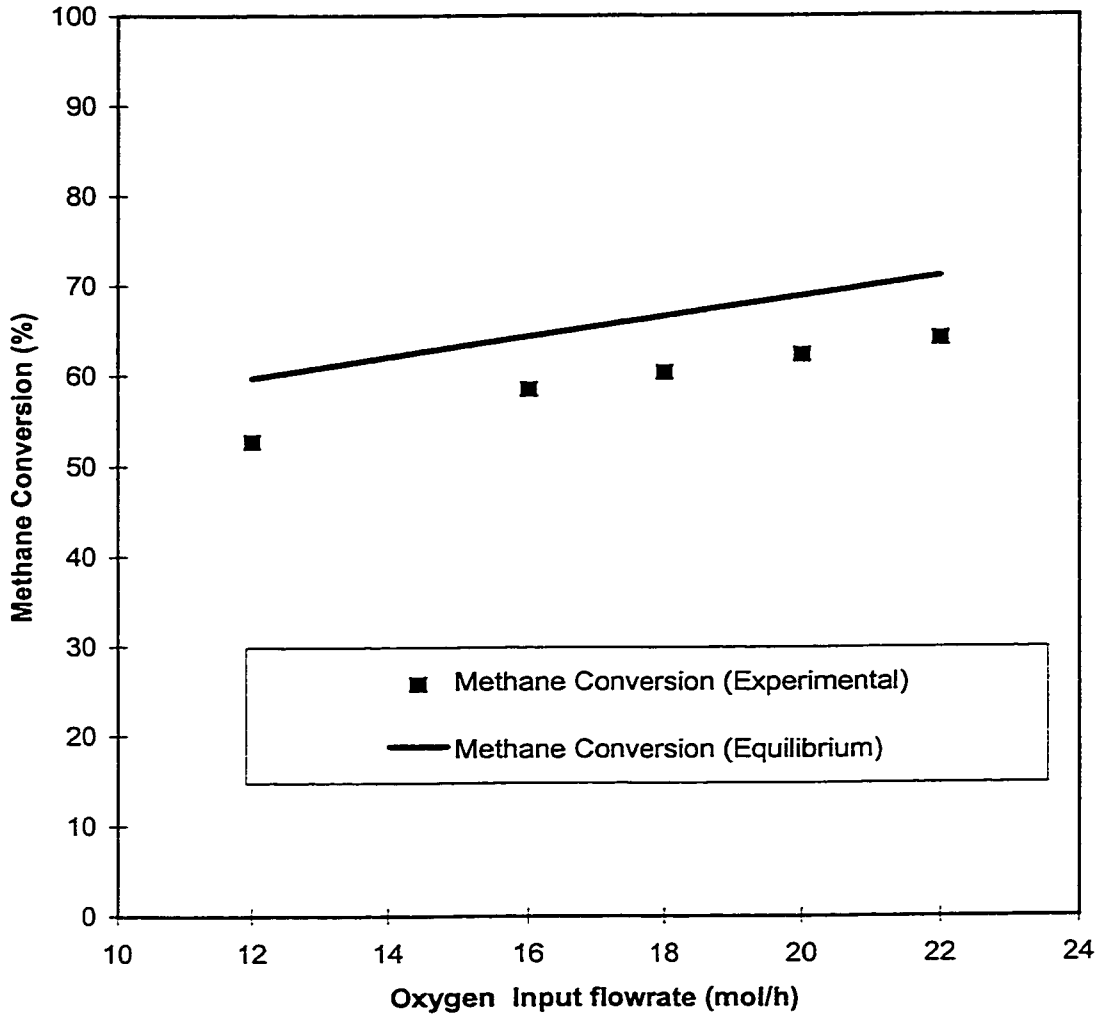

Figure 5.2: Effect of oxygen input flow variation on methane conversion

T=923 K, P=0.55 MPa, Methane flowrate=40mol/h, Steam flowrate=80mol/h.

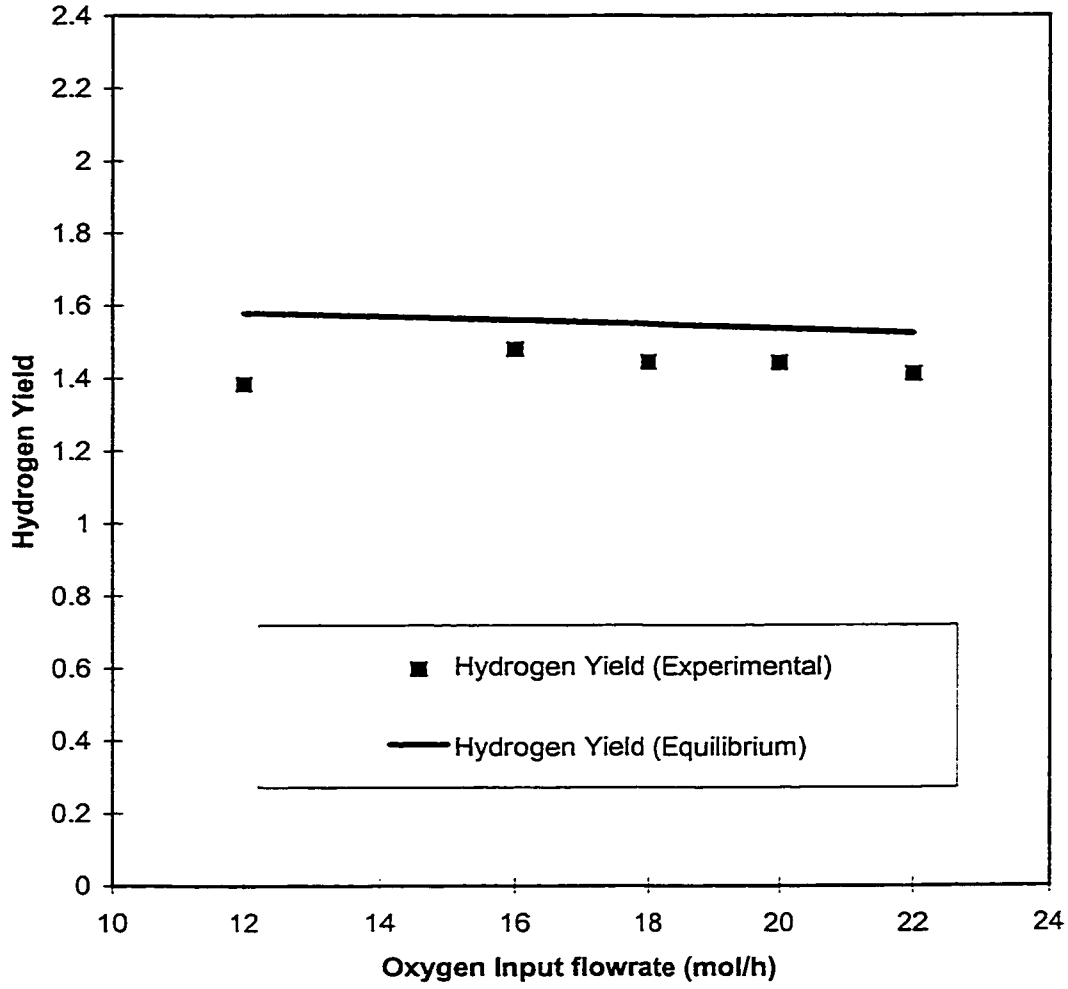

Figure 5.3: Effect of variation of oxygen input on hydrogen yield

T=923 K, P=0.55 MPa, Methane flowrate=40mol/h, Steam flowrate=80mol/h.

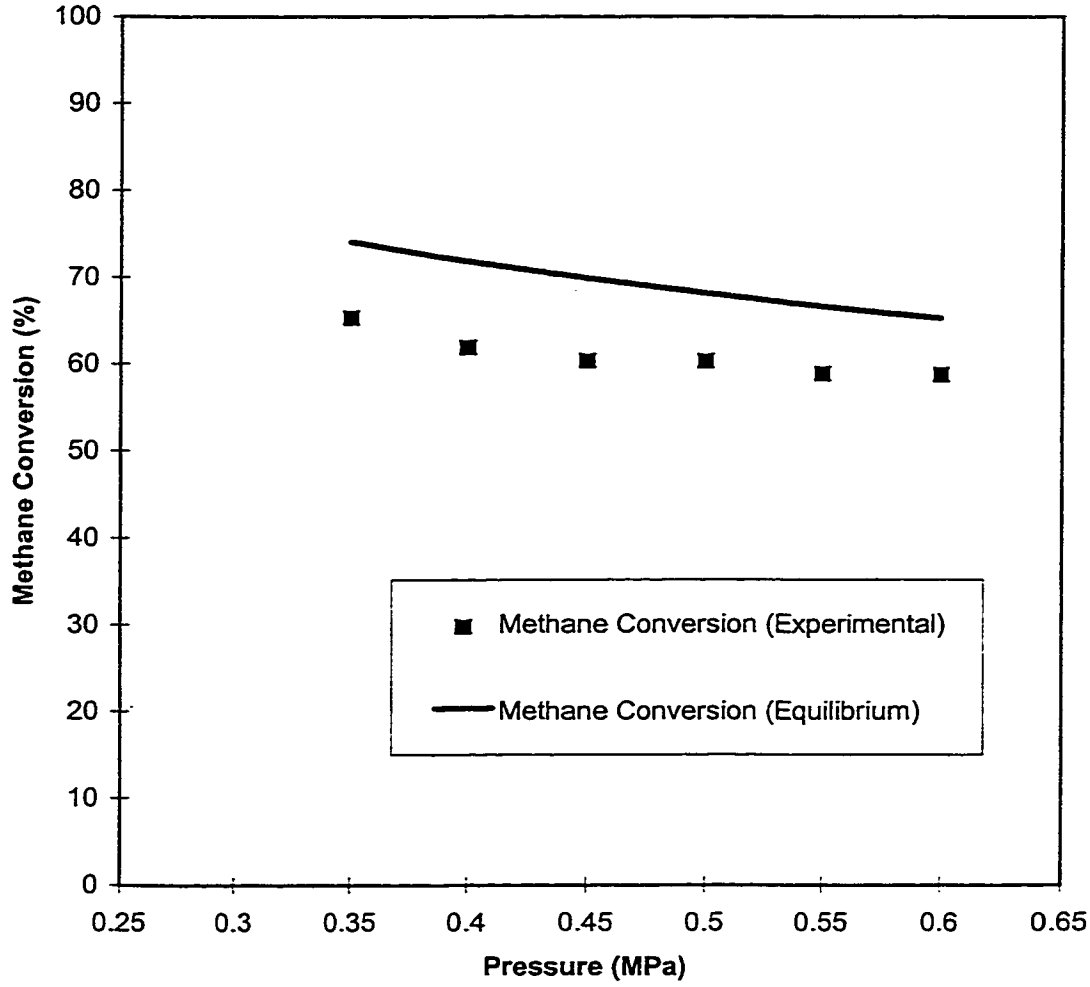

Figure 5.4: Effect of variation of pressure on methane conversion

T=923 K, Methane flowrate=40mol/h, Steam flowrate= 80mol/h, Oxygen flowrate=18mol/h.

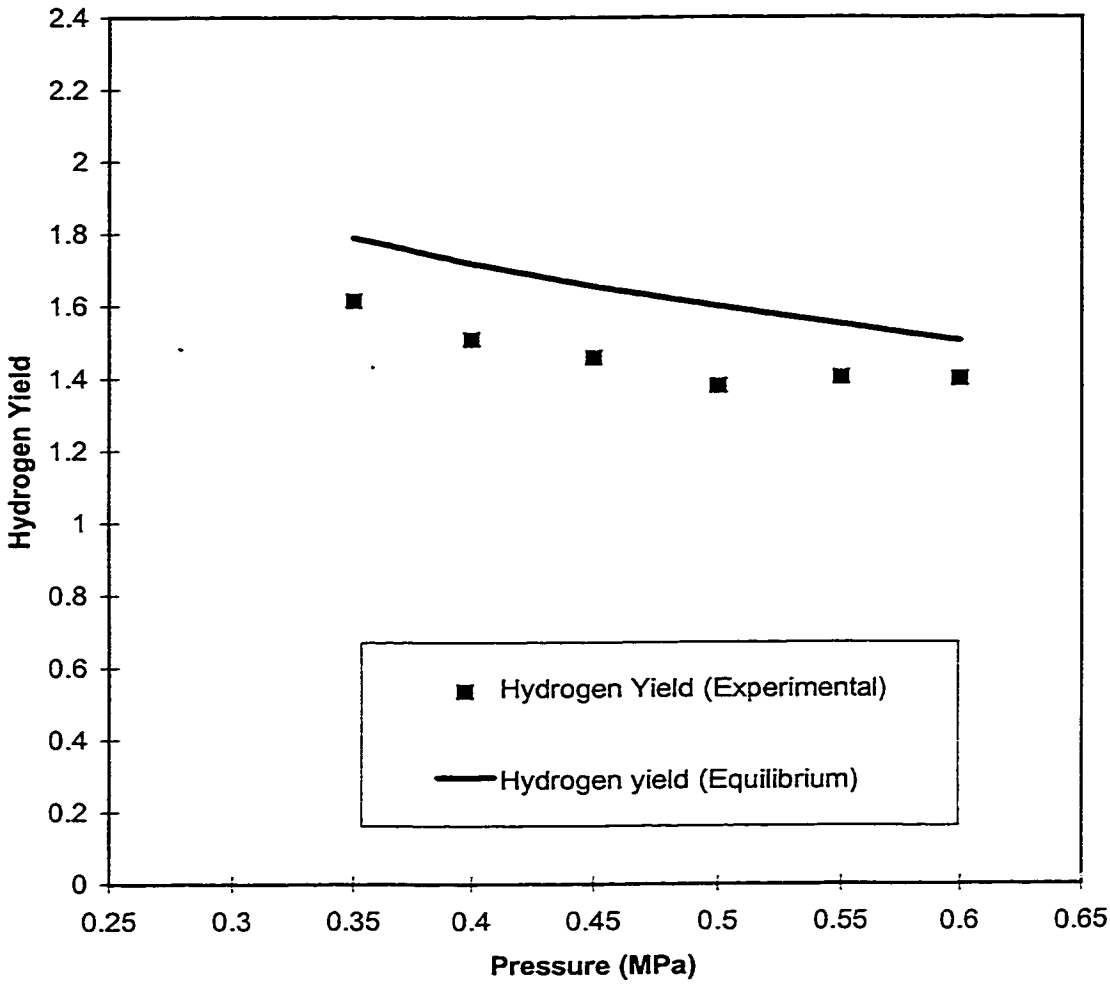

Figure 5.5: Effect of variation of pressure on hydrogen yield

T=923 K, Methane flowrate=40mol/h,Steam flowrate=80mol/h, Oxygen flowrate=18mol/h.

reactor data contained freeboard effects. These results were expected, as increasing pressure is thermodynamically unfavorable for the reforming reaction. At pressures 0.45 MPa and above, the reforming reactor reached autothermal conditions. Hydrogen yield decreased with an increase in reactor pressure as plotted in Figure 5.5.

In another set of runs, the reactor temperature was varied. In these runs the pressure in the reactor was kept at 0.5 MPa and the oxygen input flowrate at 18 mols per hour. The methane and steam flowrates were maintained constant at 40 and 80 mols per hour respectively. The methane conversion increased with an increase in reactor temperature. At a reactor temperature of around 848 K, the methane conversion was 52% and increased to 63% at a temperature of 948 K as shown in Figure 5.6. The equilibrium conversions indicate a similar trend, as expected. The experiments indicated that at all temperatures the reforming reactor reached autothermal conditions, as the electrical heat supply to the reactor was switched off by the control system in each case. Experimental runs showed that hydrogen yield increased considerably with an increase in reactor temperature as shown in Figure 5.7.

The steam methane ratio was varied from 1.5 to 3.0. In all these runs the temperature of the reactor was kept at around 923 K and the pressure at 0.5 MPa. The methane flowrate was maintained at 40 mol/h and the steam flowrate was varied to change the steam-methane ratio. Methane conversion increased from 52.6% to 65.3% when the steam-methane ratio was changed from 1.5 to 3.0 as shown in Figure 5.8. The equilibrium conversions behaved similarly but were comparatively higher. The hydrogen yield increased from 1.2 to 1.6 when the steam-methane ratio was changed from 1.5 to 3.0 as shown in Figure 5.9.

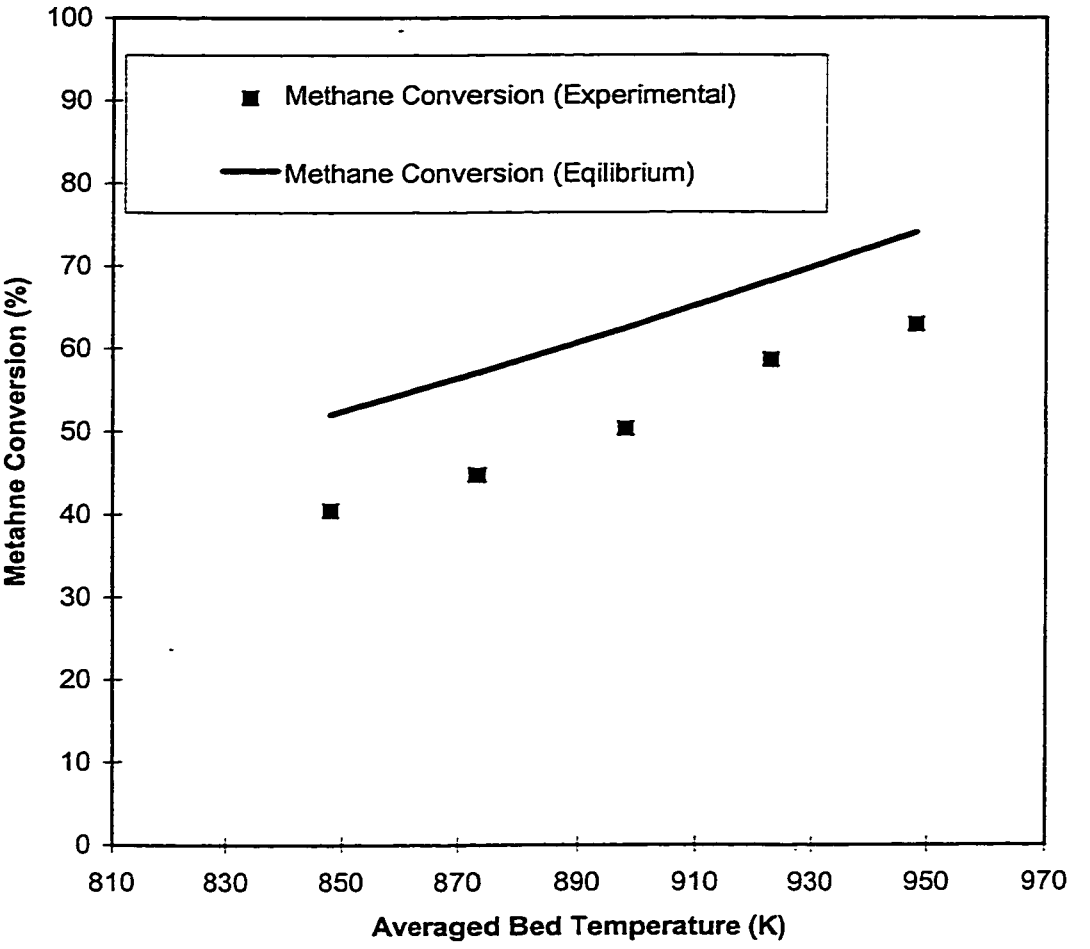

Figure 5.6: Effect of temperature vatiation on methane conversion

P=0.5 MPa, Methane flowrate=40mol/h, Steam flowrate=80mol/h, Oxygen flowrate=18mol/h

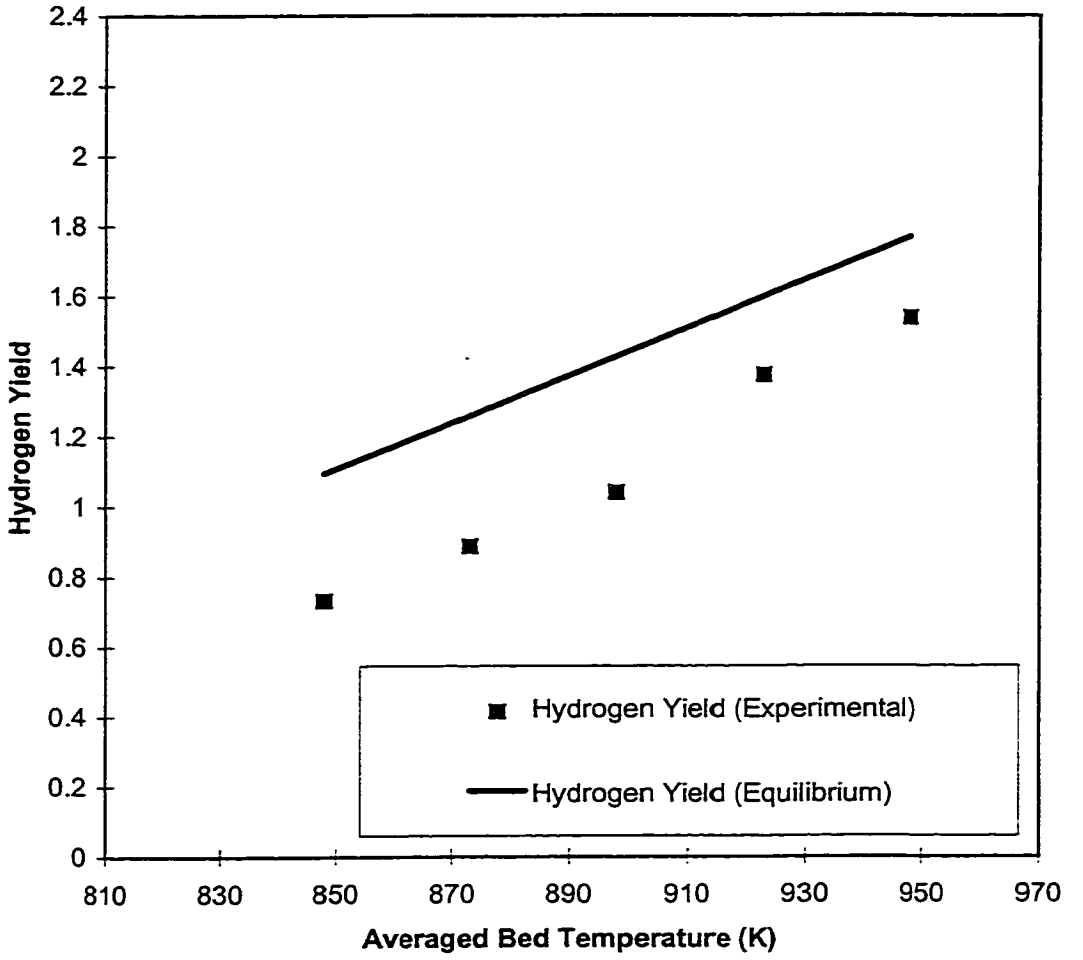

Figure 5.7: Effect of temperature variation on hydrogen yield

P=0.5 MPa, Methane Flowrate=40mol/h, Steam flowrate=80mol/h, Oxygen Flowrate=18mol/h.

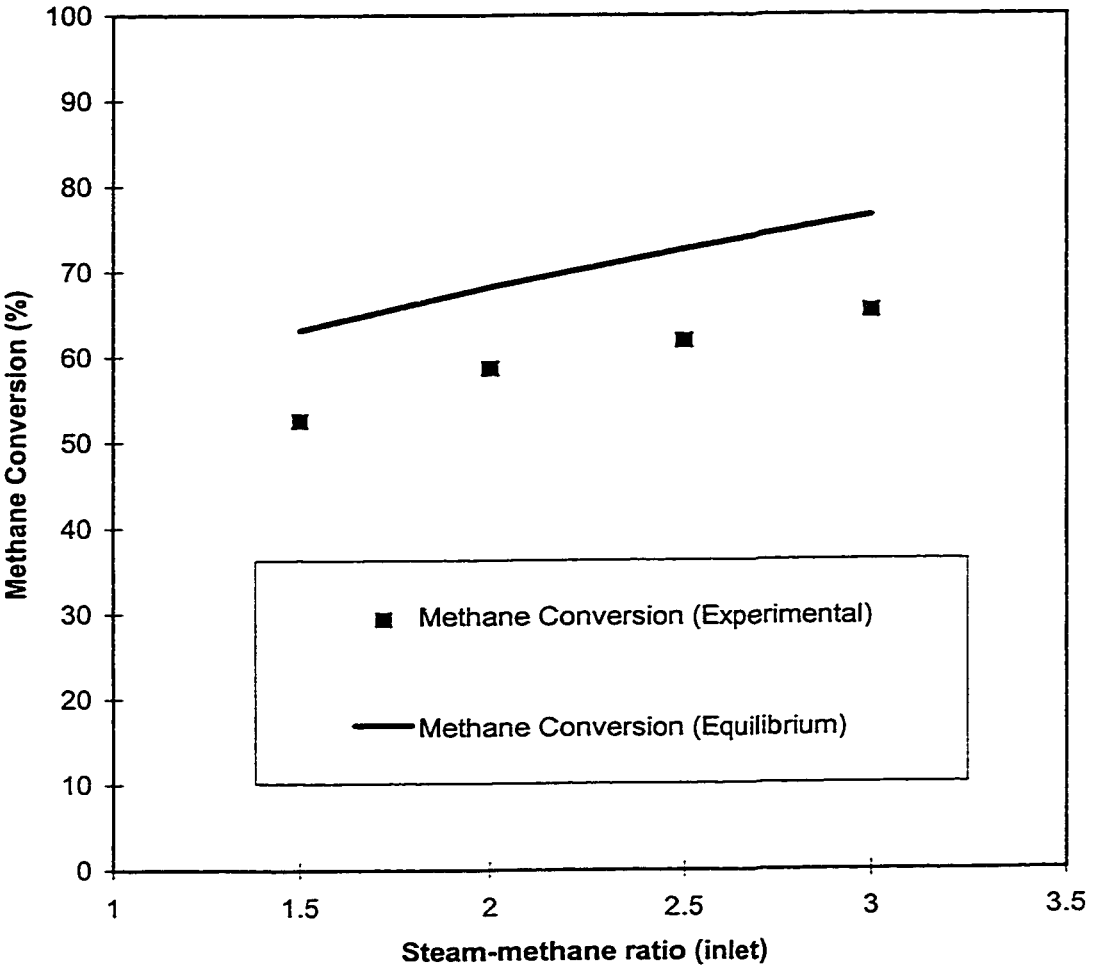

Figure 5.8: Effect of steam-methane ratio (input) variation on methane conversion

T= 923 K, P= 0.5 MPa, Methane flowrate=40mol/h, Oxygen flowrate=18mol/h.

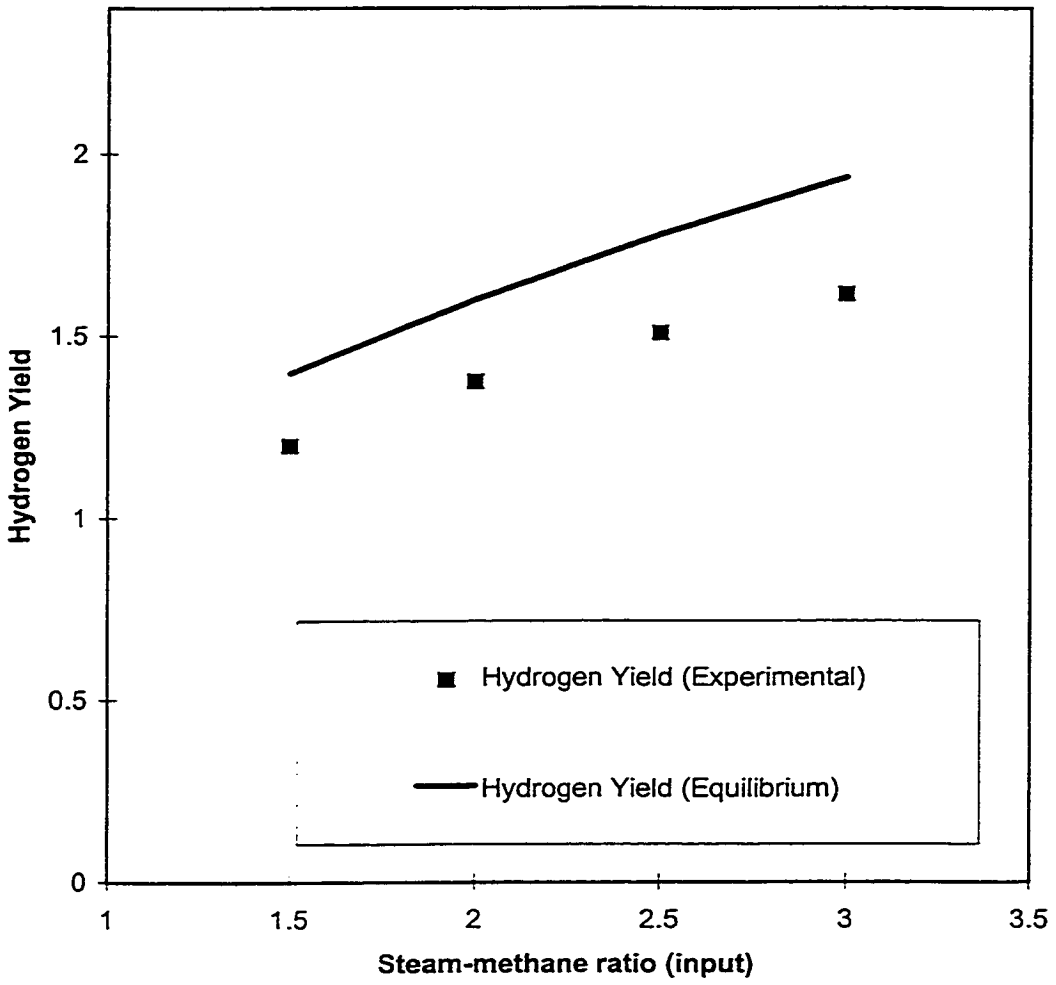

Figure 5.9 : Effect of steam-methane ratio (input) variation on hydrogen yield

T= 923 K, P= 0.5 MPa, Methane flowrate=40mol/h, Oxygen flowrate=18mol/h.

5.7 Conclusions

The study concludes that oxygen can be introduced successfully into a reforming reactor to provide for the endothermic heat of reforming reactions. There was 100% conversion of oxygen under all conditions. Most of the experimental runs reached and maintained autothermal conditions. The hydrogen yield increases with increasing temperature and steam-methane ratio, and it decreases minimally with increasing reactor pressure and oxygen flowrate.

The methane conversion increases with increasing reactor temperature, oxygen input flow rate and steam-methane ratio and decreases with increase in reactor pressure as expected. Methane conversion and hydrogen yield are compared to that expected from equilibrium.

Chapter 6

FBMR with Oxygen Input Experimentation and Analysis of Experimental Data

6.1 Objective

The primary objective of this study was to test an autothermal pilot scale fluidized bed membrane reformer with High-flux spring-reinforced palladium-coated membranes and compare the experimental results with the FBMR and equilibrium values.

A second objective was to estimate the errors in FBMR and FBMR with oxygen input data for repeated runs and by analyzing the variations in these runs. Finally the reaction-permeation data was correlated with the main operating variables (multi-variate analysis).

6.2 Introduction

The concept of FBMR with High-flux membranes was discussed in detail in Chapter 4 and the idea of FBR with oxygen input was enunciated in Chapter 5. These two concepts were integrated in this study to arrive at an autothermal FBMR configuration. This type of configuration, if implemented successfully, has many obvious advantages compared to the conventional reforming process. It includes the advantages of FBMR and eliminates the reforming furnace because of the autothermal behavior. This advantage can be translated into lower material costs for reformer

construction: stainless steel can be used instead of high metal alloys (HK 40) used in conventional reformers and the furnace which forms a major part of the capital cost of a SMR plant can be eliminated.

Because oxygen input into FBMR is a new concept, there is no literature on previous work and the literature reported in the previous chapters is relevant.

6.3 FBMR with oxygen input experimentation

Modifications were made to the reforming reactor used for the FBMR experimentation to facilitate the input of oxygen. Oxygen was distributed in the reformer using a sparger, which consisted of a 4.76 mm SS tube, 80 mm long with 0.5 mm diameter holes drilled into it. The sparger tube was placed horizontally in the reforming reactor, 85 mm above the distributor plate as shown schematically in Figure 6.1. The oxygen was preheated by an electric rope heater to a temperature of 723 K to decrease the sensible heat load.

When autothermal conditions were reached, the reactor was supplied heat solely through the exothermic reaction between methane and oxygen. This reaction took place in a region just above the distributor and the heat was distributed by the hot gases uniformly into the fluidized bed due to the existing well-mixed bed conditions. The gases exiting the surface of the fluidized bed were at bed temperature. They were cooled in the freeboard due to heat losses, resulting in some back reactions. Hence, oxygen and steam-methane ratio variation experimental runs have been compared to the equilibrium values at freeboard conditions.

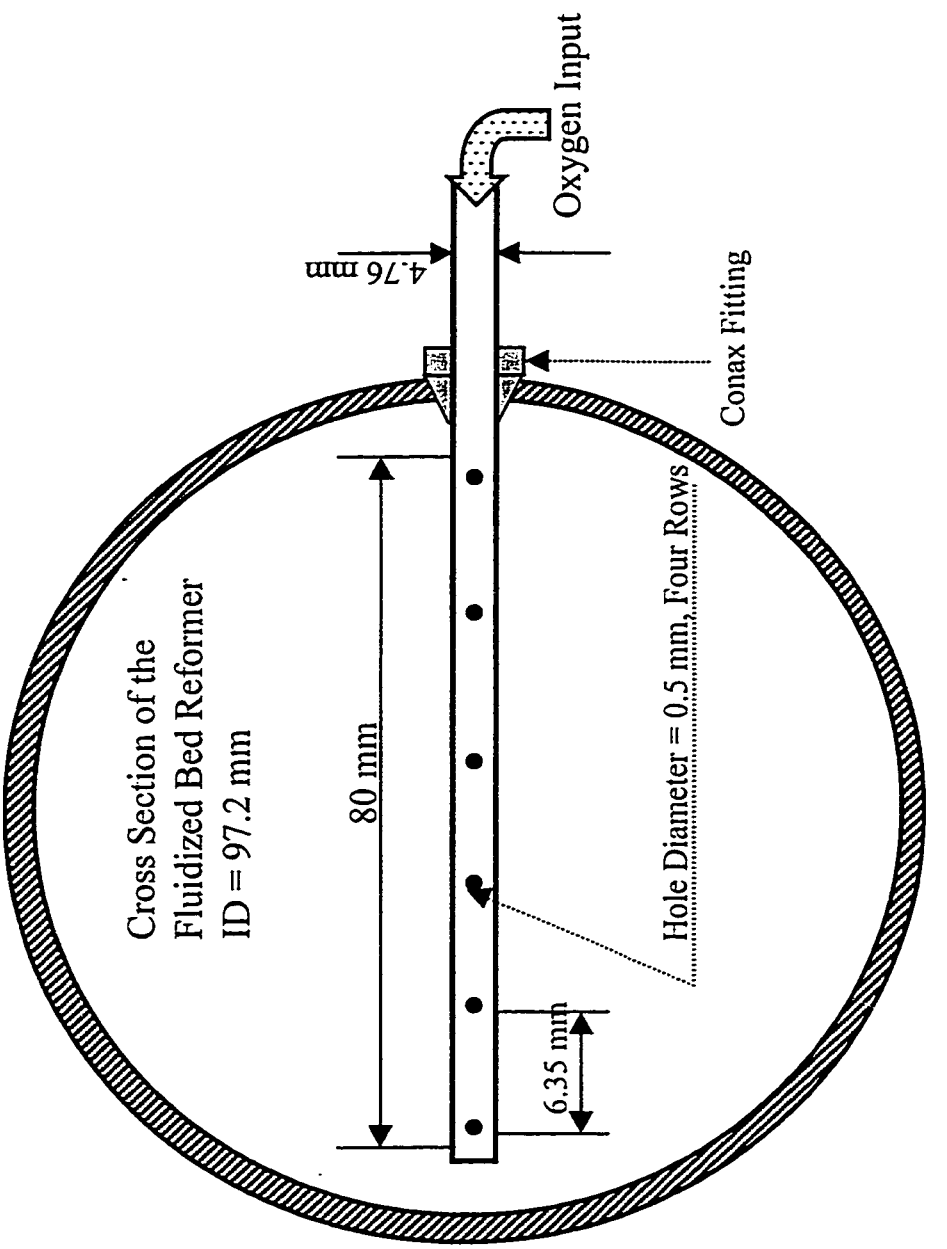

Figure 6.1: Oxygen input sparger in the fluidized bed

In one set of runs, the oxygen input flowrate was varied, and the reactor and membrane exit gas compositions were analyzed. The temperature of the reactor was kept at 923 K and the pressure at 0.68 MPa. The methane and steam flowrate were constant at 33.7 and 138 mol per hour respectively. Methane conversion increased from 76% for an oxygen flowrate of 14.6 mols per hour to about 82% for an oxygen flowrate of 21 mols per hour as shown in Figure 6.2. This result was expected as the increasing amount of oxygen reacted irreversibly with methane to produce CO or CO_2 and H_2O. The equilibrium conversions at freeboard conditions behaved similarly but were considerably lower. At an oxygen input flowrate of 15.2 mol/h the reactor reached autothermal conditions as determined by the wattmeter readings. The hydrogen yield decreased marginally with increased oxygen input flowrate. The hydrogen permeate flow also showed a decreasing trend because the partial pressure of hydrogen decreased with increasing oxygen input as shown in Figure 6.3. Oxygen flow should be kept at a minimum to maximize hydrogen production.

In another set of runs, the input steam-methane ratio was varied from 2.4 to 4.1. In these runs, the temperature of the reactor was kept at 923 K and the pressure was maintained at 0.68 MPa. The steam flowrates were maintained at 138 mol/h while the methane flowrate ranged from 58 to 33.7 mols per hour to change the ratio. The methane conversion increased from 58.5% for a steam-methane ratio of 2.4 to 73.6% for a ratio of 4.1, as shown in Figure 6.4. The equilibrium conversions at freeboard conditions behaved similarly but were considerably lower. The hydrogen yield increased with an increase in steam-methane ratio, though the hydrogen permeate flow decreased marginally, as shown in Figure 6.5. This was due to the decrease of hydrogen partial

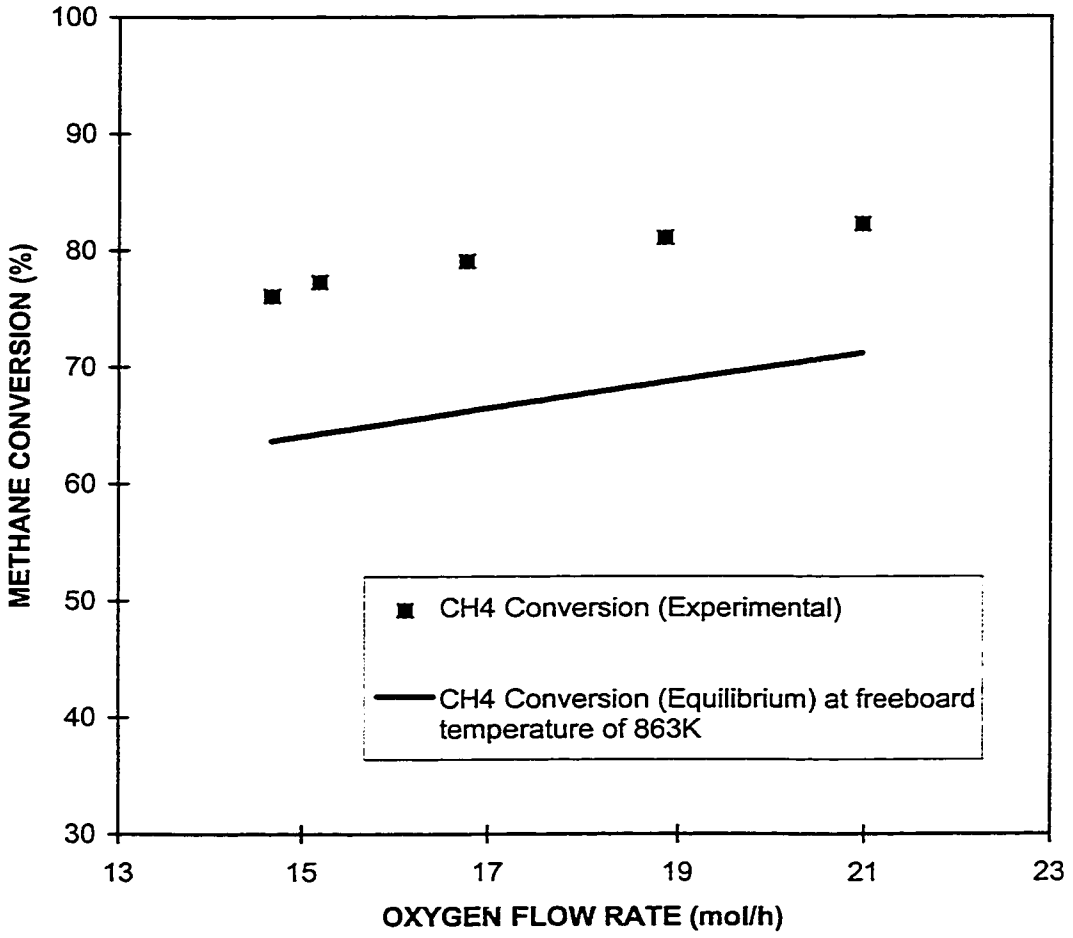

Figure 6.2: METHANE CONVERSION WITH THE VARIATION OF OXYGEN INPUT FLOW RATE

P=0.68MPa. T=923 K. Methane flowrate=33.74mol/h. Steam flowrate=138mol/h. Steam methane ratio= 4.1. Membrane pressure=0.14MPa. Sweep gas flowrate=45mol/h.

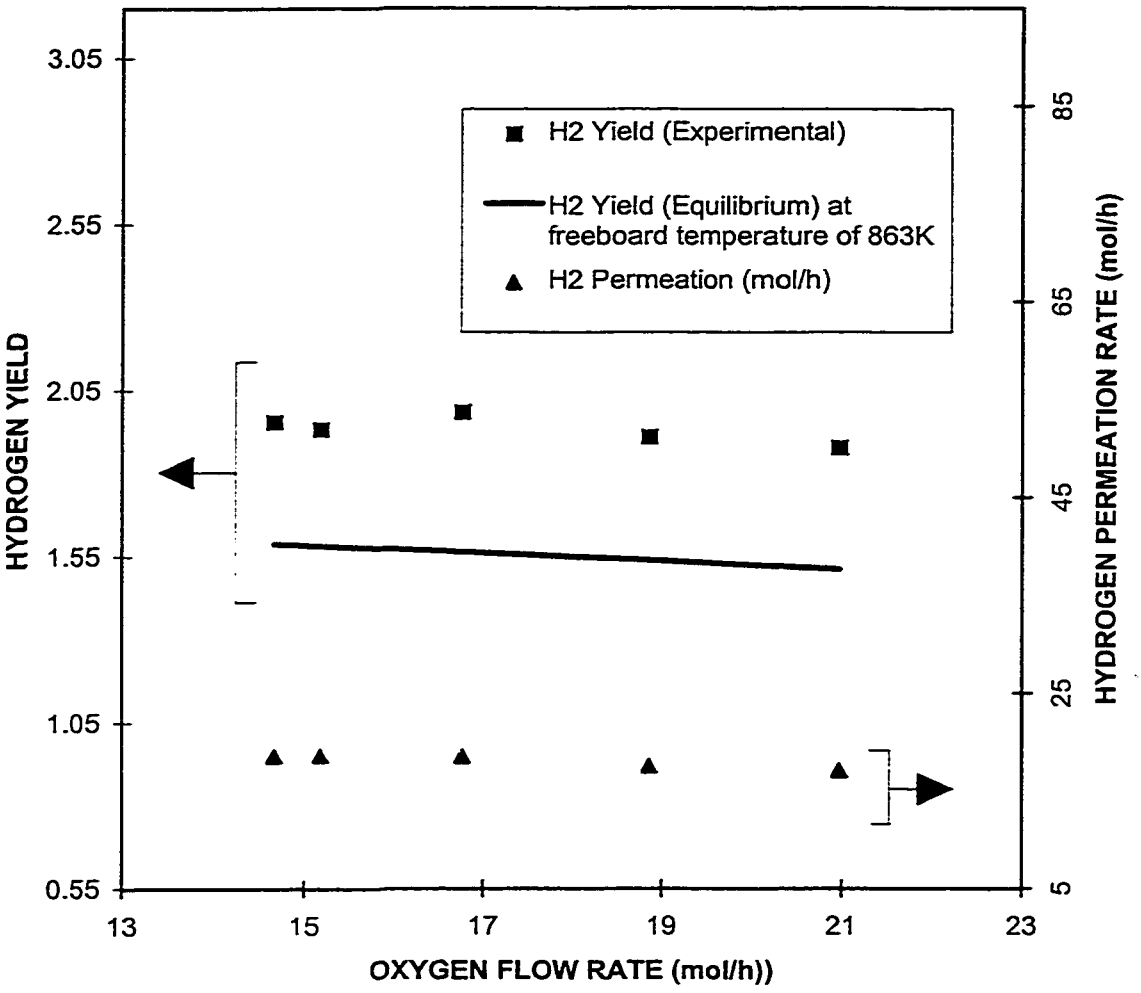

Figure 6.3: HYDROGEN YIELD AND RECOVERY WITH VARIATION OF OXYGEN INPUT FLOW RATE

P=0.68MPa. T=923 K. Methane flowrate=33.74mol/h. Steam flowrate=138mol/h. Steam methane ratio= 4.1. Membrane pressure=0.14MPa. Sweep gas flowrate=45mol/h.

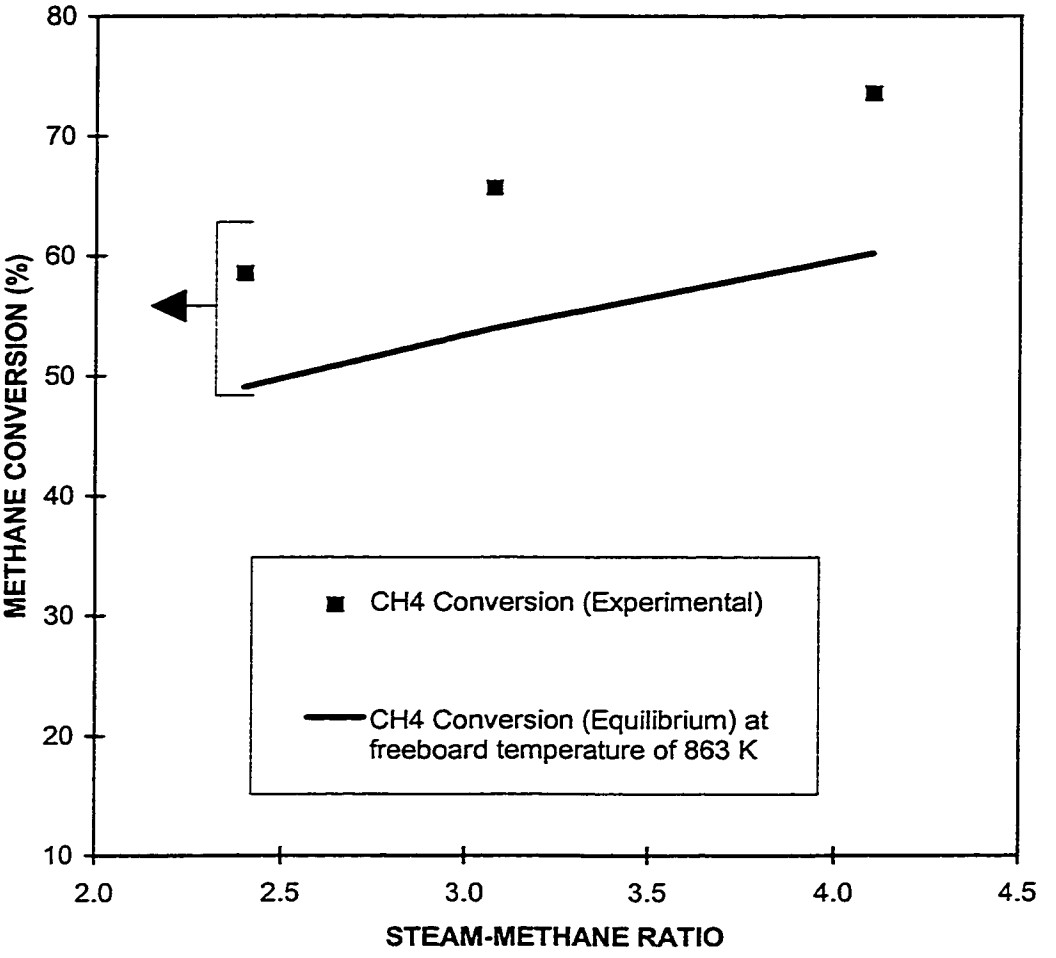

Figure 6.4: METHANE CONVERSION WITH STEAM-METHANE RATIO VARIATION

P=0.68 MPa, T=923 K. Steam flowrate=138mol/h. Sweepgas pressure=0.14MPa. Sweep gas flowrate=45mol/h. Methane:oxygen= 1.0:0.35

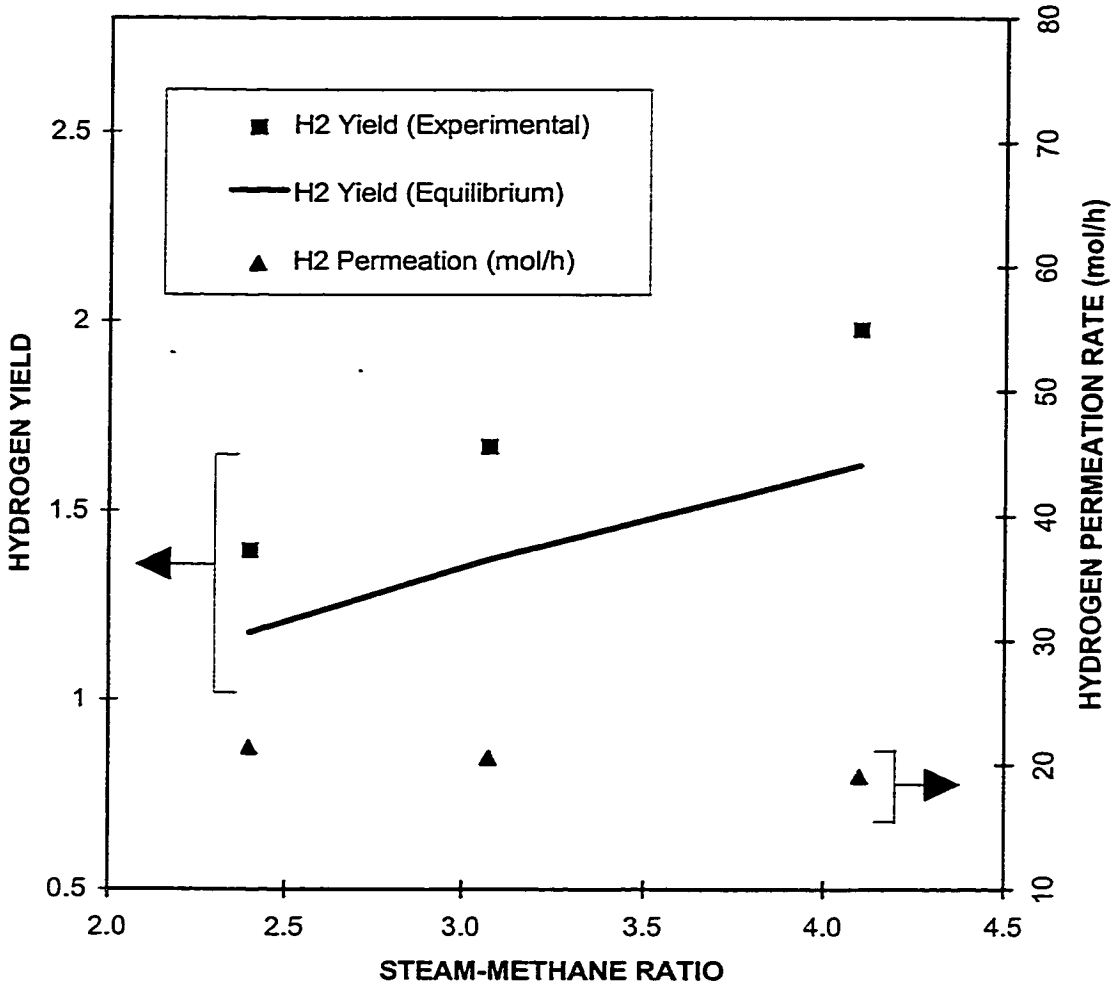

Figure 6.5: HYDROGEN YIELD AND PERMEATION RATE WITH VARIATION OF STEAM-METHANE RATIO

P=0.68 MPa, T=923 K. Steam flowrate=138mol/h. Sweepgas pressure=0.14 MPa. Sweep gas flowrate=45mol/h. Methane:oxygen= 1.0:0.35

pressure in the reactor with increasing steam-methane ratio. This set of runs proved that increasing steam-methane ratio results in higher methane conversion and hydrogen yield but will not provide an increased hydrogen permeate flow.

Comparisons have been made in Figure 6.6 among the present study (Autothermal FBMR), FBMR(without oxygen input) and the previous study (FBMR with thin-walled Pd membranes; Adris, 1994). Eight High-flux U-tubes were used for the Autothermal FBMR runs as compared to nine for the FBMR runs. Hence, the permeation area for Autothermal FBMR was about 12% less than for FBMR. The hydrogen permeate flow (mol/h) in the FBMR study was on an average ten to fifteen times higher than that of the previous study (Adris, 1994), and in the present study it was seven to ten times higher than the previous study. Autothermal behavior simplifies the heat input into the reformer but reduces hydrogen production. Figure 6.6 indicates the overall hydrogen permeation performance achieved by the present study with respect to non-autothermal configurations.

The data from FBMR with oxygen input, FBMR and equilibrium without oxygen have been compared for a set of runs in which pressure was varied. These equilibrium values can be assumed to represent conventional steam methane reforming (SMR) at the same conditions. The methane conversions of the FBMR with oxygen input are highest and show a decreasing trend with increasing pressure. This is due to the combined effect of oxygen input and permeation as shown in Figure 6.7. The hydrogen yields for FBMR with oxygen input runs are the lowest of all three as shown in Figure 6.8. The hydrogen permeation when oxygen is added is lower because the products of combustion decrease the partial pressure of hydrogen. Hydrogen permeation shows an

Figure 6.6: Comparison of hydrogen permeate flow in autothermal FBMR with non-autothermal configurations

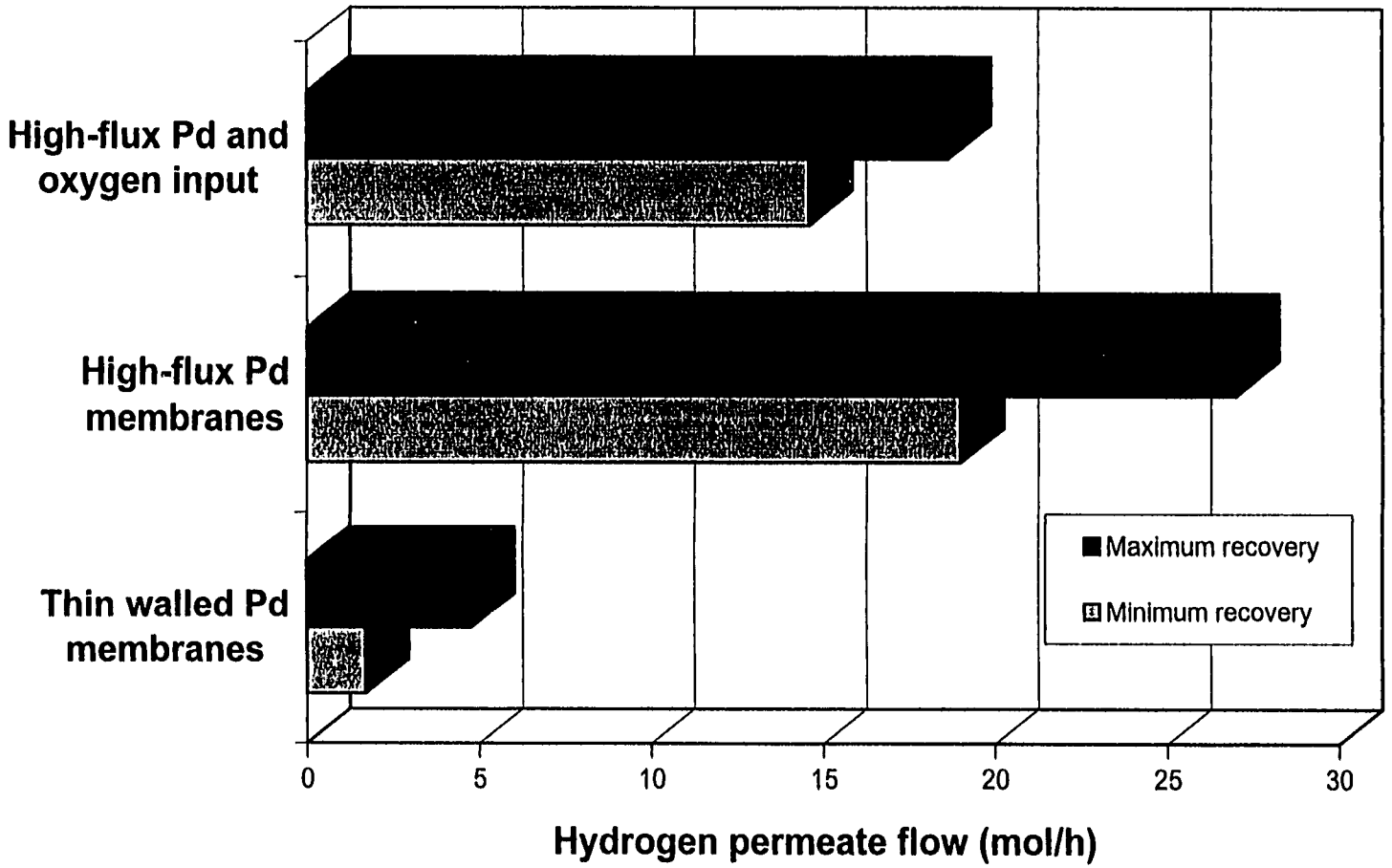

increasing trend with increased pressure as shown in Figure 6.8. This comparison shows an increase in methane conversion for the oxygen input configuration, while there is a decrease in hydrogen yield and permeation.

The effects of temperature for FBMR with oxygen input, FBMR and equilibrium without oxygen have been studied. Methane conversions for the FBMR with oxygen input runs are highest and show an increasing trend with increasing temperature. This is due to the combined effect of oxygen reaction plus permeation as shown in Figure 6.9. The hydrogen yields are lower when oxygen is added, and have an increasing trend as plotted in Figure 6.10. Again, hydrogen permeation is lower than FBMR because of the lower partial pressure of hydrogen in the reactor. The hydrogen yield and permeation show an increasing trend with increasing temperature as shown in Figure 6.10, demonstrating an increase in methane conversion, hydrogen yield, and permeation with increased temperature.

The difference between the partial pressure of hydrogen in the reactor and the inside of the membrane is the driving force for permeation. Driving force at the exit of the reactor for a selected set of runs was evaluated for the FBMR with oxygen input configuration and compared to that without oxygen input. As illustrated in Figure 6.11, there is a decrease in driving force in the FBMR with oxygen input. The percentage hydrogen recovery, which reflects the moles per hour of hydrogen recovered through the membrane divided by the total moles per hour of hydrogen produced in the reactor, expressed as a percentage, have been plotted in Figure 6.11. There was a lower rate of hydrogen recovery with oxygen addition. Therefore, the penalty for an oxygen input configuration was a reduction in hydrogen production. As there was driving force

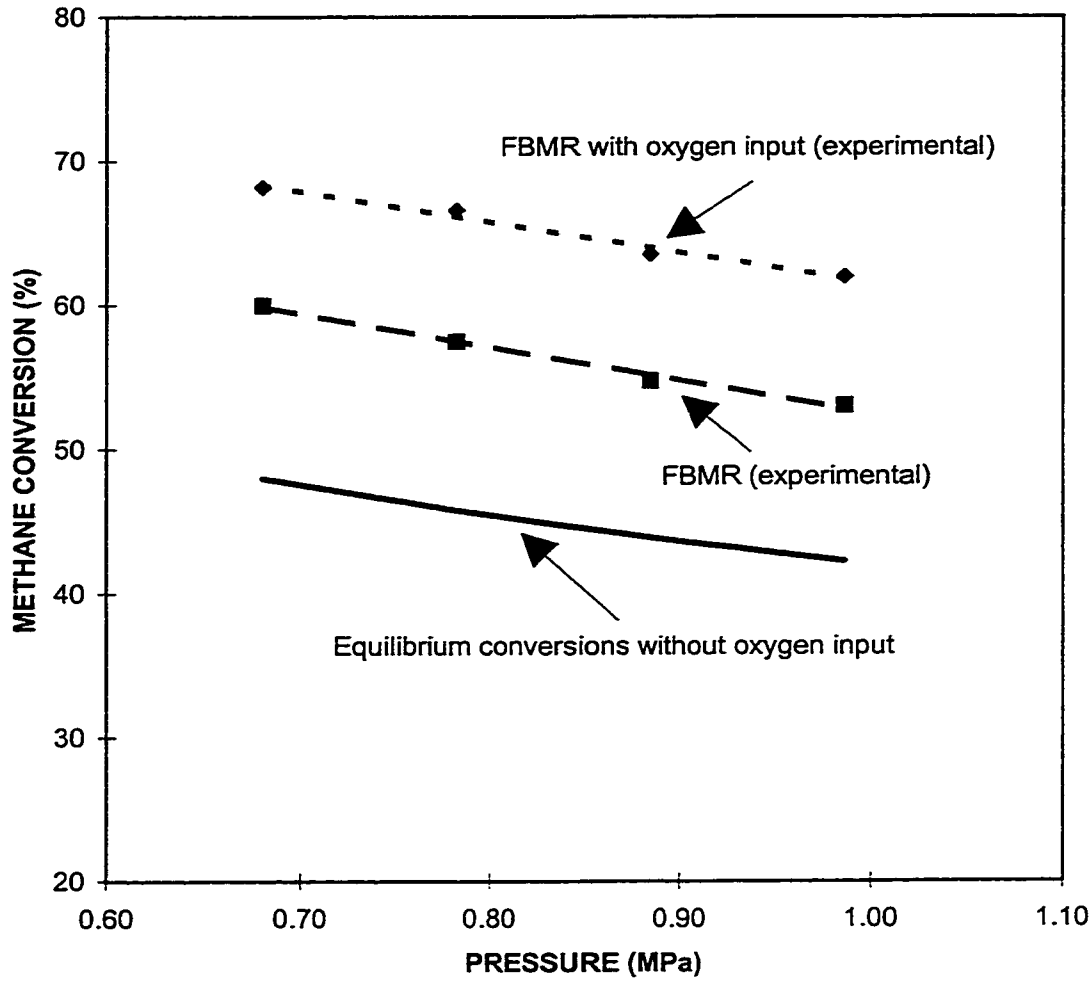

Figure 6.7: Comparison of methane conversion in FBMR with oxygen, FBMR and equilibrium without oxygen with pressure variation.

T=873K., Methane flowrate=33.74mol/h. Steam flowrate=138mol/h. Steam methane ratio= 4.1. Membrane pressure=0.14MPa. Sweep gas flowrate=45mol/h. Oxygen flowrate=15.18mol/h.

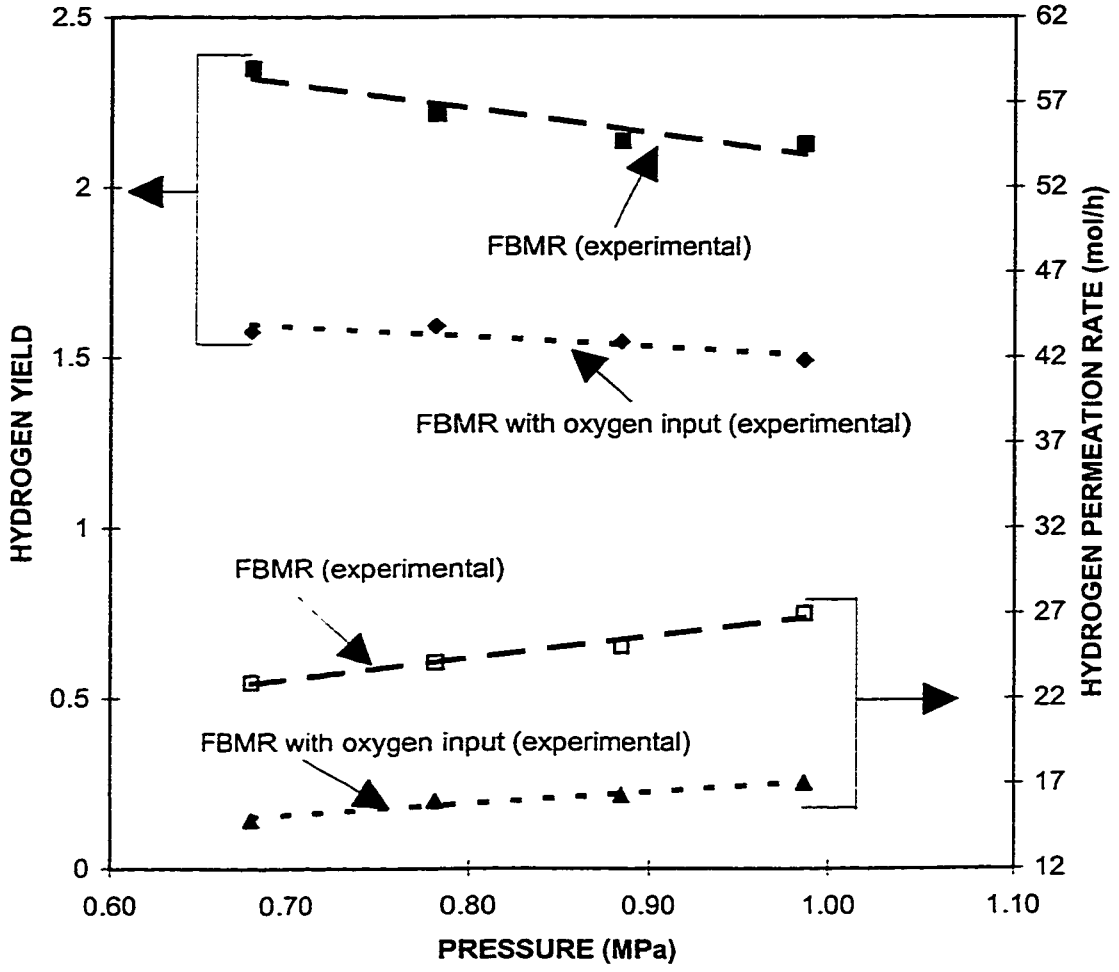

Figure 6.8: Comparison of hydrogen yield and permeation rate in FBMR with oxygen and FBMR with pressure variation.

T=873K., Methane flowrate=33.74mol/h. Steam flowrate=138mol/h. Steam methane ratio= 4.1. Membrane pressure=0.14MPa. Sweep gas flowrate=45mol/h. Oxygen flowrate=15.18mol/h.

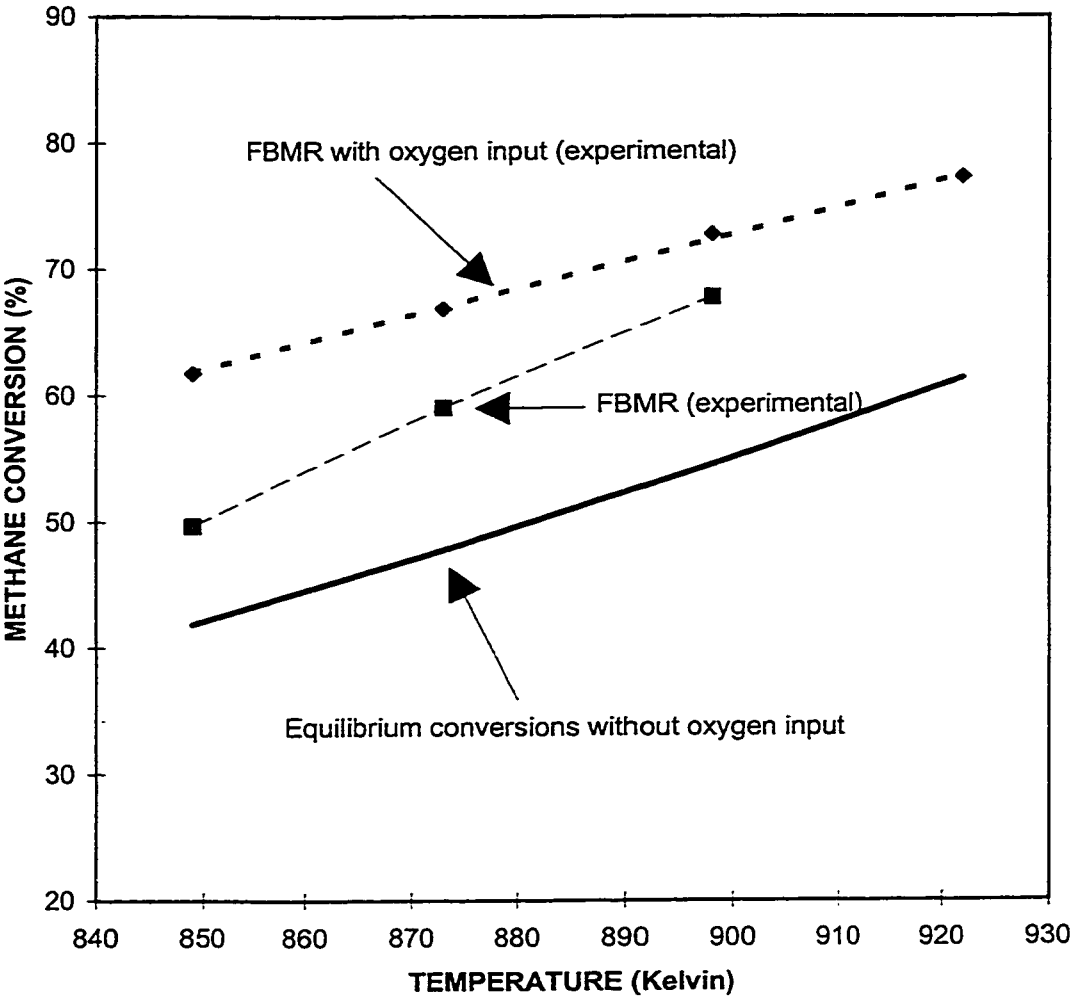

Figure 6.9: Comparison of methane conversions in FBMR with oxygen,FBMR and equilibrium without oxygen input with temperature variation

P=0.68MPa., Methane flowrate=33.74mol/h. Steam flowrate=138mol/h. Steam methane ratio= 4.1. Membrane pressure=0.14MPa. Sweep gas flowrate=45mol/h. Oxygen flowrate=15.18mol/h.

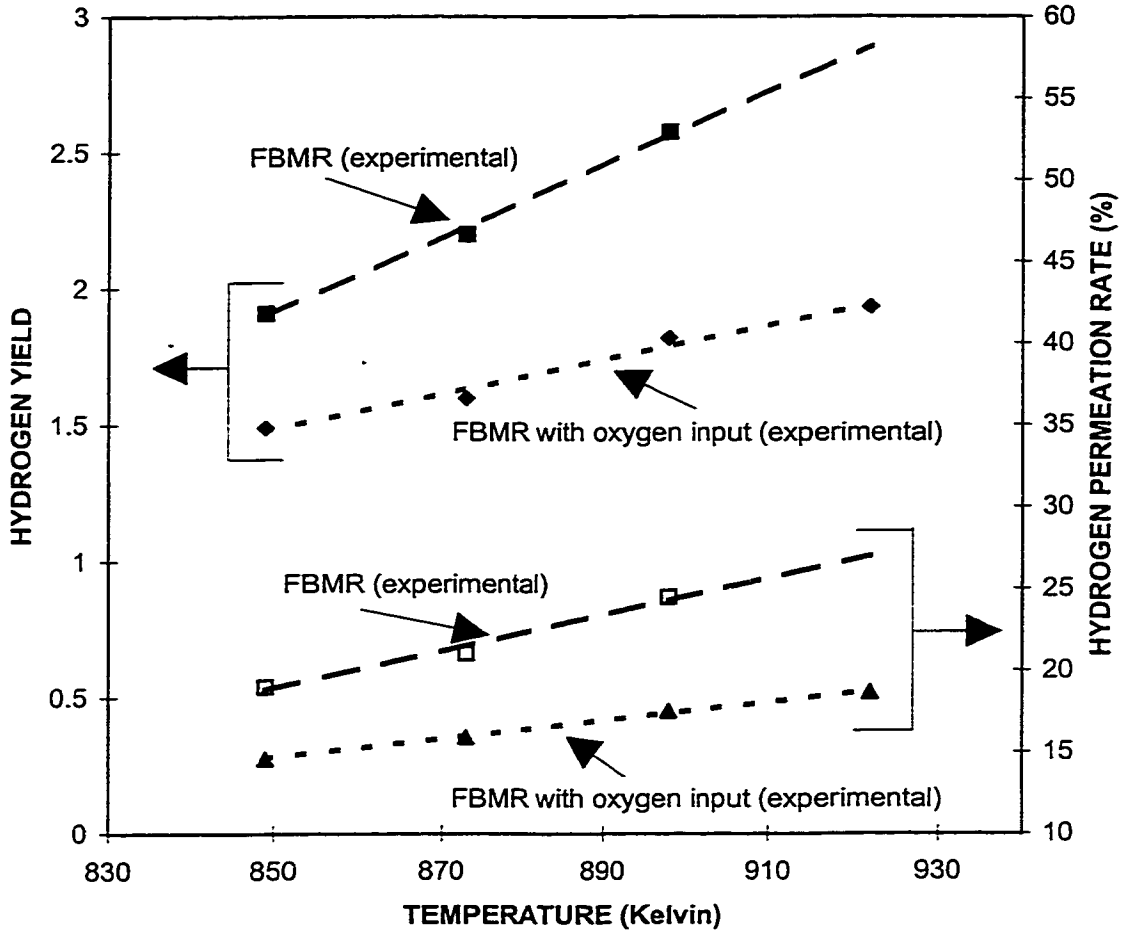

Figure 6.10: Comparison of hydrogen yield and permeation in FBMR with oxygen and FBMR with temperature variation

P=0.68MPa., Methane flowrate=33.74mol/h. Steam flowrate=138mol/h. Steam methane ratio= 4.1. Membrane pressure=0.14MPa. Sweep gas flowrate=45mol/h. Oxygen flowrate=15.18mol/h.

remaining at the reactor exit, more hydrogen could be recovered by increasing the permeation capacity.

The reaction of oxygen with methane is an exothermic reaction that provided sensible heat for reactants, heat of the reforming reaction, and heat loss through the walls of the reactor. A significant part of the heat generated by the exothermic reaction can be accounted for through heat loss. The exit composition provided the information about the heat consumed by the reforming reaction and the sensible heat requirement was calculated using temperature data. The remainder was considered to be the heat loss. The sensible heat requirement was a smaller fraction compared to the heat loss. Figure 6.12 shows the fraction of heat accounted for as reforming, as sensible heat and as heat loss out of the total exothermic heat from oxygen addition. The loss is high relative to commercial practice due to high surface/volume ratio of the pilot plant reformer.

6.4 Data Analysis

6.4.1 Multi-variate analysis of experimental data

Pilot plant data have been correlated by expressing conversion of methane as the key derived parameter. Non-linear regression was performed on appropriate experimental data. The main objective of the exercise was to quantify the relative dependence of methane conversion on the major operating variables of the FBMR.

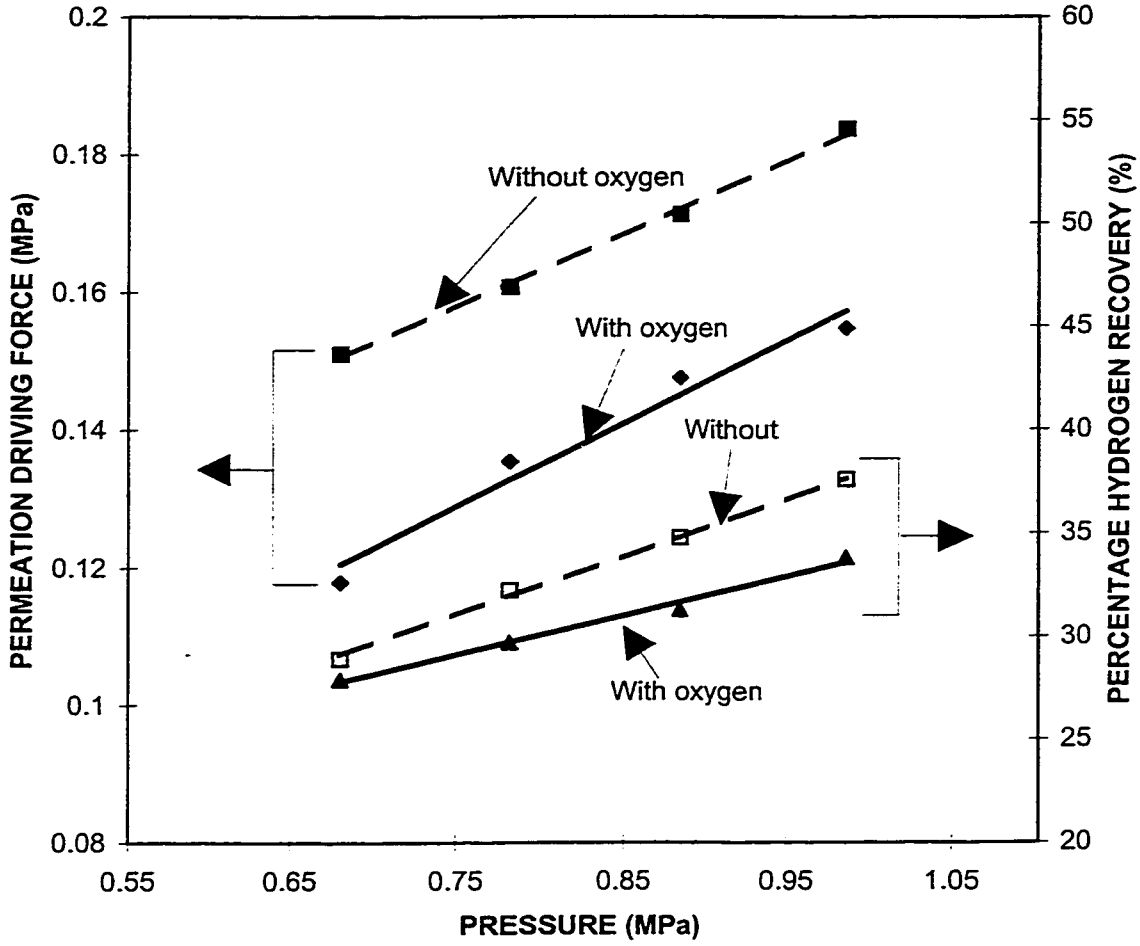

Figure 6.11: Comparison of permeation driving force and percentage hydrogen recovery between autothermal FBMR and FBMR without oxygen input

T= 873 K, Methane flowrate=33.7mol/h. Steam flowrate=138mol/h. Steam methane ratio= 3.1. Sweepgas pressure=6psi. Sweep gas flowrate=45mol/h. Oxygen flowrate(Autothremal FBMR)= 15.2mol/h

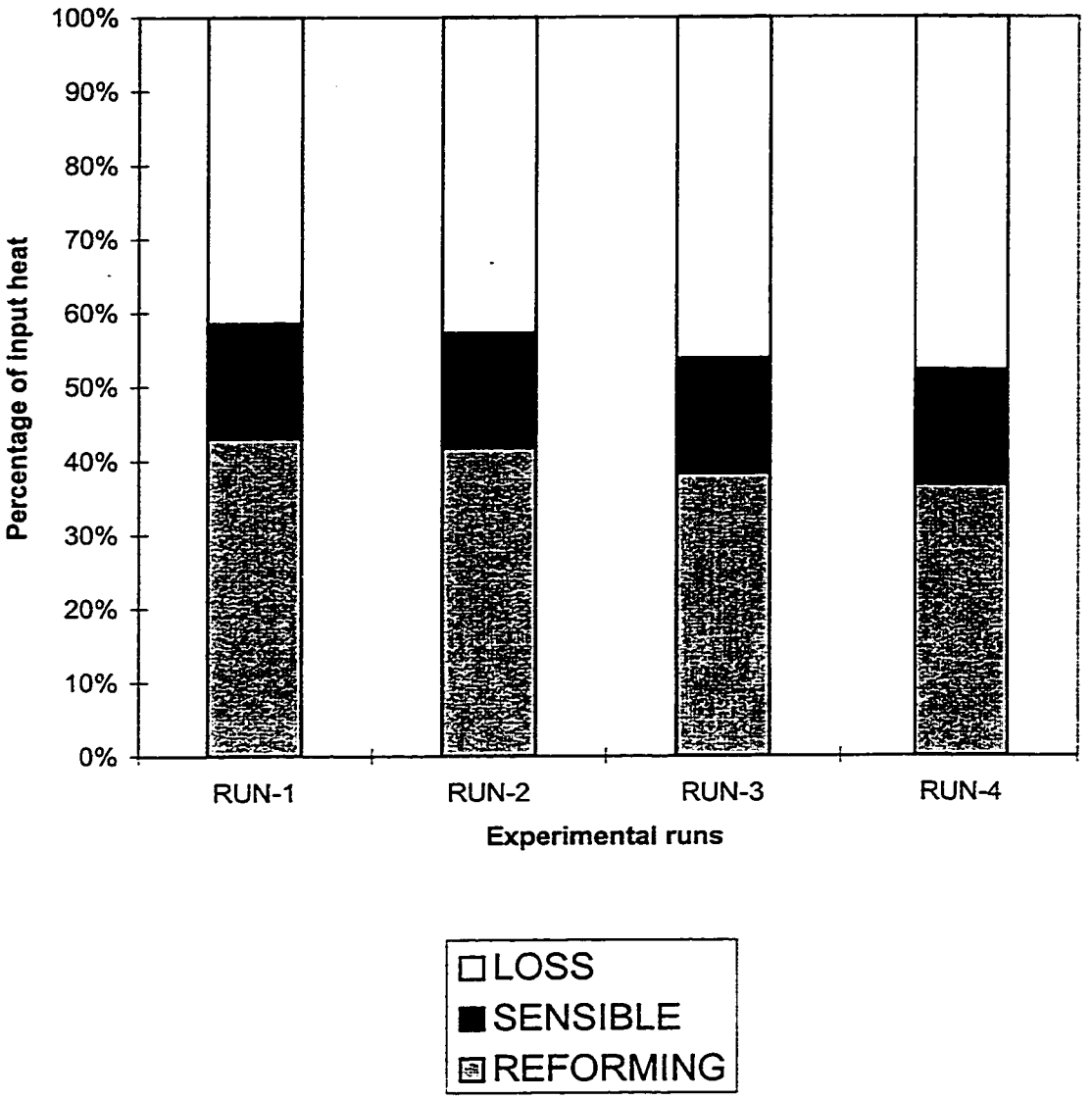

Figure 6.12: Utilization of heat in autothermal FBMR

6.4.1.1 Analysis of FBMR data

The major independent variables considered for the runs of FBMR without oxygen input were temperature (T), pressure (P) and steam-methane ratio of the feed (SC). The superficial velocity has negligible effect on methane conversion as discussed in Chapter 4. The catalyst mass, sweep gas flow and membrane side pressures were kept constant for all runs included in this analysis. Coefficients α, a, b, c were fitted for the simple power law relationship given below:

$$X_{CH4} = \alpha . T^{a} . P^{b} . SC^{c} \qquad (6.1)$$

Where X_{CH4} is the methane conversion and the units of T, P and SC are K, MPa, and dimensionless respectively.

The regression results are plotted versus the experimental runs in Figure 6.13. The regression has a multiple correlation coefficient of 0.97 and the evaluated values for the coefficients α, a, b, c are $3.27X10^{-12}$, 4.35, -0.195 and 0.713 respectively. The results correspond to anticipated trends based on equilibrium considerations. By far the strongest dependence of conversion is on the temperature; hence, the dependence on temperature surpasses that of any other variable within the domain of the present data. A weak negative dependence on pressure was indicated. Similarly, the steam-methane ratio shows a positive dependence for the domain investigated, as expected.

6.4.1.2 Analysis of FBMR with oxygen input data

The major independent variables considered for the runs of FBMR with oxygen input are temperature (T), pressure (P), steam-methane ratio of the feed (SC) and oxygen

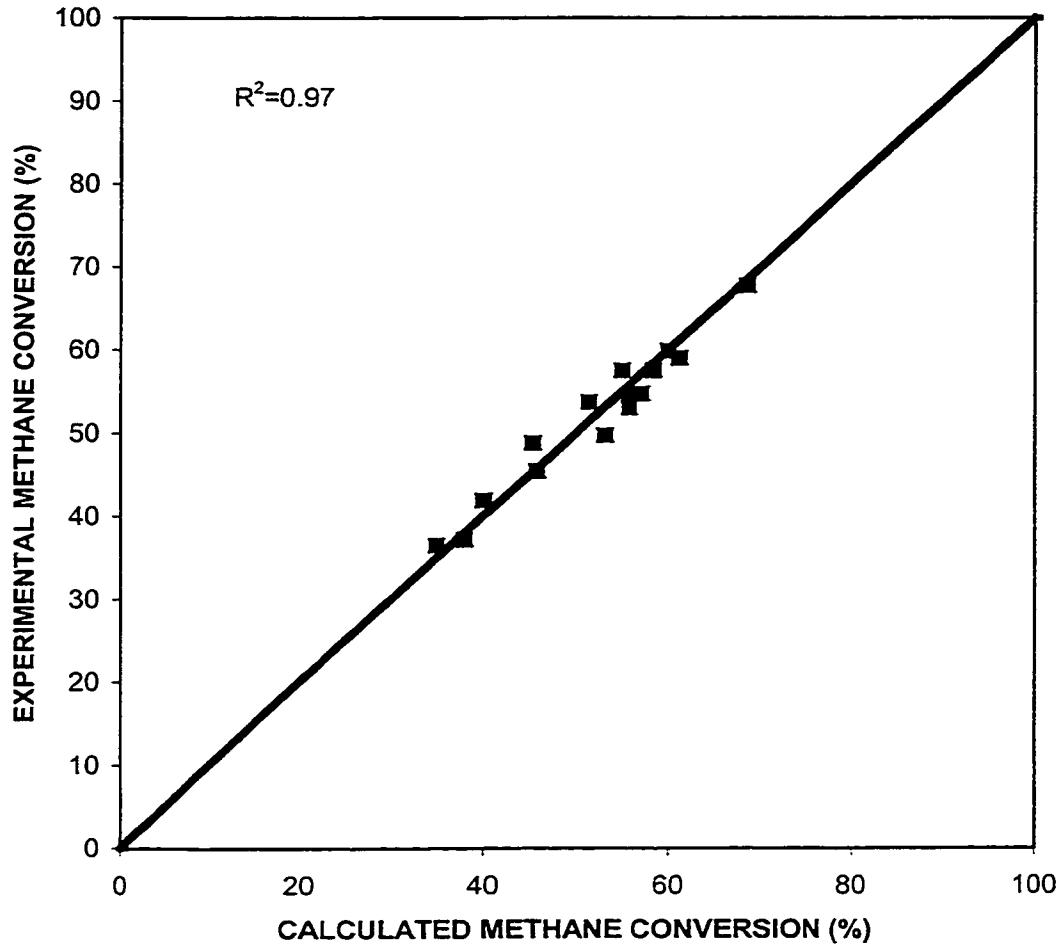

Figure 6.13: EXPERIMENTALLY MEASURED METHANE CONVERSION OF FBMR PLOTTED VERSUS PREDICTION FROM EQUATION 6.1

input flow rate (F_{O2}). The catalyst mass, sweep gas flow and membrane side pressures were kept constant in the data included for this analysis. Coefficients *αo, ao, bo, co, do* were fitted for the simple power law relationship given below:

$$X_{CH4} = \alpha o \, .T^{ao} \, .P^{bo} \, .SC^{co} \, F_{O2}{}^{do} \qquad (6.2)$$

Where X_{CH4} is the methane conversion and the units of T, P, SC and F_{O2} are K, MPa, dimensionless and mol/h. respectively.

The regression results versus the experimental runs are plotted in Figure 6.14. The regression has a multiple correlation coefficient of 0.98 and the evaluated values for the coefficients *αo, ao, bo, co and do* are $1.47X10^{-7}$, 2.75, -0.179, 0.426 and 0.215 respectively. The strongest dependence of conversion is on the temperature. The oxygen flow also has a considerable positive effect on methane conversion. A negative dependence on pressure is indicated and the steam-methane ratio shows a positive dependence for the domain investigated.

6.4.2 Error Analysis

Errors possible in the pilot plant experiments are of two types, systemic errors and random errors (Young, 1962). Errors associated with instruments, measurement procedures or calibration are systemic errors. Unknown and unpredictable variations, errors in judgement and mechanical vibrations constitute random errors. Systemic errors are more important and are difficult to avoid.

Effect of instrument errors and reproducibility errors have been computed in the following sections to evaluate the reliability of the experimental runs.

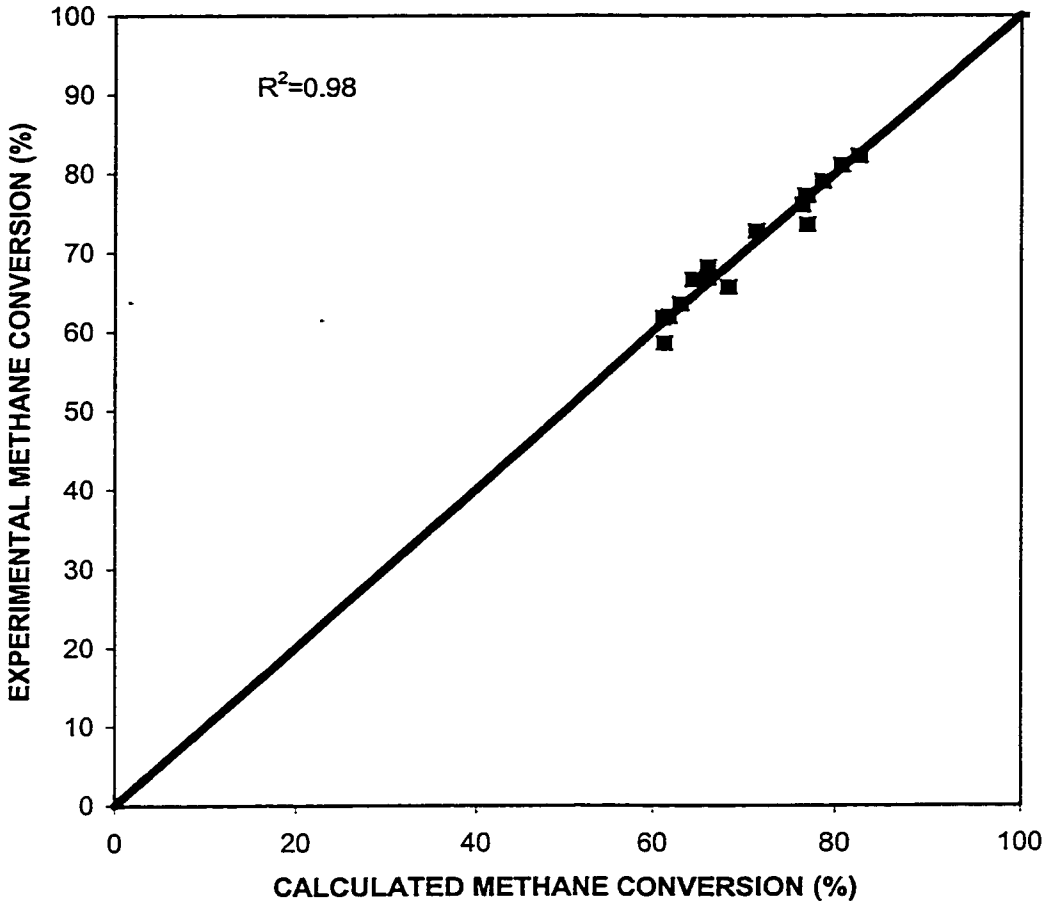

Figure 6.14: EXPERIMENTALLY MEASURED METHANE CONVERSIONS OF FBMR WITH OXYGEN INPUT VERSUS PREDICTIONS FROM EQUATION 6.2

6.4.2.1 Instrument errors

The key derived parameter of methane conversion X_{CH4} is given by the Equation 6.2 as shown the previous section. The resulting error in the methane conversion (ΔX_{CH4}), due to instrument errors is calculated by:

$$\Delta X_{CH4} = \left|\frac{\partial X_{CH4}}{\partial T}\right|\Delta T + \left|\frac{\partial X_{CH4}}{\partial P}\right|\Delta P + \left|\frac{\partial X_{CH4}}{\partial SC}\right|\Delta SC + \left|\frac{\partial X_{CH4}}{\partial F_{O2}}\right|\Delta F_{O2} \qquad (6.3)$$

Where ΔT, ΔP, ΔSC and ΔF_{O2} are the accuracy associated with the measurement temperature, pressure, steam-methane ratio and flow of oxygen respectively. The values of accuracy given by manufacturers for thermocouples, pressure transducer, rotameter and mass flow meter are ±0.4%, ±0.4%, ±2.0% and ±0.5% respectively.

The measurement errors were calculated for the domain of experimental data and the average absolute measurement error in methane conversion was 2.13%.

6.4.2.2 Reproducibility of pilot plant experiments

Measurement errors, indicating the reproducibility of the present experiments were evaluated. One data point was repeated four times and five other data points were repeated three times, days apart from each other. These data points were averaged and the deviation with respect to the average value was calculated. The average absolute deviation of these points was 0.73% in calculated methane conversions, indicating excellent reproducibility.

Runs were carried out with two different catalyst loading to ensure that there was an excess of catalyst. These also served to check reproducibility. Three data points were

repeated with catalyst loading of 3.5 kg and 4.3 kg. The average absolute deviation of these points was 0.43% in calculated methane conversions, again indicating excellent reproducibility and the presence of excess catalyst.

6.5 Conclusions

An autothermal FBMR unit producing hydrogen was successfully developed and tested. This new concept was proved and validated. The hydrogen permeate flow (mol/h) in the autothermal FBMR study was on average seven to ten times greater than in the previous study (Adris, 1994). The comparison with FBMR proves that the oxygen input configuration gives increased methane conversion but decreased hydrogen yield and permeation.

Data analysis shows good reproducibility and accuracy of pilot plant experiments and the presence excess catalyst in the reactor.

Chapter 7

Computer Simulation of FBMR

7.1 Introduction

A fluidized bed steam-methane reforming computer model has been developed as a means to simulate the catalytic process with High-flux membrane modules and oxygen input.

A model was earlier developed and validated by Adris et al. (1997). The model was based on a two-phase bubbling bed reactor model (Grace, 1984). Removal of hydrogen from the two bed phases and the dilute phase in the freeboard was computed, and reaction on entrained catalyst in the freeboard was accounted for. The original model handled a feed of steam and methane only.

In this chapter, a more rigorous model is presented. This model is also based on the two-phase bubbling bed reactor model (Grace, 1984), but with four distinct zones in the reactor. Furthermore, the model has been adapted to handle oxygen input.

The four zones in the reactor as shown in Figure 7.1 are:

ZONE 1 Bubbling bed with dense and bubbling phases

ZONE 2 Two-phase bubbling bed with High-flux membranes

ZONE 3 Freeboard with dilute and High-flux membranes

ZONE 4 Freeboard with dilute phase only

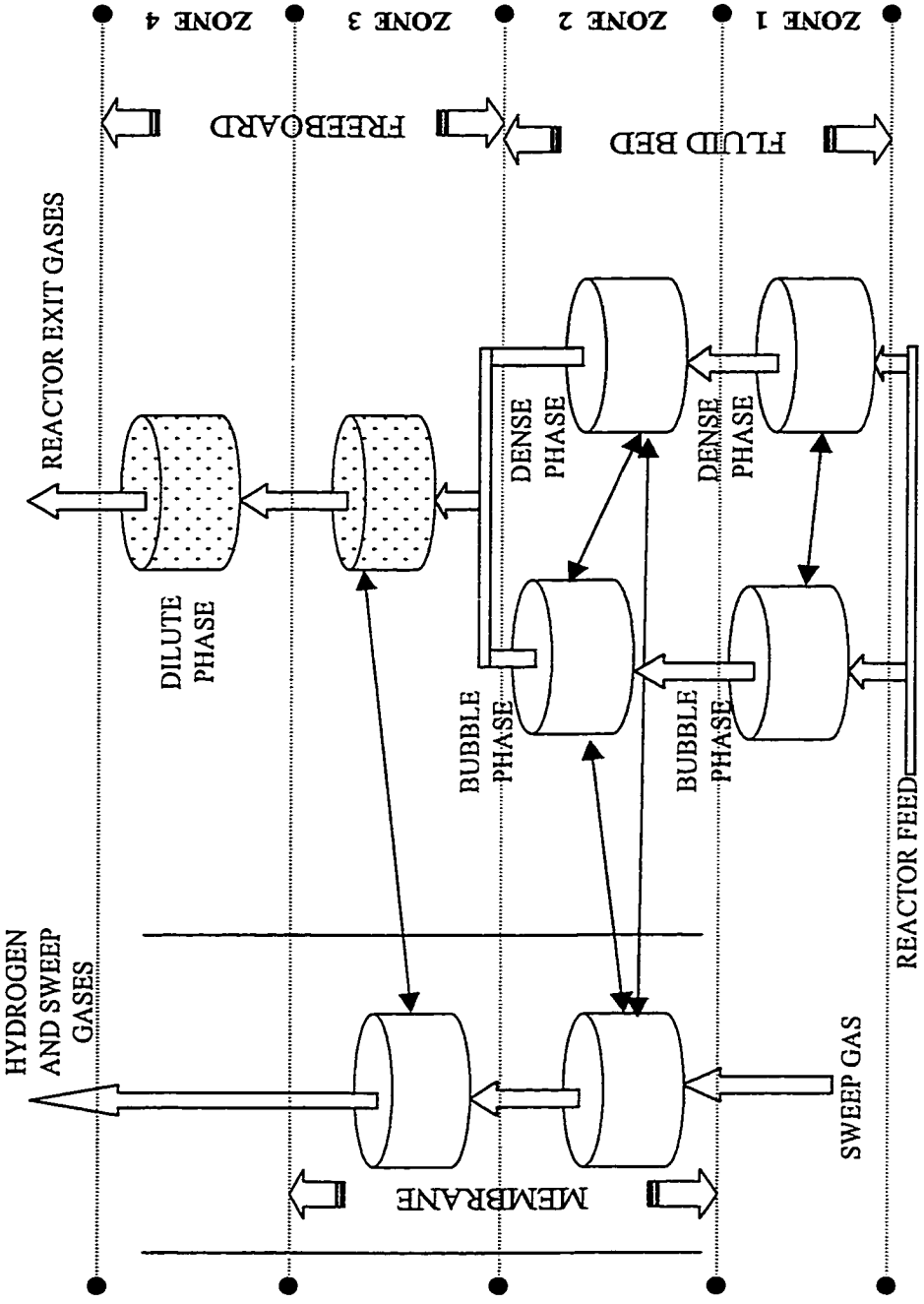

Figure 7.1: Schematic of phases and zones used in FBMR model

Reactions in the bubble phase and the freeboard region (dilute phase) were included in this work. Also, the changes in bubble size and superficial velocity along the bed height were taken into consideration. The superficial velocity increases with height as there is an increase in the total number of moles as the reactions proceed.

Minimum fluidization velocities at different temperatures, as reported in Chapter 4, were used in this study. A commercial Ni/ Al_2O_3 catalyst with size range of 90 to 350 μm, mean particle diameter of 187 μm, particle density of 3550 kg/m^3, and bulk density of 1450 kg/m^3 (Group B of Geldart's (1972) particle classification) as described in Chapter 4 was used for the model.

The model uses a reformer inner diameter of 0.097 m and a distributor plate with 134 holes. Except for the bubble diameter, all other parameters are independent of the reactor dimensions provided the feed ratio, inlet superficial velocity, temperature and pressure remain the same. Bubble diameter is a function of the internal diameter of the reactor and the number of orifices in the distributor plate.

The model was validated with the FBMR data (with and without oxygen input) involving no fitting of parameters except effectiveness of the permeation.

7.2 Model development

7.2.1 High-flux membrane tube model

The mechanism of hydrogen permeation and the parameters used to evaluate permeation of hydrogen through High-flux membrane have been reported in Chapter 3.

In the reformer environment, the high pressure side is the reactor side while the low pressure side is the permeate side (membrane).

In the fluidized bed membrane configuration the effective permeability will be less than that measured under ideal conditions. This permeability may be affected by the following factors:

1. Spring reinforcement coverage of membrane surface, which reduces inside surface area.

2. Variation in palladium coating thickness,

3. Coverage of membrane outside surface by catalyst dust, which affects the permeation process.

4. Exposure of membrane tube to two different phases, the bubble phase and the dense phase, each of which may have different hydrogen permeation rates.

5. Gas phase mass transfer resistance.

A parameter, called the effectiveness of permeation, η_P, was used to account for the influence of the above factors on the permeation rate constant. The effective permeability is the product of η_P and the permeability,

$$P_{Meff} = \eta_P . P_M \tag{7.1}$$

The permeability is given by the following equation:

$$P_M = P_{MO} \exp\left(-\frac{E_p}{R_g T}\right) \tag{7.2}$$

The permeability pre-exponential factor (P_{MO}), the activation energy (E_P) and the pressure exponent (n) were determined from experimentally obtained permeation rates reported in Chapter 3.

The molar permeation rate of hydrogen (N_{H2}) was estimated by the equation reported below, derived from Equation 3.1 $\{J_{H2} = P_M\left(\frac{P_{H2h}^n - P_{H2l}^n}{t}\right)\}$:

$$N_{H2} = \eta_P P_M A_m \frac{(P_{H2h}^n - P_{H2i}^n)}{t_{tot}} \tag{7.3}$$

where:

$$A_m = \pi d_i l = \pi l (d_o - 2t_{tot}) \tag{7.4}$$

and, l is the length and t_{tot} is the total thickness of the membrane tube.

The mass balance of an element of High-flux tube for length 'dh' gives a differential equation which relates molar hydrogen permeation rate at any point along the length h to other parameters. An equation in such a form can be incorporated with the FBMR model equations. The equation is written as:

$$\frac{dn_{H2}}{dh} = \eta_P P_M \pi (d_o - 2t_{tot}) \frac{(P_{H2h}^n - P_{H2l}^n)}{t_{tot}} \tag{7.5}$$

where P_M was evaluated by Equation 7.2. The High-flux membrane tubes used for the FBMR experimentation had a substrate thickness of 76 μm and palladium coating of 5.2 μm on both the outside and inside surfaces. This coating thickness was supplied by REB research for these tubes. The outer diameter d_o of the tubes were 3.175 mm.

Considering the dimensions of the High-flux membrane the parameters evaluated by experimentation were as follows: the permeability pre-exponential factor (P_{MO}) was

7.85×10^{-9} mol/(m.s.$Pa^{0.72}$); activation energy (E_P) was 11.5 kJ/mol; and the pressure exponent (n) was 0.72.

7.2.2 Model assumptions

The model equations are based on the following assumptions:

1) Steady state conditions.

2) Ideal gas law behavior for all gases.

3) The catalyst bed is composed of a bubble phase and a dense phase.

4) No axial dispersion of gas in either phase.

5) No intraparticle mass transfer resistance.

6) Freeboard has only a single phase (dilute phase) with entrained catalyst.

7) Reaction takes place on the surface of the entrained catalyst particles in the freeboard region. The concentration of catalyst particles decreases exponentially with height.

8) The membrane is taken as a separate phase and permeates only hydrogen from the bubble, dense and dilute phase.

9) Gases on the membrane side are in plug flow.

10) Mass exchange of components between the bubble phase and the dense phase is due to concentration gradients.

11) There are no axial or radial temperature gradients in the catalyst bed i.e. the bed is isothermal.

12) All the reactions occurring over the surface of the catalyst particles (in the fluidized bed as well as in the dilute phase) can be described by the kinetic rate equations.

13) Reformer has four separate zones as mentioned previously.

7.2.3 Bed hydrodynamics

The hydrodynamics of the fluidized bed reactor were described by an adaptation of the two-phase bubbling bed reactor model of Grace (1984). It was assumed that at the inlet gas flows through the dense phase at the minimum fluidization velocity (U_{mf}) and the remaining gas flows as bubble phase. All hydrodynamic parameters as well as mass transfer coefficients were dependent on the height above the distributor.

The Mori and Wen (1975) correlation which accounts for bubble growth due to coalescence was used to estimate bubble size, d_b, at any height, h, above the distributor:

$$\frac{d_{bm} - d_b}{d_{bm} - d_{bo}} = \exp(-0.3h / D) \tag{7.6}$$

where D is the internal diameter of the reactor, and d_{bo} is the initial bubble size produced just above the distributor level as estimated using the correlation proposed by Miwo (1972):

$$d_{bo} = \frac{1.38}{g^{0.2}}\left[\frac{A_i.(U_o - U_{mf})}{N_{or}}\right]^{2/5} \tag{7.7}$$

where U_o is the superficial velocity, A_i is the internal cross sectional area of the reactor, N_{or} is the number of orifices in the distributor plate, and d_{bm} is the maximum bubble diameter at the given gas flow rate given by:

$$d_{bm} = 1.64\left[A_i.(U_o - U_{mf})\right]^{2/5} \tag{7.8}$$

Assuming all the bubbles are spherical, the ratio of bubble surface area to volume, a_b, is given by the relation:

$$a_b = \frac{6}{d_b} \tag{7.9}$$

The volume fraction of bed occupied by bubbles, ε_b, was estimated by:

$$\varepsilon_b = \frac{U_o - U_{mf}}{U_{abs}} \tag{7.10}$$

where U_{abs} is the absolute rise velocity of bubbles and was calculated from:

$$U_{abs} = U_o - U_{mf} + U_{br} \tag{7.11}$$

Here U_{br} is the relative rise velocity of bubbles and can be estimated using the correlation proposed by Davidson and Harrison (1963):

$$U_{br} = 0.711(g.\, d_b)^{1/2} \tag{7.12}$$

For the volume fraction of bed occupied by solids dispersed in the bubble phase, ϕ_b, Kunii and Levenspiel (1969) found that:

$$0.001\varepsilon_b < \phi_b < 0.01\varepsilon_b \tag{7.13}$$

In this model the average of these two limiting values was used to estimate ϕ_b.

The volume fraction occupied by dense phase solids (including all of the solids in the clouds and wakes), ϕ_e, was approximated by assuming that the dense phase voidage was constant and equal to the voidage corresponding to the minimum fluidization velocity (ε_{mf})(Grace, 1986):

$$\phi_e = (1-\varepsilon_b)(1-\varepsilon_{mf}) \tag{7.14}$$

The effective diffusivity of any component i in a mixture (D_{id}) was used to calculate the interphase mass exchange coefficient for each component. D_{id} was estimated based on the average composition (mole fraction) in the bubble phase and the dense phase [i.e.$y_{id}=(y_{ib}+y_{ie})/2$] using a relation given by Wilke and Lee (1955):

$$\frac{(1-y_{id})}{D_{id}} = \sum_{j=1}^{n}(y_j / D_{ij}) \tag{7.15}$$

where D_{ij} is the binary diffusivity of components i and j, and was estimated from critical constants using the relation proposed by Slattery and Bird (1958):

$$D_{ij} = \frac{0.01498\, T^{1.81}\left(\frac{1}{M_i}+\frac{1}{M_j}\right)^{0.5}}{P(T_{ci}T_{cj})^{0.1405}(V_{ci}^{0.4}+V_{cj}^{0.4})^2} \tag{7.16}$$

where T, T_{ci},T_{cj} are in degrees kelvin; V_{ci}, V_{cj} in $cm^3/gmol$, P in atm., and D_{ij} is in cm^2/sec.

Finally, the interphase mass exchange coefficient for component i, k_{iq}, was calculated using the semi-empirical equation of Sit and Grace (1981):

$$k_{iq} = \frac{U_{mf}}{3} + \left(\frac{4D_{id}\cdot\varepsilon_{mf}\cdot U_{abs}}{\pi . d_b}\right)^{1/2} \tag{7.17}$$

For the freeboard region, it was assumed that the entrainment flux of solids decreased exponentially with respect to the distance above the bed surface (h_{dil}) (Wen and Chen, 1982):

$$\frac{\Psi_{h_{dil}}-\Psi_\infty}{\Psi_o-\Psi_\infty} = e^{-a_c . h_{dil}} \tag{7.18}$$

where, Ψ_{dil} is the entrainment flux of solids at any height, h_{dil}, above the catalyst bed (in the dilute phase), Ψ_o is the entrainment flux of solids at the bed surface, Ψ_∞ is the

entrainment flux above the transport disengagement height (TDH) of fine particles; and a_c is the overall decay constant. The above parameters were calculated using the method given by Geldart (1986) and the values are:

$\Psi_0 = 0.2$ kg/(m^2.s)

$\Psi_\infty = 0.004$ kg/(m^2.s)

$a_c = 4$ m^{-1}

7.2.4 Reaction kinetics

The reaction network was assumed to consist of the following reactions: complete oxidation of methane, partial oxidation of methane to carbon monoxide, steam reforming of methane to carbon monoxide, water-gas shift and steam reforming of methane to carbon dioxide.

$$CH_4 + 2O_2 = CO_2 + 2H_2O \qquad (7.19)$$

$$CH_4 + 1.5O_2 = CO + 2H_2O \qquad (7.20)$$

The two reactions (Equations 7.19 and 7.20) were used to describe the oxidation of methane in the catalyst bed. Oxidation of methane has been studied extensively and a number of mechanistic reaction networks comprised of a large number of elementary reactions are available. Global rate expressions are difficult to find in the literature. Most of the reaction networks were developed for the homogeneous combustion of methane in air or oxygen, but our requirement is catalytic combustion in presence of other components. Some studies have reported on the heterogeneous (catalytic) oxidation of methane, but most of them focused on syngas generation by partial oxidation of methane. Very few attempts have been made to develop kinetic rate expressions for two

reasons: i) above the light-off temperature of the catalyst particles, complete conversion of oxygen is achieved and the reaction reaches equilibrium instantaneously; ii) the rate of reaction is so fast that the diffusional resistance in the catalyst pore becomes rate controlling.

After correlating experimental data, Yermakova et al. (1993) developed intrinsic rate expressions for the catalytic oxidation of methane over alumina catalysts for the temperature range 913 K to 1103 K. Oxygen was the limiting reactant in all the experiments and the reactions were carried out in the presence of an inert gas. Yermakova et al. considered two different reaction mechanisms. The first was based on parallel reactions Equations 7.19 and 7.20 whereas the second considered series reactions, the oxidation of methane to carbon monoxide and then oxidation of carbon monoxide to carbon dioxide. The experimental data validated the parallel reactions 7.19 & 7.20, for which the rate expressions were given as:

$$R_1 = k_1 y_{CH_4}^{0.5} y_{O_2} \tag{7.21}$$

$$R_2 = k_2 y_{CH_4}^{0.5} y_{O_2}^{0.75} \tag{7.22}$$

and the rate constants are:

Rate/ Adsorption constants	Pre-exponential factor	Activation energy/ Heat of adsorption kJ/mol
k_1	4.54×10^{12}	170.3
k_2	1.11×10^{11}	139.7

where R_1 and R_2 are the rate of the reactions 7.19 and7.20, respectively, k_1 and k_2 are the corresponding rate constants, and y_{CH4} and y_{O2} are the mole fractions of methane and oxygen, respectively.

Xu and Froment (1989) developed rate expressions for steam ethane reforming based on the Langmuir-Hinshelwood-Hougen-Watson approach after correlating data over a wide range of operating conditions. The 13 step reaction scheme represents 3 global reactions given by Equations 1.1, 1.2 and 1.3 of Chapter 1. The rate equations for the global reactions are given in Chapter 2 and described by Equations 2.1, 2.2, 2.3 and 2.4. R3, R4 and R5 (Chapter 2, Equations 2.1, 2,2 & 2.3) represent the global reaction rates for Equations 1.1, 1,2 & 1.3

The rates of formation for individual components are given by{kmol/(kg cat.h)}:

$$R_{CH4} = -R_1 - R_2 - R_3 - R_5 \tag{7.23}$$

$$R_{H2O} = 2R_1 + 2R_2 - R_3 - R_4 - 2R_5 \tag{7.24}$$

$$R_{H2} = 3R_3 + R_4 + 4R_5 \tag{7.25}$$

$$R_{CO} = R_2 + R_3 - R_4 \tag{7.26}$$

$$R_{CO2} = R_1 + R_4 + R_5 \tag{7.27}$$

$$R_{O2} = -2R_1 - 1.5R_2 \tag{7.28}$$

$$R_{N2} = 0 \tag{7.29}$$

With minor modification in the inlet flow rate, the same model can be used if natural gas is used instead of methane. The higher molecular weight alkanes in the natural gas feed can be assumed to dissociate instantaneously at the reactor inlet to form methane according to the following reactions (Hyman, 1968):

$$C_2H_6 + H_2 = 2CH_4 \tag{7.30}$$

$$C_3H_8 + 2H_2 = 3CH_4 \quad (7.31)$$

The generalized form is (where n_k is the molar flow rate of hydrocarbon having k carbon atoms per molecule):

$$C_kH_{2k+2} + (k-1)H_2 = kCH_4 \quad (7.32)$$

$$CH_4 \text{ (at the reactor inlet)} = \text{original } CH_4 + \sum_{\text{all k}} kn_k \quad (7.33)$$

$$H_2 \text{ (at the reactor inlet)} = \text{original } H_2 - \sum_{\text{all k}} (k-1)n_k \quad (7.34)$$

7.2.5 Reactor model

The mole balances of each component in dense, bubble, dilute and separation phases for a differential elemental height of the reactor constitutes the differential equations for the model. The components are denoted i where i equals 1 for methane, 2 for steam, 3 for hydrogen, 4 for carbon monoxide, 5 for carbon dioxide, 6 for oxygen and 7 for nitrogen.

7.2.5.1 Zone 1 equations

Zone 1 consists of the catalyst-bed below the membranes and is represented by these equations:

A mole balance on component i in the bubble phase give:

$$\frac{dn_{ib}}{dh} = k_{iq}.a_b.\varepsilon_b.A_i.(C_{ie} - C_{ib}) + \phi_b.\rho_S.A_i.R_{ib} \quad (7.35)$$

where ρ_S is the particle density of the catalyst; R_{ib} is the rate of formation of component i in the bubble phase; n_{ib} is the molar flow rate of component i in the bubble phase; and C_{ib}

and C_{ie} are the concentration of component i in the bubble and dense phase, respectively. All other parameters were previously defined.

Similarly, a mole balance on component i in the dense phase gives:

$$\frac{dn_{ie}}{dh} = k_{iq}.a_b.\varepsilon_b.A_i.(C_{ib} - C_{ie}) + \phi_e.\rho_S.A_i.R_{ie} \qquad (7.36)$$

where R_{ie} is the rate of formation of component i in the dense phase and n_{ie} is the molar flow rate of component i in the dense phase.

The initial conditions for the above differential equations are:

$$n_{ib} = n_{ibo} \quad \text{and} \quad n_{ie} = n_{ieo} \qquad \text{at } h = 0,$$

where, n_{ibo} and n_{ieo} can be calculated from the molar feed rate, n_{io}, using the assumption that the gas flow through the dense phase equals that needed for minimum fluidization:

$$n_{ibo} = \left(\frac{U_o - U_{mf}}{U_o}\right).n_{io} \qquad (7.37)$$

$$n_{ieo} = \left(\frac{U_{mf}}{U_o}\right).n_{io} \qquad (7.38)$$

7.2.5.2 Zone 2 equations

Zone 2 consists of the catalyst-bed in which membranes are immersed and is represented by these equations:

A mole balance on non-hydrogen components (where i equals to 1, 2, 4, 5, 6 or 7) in the bubble phase gives:

$$\frac{dn_{ib}}{dh} = k_{iq}.a_b.\varepsilon_b.A_i.(C_{ie} - C_{ib}) + \phi_b.\rho_S.A_i.R_{ib} \qquad (7.39)$$

a mole balance on hydrogen (i=3) in bubble phase is given by equation:

$$\frac{dn_{ib}}{dh} = k_{iq}.a_b.\varepsilon_b.A_i.(C_{ie} - C_{ib}) + \phi_b.\rho_S.A_i.R_{ib} -$$

$$\varepsilon_b.\eta_p.P_M.\pi(d_o - 2t_{tot}).\frac{(P^n_{H2b} - P^n_{H2s})}{t_{tot}} \qquad (7.40)$$

Similarly, a mole balance on non-hydrogen components (i=1,2,4,5,6 or 7) in the dense phase gives:

$$\frac{dn_{ie}}{dh} = k_{iq}.a_b.\varepsilon_b.A_i.(C_{ib} - C_{ie}) + \phi_e.\rho_S.A_i.R_{ie} \qquad (7.41)$$

a mole balance on hydrogen (i=3) in dense phase is given by equation:

$$\frac{dn_{ie}}{dh} = k_{iq}.a_b.\varepsilon_b.A_i.(C_{ib} - C_{ie}) + \phi_e.\rho_S.A_i.R_{ie} -$$

$$(1-\varepsilon_b).\eta_p.P_M.\pi(d_o - 2t_{tot}).\frac{(P^n_{H2e} - P^n_{H2s})}{t_{tot}} \qquad (7.42)$$

A mole balance on hydrogen (i=3) gives the membrane side equation:

$$\frac{dn_{is}}{dh} = \varepsilon_b.\eta_p.P_M.\pi(d_o - 2t_{tot}).\frac{(P^n_{H2b} - P^n_{H2s})}{t_{tot}} +$$

$$(1-\varepsilon_b).\eta_p.P_M.\pi(d_o - 2t_{tot}).\frac{(P^n_{H2e} - P^n_{H2s})}{t_{tot}} \qquad (7.43)$$

7.2.5.3 Zone 3 equations

Zone 3 is that part of the freeboard region which contains membranes.

The dilute phase equations for hydrogen (i=3) given by their mole balance yields:

$$\frac{dn_{idil}}{dh_{dil}} = \phi_{dil}.\rho_S.A_i.R_{idil} -$$

$$\eta_P . P_M . \pi (d_o - 2t_{tot}) . \frac{(P^n_{H2dil} - P^n_{H2s})}{t_{tot}} \qquad (7.44)$$

The dilute phase equations for non-hydrogen component (i=1, 2, 4, 5, 6 or 7) given by their mole balance yields:

$$\frac{dn_{idil}}{dh_{dil}} = \phi_{dil} . \rho_S . A_i . R_{idil} \qquad (7.45)$$

where h_{dil} is the distance above the bed surface; R_{idil} is the rate of reaction of component i in the dilute phase; n_{idil} is the molar flow rate of component i in the dilute phase; and ϕ_{dil} is the catalyst mass concentration in the freeboard region and is related to entrainment flux of solids by:

$$\phi_{dil} = \frac{\Psi_{h_{dil}}}{U_o} \qquad (7.46)$$

The initial conditions are:

$$n_{idil} = n_{idilo} = n_{ibf} + n_{ief} \qquad \text{at } h_{dil} = 0$$

A mole balance on hydrogen (i=3) gives the membrane side equation:

$$\frac{dn_{is}}{dh_{dil}} = \eta_P . P_M . \pi (d_o - 2t_{tot}) . \frac{(P^n_{H2dil} - P^n_{H2s})}{t_{tot}} \qquad (7.47)$$

7.2.5.4 Zone 4 equations

Zone 4 is the freeboard region without membranes and has dilute phase only.

The dilute phase equations for hydrogen, component i (i=3) given by their mole balance yields:

$$\frac{dn_{idil}}{dh_{dil}} = \phi_{dil} . \rho_S . A_i . R_{idil} \qquad (7.48)$$

The conversion of any feed component can be calculated at any height using the relation:

$$X_i = \frac{n_{io} - n_i}{n_{io}} \tag{7.49}$$

where n_{io} is the molar feed rate of component i. The freeboard region, n_i is the molar flow rate of component i at any particular height (i.e. $n_i = n_{idil}$), and for the dense catalyst bed n_i is the sum of the molar flow rates in the bubble and dense phases ($n_i = n_{ib} + n_{ie}$).

The concentration, partial pressure, molar flow rate and mole fraction of a component at any phase are interrelated by the following relations,

$$C_i = \frac{P}{R_g T} \frac{n_i}{\sum n_i} \tag{7.50}$$

$$y_i = C_i \frac{R_g T}{P} \tag{7.51}$$

$$p_i = C_i R_g T \tag{7.52}$$

$$y_i = \frac{p_i}{P} \tag{7.53}$$

7.2.6 Model solution algorithm

The simulation program was written in C and solved using MATLAB™, computing software of Math Works Inc. The solution algorithm comprised Modules 1-4 to solve for the Zones 1-4 respectively:

1) Module 1 calculates the molar flow rates of all the components in Zone 1 at any reactor height for the dense and bubble phases.

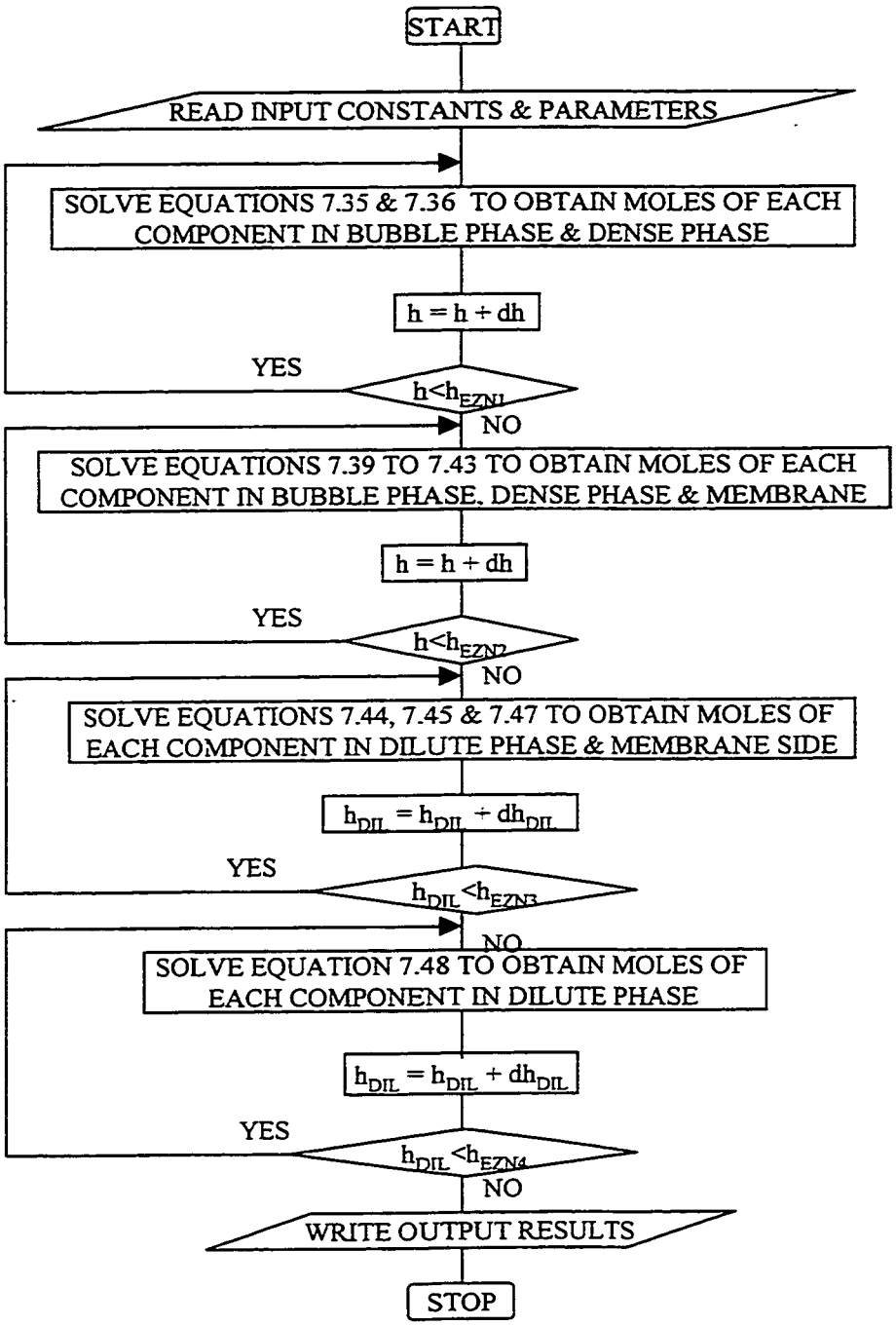

Figure 7.2: Flowchart of FBMR model solution algorithm

2) Module 2 calculates the molar flows rates of all the components in Zone 2 at any reactor height for dense and bubble phases, and the membrane side.

3) Module 3 calculates the molar flow rates in all of the components in Zone 3 at any reactor height for dilute phase and the membrane side.

4) Module 4 calculates the molar flow rates of all the components in Zone 4 at any reactor height for dilute phase only.

Each of the modules calculated the parameters needed for the differential equations from the initial input data supplied. The equations use a numerical routine 'ode45' (fourth order Runge-Kutta method with variable step size) to solve for an incremental height of the reactor. As the intrinsic rates of the reactions are very fast, integration is initiated with a very small step size (less than 10^{-10} m). The program has the ability to simulate fluidized bed membrane reforming with or without oxygen input.

The solution followed the sequence given by the flow chart in Figure 7.2, where h_{EZN1}, h_{EZN2}; h_{EZN3} and h_{EZN4} are height at end of Zones 1 to 4 respectively. Each module in the model is assumed to have uniform temperature but separately they can handle different temperatures. The output of the model gave the exit composition, methane conversion, hydrogen yield and hydrogen permeate flow.

7.3 Model validation

7.3.1 FBMR experimental data vs. model prediction

Experimental results of FBMR runs with and without oxygen input performed during the present investigation, have been simulated using the computer model. A

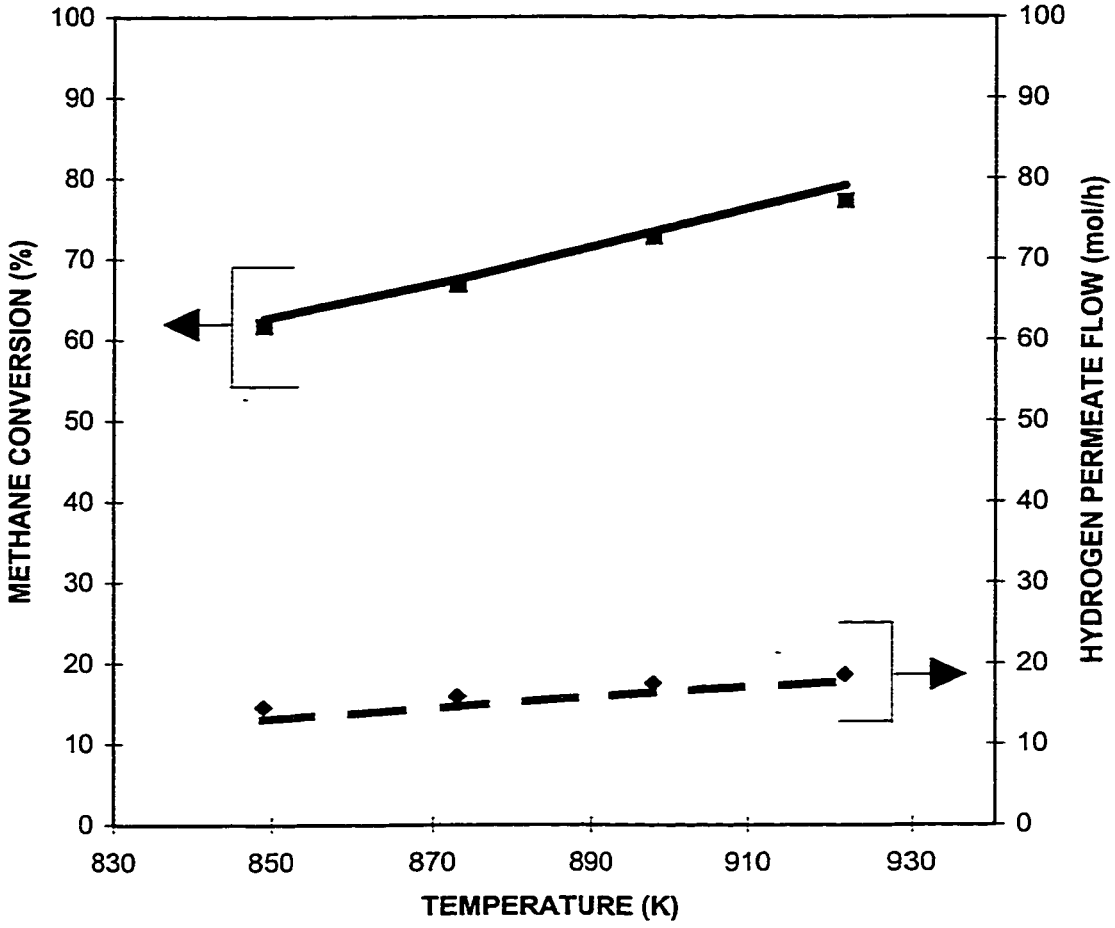

Figure 7.3: Experimental results of FBMR with oxygen input compared to predictions from the model

P=0.68 MPa, Methane flowrate = 33.78 mol/h, Steam flowrate = 138 mol/h, Oxygen flowrate = 15.18 mol/h and Sweep gas flowrate = 45 mol/h.

comparison between the experimental results and model predictions for a set of temperature variation runs for the FBMR with oxygen input has been shown in Figure 7.3. Similarly, a comparison between the experimental results and model results for a set of temperature variation runs for the FBMR is shown in Figure 7.4. Both figures show a very good match between experimental results and model predictions.

7.3.2 Sensitivity analysis

The predicted methane conversion was examined for its sensitivity to four estimated parameters used in the model: catalyst activity, bubble size, solids concentration in the bubble phase and interfacial mass exchange coefficient. Data for all simulation runs are given in terms of methane conversion at the same catalyst bed height. This procedure excluded the freeboard, which may obscure the effects of these parameters.

7.3.2.1 Catalyst activity

Two separate sets of kinetic rate expressions were used in the model: one for oxidation reactions and the other for reforming reactions. The rate expressions were previously developed for similar type of catalyst but having different nickel contents. The difference in catalyst activity between two commercial catalysts can affect the reaction rate estimation by as much as 50% (Elnashaie et al., 1990). The activity evaluated by the rate expressions was multiplied by different factors ranging from 0.01 to 1.0 to examine its effect on the methane conversion as shown in Table 7.1. For a factor of 0.5, the conversion did not change significantly which indicates that mass exchange

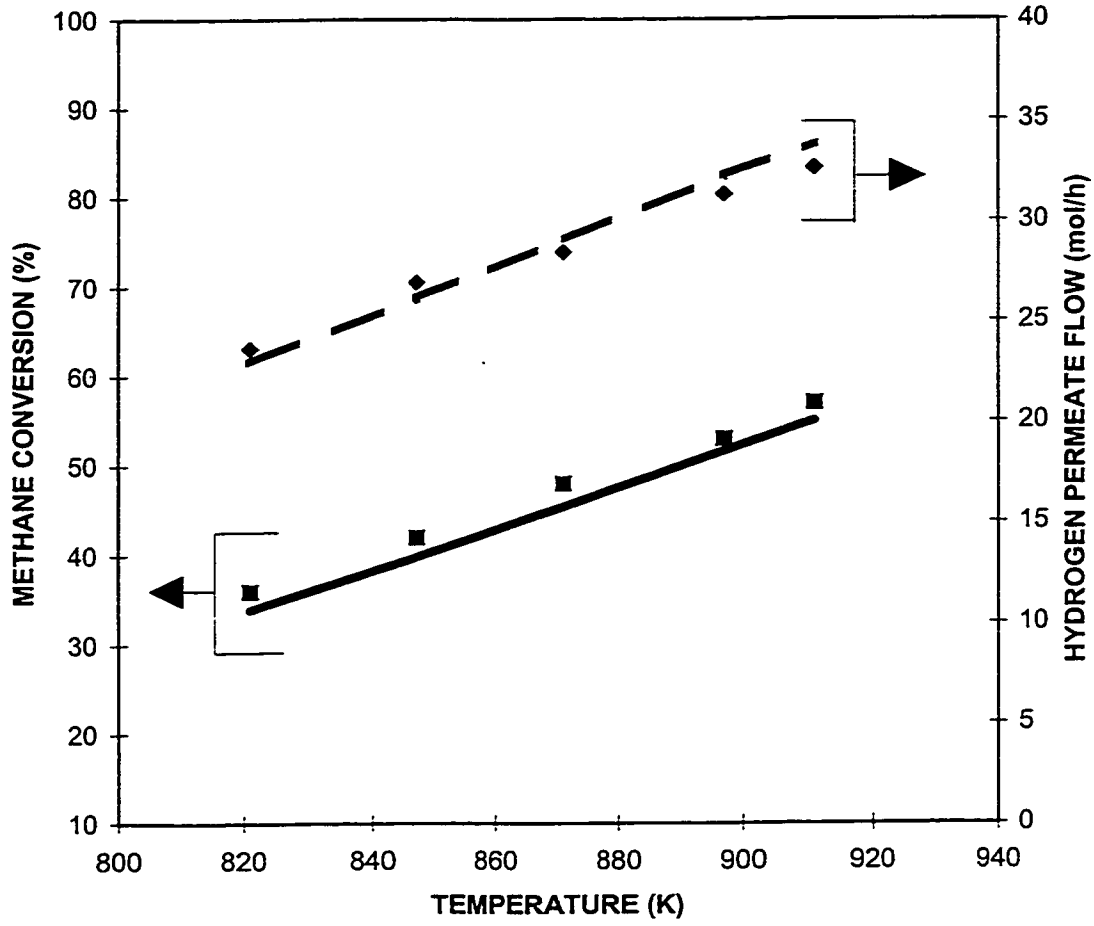

Figure 7.4: Experimental results of FBMR compared to model predictions

P=0.99 MPa, Methane flowrate = 45 mol/h, Steam flowrate = 138 mol/h and Sweep gas flowrate = 45 mol/h.

between the bubble and the emulsion phase is the limiting step. For a very low activity (a factor of 0.01), a longer bed height was required to accomplish the same conversion.

Table 7.1: Model sensitivity to catalyst activity level. T = 973 K, P = 1.0 MPa, Methane flowrate = 100 mol/h, Ratio of CH_4:H_2O:O_2 = 1.0:1.5:0.4.

Catalyst activities multiplied by	1.0	0.5	0.1	0.01
Methane conversion at bed ht. 0.1 m	63.3	62.9	61.5	57.5
% change in at bed ht. of 0.1 m	0.0	-0.6	-2.8	-9.2
Methane conversion at bed ht. 0.2 m	63.3	63.2	62.2	60.4
% change in at bed ht. of 0.2 m	0.0	-0.2	-1.7	-4.6

7.3.2.2 Bubble size

In fluidized bed reactors, bypassing of gas in bubbles has a negative effect on reaction conversion as it reduces gas-solid contacting and deprives part of the reacting gases from exposure to catalyst particles. However for reversible reactions, bubbles can play a positive role by removing reaction products from the reacting mixture, thereby enhancing the forward reactions and suppressing the backward ones.

In the present system membrane tubes are placed vertically in the reactor and the bubble diameters could well be different from estimated ones. The Mori and Wen (1975) correlation (Equation 7.6) was used in this model to estimate the bubble diameter as a function of height. This estimated diameter was multiplied by factors of 0.5, 1.0 and 2.0 to study the effect on methane conversion as shown in Table 7.2. For values less than the Mori and Wen (1975) prediction, bubble size had a limited effect on the conversion.

Table 7.2: Model sensitivity to estimated bubble size. T = 973 K, P = 1.0 MPa, Methane flowrate = 100 mol/h, Ratio of CH_4:H_2O:O_2 = 1.0:1.5:0.4.

Estimated bubble size multiplied by	0.5	1.0	2.0
Methane conversion at bed ht. 0.05 m	63.3	62.6	61.5
% change in at bed ht. of 0.05 m	1.1	0.0	-6.9
Methane conversion at bed ht. 0.1 m	63.3	63.3	61.9
% change in at bed ht. of 0.1 m	0.0	0.0	-2.2

7.3.2.3 Solids concentration in the bubble phase

Kunii and Levenspiel (1969) reported that the solids concentration in the bubble phase (ϕ_b) lies between:

$0.001\varepsilon_b < \phi_b < 0.01\varepsilon_b$ (ε_b = void fraction of bubbles in the catalyst bed)

Table 7.3: Model sensitivity to solids concentration in the bubble phase (ϕ_b). T = 973 K, P = 1.0 MPa, Methane flowrate = 100 mol/h, Ratio of CH_4:H_2O:O_2 = 1.0:1.5:0.4.

Solids concentration in the bubble phase	0.0	0.0055 ε_b	0.01 ε_b
Methane conversion at bed ht. 0.05 m	53.9	62.6	63.3
% change in at bed ht. of 0.05 m	-13.9	0.0	1.1
Methane conversion at bed ht. 0.1 m	58.3	63.3	63.3
% change in at bed ht. of 0.1 m	-7.9	0.0	0.0

In the present model, an average of these limiting values (ϕ_b = 0.0055 ε_b) was used. For this sensitivity analysis, ϕ_b was varied from 0.0 to 0.01ε_b. When solids were eliminated from the bubble phase altogether (ϕ_b=0), there was a decrease in conversion. For a value of ϕ_b=0.01ε_b, the maximum suggested by Kunii and Levenspiel (1991), the conversion remained almost same as that for ϕ_b=0.0055ε_b as shown in Table 7.3.

7.3.2.4 Interfacial mass exchange coefficient

The interphase mass exchange coefficient (k_{iq}) was calculated using the semi-empirical equation of Sit and Grace (1981) (Equation 7.17). Table 7.4 shows four different cases where the mass exchange coefficient was varied from 0.1 to 2.0 times the value predicted by Equation 7.17. When k_{iq} was reduced by half, there was a decrease in conversion but the same conversion was reached at the bed height of 0.10 m.

Table 7.4: Model sensitivity to interphase mass exchange coefficient (k_{iq}). T = 973 K, P = 1.0 MPa, Methane flowrate = 100 mol/h, Ratio of CH_4:H_2O:O_2 = 1.0:1.5:0.4.

k_{iq} multiplied by	0.01	0.5	1.0	2.0
Methane conversion at bed ht. 0.05 m	53.2	61.2	62.6	63.7
% change in at bed ht. of 0.05 m	-15.0	-2.2	0.0	1.8
Methane conversion at bed ht. 0.1 m	56.8	62.9	63.3	63.7
% change in at bed ht. of 0.1 m	-10.3	-0.6	0.0	0.6

When k_{iq} was decreased to one tenth there was a considerable decrease in conversion, which meant that a larger bed height was required to achieve the desired conversion.

7.4 Conclusions

A comprehensive computer model to simulate the FBMR (High-flux membranes) with or without oxygen input was developed. The simulation work is based on a two-phase bubbling bed reactor model (Grace, 1984) with the membrane considered as a separate side selectively separating hydrogen from other phases. The model was validated by experimental data from the present study. The simulation results showed good agreement with experimental data.

Chapter 8

Conclusions and Future Work

8.1 Conclusions of the present investigation

This chapter concludes the developments and modifications made to the FBMR in due course of the entire thesis project. The conclusions of the present investigation can be summarized in six different sections, each of them comprised of a chapter in this thesis. The following paragraphs explain the conclusions and achievements of each of these studies.

8.1.1 Economic study of FBMR

This study outlined the general direction of the present investigation. It identified the shortcomings and proposed solutions in this process. The study confirmed that fluidized bed membrane reforming has up to a 35% gain in conversion of methane over conventional technology at comparable operating temperature and pressure when hydrogen can be efficiently removed in the reactor. The configuration with High-flux membranes had a lower capital and operating cost than conventional SMR, and had a hydrogen supply cost 5% lower than commercial SMR showing the promise of this new technology. The study showed that work had to be done in two major areas for substantial improvement, the supply of heat to the reformer and development of

palladium membranes with improved permeation capability. The following studies provided solutions to these two problems.

8.1.2 Development of High-flux membrane module

The writeup described the successful development of palladium coated metal alloy tubular (High-flux) membranes for use at high temperatures and differential pressures. The spring reinforced High-flux membrane tubes were tested for permeation over the temperature range of 673-973 K and at differential pressures up to 1480 kPa. This was a significant improvement, as these types of membranes were tested in earlier studies only up to a temperature of 698 K and a differential pressure of 110.3 kPa. In addition, the abrasion resistance of the palladium coating was tested in the fluidized bed of catalyst particles and found to be satisfactory.

Due to their stability at high temperatures, with differential pressures and in a fluidized bed environment, the High-flux membrane tubes could be used in membrane reactors including fluidized bed membrane reformers that require operation at relatively high temperatures and with high transmembrane pressure differences. A U-tube spring reinforced High-flux membrane module was also developed for use in the FBMR pilot plant.

8.1.3 FBMR with High-flux membranes

The study proved the viability of U-tube spring reinforced High-flux membrane modules in a pilot plant reformer. The membranes were able to successfully perform in the reforming reactor environment.

The experimental results showed a greatly improved performance compared to the equilibrium reactor and previous investigation. The hydrogen permeate flow was ten to fifteen times more than the previous study. The study also showed that there was room in the reformer to handle increased permeation capacity.

The dependent variables methane conversion and hydrogen yields behaved as anticipated and were about 15% higher than equilibrium values.

8.1.4 Fluidized bed steam methane reforming with oxygen input

The study concluded that oxygen could be introduced successfully into a reforming reactor to provide for the endothermic heat of reforming reactions. There was 100% conversion of oxygen under all conditions. Most of the experimental runs reached and maintained autothermal conditions. The hydrogen yield increased with increasing temperature and steam-methane ratio and it decreased minimally with increasing reactor pressure and oxygen flowrate.

The methane conversion increased with increasing reactor temperature, oxygen input flowrate and steam-methane ratio and decreased with increasing reactor pressure as expected. Methane conversion and hydrogen yield were compared to those expected from equilibrium.

8.1.5 FBMR with oxygen input experimentation and analysis of experimental data

An autothermal FBMR unit producing hydrogen was successfully developed and tested. This new concept was proved and validated. The hydrogen permeate flow (mol/h) in the autothermal FBMR study was on average seven to ten times greater than in

the previous study (Adris, 1994). The comparison with FBMR proves that the oxygen input configuration gives increased methane conversion but decreased hydrogen yield and permeation.

Data analysis shows good reproducibility and accuracy of pilot plant experiments and the presence of excess catalyst in the reactor.

8.1.6 Computer simulation of FBMR

A comprehensive computer model to simulate the FBMR (High-flux membranes) with or without oxygen input was developed. The simulation work is based on a two-phase bubbling bed reactor model (Grace, 1984) with the membrane considered selectively separating hydrogen from both phases. The model was validated by experimental data from the present study. The simulation results showed good agreement with experimental data.

8.2 Future Work

Though major drawbacks associated with the FBMR technology have been successfully addressed by this study, there are issues related to commercial use of this technology that still need to be addressed. The durability of the membrane tubes, effect on the catalyst during prolonged operation, thermal efficiency, reformer design, effect of prolonged oxygen input on the equipment, and oxygen sparger or nozzle design are the major issues. Hence the next step would be the optimization of process variables and equipment with respect to a specific applications and throughput. These studies should preferably be done on a demonstration scale plant.

The present work has dwelt on solutions to two specific problems regarding the membrane and heat input. In commercial SMR the ratio of mols of hydrogen produced per mol of CH_4 fed is about 2.2. The present pilot plant was able to reach a ratio of 1.0 based on hydrogen permeating through the membranes and it has to be increased to about 2.0 to be competitive with existing technology. This can be achieved with a redesigned configuration.

These following investigations should be undertaken to achieve the goals of commercialization of the FBMR process with High-flux membranes and oxygen input:

➔ Technical and economic evaluation including:

Computer simulation

Preliminary engineering design

Cost evaluation

➔ Durability tests on membranes and catalyst under full process conditions

➔ Further improvements to the structural design of the membranes

➔ Engineering design of a demonstration plant involving an EPC company

➔ Testing and improvements under plant conditions

➔ Technology demonstration for selected applications

These steps should lead to eventual acceptance of the process as a viable alternative to the existing ones.

References

Adris, A. M., "A Fluidized Bed Membrane Reactor for Steam Methane Reforming: Experimental Verification and Model Validation", Ph.D. Thesis, University of British Columbia, Vancouver, Canada, April 1994.

Adris, A. M., "A Fluidized Bed Steam Reformer for Methane", M.Sc. Thesis, University of Salford, Salford, England, 1989.

Adris, A. M., Elnashaie, S. S. E. H and Hughes, R., "A Fluidized Bed Membrane Reactor for the Steam Reforming of Methane", *Canadian Journal of Chemical Engineering*, Vol. 69, 1061-1069, Oct. (1991).

Adris, A. M., Grace, J. R., Lim, C. J. and Elnashaie, S. S. E. H., "Fluidized Bed Reaction System for Steam/Hydrocarbon Gas Reforming to Produce Hydrogen", U.S. Pat. No. 5,326,550, 1994.

Adris, A. M., Lim, C. J. and Grace, J. R., "The Fluidized –bed Membrane Reactor for Steam Methane Reforming: Model Verification and Parametric Study", *Chemical Engineering Science*, Vol. 52, No. 10, 1609-1622 (1997).

Adris, A. M., Pruden, B. B., Lim, C. J. and Grace, J. R., "On the Reported Attempts to Radically Improve the Performance of the Steam Methane Reforming Reactor", *Canadian J. Chem. Engg.*, 74 (April), 177-186 (1996).

Akers, W. W., and Camp, D. P., "Kinetics of Methane Steam Reactions", *AIChE J.*, 1(4), 471 (1955).

Allen, D. W., Gehard, E. R. and Likins, M. R. Jr., "Kinetics of the Methane-Steam Reaction", *Ind. Eng. Chem. Process Des. Dev.*, 14, 256 (1975).

Amano, M., Komaski, M., Nishimura, C., "Hydrogen Permeation Characteristics of of Palladium Plated V-Ni Alloy Membranes", *J. Less-Common Met.*, 172-174, 727-731 (1991).

Athavale, S. N. and Totlani, M. K., "Electroless Plating of Palladium", *Met. Fin.*, 87, 23-27 (1989).

Athayde, A. L., Baker, R. W. and Nguyen, P., "Metal Composite Membranes for Hydrogen Separation", *J. Membr. Sci.*, 94, 299-311 (1994).

Baker, G. N., Gallagher, M. J. and Wear, T. J. "Ultrathin Metal Composite Membranes for Gas Separation", US Patent 4,857,080, 1989.

Balthasar W., "Hydrogen Production and Technology: Today, Tomorrow and Beyond", *Int. J. Hydrogen Energy*, 9, 649-668 (1984).

Barrer, R. M., "Diffusion in and through Solids", Cambridge University Press, London, 1951.

Barrer, R. M., *Trans. Faraday Soc.*, 36, 1235 (1940).

Bharadwaj, S. S. and Schmidt, L. D., "Synthesis Gas Formation by Catalytic Oxidation of Methane in Fluidized Bed Reactors", *J. Catal.*, 146, 11-21 (1994).

Bhave, R. R., "Inorganic Membranes: Synthesis, Characteristics and Applications", Chapman & Hall, New York, 1991.

Bitter, J. G. A., "Dehydrogenation Using Porous Inorganic Membranes", GB Patent Appl. 8,629,135, 1986.

Bohmholdt, G. and Wicke, E., "Diffusion of H_2 and D_2 in Pd and Pd-alloys", *Z.Physik. Chem.*, Neue Folge, 56, 133-148 (1967).

Brown, C. C. and Buxbaum, R. E., "Kinetics of Hydrogen Absorption in Alpha Titanium", *Metall. Trans. A*, 19A, 1425-1427 (1988).

Brun-Tsekhovoi, A. R., Zadorin, A. N., Katsobashvili, Ya. R. and Kourdumov, S. S., "The Process of Catalytic Steam - Reforming of Hydrocarbons in the Presence of Carbon Dioxide Acceptor", Hydrogen Energy Progress VII, Proceedings of the 7th World Hydrogen Energy Conference, Vol. 2, Pergamon Press, 885-900 (1988).

Buxbaum, R. E. and Hsu, P. C., "Method for Plating Palladium", US Patent 5,149,420, 1992.

Buxbaum, R. E. and Kinney, A. B., "Hydrogen Transport through Tubular Membranes of Palladium-Coated Tantalum and Niobium", *Ind. Eng. Chem. Res.*, 35(2), 530-537 (1996).

Buxbaum, R. E. and Marker, T. L., "Hydrogen Transport through Non-Porous Membranes of Palladium-Coated Niobium, Tantalum and Vanadium", *J. Membr. Sci.*, 85, 29-38 (1993).

Buxbaum, R. E., "Composite Metal Membranes for Hydrogen Extraction", US Patent 5,108,724, 1991.

Chai, M., Yamashita, Y., Machida, M., Eguchi, K. and Arai, H., "Preparation and Characterization of Metal-Dispersed Alumina Membranes for Selective Separation of Hydrogen", *J. Membr. Sci.*, 97, 199-207 (1994).

Chopra, K. L., "Thin Film Phenomena", McGraw-Hill Book Co., 1969.

Choudhary, V. R., Rajput, A. M. and Prabhakar, B., "Nonequilibrium Oxidative Conversion of Methane to CO and H_2 with High Selectivity and Productivity over Ni/Al_2O_3 at Low Temperatures", *J. Catal.*, 139, 326-328 (1993).

Clayson, D. M. and Howard, P., "Process and Catalysts for Manufacture of Aromatic Hydrocarbons from C_{2-6} Alkanes", GB Patent 2,190,397 A, 1987.

Cole, M. J., "The Generation of Pure Hydrogen for Industrial Applications", *Plat. Met. Rev.*, 25, 12-13 (1981).

Collins, J. P. and Way, J. D., "Preparation and Characterization of a Composite Palladium-Ceramic Membrane", *Ind. Eng. Chem. Res.*, 32, 3006-3013 (1993).

Davidson, J. F. and Harrison, D., Fluidization Particles, Cambridge University Press, Cambridge, UK, 1963.

Davidson, J. F., "The Two-phase Theory of Fluidization, Successes and Opportunities", *AIChE Symp. Ser.*, 87, 1-12 (1991).

De Deken, J., Devos, E. F. and Froment, G. F., "Steam Reforming of Natural Gas: Intrinsic Kinetics, Diffusional Influences and Reactor Design", *Chem. React. Eng., ACS Symp. Ser.*, 196, Boston (1982).

DeRosset, A. J., "Diffusion of Hydrogen through Palladium Membranes", *Ind. Eng. Chem. Res.*, 52, 525-528 (1960).

Dibbern, H. C., Olsen, P., Rostrup-Nielsen, J. R., Tottrup, P. B. and Udengard, N. R., "Make Low H2/CO Syngas Using Sulfur Passivated Reforming", *Hydrocarbon Processing*, January, 71-74 (1986).

Dissanayake, D., Rosynek, M. P., Kharas, K. C. C. and Lunsford, J. H., "Partial Oxidation of Methane to Carbon Monoxide and Hydrogen over a Ni/Al_2O_3 Catalyst", *J. Catal.*, 132, 117-127 (1991).

Edlund, D. J., "A membrane Process for Hot-Gas Cleanup and Decomposition of H_2S to Elemental Sulfur", Phase I Final Report to the U.S. Department of Energy on Contract No. DE-FG03-91ER81228 from Bend Research, Inc., Bend, OR, 1992.

Elnashaie, S. S. E. H., Adris, A. M., Al-Ubaid, A. S. and Soliman, M. A., "On the Non-monotonic Behaviour of Methane Steam Reforming Kinetics", *Chem. Eng. Sci.*, 45, 491-501 (1990).

Ermilova, M. M., Orekhova, N. V., Morozova, L. S. and Skakunova, E. V., *Membr. Katal.*, 70 (1985).

Fleming, H. L., "Latest Developments in Inorganic Membranes", Presented at BBC Membrane Planning Conference, October 20-22, Cambridge, MA, 1987.

Foka, M., Chaouki, J., Guy, C. and Klvana, D., "Natural Gas Combustion in a Catalytic Turbulent Fluidized Bed", *Chem. Eng. Sci.*, 49(24A), 4269-4276 (1994).

Fuderer, A., "Integrated Process and Apparatus for the Primary and Secondary Catalytic Steam Reforming of Hydrocarbons", U.S. Pat. No. 4,650,651, 1987.

Furneaux, R. C. and Davidson, A. P. and Ball, M. D., "Porous Anodic Aluminium Oxide Membrane Catalyst Support", European Patent Appl. 0,244,970A1, 1987.

Geldart, D., "Chapter 6: Particle Entrainment and Carryover", Gas Fluidization Technology (Editor D. Geldart), John Wiley and Sons Ltd., 1986.

Geldart, D., "The Effect of Particle Size and Size Distribution on the Behaviour of Gas-Fluidized Beds", Powder Technology, 6, 201-205 (1972).

Geldart, D., "Types of Gas Fluidization", Powder Technology, 7, 285-292 (1973).

Goetsch, D. A. and Say, G. R., "Synthesis Gas Preparation and Catalyst Therefor", U.S. Pat. No. 4,877,550, 1989.

Govind, R. and Atnoor, D., "Development of a Composite Palladium Membrane for Selective Hydrogen Separation at High Temperature", *Ind. Eng. Chem. Res.*, 30, 591-594 (1991).

Grace, J. R., "Fluid Beds as Chemical Reactors", Gas Fluidization Technology (Editor D. Geldart), John Wiley and Sons Ltd., 1986.

Grace, J. R., "Generalized models for Isothermal Fluidized Bed Reactors", Recent Advances in the Engineering Analysis of Chemically Reacting Systems (Editor L. K. Doraiswamy), Wiley, New Delhi, 1984.

Graham, T., *Phil. Trans. Roy. Soc.*, London, 156, 399 (1866).

Gryaznov, V. M., "Hydrogen Permeable Palladium Membrane Catalysts. An Aid to the Efficient Production of Ultra Pure Chemicals and Pharmaceuticals", *Plat. Met. Rev.*, 30, 68-72 (1986b).

Gryaznov, V. M., Ermilova, M. M., Morozova, L. S. and Orekhova, N. V., "Palladium Alloys as Hydrogen Permeable Catalysts in Hydrogenation and Dehydrogenation Reactions", *J. Less-Common Metals*, 89, 529-535 (1983).

Gryaznov, V. M., Karavanov, A. N., *Khim.-Farm. Zh.*, 13, 74 (1979a).

Gryaznov, V. M., Mishchenko, A. P., Smirnov, V. S. and Aladiyshev, S. I., "Catalytic Reactor for Executing Coupled Chemical Reactions", GB Patent 1,358,297, 1973a.

Gryaznov, V. M., Smirnov, V. S. and Slin'ko, M. G., *Proc. 5th Int. Congr. Catal.*, 2, 1139 (1973b).

Gryaznov, V. M., Smirnov, V. S., Dyumaev, K. M., Ermilova, M. M. and Fedorova, N. V., "Tetralin", Soviet Patent 706,936, 1979b.

Gryaznov, V. M., Vestn. Akad. Nauk SSSR, 21 (1986a).

Gryaznov, V. M.and Smirnov, V. S., "Selective Hydrogenation on Membrane Catalysts", *Kinet. Catal.*, 18, 485 (1977).

Guerrieri, S. A., "Steam Reforming of Hydrocarbons", U.S. Pat. No. 3,524,819, 1970.

Hill, E. F., "Feasibility study: Removal of Tritium from Sodium During the MDEC Process by Oxidative Diffusion, Argonne West, DOE N707T1830035, 1982.

Hill, E. F., "Hydrogen Separation Using Coated Titanium Alloys", US Patent 4,468,235, 1984.

Holleck, G. L., "Diffusion and Solubility of Hydrogen in Palladium and Palladium-Silver Alloys", *J. Phys. Chem.*, 74, 503-511 (1970).

Hsieh, H. P., "Inorganic Membrane Reactors - A Review", *AIChE Symp. Ser.268*, 85, 53-67 (1989).

Hsieh, H. P., "Inorganic Membrane Reactors", *Catal. Rev. - Sci. Eng.*, 33 (1&2), 1-70 (1991).

Hsieh, H. P., "Inorganic Membranes", *AIChE Symp. Ser. 261*, 84, 1-18 (1988).

Hunter, J. B., "Ultrapure Hydrocarbon by Diffusion through Palladium Alloys", Paper Presented at the Symposium on the Production of Hydrogen, ACS Fall Meeting, New York, NY, 1963.

Hurlbert, R. C. and Konecny, J. O., "Diffusion of Hydrogen Through Palladium", *J. Chem. Phys.*, 34, 655-668 (1961).

Hyman, M. H., "Simulate Methane Reformer Reactions", *Hydrocarbon Process.*, 47, 131 (1968).

Islam, M. T., "Palladium Coated High-flux Tubular Membranes for Hydrogen Separation at High Temperatures and Differential Pressures and Mathematical Modelling of Fluidized Bed Reformer with Oxygen Input", M.Sc. Thesis, University of Calgary, Calgary, Canada, Aug. (1997).

Itoh, N. and Govind, R., "Combined Oxidation and Dehydrogenation in a Palladium Membrane", *Ind. Eng. Chem. Res.*, 28, 1554-1557 (1989).

Itoh, N., "A membrane Reactor Using Palladium", *AIChE J.*, 33, 1576-1578 (1987).

Jost, W. and Widman, A., *Z. Physik. Chem. (Leipzig)*, B45, 285 (1940).

Kameyama, T., Fukuda, K., Fujishige, M., Yokokawa, H. and Dokiya, M., "Production of Hydrogen from Hydrogen Sulfide by Means of Selective Diffusion Membranes", *Int. J. Hydrogen Energy*, 8(1), 5 (1983).

Katsuta, H., Farraro, R. B., McLellan, R. B., Acta Met., 27, 1111-1114 (1979).

Kikuchi, E., Uemiya, S., Sato, N., Inoue, H., Ando, H. and Matsuda, T., "Membrane Reactor Using Microporous Glass-Supported Thin Film of Palladium. Application to the Water Gas Shift Reaction", *Chem. Lett.*, 3, 489-492 (1989).

Kondrasheva, V. S., Gryaznov, V. M., Buravkov, S. V. and Skundin, A. M., "Structure of Chemically Deposited Palladium, Platinum and Ruthenium Thin Films", Izv. Vyssh, Uchebn. Zaved., *Khim. Khim. Tekhnol*, 28, 122-123 (1985).

Konno, M., Shindo, M., Sugawara, S. and Satio, S., "A Composite Palladium and Porous Aluminum Oxide Membrane for Hydrogen Gas Separation", *J. Membr. Sci.*, 37, 193 (1988).

Koresh, J. and Soffer, A., "The Carbon Molecular Sieve Membranes. General Properties and Permeability of CH_4/H_2 mixtures", *Separ. Sci. Technol.*, 22(2&3), 972-982 (1987).

Kunii, D. and Levenspiel, O., "Fluidization Engineering", 2nd edition, Butterworth-Heinmann, Massachusetts, 1991.

Kunii, D. and Levenspiel, O., "Fluidization Engineering", John Wiley & Sons Inc., 1969.

Lange de, R. S. A., Keizer, K. and Burggraaf, A. J., "Analysis and Theory of Gas Transport in Microporous Sol-Gel Derived Ceramic Membranes", *J. Membr. Sci.*, 104, 81 (1995).

Le Claire, A. D., "Permeation of Gases through Solids: I. Principles", *Diffusion and Defect Data*, 33, 1-66 (1983).

LeBlanc, J. R., "Autothermal Steam Reforming Process", U.S. Pat. No. 5,011,625, 1991.

Lee, S. J., Yang, S. M. and Park, S. B., "Synthesis of Palladium Impregnated Alumina Membrane for Hydrogen Separation", *J. Membr. Sci.*, 96, 223-232 (1994).

Lee, S. M., "Film Deposition Techniques", in "Encyclopedia of Chemical Technology", Editors Kirk, R. E. and Othmer, D. F., Vol. 10, 3rd Edition, John Wiley and Sons, New York, 247-283 (1978).

Li, Z. Y., Maeda, H., Kusakabe, K., Morooka, S., Anzai, H. and Akiyama, S., "Preparation of Palladium-Silver Alloy Membranes for Hydrogen Separation by the Spray Pyrolysis Method", *J. Membr. Sci.*, 78, 247-254 (1993).

Lowenheim, F. A., "Modern Electroplating", John Wiley & Sons, New York, 342-357, 739-747 (1974).

Markides, A. C., Wright, M. A. and Jewett, D. N., "Separation of Hydrogen by Permeation", US Patent 3,350,846, 1967.

Mikhalenko, N. N., Khrapova, E. V. and Gryaznov, V. M., "Influence of Hydrogen on the Dehydrogenation of Isopropyl Alcohol in the Presence of a Palladium Membrane Catalyst", *Kinet. Catal.*, 26, 125-128 (1986).

Mishchenko, A. P., Gryaznov, V. M., Smirnov, V. S., Senina, E. P., Parbuzina, I. L., Roshan, N. R., Polyakova, V. P. and Savitskii, E. M., "Aniline", German Patent 3,013,799, 1981.

Miwo, K., *Int. Chem. Eng.*, 12, 187 (1972).

Mohan, K. and Govind, R., "Effect of Temperature on Equilibrium Shift in Reactors with a Permselective Wall", *Ind. Eng. Chem. Res.*, 27, 2064-2070 (1988).

Mori, S. and Wen, C. Y., "Estimation of Bubble Diameter in Gaseous Fluidized Beds", *AIChE J.*, 21, 109-115 (1975).

Mulder, M., "Basic Principles of Membrane Technology", Kluwer Academic Publishers, Dordrecht, 1991.

Nagamoto, H. and Inoue, H., "A Reactor with Catalytic Membrane Permeated by Hydrogen", *Chem. Eng. Commun.*, 34, 315-323 (1985).

Nazarkina, E. B. and Kirichenko, N. A., "Improvement in the Steam Catalytic Conversion of Methane by Hydrogen Liberation via Palladium Membranes", *Khim. Tekhnol. Topl. Masel*, 3, 5-7 (1979).

Olsbye, U., Slagtern, A. and Dahl, I. M., Proc. Natural Gas Conversion Symposium, Sydney, 1993.

Orcut, J. C., Davidson, J. F. and Pigford, R. L., "Reaction Time Distributions in Fluidized Catalytic Reactors", *Chem. Eng. Prog. Symp. Ser.*, 85, No. 38, 1-15 (1962).

Paloumbis, S. and Petersen, E. E., "Coke Deposition on a Commercial Nickel Oxide Catalyst During the Steam Reforming of Methane", Chemical Reaction Engineering, *ACS Symp. Ser.*, 38, 489-494 (1982).

Partington, J. R., "General and Inorganic Chemistry", MacMillan, London, 1954.

Pfefferie, W. C., "Process for Dehydrogenation", US Patent 3,290,406, 1966.

Philpott, J. E., "Hydrogen Diffusion Technology. Commercial Applications of Palladium Membrane", *Plat. Met. Rev.*, 29, 12-16 (1985).

Pruden, B. B, Roy, S. and Cox, B. G., "Economics and Simulation of Fluidized Bed Membrane Reforming", Report No: 95-01, Dept. of Chemical and Petroleum Engg., University of Calgary, Sept. 1995.

Quartuli et al., U.S. Pat. No. 3,264,066, 1966.

Rao, M. B. and Sircar, S., "Nanoporous Carbon Membranes for Gas Separation", *Gas Sep. Purif.*, 7(4), 279 (1993).

Reichel, W. and Lippert, H., "Wirbelbett-Reaktorsystem", Deutsches Pat. No. DE 33 31 202, 1984.

Richardson, S. A., Paripatyadar, S. A. and Shen, J. C., "Dynamics of a Sodium Heat Pipe Reforming Reactor", *AIChE Journal*, 34, 743-752 (1988).

Rostrup-Nielsen J. R., Dybkjarer, I. B and Christiansen, L. J., "Steam Reforming: Opportunities and Limits of the Technology", *Chemical Reactor Technology for Environmentally Safe Reactors and Products*, Lyngby, Denmark (1992).

Rostrup-Nielsen, J. R., "Catalytic Steam Reforming", Catalysis Science and Technology (Editors - J. R. Anderson and M. Boudard), Vol. 4, Springer, Berlin, 1983.

Rostrup-Nielsen, J. R., "Catalytic Steam Reforming", *Catalysis Science and Technology*, Springer, Verlag, Berlin (1984).

Rostrup-Nielsen, J. R., *Steam Reforming Catalyst*, Danish Technical Press, Inc., Copenhagen, 1975.

Roy, S., Cox, B. G., A. M. Adris, and Pruden, B. B., "Economics and Simulation of Fluidized Bed Membrane Reforming", *Int. J. Hydrogen Energy*, Vol. 23, No. 9, 745-752 (1998).

Sakai, T., Takenaka, H., Wakabayashi, N., Kawami, Y. and Torikai, E., "Hydrogen Separation by Nafion-Pd Composite Membranes", *Osaka Kogyo Gijutsu Shikensho Kiho*, 36, p.36 (1985).

Santos, A., Menendez, M. and Santamaria, J., "Partial Oxidation of Methane to Carbon Monoxide and Hydrogen in a Fluidized Bed Reactor", *Catal. Today*, 21, 481-488 (1994).

Sawatzki, A. and Ledoux, G. A., "The Use of Palladium to Remove Hydrogen from Zirconium", Presented at the 2nd International Congress on Hydrogen in Metals, Paris, France, 1977.

Schmidt, L. D., Huff, M. and Bharadwaj, S. S., "Catalytic Partial Oxidation Reactions and Reactors", *Chem. Eng. Sci.*, 49(24A), 3981-3994 (1994).

Schmitz, J. and Gerke, H., "Conversion Increase in Steam Reforming of Natural Gas by Hydrogen Permeation Membranes", CLB, *Chem. Labor. Betr.*, 39, 75-76 (1988).

Scott, D. S., "Hydrogen, National Mission for Canada", Report by the Advisory Group on Hydrogen Opportunities , Ministry of Supply and Services Canada, Cat No. M27-86/1987E, 1987.

Shu, J., Grandjean, P. A., Van Neste, A. and Kaliaguine, S., "Catalytic Palladium-based Membrane Reactors: A Review", *Canad. J. Chem. Eng.*, 69, 1036-1060 (1991).

Silberg, P. A. and Bachman, C. H., *J. Chem. Phys.*, 29, 777 (1958).

Singh, C. P. P., and Saraf, D. N., "Simulation of Side Fired Steam-Hydrocarbon Reformers", *Ind. Eng. Chem. Process. Des. Dev.*, 18, 1 (1979).

Sit, S. P. and Grace, J. R., "Effect of Bubble Interaction on Interphase Mass Transfer in Gas-Fluidized Beds", *Chem. Eng. Sci.*, 36, 327-335 (1981).

Slattery, J. C. and Bird, R. B., *AIChE J.*, 4, 137-142 (1958).

Smirnov, V. S., Gryaznov, V. M., Lebedeva, V. I., Mishchenko, A. P., Polyakova, V. P. and Savitsky, E. M., "Method of Dehydrogenation, Dehydrocyclization and Hydrodealkylation", US Patent 4,041,093, 1977.

Soliman, M. A., El-Nashaie, S. S. E. H., Al-Ubaid, A. S. and Adris, A. M., "Simulation of Steam Reformers for Methane", *Chem. Eng. Sci.*, 43, 1801 (1988).

Stephanopoulos, M. F. and Voecks, G. E., "Catalytic Autothermal Reforming Increases Fuel Cell Flexibility", *Energy Progress*, 1(1-4), 52-58 (1981).

Sun, Y. M. and Khang, S. J., "Catalytic Membrane for Simultaneous Chemical Reaction and Separation Applied to a Dehydrogenation Reaction", *Ind. Chem. Eng. Res.*, 27(7), 1136-1142 (1988).

Suzuki, F., Onozato, K. and Kurokawa, Y., "Gas Permeability of a Porous Alumina Membrane Prepared by the Sol-Gel Process (Aluminium iso-Propoxide) ", *J. Non-Crystl. Solids,* 94, 160-162 (1987).

Torniainen, P. M., Chu, J. and Schmidt, L. D., "Comparison of Monolith-Supported Metals for the Direct Oxidation of Methane to Syngas", *J.Catal.,* 146, 1-10 (1994).

Tsotsis, T. T., Minet, R. G., Champagnie, A. M. and Liu, P. K. T., "Catalytic Membrane Reactors", In Computer Aided Design of Catalysts, Chemical Industries, Marcel Dekker, New York. 1993.

Uemiya, S., Kude, Y.. Sugino, K., Sato, N., Matsuda, T. and Kikuchi, E., "A Palladium/ Porous Glass Composite Membrane for Hydrogen Separation", *Chem. Lett.,* 10, 1687-1690 (1988).

Uemiya, S., Matsuda. T. and Kikuchi, E., "Hydrogen Permeable Palladium-Silver Alloy Membrane Supported on Porous Ceramics", *J. Membr. Sci.,* 56, 315-325 (1991b).

Uemiya, S., Sasaki, H.. Matsuda, T. and Kikuchi, E., "Preparation of Thin Palladium Films by Use of an Electroless Plating Technique", *Nippon Kagaku Kaishi,* 6, 669-675 (1990).

Uemiya, S., Sato, N., Ando, H. and Kikuchi, E., "Steam Reforming of Methane in a Hydrogen-Permeable Membrane Reactor", *Appl. Catal.,* 67, 223-230 (1991c).

Uemiya, S., Sato, N., Ando, H., Kude, Y., Matsuda, T. and Kikuchi, E., "Separation of Hydrogen through Palladium Thin Film Supported on a Porous Glass Tube", *J. Membr. Sci.,* 56, 303-313 (1991a).

Uhlhorn, R. J., Keizer, K. and Burggraaf, A. J., "Gas and Surface Diffusion in (modified) γ-Alumina Syatems", *J. Membr. Sci.,* 46, 225-246 (1989).

Van der Vaart, D. R. and Davidson, J. F., "The Combustion of Hydrocarbon Gas, Pre-Mixed with Air, in a Fluidized Bed", Fluidization V, Elsinore, Denmark; Engineering Foundation: New York, 539-546 (1986).

Van der Vaart, D. R., "Mathematical Modeling of Methane Combustion in a Fluidized Bed", *Ind. Eng. Chem. Res.*, 31, 999-1007 (1992).

Vandaveer, F. E. and Segeler, C. G., Chapter 5: Combustion, *Fuels, Combustion and Heat Transfer,* Gas Engineers Handbook, Editor in Chief Segeler, C. G., Industrial Press, NY, 2/46 - 2/100, 1965.

Veser, G. and Schmidt, L. D., "Ignition and Extinction in the Catalytic Oxidation of Hydrocarbons Over Platinum", *AIChE J.*, 42(4), 1077-1087 (1996).

Wagner, E. S. and Froment, G. F., "Steam Reforming Analyzed", *Hydrocarbon Processing*, 69-77, July (1992).

Wen, C. Y. and Chen, L. H., *AIChE J.*, 28, 117 (1982).

Wen, C. Y. and Yu, Y. H., "A generalized Method for Predicting the Minimum Fluidization Velocity", *AIChE J.*, 12, 610-612 (1966).

Wijmans, J. G. and Baker, R. W., "The Solution-Diffusion Model: A Review", *J. Membr. Sci.*, 107, 1-21 (1995).

Wilke, C. R. and Lee, C. Y., *Ind. Eng. Chem.*, 47, 1253 (1955).

Wu, J. C. S., Gerdes, T. E., Pszczolkowski, J. L., Bhave, R. R. and Liu, P. K. T., "Dehydrogenation of Ethylbenzene to styrene Using Commercial Ceramic Membranes as Reactors", *Separ. Sci. Technol.*, 25(13-15), 1489-1510 (1990).

Xu, J. and Froment, G. F., "Methane Steam Reforming -II. Diffusional Limitations and Reactor Simulation", *AIChE J.*, 35, 97 (1989a).

Xu, J. and Froment, G. F., "Methane Steam Reforming, Methanation, and Water-gas shift - I. Intrinsic Kinetics", *AIChE J.*, 35, 88 (1989).

Xu, J., "Kinetic Study of Steam Reforming of Methane", Ph.D. Thesis, University of Ghent, Belgium, 1988.

Yan, S., Maeda, H., Kusakabe, K. and Morooka, S., "Thin Palladium Membrane Formed in Support Pores by Metal-Organic Chemical Vapor Deposition Method and Application to Hydrogen Separation", *Ind. Eng. Chem. Res.*, 33, 616-622 (1994).

Yermakova, A., Anikeev, V. I. and Bobrin, A. S., "Kinetics of Catalytic Oxidation of Methane", *React. Kinet. Catal. Lett.*, 51(2), 325-330 (1993).

Young, H. D., "Statistical Treatment of Experimental Data", 1st Ed., McGraw-Hill Inc., New York (1962).

APPENDIX

Experimental and Calculated Data

Table A.1: Oxygen input variation in FBR

(T = 923 K, P = 0.55 MPa, Methane flowrate = 40 mol/h & Steam-methane ratio = 2)

Oxygen flowrate	Methane (Expt.) conversion	Hydrogen Yield (Expt.)	Methane (Eqil.) conversion	Hydrogen Yield (Eqil.)
mol/h	%		%	
12	52.7	1.38	59.7	1.58
14	52.9	1.34	62.0	1.57
16	58.5	1.48	64.3	1.56
18	60.4	1.44	66.6	1.55
20	62.3	1.44	68.8	1.54
22	64.1	1.41	71.0	1.52

Table A.2: Pressure variation in FBR

(T = 923 K, Methane flowrate = 40 mol/h, Oxygen flowrate = 18 mol/h & Steam-methane ratio = 2)

Reactor pressure	Methane (Expt.) conversion	Hydrogen Yield (Expt.)	Methane (Eqil.) conversion	Hydrogen Yield (Eqil.)
MPa	%		%	
0.35	65.3	1.61	74.0	1.79
0.4	61.9	1.5	71.8	1.72
0.45	60.4	1.46	69.9	1.66
0.5	60.3	1.38	68.2	1.6
0.55	58.8	1.4	66.6	1.55
0.6	58.7	1.4	65.2	1.5

Table A.3: Temperature variation in FBR

(P = 0.5 MPa, Methane flowrate = 40 mol/h, Oxygen flowrate = 18 mol/h & Steam-methane ratio = 2)

Reactor Temperature	Methane (Expt.) conversion	Hydrogen Yield (Expt.)	Methane (Eqil.) conversion	Hydrogen Yield (Eqil.)
K	%		%	
848	40.5	0.73	52.0	1.09
873	44.7	0.89	57.0	1.26
898	50.3	1.04	62.4	1.43
923	58.6	1.37	68.2	1.56
948	62.9	1.54	74.0	1.77

Table A.4: Steam-methane ratio variation in FBR

(T = 923 K, P = 0.5 MPa, Methane flowrate = 40 mol/h, Oxygen flowrate = 18 mol/h)

Steam-methane ratio	Methane (Expt.) conversion	Hydrogen Yield (Expt.)	Methane (Eqil.) conversion	Hydrogen Yield (Eqil.)
	%		%	
1.5	52.6	1.20	63.1	1.40
2.0	58.6	1.37	68.2	1.60
2.5	61.9	1.51	72.6	1.78
3.0	65.3	1.62	76.5	1.94

Table A.5: Temperature variation (I) in FBMR

(P = 0.99 MPa, Methane flowrate = 45 mol/h, Steam flowrate = 138.33 mol/h, Sweep gas pressure = 0.24 MPa, Sweep gas flowrate = 45 mol/h)

Reactor Temperature	Methane Conversion	Hydrogen Yield	Hydrogen Permeate rate	Hydrogen Recovery
K	%		mol/h	%
826	33.3	1.33	18.7	31.1
856	38.2	1.53	21.2	30.8
870	45.0	1.75	24.9	31.6
898	50.9	1.92	26.3	30.4

Table A.6: Temperature variation (II) in FBMR

(P = 0.99 MPa, Methane flowrate = 45 mol/h, Steam flowrate = 138.33 mol/h, Sweep gas pressure = 0.14 MPa, Sweep gas flowrate = 45 mol/h)

Reactor Temperature	Methane Conversion	Hydrogen Yield	Hydrogen Permeate rate	Hydrogen Recovery
K	%		mol/h	%
821	36.5	1.52	23.6	34.5
847	42.0	1.69	27.0	35.3
871	48.9	1.85	28.4	34.1
897	53.8	2.06	31.3	33.8
911	57.5	2.16	32.6	33.6

Table A.7: Temperature variation (III) in FBMR

(P = 0.68 MPa, Methane flowrate = 33.74 mol/h, Steam flowrate = 138.33 mol/h, Sweep gas pressure = 0.14 MPa, Sweep gas flowrate = 45 mol/h)

Reactor Temperature	Methane Conversion	Hydrogen Yield	Hydrogen Permeate rate	Hydrogen Recovery
K	%		mol/h	%
849	49.7	1.91	19.0	29.5
877	59.0	2.20	21.0	28.3
900	67.7	2.6	24.5	28.2

Table A.8: Temperature variation (IV) in FBMR with no sweep

(P = 0.99 MPa, Methane flowrate = 45 mol/h, Steam flowrate = 138.33 mol/h, Sweep gas pressure = 0.14 MPa)

Reactor Temperature	Methane Conversion	Hydrogen Yield	Hydrogen Permeate rate	Hydrogen Recovery
K	%		mol/h	%
871	44.9	1.83	23.1	28.2
897	52.0	2.08	26.9	28.8
911	56.5	2.19	28.1	28.6

Table A.9: Pressure variation (I) in FBMR

(P =873 K, Methane flowrate = 45 mol/h, Steam flowrate = 138.33 mol/h, Sweep gas pressure = 0.24 MPa, Sweep gas flowrate = 45 mol/h)

Reactor Pressure	Methane Conversion	Hydrogen Yield	Hydrogen Permeate rate	Hydrogen Recovery
MPa	%		mol/h	%
0.68	46.3	1.80	18.7	31.1
0.78	46.1	1.80	21.2	30.8
0.88	45.6	1.79	24.9	31.6
0.99	44.5	1.72	26.3	30.4

Table A.10: Pressure variation (II) in FBMR

(T = 873 K, Methane flowrate = 45 mol/h, Steam flowrate = 138.33 mol/h, Sweep gas pressure = 0.14 MPa, Sweep gas flowrate = 45 mol/h)

Reactor Pressure	Methane Conversion	Hydrogen Yield	Hydrogen Permeate rate	Hydrogen Recovery
MPa	%		mol/h	%
0.68	60.0	2.35	18.7	29.4
0.78	57.5	2.22	21.2	24.1
0.88	54.7	2.14	24.9	25.1
0.99	53.0	2.13	26.3	27.0

Table A.11: Steam-methane ratio variation in FBMR

(T= 872 K, P = 0.99 MPa, Steam flowrate = 138.33 mol/h, Sweep gas pressure = 0.14 MPa, Sweep gas flowrate = 45 mol/h)

Steam-methane ratio	Methane Conversion	Hydrogen Yield	Hydrogen Permeate rate	Hydrogen Recovery
K	%		mol/h	%
4.1	54.6	2.15	26.0	35.7
3.1	45.5	1.81	26.8	32.7
2.4	37.3	1.46	27.1	32.1

Table A.12: Superficial velocity variation in FBMR

(P = 0.99 MPa, Steam-methane ratio = 3.1, Sweep gas pressure = 0.14 MPa and Sweep gas flowrate = 45 mol/h)

Superficial velocity	Methane Conversion	Hydrogen Yield	Hydrogen Permeate rate	Hydrogen Recovery
cm/s	%		mol/h	%
11.2	46.5	1.82	26.8	32.7
8.5	45.9	1.80	26.2	32.4
6.3	45.7	1.80	26.0	32.2

Table A.13: Oxygen input variation in FBMR with oxygen onput

(T = 923 K, P = 0.68 MPa, Methane flowrate = 33.74 mol/h, Steam flowrate = 138.33 mol/h, Sweep gas pressure = 0.14 MPa, Sweep gas flowrate = 45 mol/h)

Oxygen Flowrate	Methane Conversion	Hydrogen Yield	Hydrogen Permeate rate	Hydrogen Recovery
mol/h	%		mol/h	%
14.7	76.01	1.95	18.6	28.2
15.2	77.2	1.93	18.6	28.6
16.8	79.1	1.93	18.5	27.7
18.9	81.1	1.91	17.6	27.3
21.0	82.2	1.88	17.1	27.0

Table A.14: Steam-methane ratio variation in FBMR with oxygen

(T= 923 K, P = 0.68 MPa, Steam flowrate = 138.33 mol/h, Sweep gas pressure = 0.14 MPa, Sweep gas flowrate = 45 mol/h and Methane:Oxygen = 1.0:0.35)

Steam-methane ratio	Methane Conversion	Hydrogen Yield	Hydrogen Permeate rate	Hydrogen Recovery
	%		mol/h	%
4.1	73.6	1.98	19.1	28.6
3.1	65.7	1.67	20.5	27.3
2.4	58.5	1.40	21.4	26.6

Table A.15: Temperature variation (I) in FBMR with oxygen

(P = 0.99 MPa, Methane flowrate = 45 mol/h, Steam flowrate = 138.33 mol/h, Sweep gas pressure = 0.14 MPa, Sweep gas flowrate = 45 mol/h and Methane:Oxygen = 1.0:0.4)

Reactor Temperature	Methane Conversion	Hydrogen Yield	Hydrogen Permeate rate	Hydrogen Recovery
K	%		mol/h	%
873	52.1	1.26	19.0	33.3
898	55.9	1.41	21.0	33.0
923	60.4	1.55	23.2	33.2

Table A.16: Temperature variation (II) in FBMR with oxygen input

(P = 0.68 MPa, Methane flowrate = 33.74 mol/h, Steam flowrate = 138.33 mol/h, Sweep gas pressure = 0.14 MPa, Sweep gas flowrate = 45 mol/h & Methane: Oxygen = 1.0:0.45)

Reactor Temperature	Methane Conversion	Hydrogen Yield	Hydrogen Permeate rate	Hydrogen Recovery
K	%		mol/h	%
849	61.7	1.49	14.6	29.0
873	66.8	1.60	15.9	29.5
898	72.7	1.82	17.5	28.5
922	77.2	1.93	18.6	28.6

Table A.17: Pressure variation in FBMR with oxygen input

(T = 873 K, Methane flowrate = 33.74 mol/h, Steam flowrate = 138.33 mol/h, Sweep gas pressure = 0.14 MPa, Sweep gas flowrate = 45 mol/h & Methane: Oxygen = 1.0:0.45)

Reactor Pressure	Methane Conversion	Hydrogen Yield	Hydrogen Permeate rate	Hydrogen Recovery
MPa	%		mol/h	%
0.68	68.1	1.58	14.8	27.9
0.78	66.6	1.59	16.0	29.7
0.88	63.5	1.54	16.3	31.3
0.99	61.9	1.49	17.0	33.8

Table A.18: Driving force and percentage hydrogen recovery in FBMR with and without oxygen input (pressure variation runs)

(T = 873 K, Methane flowrate = 33.74 mol/h, Steam flowrate = 138.33 mol/h, Sweep side pressure = 0.14 MPa, Sweep gas flowrate = 45 mol/h & Methane: Oxygen = 1.0:0.45)

{ P_{H2R} is hydrogen partial pressure at reactor exit & P_{H2M} is hydrogen partial pressure at membrane exit}

Reactor Pressure	Driving Force (FBMR) $P_{H2R} - P_{H2M}$	Hydrogen Recovery (FBMR)	Driving Force (FBMR with O_2) $P_{H2R} - P_{H2M}$	Hydrogen Recovery (FBMR with O_2)
MPa	MPa	%	MPa	%
0.68	0.15	28.9	0.12	27.9
0.78	0.16	32.3	0.13	29.7
0.88	0.17	34.8	0.15	31.3
0.99	0.18	37.6	0.16	33.8

Table A.19: FBMR data used for multi-variate analysis

(Sweep side pressure = 0.14 MPa, sweep gas flowrate = 45 mol/h)

Code	Methane Conversion	Temperature	Pressure	Steam-methane ratio
	%	K	MPa	
MR2T1	49.7	849	0.68	4.1
MR2T2	59.0	877	0.68	4.1
MR2T3	67.7	900	0.68	4.1
MR1P1	59.9	873	0.68	4.1
MR1P2	57.5	873	0.78	4.1
MR1P3	54.7	873	0.88	4.1
MRIP4	53.0	873	0.99	4.1
MRS1	54.5	873	0.99	4.1
MRS2	45.4	873	0.99	3.1
MRS3	37.2	873	0.99	2.4
MR1T1	36.5	821	0.99	3.1
MRIT2	41.9	847	0.99	3.1
MRIT3	48.8	871	0.99	3.1
MRIT4	53.7	897	0.99	3.1
MR1T5	57.5	911	0.99	3.1

Table A.20: FBMR with oxygen input data used for multi-variate anlysis

(Sweep side pressure = 0.14 MPa, sweep gas flowrate = 45 mol/h)

Code	Methane Conversion	Temperature	Pressure	Steam-methane ratio	Oxygen flowrate
	%	K	MPa		mol/h
MA1T1	61.7	849	0.68	4.1	15.2
MA1T2	66.8	873	0.68	4.1	15.2
MA1T3	72.7	898	0.68	4.1	15.2
MA1T4	77.3	922	0.68	4.1	15.2
MAP1	68.2	873	0.68	4.1	15.2
MAP2	66.6	873	0.78	4.1	15.2
MAP3	63.5	873	0.88	4.1	15.2
MAP4	61.9	873	0.99	4.1	15.2
MAS1	73.6	923	0.68	4.1	15.2
MAS2	65.7	923	0.68	3.1	15.2
MAS3	58.5	923	0.68	2.4	15.2
MAO1	76.1	923	0.68	4.1	14.7
MAO2	77.3	923	0.68	4.1	15.2
MAO3	79.1	923	0.68	4.1	16.8
MAO4	81.1	923	0.68	4.1	18.9
MAO5	82.3	923	0.68	4.1	21.0

Table A.21: Data reproducibility analysis for pilot plant experiments

Code	Number of reproducibility runs (k)	Average CH_4 conversion (X_{av}) $\sum_k X_k / k$	Absolute deviation (DEV) $\sum_k \lvert X_k - X_{av} \rvert / k$	Average absolute deviation (AADEV)
		(%)	(%)	(%)
R1	4	46.77	1.02	0.73
R2	3	59.50	0.48	
R3	3	53.78	0.78	
R4	3	44.75	0.23	
R5	3	67.47	0.67	
R6	3	75.43	1.20	

Table A.22: Data reproducibility analysis with catalyst loading of 3.4 kg and 4.3 kg.

Code	Number of reproducibility runs (k)	Average CH_4 conversion (X_{av}) $\sum_k X_k / k$	Absolute deviation (DEV) $\sum_k \lvert X_k - X_{av} \rvert / k$	Average absolute deviation (AADEV)
		(%)	(%)	(%)
RC1	2	50.11	0.42	0.43
RC2	2	59.52	0.48	
RC3	2	67.36	0.49	

Table A.23: Process parameters of experiments described in Tables A.21 & A.22

Code	Temperature	Pressure	Methane flowrate	CH_4:H_2O:O_2 ratio	Sweep side pressure
	K	MPa	mol/h		MPa
R1	873	0.99	45.0	1.0:3.1:0.0	0.14
R2	873	0.68	33.7	1.0:4.1:0.0	0.14
R3	873	0.99	33.7	1.0:4.1:0.0	0.14
R4	873	0.99	45.0	1.0:3.1:0.0	0.24
R5	873	0.68	33.7	1.0:4.1:0.45	0.14
R6	923	0.68	33.7	1.0:4.1:0.45	0.14
RC1	848	0.68	33.7	1.0:4.1:0.0	0.14
RC2	873	0.68	33.7	1.0:4.1:0.0	0.14
RC3	923	0.68	33.7	1.0:4.1:0.0	0.14